

SODANKYLÄ GEOPHYSICAL OBSERVATORY  
PUBLICATIONS



No. 98

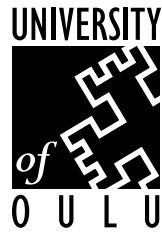
SOME ASPECTS OF ELF-VLF EMISSIONS  
IN GEOPHYSICAL RESEARCH

JYRKI MANNINEN

Oulu 2005



SODANKYLÄ GEOPHYSICAL OBSERVATORY  
PUBLICATIONS



No. 98

SOME ASPECTS OF ELF-VLF EMISSIONS  
IN GEOPHYSICAL RESEARCH

JYRKI MANNINEN

*Academic Dissertation to be presented, with the permission of the Faculty of Science of the University of Oulu, for public discussion in Polaria Lecture Hall, Sodankylä, on 17<sup>th</sup> December, 2005, at 12 o'clock noon.*

Oulu 2005

SODANKYLÄ GEOPHYSICAL OBSERVATORY PUBLICATIONS

Editor: Johannes Kultima  
Sodankylä Geophysical Observatory  
FIN-99600 SODANKYLÄ, Finland

This publication is the continuation of the former series  
“Veröffentlichungen des geophysikalischen Observatoriums  
der Finnischen Akademie der Wissenschaften”

Sodankylä Geophysical Observatory  
Publications

ISBN 951-42-6047-3  
ISBN 951-42-6048-1 (pdf)  
ISSN 1456-3673

**OULU UNIVERSITY PRESS**  
Oulu 2005

## Abstract

This thesis concentrates on electromagnetic waves in the ELF-VLF frequency range, which propagate in a magnetized plasma in the whistler mode. Their frequency range is from 3 Hz to 30 kHz, which means that they can be demodulated to audible sounds and therefore can be listened to with the aid of a simple radio receiver. The source of these waves can be a lightning discharge in the troposphere, natural wave-particle interaction in the magnetosphere, or wave-particle interaction triggered by an artificial man-made wave. Relations to other plasma physical phenomena are still partly unknown. In this thesis I have introduced several observations, which still need a theoretical explanation.

The ELF-VLF waves discussed in the thesis can be divided into four main classes: 1) Whistlers are the waves, whose source is audio-frequency radiation from a lightning discharge; 2) Discrete ELF-VLF emissions are generated in wave-particle interactions in the equatorial region of the magnetosphere; 3) The hiss spectrum resembles that of band-limited noise, and its source can be either in the equatorial region of the magnetosphere or just a couple of thousands of kilometres above the ionosphere. The latter one is called an auroral hiss, which is caused by precipitating electrons; 4) Man's influence extends thousands of kilometres into the space. VLF transmitter signals can interact with trapped energetic particles in the radiation belts. Similarly, power line harmonic radiation (PLHR) enters into the magnetosphere and interacts with particles.

All above mentioned phenomena have been studied in this thesis, but a particular attention is drawn to the PLHR-triggered emissions and the effects of PLHR on natural ELF-VLF waves. Although these phenomena were known almost 30 years, they have never been studied with similar analysis methods as described in this thesis. The new analysis brings out features like the left-hand polarisation of PLHR-triggered emissions, which have not been known earlier. It seems that the Earth-ionosphere wave-guide plays a very important role in the ground-based ELF-VLF observations.

The largest part of the thesis (Chapter 5) deals with magnetospheric line radiation (MLR). Here we have analysed five events in detail. We have narrowed down the source region for MLR, and provided evidence that it is, initially, triggered by PLHR. The generation region of MLR can be much lower than expected earlier. Many new features have been introduced.

New ELF-VLF phenomena like the narrow band hiss events and the hiss clouds are introduced, which is possible only due to continuous wide-band observations. This thesis is based on the data observed during several campaigns lasting for 1-3 weeks each. All observations were made in the auroral zone in northern Finland ( $L \approx 5-6$ ).

This is the first doctoral thesis studying ELF-VLF waves in Finland.



## Acknowledgements

I thank the Sodankylä Geophysical Observatory, initially observatory of the Finnish Academy of Science and Letters, later institute of the University of Oulu, for hosting me during my thesis work. I am grateful to directors Prof. Tauno Turunen (–1997 and 2003–) and Prof. Jorma Kangas (1998–2002) for being curious enough to let me pursue my rather new research, which extends the frequency range traditionally studied in Finland. Sincere thanks to Prof. Jorma Kangas, then Finnish EISCAT Research Co-ordinator, and to the Finnish Graduate School of Solar-Terrestrial Physics for funding me during this time. I am very thankful that Prof. Tuomo Nygrén has supported me in many ways.

I am very grateful to the technical personnel of SGO, who were always ready to stretch out their helping hands. Lots of help was provided by Mr. Keijo Nuutinen, Mr. Erkkö Saviaro, Mr. Jari Lehtinen, and Mr. Antero Väänänen during campaigns in 1990s.

I wish to thank the referees of this thesis, Prof. Michael Rycroft and Dr. Craig Rodger, for reading the manuscript and giving a lot of very valuable comments.

I thank all my INTAS colleagues (especially, Prof. David Nunn, Prof. Victor Trakhtengerts, Dr. Elena Titova, Dr. Andrei Demekhov, Dr. Boris Kozelov, and Dr. Ilya Kornilov), who were always ready to discuss the various aspects of my work with me. Also Mr. Tero Raita has assisted me with many things related to the computers.

Special thanks are due to the staff of the Sodankylä Geophysical Observatory as a whole for providing an excellent environment in which it was always fun to work. I am esp. grateful to Mr. Johannes Kultima, who, since November 1991, participated in nearly all VLF field campaigns. Also I am indebted to Timo Rantala for his excellent support in computational matters, much of which went unnoticed since “things simply worked.” Mrs. Tarja Mäkihalvari deserves thanks due to endless capability to find “important” things in my room. I wish to thank Mrs. Pirkko Kaukonen, who has tirelessly found and copied hundreds of articles from our library and ordered tens of papers from other libraries for me.

Special thanks to Prof. Tauno Turunen, my thesis supervisor, for his permanent trust in me. I am very grateful to him and to my “secret supervisor” and friend Dr. Thomas Ulich for their valuable help during all phases of my studies in scientific as well as private matters. Without Thomas’ help in English language my text would have been difficult to understand.

Finally, but most importantly, I thank my beloved mother. I thank my family Teija, Jemina, Siina, and Meri. Without their encouragement and support all this would have been impossible.



# Contents

Abstract . . . . .	iii
Acknowledgements . . . . .	v
<b>List of Acronyms and Symbols</b>	<b>1</b>
<b>Prologue</b>	<b>5</b>
<b>1 Introduction to ELF-VLF Waves</b>	<b>9</b>
1.1 Whistlers . . . . .	11
1.1.1 Ground-based observations . . . . .	11
1.1.2 Satellite observations . . . . .	12
1.2 Discrete Emissions and Chorus . . . . .	13
1.2.1 Periodic and quasiperiodic emissions . . . . .	15
1.2.2 Triggered emissions . . . . .	17
1.3 Hiss . . . . .	18
1.3.1 Auroral hiss . . . . .	19
1.3.2 Mid-latitude hiss . . . . .	20
1.3.3 Plasmaspheric hiss . . . . .	21
1.4 Power Line Harmonic Radiation – PLHR . . . . .	21
1.5 Locations of Receivers in Finland . . . . .	23
<b>2 Instrumentation</b>	<b>29</b>
2.1 Antennae . . . . .	30
2.1.1 IGY aerials . . . . .	30
2.1.2 “Aktivnyij” aerials . . . . .	31
2.1.3 Coaxial cable aerials . . . . .	33
2.1.4 UEV2300 aerials . . . . .	33
2.2 Amplifiers . . . . .	33
2.3 Recording Unit . . . . .	35
2.4 Data Storage . . . . .	36
<b>3 Digital Analysis of ELF-VLF Data</b>	<b>37</b>
3.1 Analysis Method . . . . .	39
3.2 Digital Analysis . . . . .	42
3.3 Examples of Analyzed ELF-VLF Data . . . . .	44
3.3.1 Quick-look plots . . . . .	44

3.3.2	Detailed plots . . . . .	49
<b>4</b>	<b>Power Line Harmonic Radiation</b>	<b>53</b>
4.1	History of PLHR Observations . . . . .	54
4.2	Nonlinear Effects . . . . .	56
4.3	Theoretical Background . . . . .	56
4.4	Observations of PLHR TEs . . . . .	59
4.5	Special Features of PLHR . . . . .	64
4.5.1	Spectra of PLHR . . . . .	75
4.6	Discussion . . . . .	79
4.7	Conclusions . . . . .	84
<b>5</b>	<b>Magnetospheric Line Radiation</b>	<b>85</b>
5.1	Analysis of Five Events . . . . .	86
5.2	Frequency Spacing . . . . .	101
5.3	Statistics of 31 Events . . . . .	105
5.4	Discussion . . . . .	107
5.5	Conclusions . . . . .	110
<b>6</b>	<b>Bursts of Very Narrow Band VLF hiss</b>	<b>111</b>
6.1	ULF Bursts . . . . .	112
6.2	Observations . . . . .	112
6.3	Discussion and Conclusions . . . . .	117
<b>7</b>	<b>Whistlers and Auroral Substorm</b>	<b>119</b>
7.1	Properties of Whistlers in Earlier Studies . . . . .	119
7.2	Whistler Analysis . . . . .	121
7.3	Observations . . . . .	122
7.3.1	Whistlers and magnetic activity . . . . .	122
7.3.2	Auroral activity . . . . .	123
7.4	Discussion and Conclusions . . . . .	126
<b>8</b>	<b>Chorus and ULF Bursts</b>	<b>127</b>
8.1	HM Emission Bursts . . . . .	127
8.2	ELF-VLF Frequencies <3 kHz . . . . .	129
8.2.1	Relation between upper cutoff frequencies . . . . .	130
8.3	VLF Frequencies at 3-4 kHz . . . . .	130
8.4	VLF Frequencies >4 kHz . . . . .	131
8.4.1	Relation between intensities . . . . .	131
8.5	Discussion and Conclusions . . . . .	132
<b>9</b>	<b>ELF-VLF and Auroral Emissions Related to Pc 3</b>	<b>133</b>
9.1	Observations . . . . .	134
9.2	Discussion and Conclusions . . . . .	136

<b>10 Hiss Clouds</b>	<b>137</b>
10.1 Observations . . . . .	137
10.2 Relations to Other Parameters . . . . .	146
10.3 Discussion . . . . .	147
10.4 Conclusion . . . . .	148
<b>11 Some Unusual ELF-VLF events</b>	<b>149</b>
11.1 Banded VLF Hiss . . . . .	149
11.2 Mysterious Man-made ELF-VLF Bursts . . . . .	154
<b>12 Conclusions</b>	<b>157</b>
<b>Bibliography</b>	<b>160</b>



# List of Acronyms and Symbols

- AC** Alternating Current.
- AD** Analog-Digital, term used in electronics.
- Activnyi** Russian Active satellite, Intercosmos-24, 28 September 1989 – 13 October 1993.
- AKR** Auroral Kilometric Radiation.
- APEX** Active Plasma EXperiments, Russian satellite, Intercosmos-25, launched on 18 December 1991.
- B** Magnetic flux density [ $T = \text{Wb}/\text{m}^2$ ].
- BAS** British Antarctic Survey.
- CD** Compact Disc, mass media.
- CGM** Corrected Geomagnetic coordinates.
- CL** Collisionless model (same as R-4), whistler analysis.
- centre-tapping** Enables symmetrical input for the differential amplifier. Symmetrical input improves the suppression of electric fields.
- dB** deciBel, logarithmic scale used often with amplitudes and powers.
- DC** Direct Current.
- DE** Diffuse Equilibrium model, whistler analysis.
- DVD** Digital Versatile Disc, mass media.
- EISCAT** European Incoherent SCATter Scientific Association.
- ELF** Extreme Low Frequency, 3–30 Hz (according to latest ITU rules).
- EM** ElectroMagnetic.
- EW** East-West, used with the antenna direction.
- $f_{eq}$  Wave frequency at the magnetic equator.
- $f_{LHR}$  Lower Hybrid Resonance frequency.
- $F(\omega)$  Fourier coefficient at frequency  $\omega$ .

- FLR** Field Line Resonance.
- GMT** Greenwich Mean Time. It's ambiguous, and is used (although not in astronomy) in the sense of UTC in addition to the earlier sense of UT. Prior to 1925, it was reckoned for astronomical purposes from Greenwich mean noon (12h UT).
- GPS time** is TAI –19 seconds. GPS time matched UTC from 1 January 1980 to 1 July 1981. No leap seconds are inserted into GPS time, thus GPS time was 13 seconds ahead of UTC on 1 January 2000. The GPS epoch is 00:00 (midnight) UTC on 6 January 1980.
- HM** HydroMagnetic.
- IGY** International Geophysical Year, July 1957 – December 1958.
- IMAGE** International Monitor for Auroral Geomagnetic Effects, magnetometer network in Scandinavia.
- IMF** Interplanetary Magnetic Field.
- ITU** International Telecommunication Union.
- K** Magnetic index, 3-hourly, usually local, varies between 0 and 9.
- $K_p$**  Planetary magnetic index, 3-hourly, varies between 0 and 9.
- L** L value, distance of the magnetic field line from the ground at the equator given in Earth radii.
- LF** Low Frequency, 30–300 kHz.
- LHR** Lower Hybrid Resonance.
- $L_{pp}$**  Location of the plasmopause.
- LT** Local Time.
- MLR** Magnetospheric Line Radiation.
- MLT** Magnetic Local Time.
- $N_{eq}$**  Equatorial electron density.
- NS** North-South, used with the antenna direction.
- OGO-3** Satellite.
- Pc 1-5** Pulsation continuous, magnetic pulsations in the frequency range from 1 mHz to 5 Hz.
- PE** Periodic Emission.
- PL** Pro-longitudinal whistler propagation.
- PLHR** Power Line Harmonic Radiation.
- Q factor** Quality factor of a resonant circuit is a measure of the ratio of the energy stored in it to the energy lost during one cycle of operation. The Q factor of a coil is important when it is used in a resonant circuit because it affects the 'sharpness' of the response curve. A good loop antenna has a very high Q-factor, which must be damped to avoid resonance where the signal is growing to uncontrolled level.

- QP** Quasiperiodic emission.
- R** Right-handed polarisation.
- R-4** Collisionless model (same as CL), whistler analysis.
- SGO** Sodankylä Geophysical Observatory, established in 1913.
- SI** Sudden Impulse, magnetospheric compression.
- SLF** Super Low Frequency, 30–300 Hz (according to latest ITU rules).
- SSC** Storm Sudden Commencement, magnetospheric compression.
- $\theta$  Angle between wave propagation direction and ambient magnetic field.
- $t$  Time.
- TAI** International Atomic Time. Defined by about a dozen atomic clocks distributed worldwide. TAI-UT1 was approximately 0 on 1 January 1958.
- TE** Triggered Emission.
- TLE** Transient Luminous Event, like red sprite, blue jet, and elve.
- TVLF** Transportable Very-Low-Frequency transmitter.
- tweaks** Tweaks result when sferics are ducted in the earth-ionosphere waveguide distances much greater than a couple of thousand kilometers. When ducted over large distances, the VLF radio waves undergo dispersion. Tweaks sound much different than sferics. Instead of the sharp crackling sound, tweaks have a quick musical sound like chirp or tweek.
- UEV2300** ULF-ELF-VLF 2300 m<sup>2</sup>, the name of the receiver built by SGO in 2005.
- ULF** Ultra Low Frequency, 0.3–3 kHz (according to latest ITU rules), but in this thesis it means 0–10 Hz, i.e. frequencies of magnetic pulsations.
- URSI** International Union of Radio Science.
- UT** Universal Time. Defined by the Earth’s rotation, and determined by astronomical observations. This time scale is slightly irregular. There are several different definitions of UT, but the difference between them is always less than about 0.03 s.
- UT0** “Raw”, uncorrected UT as derived from meridian circle observations or from more modern methods involving GPS satellites.
- UT1** UT0 corrected for polar wandering - usually one means UT1 when saying UT.
- UTC** Coordinated Universal Time. Differs from TAI by an integral number of seconds. When needed, leap seconds are introduced in UTC to keep the difference between UTC and UT less than 0.9 s. UTC was introduced in 1972.
- VLF** Very Low Frequency, 3–30 kHz.
- $W_{\parallel}$  Energy of the precipitating electrons parallel with the magnetic field.
- X** Horizontal component of magnetic field, positive northward.
- Y** Horizontal component of magnetic field, positive eastward.
- Z** Vertical component of magnetic field, positive downward on the northern hemisphere.



# Prologue

*Mr. Donnithorne, in Llanfair P.G., Anglesea, reports: – “At 2.0 a.m. (Saturday) the telephone receiver was again tried, and then ‘twangs’ were heard as if a stretched wire had been struck, and a kind of whistling sound. The strength of the earth current was 17.7 milliamperes.” Mr. Miles, in Lowestoft, reports: – “Noise on 408 (Liverpool–Hamburg) wire seemed like that heard when a fly-wheel is rapidly revolving,” and “sounds in telephone appear like heavy carts rumbling in the distance.” Mr. Scaife, in Haverfordwest, reports: – ‘March 31, 2.5 a.m. Earth currents on all wires; wires completely stopped. ... Peculiar and weird sounds distinctly perceived, some highly-pitched musical notes, others resembling murmur of waves on a distant beach. ... The musical sounds would very much resemble those emitted by a number of sirens driven at first slowly, then increased until a ‘screech’ is produced, then again dying away. Duration of each averaged about twenty seconds.” These experienced observers, situated at three distant points, and perfectly acquainted with the ordinary inductive disturbances on telephone circuits, simultaneously observed and independently recorded their own impressions of peculiar sounds exerted in telephones by very rapid alternations or pulsations of currents which accompanied or were consequent on sun-spots, earth currents, and the Aurora Borealis. [Preece, 1894].*

The short letter by Preece [1894] to the editor of Nature was very likely the first scientific writing about plasma waves in the audio-frequency range. The signals were heard in long-distance telephone lines. The next time these ‘strange’ sounds were reported after World War I. The first unambiguous scientific report of whistlers was made by Barkhausen, who eavesdropped on enemy telephone conversations at the front [Barkhausen, 1919]. Barkhausen carried out a systematic study of whistlers and suggested that whistlers originated in lightning discharges and that their long descending tone was the result of propagation within a dispersive medium [Barkhausen, 1919, 1930]. However, a theoretical explanation was not possible before Eckersley [1931, 1935] developed the wave propagation theory in a magnetoactive plasma, which lead to the whistler dispersion law in the low frequency limit.

Eckersley and his colleagues also found many other examples of VLF noises now known as ELF-VLF emissions (chorus, hiss, etc.). At the same time Burton [1930] and Burton and Boardman [1933a,b] investigated whistlers and VLF emissions that were picked up by submarine cables. They made observations during the solar activity maximum. Some hooks (an emission, whose frequency first decreases and then increases) were also found, but their first spectrogram has been published by Potter

[1951].

In the 1920s and 1930s sounds related to aurora were discussed by many authors [e.g. *Chapman*, 1931; *Williams*, 1932]. Some of those audio-frequency disturbances were also connected to meteors [e.g. *Lindemann and Dobson*, 1923; *Skellett*, 1931].

The breakthrough happened when the pioneering work by *Storey* [1953] was published. This paper showed conclusive evidence that whistlers originated in lightning discharges in the opposite hemisphere and then propagated along the geomagnetic field lines to the hemisphere of the observer. Furthermore, he suggested that the electron density was of the order of several hundred particles per  $\text{cm}^3$  in the remotest parts of the whistler paths. This was the first evidence that plasma exists also well above the ionosphere.

During the past four decades, the ELF-VLF science has progressed: more observations have been made [*Helliwell*, 1965; *Kokubun et al.*, 1969; *Tanaka et al.*, 1976; *Makita*, 1979; *Sato*, 1980; *Yamagishi*, 1989; *Helliwell*, 2000; *Johnson and Inan*, 2000; *Salvati et al.*, 2000; *Singh et al.*, 2000; *Lorentzen et al.*, 2001; *Lauben et al.*, 2002; *Inan et al.*, 2004; *Engbretson et al.*, 2004] and more advanced theories have been developed [*Helliwell*, 1967; *Rycroft*, 1976; *Kimura*, 1989; *Hobara et al.*, 2000; *Trakhtengerts and Rycroft*, 2000; *Lauben et al.*, 2001; *Bortnik et al.*, 2002, 2003].

In the present thesis, I introduce ELF-VLF phenomena, which usually require continuous wide-band recordings, instead of traditional narrow band observations with one minute wide-band recordings every 15th minute. Also the idea to record other geophysical data on the same video tape has turned out to be very useful when correlating optical phenomena and/or geomagnetic pulsations to ELF-VLF observations. Even if absolute timing was missing, the relative timing between the phenomena recorded on the same tape is perfect. The enormous development of computers and mass storages has made digital analysis possible allowing to produce easily quick-look plots of the ELF-VLF recordings of the 1990s.

## Contents of this thesis

The first part of this thesis is an introduction to ELF-VLF phenomena and the instrumentation of my scientific work. This thesis is based mostly on purely empirical observations due to my long experience in field campaigns. Here, we present ELF-VLF phenomena, which nobody has reported earlier, and new aspects of relations to other phenomena. Some results have been discussed in separate papers where I have been involved and which are referred to in the text.

The most important inventions and discoveries I have made or contributed to are: 1) the left-hand polarisation of the PLHR-triggered emissions; 2) the 1-hour, the 6-hour, the 12-hour, and the 24-hour quick-look plots for a more effective search for the ELF-VLF events; 3) the hiss clouds; 4) the fine structure of the MLR events; 5) the relative motion of the whistler ducts during an auroral substorm; 6) the narrow band hiss events at 'high' frequencies; 7) a relation between the ELF-VLF chorus and hydromagnetic emission bursts; 8) a whistler-triggered optical emission; 9) a banded VLF hiss; 10) the whistler-triggered chorus events (these are not presented in this thesis).

## Outline of the chapters

In **Chapter 1**, the various types of ELF-VLF phenomena are introduced. Whistlers, discrete emissions, chorus, hiss, and power line harmonic radiation are most interesting and most relevant for this thesis. Also the locations of ELF-VLF receivers during Finnish campaigns are shown.

**Chapter 2** introduces the instrumentation used during different Finnish campaigns between 1989 and 2005. Four types of aerials, amplifiers, recording units, and data storage are explained.

**Chapter 3** explains the analysis of digital ELF-VLF data. The basic formulae of the analysis are shown, and a number of example plots are presented.

In **Chapter 4**, Power Line Harmonic Radiation (PLHR) related phenomena are presented. PLHR-triggered emissions seem to be left-hand polarised, which is a new result. Also other special features are introduced.

**Chapter 5** gives an extensive description of Magnetospheric Line Radiation (MLR). The observations of MLR in Northern Finland give more detailed information on the phenomenon. Many new features are demonstrated for the first time. Continuous wide-band ELF-VLF data allows to study MLR events in their full extent and detail.

**Chapter 6** introduces the bursts of very narrow band VLF hiss events observed only during one morning in January 1993. Altogether 17 bursts were observed. Some burst-like ULF pulsations in the Pc 1 frequency range occurred simultaneously.

**Chapter 7** presents the movements of the whistler duct boundary before, during, and after an auroral substorm. During 4.5 hours the whistler activity at high latitudes was exceptionally high (860 analysed whistlers).

**Chapter 8** shows for the first time a one-to-one correlation between upper cutoff frequencies of ULF Pc 1 bursts and ELF-VLF morning chorus. The ratio between frequencies is surprisingly close to 1840, which is the ratio between electron and proton gyro-frequencies.

**Chapter 9** displays a clear correlation between optical and magnetic Pc 3 pulsations during an event where Pc 3 correlated most of the time very well with quasi-periodic ELF-VLF emissions. However, riometers did not show any indication of pulsating absorption.

**Chapter 10** manifests a new type of ELF-VLF emissions, which we have named ‘hiss clouds’. These phenomena can be observed only in continuous wide-band recordings. They occur early in the morning hours in the frequency range of 0.7–7 kHz, and their duration varies from 3 to 10 hours.

**Chapter 11** introduces some unusual ELF-VLF events, the first of which is the banded VLF hiss. Altogether 24 events were observed. The second unusual event consists of mysterious ELF-VLF bursts, which have been observed only while Russian APEX satellite signals should have been received on the ground.

## Annotations

In the context of this thesis, “wide-band” refers to the frequency range of 0.2–10 kHz. ELF and VLF frequencies are defined by ITU (International Telecommunication Union) as 3–30 Hz and 3–30 kHz, respectively, but in this thesis I have only used

frequencies up to 15 kHz. This is due to the receiver parameters. Earlier, ELF denoted 3 Hz–3 kHz, but nowadays there are two other designations between ELF and VLF, namely SLF for 30–300 Hz, and ULF for 0.3–3 kHz. However, the term ELF-VLF frequencies in this thesis does not violate the new ITU rules, because it refers to the frequency range of 3 Hz–30 kHz.

“Continuous recording” means in this thesis that the recording lasts at least several hours, and mostly many days or even weeks during campaigns. This is to be contrasted with the procedure common in many other international research groups, called synoptic broadband recording (1 minute out of every 15 minutes at 5, 20, 35, and 50 minutes after the hour). Usually the remaining 56 minutes are recorded only in narrow bands, whose centre frequencies are, e.g., 0.5, 1.0, 1.5, 2.0, 3.0, 4.25, 6.0, 9.3, and 10.2 kHz, with bandwidths of 0.5–2.0 kHz. This system was developed for long-term recordings at a time of small capacities of storing digital data. One-minute wide-band data with 16-bit digitising requires more than 9 MB of disk space, i.e. 13.2 GB per 24 hours.

The terms “ULF wave” or “ULF pulsations” in the context of ELF-VLF waves in this thesis mean electromagnetic ion-cyclotron waves in the frequency range of 0–10 Hz. According to the most recent rules of ITU, ULF refers to the frequency band of 0.3–3 kHz. However, historically the term “ULF waves” means waves, which are generated or amplified below proton or ion gyrofrequencies. This new frequency designation will cause many confusions in the future – at least, before some reasonable solution for magnetic pulsations will be invented.

There are both black and white plots and colour plots in this thesis. Some of them are more informative just in b/w, but colour coded plots can show new features of the same data.

### **Additional publications**

There are altogether 22 earlier published refereed articles, to which I have mainly contributed ELF-VLF, ULF, and/or ionospheric absorption observations and data analysis. Those articles are not directly related to this thesis, but they represent wide scientific activity outside the topic of this work. They can be divided into 6 groups: 1) papers related to ELF-VLF waves, ionospheric absorption, and aurora; 2) papers reporting on ULF pulsations observed mostly on the ground; 3) a paper studying theoretically the ionospheric demodulation of MF/HF radio transmitter signals; 4) a paper related to VLF heating experiments; 5) a paper dealing with the satellite observations of energetic electrons; and 6) a paper studying a possible mechanism of the ELF-VLF chorus generation. Especially, papers treating magnetic pulsations are useful to understand observed relations between ELF-VLF waves and ULF waves.

# Chapter 1

## Introduction to ELF-VLF Waves

This thesis concentrates on electromagnetic waves in the ELF-VLF frequency range that propagate in a magnetized plasma in the whistler mode. Their frequency range is from 3 Hz to 30 kHz, which means that they can be transformed to audible sounds and therefore could be listened to by naked ears. This mode of propagation is possible only in magnetized plasma and at frequencies below both the plasma frequency and the electron gyrofrequency. The whistler-mode is named after lightning generated ‘whistlers’ which propagate in this mode [*Helliwell, 1965*]. It has the lower cutoff at the lower hybrid resonance frequency,  $f_{LHR}$ , when propagating perpendicular to the ambient magnetic field, and the waves undergo a reflection when the wave frequency is equal to the local  $f_{LHR}$ . It has a right-hand circular (R) polarisation when propagating parallel to the magnetic field. Waves propagating in this mode are found throughout the magnetosphere, including the equatorial and polar regions, polar cusp, near the magnetopause, and in the magnetosheath and the bow shock.

Wave propagation in a magnetoplasma is both anisotropic and dispersive. In such a medium, the direction of propagation (ray direction) of a wavepacket of finite temporal duration and spatial extent is different from the wave normal direction. Most of the rays from a magnetospheric source cannot reach a ground receiver because they either undergo total internal reflection at the Earth-ionosphere boundary, where the refractive index changes suddenly from a large value ( $\approx 10$  to 100) to unity, or they undergo reflections at  $f_{LHR}$  in the magnetosphere. In the presence of field-aligned columns of enhanced or depressed ionization called ducts, some of the rays can be guided to the low altitude ionosphere with their wave normal at small angles with the local vertical, and these rays can be observed at a ground receiver after propagating within the Earth-ionosphere waveguide [*Helliwell, 1965*]. Experience indicates that most of the whistler-mode waves observed on the ground, however, propagate in one or more ducts and in general a signal observed at the ground is a sum of the signals that have been excited in various ducts located at different latitudes and longitudes.

Resonant interactions between ELF-VLF waves and energetic particles are occurring throughout the Earth’s magnetosphere and are believed to play a controlling role

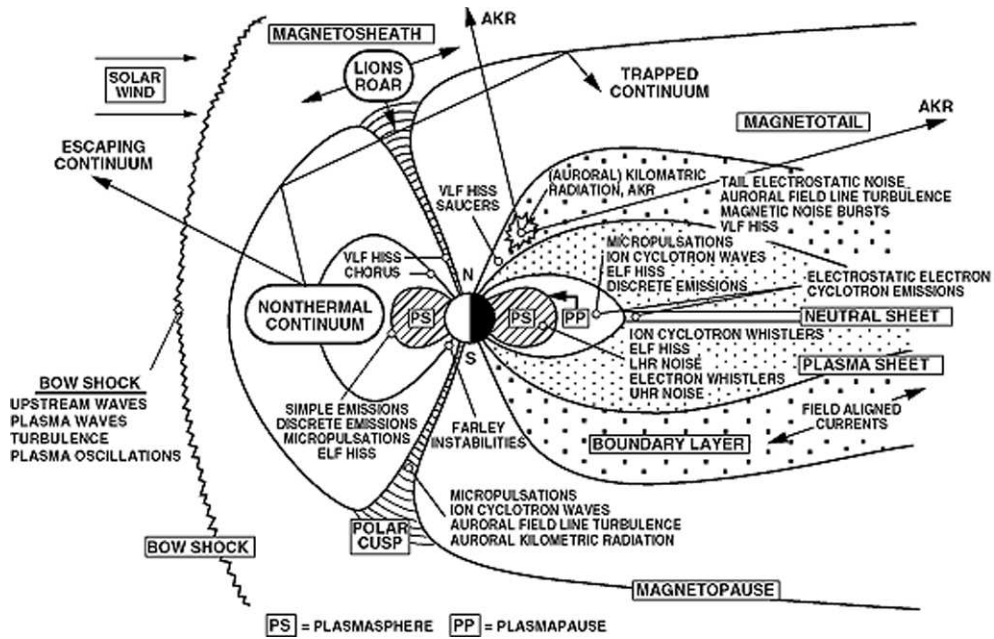


Figure 1.1: Regions of plasma wave occurrence located in a noon-midnight meridian cross section of the Earth's magnetosphere [From *Shawhan*, 1979].

in the dynamics of the inner and outer radiation belts [*Helliwell*, 1967].

Figure 1.1 shows a sketch of the various regions and boundaries of the Earth's magnetosphere in a noon-midnight meridian cross section. There are also marked different wave phenomena and where in the magnetosphere they have been observed.

Other plasma waves generated in the magnetosphere are: Lion's roar, Auroral kilometric radiation (AKR), VLF saucers, LHR noise, which can only be observed on satellites, as well as man-made signals. The lion's roar (that is how it is aurally perceived) is an intense sporadic whistler-mode wave burst observed in the Earth's magnetosheath. Its frequency ranges between 100 and 200 Hz and typically lasts for  $\approx 10$  s, but can even be longer than 5 min [*Smith and Angerami*, 1968]. AKR is an intense radio emission generated along the auroral field lines in association with discrete auroral arcs. It has been observed at frequencies between 20 kHz and 2 MHz. It is primarily an  $R - X$  mode (right-hand polarised extraordinary mode) radiation that escapes from Earth into interplanetary space. *Baumback and Calvert* [1987] showed that the minimum bandwidth of single AKR emissions could be 5 Hz or less.

VLF saucers are whistler-mode emissions with spectra having a characteristic saucer or V shape observed in the auroral regions in the frequency range  $\approx 100$  Hz to 20 kHz, and in the altitude range from 500 to 4000 km [*Smith*, 1960; *James*, 1976]. In spite of the low altitude observations it cannot be seen on the ground, because it propagates upwards. A typical source region has 0.5 km extent in the horizontal

and 10 km in the vertical direction. It is believed that VLF saucers are generated by beams of suprathermal electrons with energies not exceeding 5 eV via coherent Cerenkov processes [James, 1976].

LHR noise showing quasi-electrostatic plasma wavebands with a sharp cutoff near  $f_{LHR}$  has often been observed by satellites [e.g. Barrington and Belrose, 1963; Laaspere and Johnson, 1973].

## 1.1 Whistlers

Lightning radiates electromagnetic energy over a very wide bandwidth, from a few Hz [Burke and Jones, 1992] to many tens of MHz [Weidman and Krider, 1986]. However, because of the time scales and spatial extent of the radiating current, most of this energy is radiated in the VLF and ELF bands.

The radiated ELF-VLF energy thus propagates in a guided fashion between the two boundaries, which form what is known as the Earth-ionosphere waveguide. This guided propagation occurs with low attenuation rates at ELF and VLF frequencies (a few dB per 1000 km), allowing ELF and VLF radio atmospherics (or sferics, for short) to be observed literally around the world from a single source of lightning discharge.

The source of the whistler is audio-frequency range radiation from a lightning discharge. This radiation propagates through the ionosphere and magnetosphere in the whistler mode.

The time between local midnight and an hour after sunrise is the local time sector where most of the whistlers are observed, although the dusk to midnight sector may reveal substantial whistler activity, and sometimes strong whistlers may be observed a couple of hours before sunset [Helliwell, 1965]. Intense whistler events of short duration can occur at any time between just before the local sunset through one to two hours after the sunrise.

Mostly one whistler a minute may be heard on the average, but as is often the case, whistlers are not observed at all. Occasionally, during a geomagnetic storm over 100 whistlers a minute or even more can be received. That is called a whistler storm. Whistlers may or may not have echoes, may be few and far between but are intense, or may occur frequently but quite weak. The characteristic intensity, and number of whistlers can change from hour to hour, which depends upon the sensitivity of the receiver and conditions of Earth's magnetosphere and location of lightning storms and magnetospheric ducts in relation to the receiver.

Whistlers are seldom observed in the noon sector, except during a geomagnetic storm and when lightning is within a few hundred kilometres of the receiver. It is difficult to predict when whistlers will occur based on geomagnetic indices.

### 1.1.1 Ground-based observations

A very small fraction of all whistlers propagates field-aligned from one hemisphere to another and thus can be observed on the ground. Most whistlers are magnetospherically reflected and they cannot reach the ground receivers. The most dense whistler activity can be observed at  $L=2.0-4.5$  [Helliwell, 1965]. Nowadays many ground areas

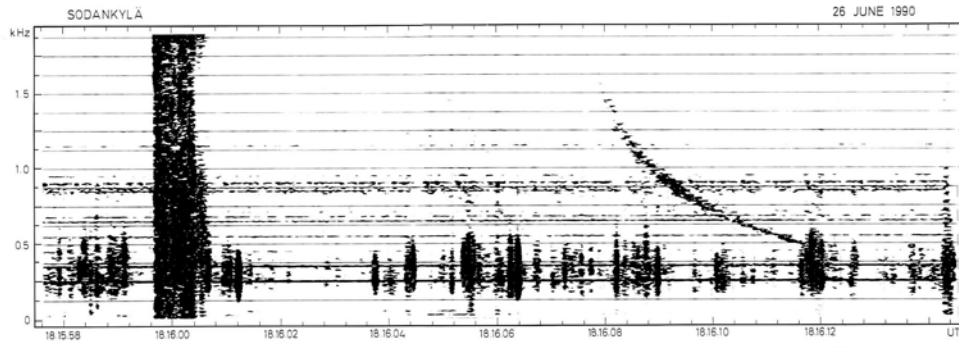


Figure 1.2: An example of a whistler recorded on the ground. This was an exceptionally low-frequency whistler, whose nose frequency was as low as 1.7 kHz, and its propagation L shell was 6.2. Thick vertical signal on the left was a causative sferics. Vertical structures below 0.6 kHz are due to mode 0 of Earth-ionosphere wave-guide propagation of sferics. Recording was made on 26 June 1990 in Sodankylä.

at this latitude range are full of man-made noise, which makes whistler observations very difficult.

Ground-based observations allow to study temporal behaviour of whistlers, where time scales can be days, weeks, months, years, or even solar cycles. In order to get some information of spatial distribution, several identical receivers should be located around the globe. Stable ground-based receiver data enable long-term studies, which is now more important than earlier.

A new area of whistler studies has risen recently due to the so-called transient luminous events (TLEs) like red sprites, blue jets and elves. As whistlers are generated by lightning discharges, and TLEs have the same origin, many unknown or unexplained features may come up. There are no studies of this possible relation so far, but an extensive summary of TLEs has been given by *Rodger* [1999].

### 1.1.2 Satellite observations

A satellite can practically observe all whistlers; both field-aligned and magnetospherically reflected. Most magnetospheric whistler-mode energy propagates in the nonducted mode [*Edgar*, 1976; *Bell et al.*, 1981]. These obliquely propagating whistlers are reflected between hemispheres, often persisting for many tens of seconds [*Gurnett and Inan*, 1988; *Jasna et al.*, 1990; *Draganov et al.*, 1992]. Recent studies show that oblique whistler precipitation contributes significantly to the loss of energetic radiation belt electrons from the magnetosphere. That happens especially over the range  $2.2 \leq L \leq 3.5$  where the slot region forms [*Lauben et al.*, 2001]. Nonducted whistler waves cause electron precipitation even several degrees of latitude away from the original lightning discharge [*Peter and Inan*, 2004].

## 1.2 Discrete Emissions and Chorus

One of the most interesting kinds of magnetospheric plasma waves are discrete emissions, lasting for a few seconds or less and covering a bandwidth of a few hundred Hz to a few kHz in frequencies of up to 10 kHz [Helliwell, 1965; Anderson and Kurth, 1989; Sazhin and Hayakawa, 1992]. Depending on their dynamic spectral form, principal elementary types of discrete emissions have been called rising tones (risers; Figure 1.3), falling tones (fallers), and hooks, which can also be inverted.

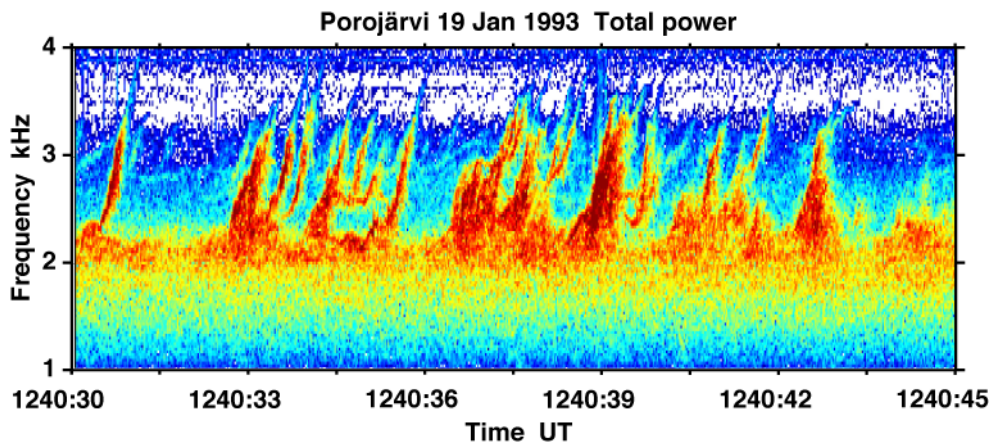


Figure 1.3: Example of discrete emissions observed in the afternoon (LT=UT+2h) on 19 January 1993 at Porojärvi. The intensity is colour coded, red is strongest, through the spectrum to blue, which is the weakest. The same coding is used in all subsequent figures showing spectra. The power difference between red and blue is typically 40 dB.

The most common natural discrete emission observed both on the ground and by satellites is the whistler-mode chorus, which is well known as the most intense electromagnetic emission in near-Earth space. Its spectral form looks like a closely spaced superposition of three elementary types of discrete emissions, though in most cases it consists of a superposition of risers. An example of dawn chorus is shown in Figure 1.4. It was found already in the 1950s that chorus activity exists mostly in the early morning hours, and therefore it was given the name ‘dawn chorus’ by *Isted and Millington* [1957]. Dawn chorus can resemble the sound of a flock of birds singing and squawking, or dogs barking. *Helliwell* [1965] and *Francis et al.* [1983] have shown that both the frequency range and local time maximum of chorus intensity is dependent on the latitude of the ground station. *Sato* [1980] showed that dawn chorus tends to peak in intensity around noon, and our observations at high latitudes support him.

Dawn chorus occurs commonly during high solar activity years mostly after solar flares or coronal mass ejections causing a magnetic storm as well as aurora. However, in years of low solar activity and few solar flares, coronal mass ejections can still cause magnetic storms and chorus can be observed - but more rarely.

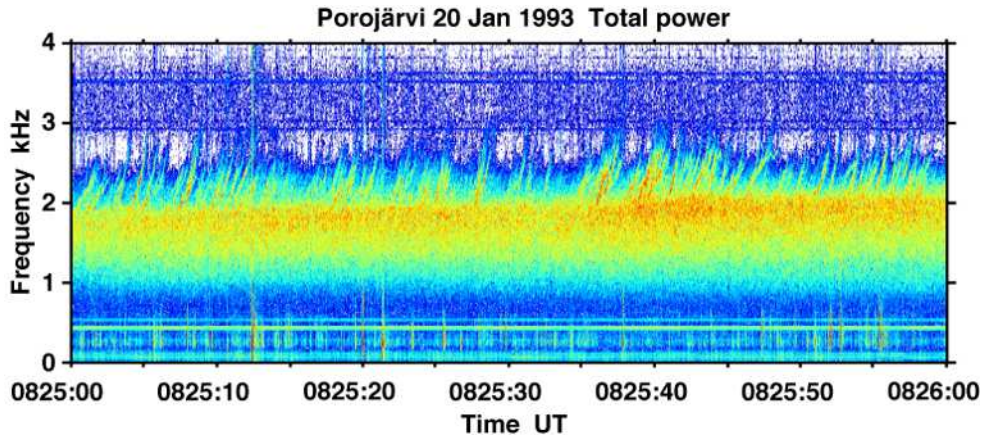


Figure 1.4: Example of dawn chorus emissions observed on 20 January 1993 at Porojärvi. This chorus event lasted for more than 4 hours. This example is from the event studied in detail in Chapter 8.

Chorus is a driver of electron precipitation, believed to be responsible for pulsating aurora and morning-side diffuse aurora [Helliwell *et al.*, 1980]. Demekhov and Trakhtengerts [1994] have made an analytical and numerical investigation of the flow cyclotron maser model, which can explain observed characteristics of morning-side pulsating aurorae. This model has been introduced first by Trakhtengerts *et al.* [1986]. Chorus occurs primarily on closed field lines, typically outside the plasmasphere, and can thus be almost optimally observed from Porojärvi ( $69.17^\circ$  N,  $21.47^\circ$  E,  $L=6.15$ ). It is often associated with particle precipitation bursts, leading to secondary ionization (as may be viewed with riometers and ionosondes), optical emissions (as may be viewed by photometers and all-sky cameras), x-rays (as may be observed on high-altitude balloons), and micropulsations (ULF receivers), thus requiring coordinated sets of observations.

Chorus can occur also during dusk and night-time, especially at high latitudes. This so-called auroral zone is the source of a vast amount of natural VLF phenomena. During auroral events chorus is often heard, as well as hiss of various pitches. The chorus, which occurs during auroral events is called auroral chorus.

Most of the present observations of this phenomenon are being carried out on satellites. Ground-based observations of ionospheric effects of the associated precipitation enhancements can complement spacecraft data by providing continuity in time and by documenting also the associated wave activity. ELF-VLF chorus and relativistic electron enhancements are just two examples of subauroral phenomena, which lend themselves to coordinated observation from the ground.

Both auroral chorus and dawn chorus occur during magnetic storms. Increasing magnetic activity causes an enhancement of the chorus intensity and chorus can be observed at lower latitudes. Auroral chorus, like whistlers, is best heard after midnight.

*Kornilov et al.* [1998] have shown that there is a sunrise effect in ELF-VLF chorus. The time of chorus intensification corresponds to the sunrise time at an altitude of 200 km.

### 1.2.1 Periodic and quasiperiodic emissions

A sequence of discrete emissions or clusters of discrete emissions showing regular temporal spacing is called periodic emissions (PE) [*Helliwell, 1965; Sazhin and Hayakawa, 1992*]. Usually their period is constant. The top panel of Figure 1.5 shows a spectrogram of periodic emissions recorded at Porojärvi, Finland. The bandwidth is typically a few kHz and the period can be related to the bouncing period of electrons at a certain latitude, i.e. from 2 to 6 s. Periodic emissions are observed at latitudes that correspond to closed magnetic field lines and are rarely observed on satellites.

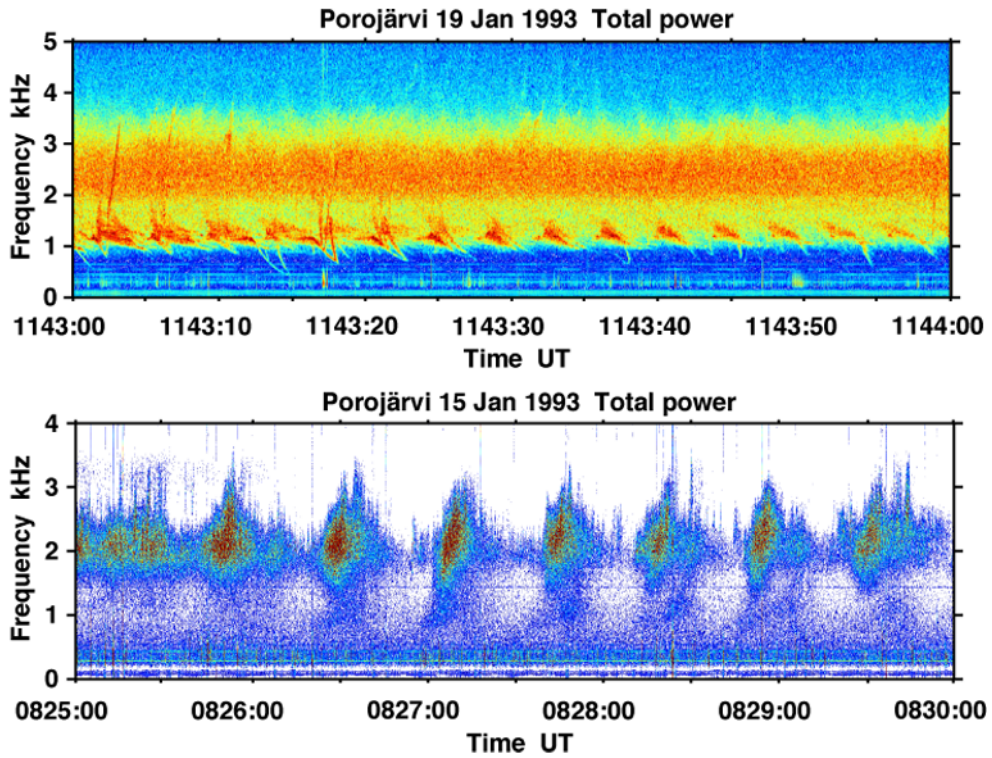


Figure 1.5: Examples of periodic (top panel) and quasiperiodic (bottom panel) emissions observed at Porojärvi. In the example shown, individual bursts of quasiperiodic emissions consist of periodic emissions. This event is studied in Chapter 9.

Periodic emissions are classified into various categories: if the period varies with frequency, they are called dispersive; if there is little or no variation in period with frequency, they are called non-dispersive; two or more interleaved sets with the same

period are called multiphase periodic emissions; and if their frequency is increasing between individual emissions, they are called drifting periodic emissions.

The periodic signals are assumed to have propagated in field-aligned ducts. It is easy to prove that the emission period is the same as the two-hop whistler transit time (first reported by *Helliwell* [1962]). For the dispersive type the variations are often the same as those found in echoing whistlers. Thus, each burst is the result of whistler-mode echoing in a duct. *Helliwell* [1965] suggested that each nondispersive periodic emission burst was triggered by the previous one, and that the whistler-mode cyclotron instability may be the trigger mechanism.

Quasiperiodic (QP) emissions are a sequence of repeated noise bursts of a relatively long period, in which each burst may consist of a number of discrete events such as periodic emissions or chorus or may consist of diffuse hiss [*Helliwell*, 1965]. The bottom panel of Figure 1.5 shows a spectrogram of QP emissions recorded at Porojärvi. The period between bursts is usually from 10 to 200 s, and is irregular compared with that of PE. QP emissions are a special phenomenon in the sense that they have been observed much more rarely on satellites than on the ground [see *Sazhin and Hayakawa*, 1994, and references therein].

Type of Event	Classification of Event
QP Type I only (QP1)	An event (with centre frequency) between 0 and 100 mHz, without any PEs, but with Pc 3 pulsations occurring sometime during it.
QP Type II only (QP2)	An event between 0 and 100 mHz without any PEs or Pc 3 pulsation during it.
PE Type I only (PE1)	An event between 100 and 500 mHz without any QPs, but with Pc 3 pulsations during it.
PE Type II only (PE2)	An event between 100 and 500 mHz without any QPs or Pc 3 pulsations during it.
QP and PE Type I (QPPE1)	An event in which a QP and a PE are seen overlapping in time, and which also has a Pc 3 pulsation during at least part of the QP.
QP and PE Type II (QPPE2)	An event during which a QP and a PE are seen overlapping in time, but which has no Pc 3 pulsation.

Table 1.1: Event categories used in statistical studies of QP and PE events [Table 2 from *Engebretson et al.*, 2004].

QP emissions have similar periods to magnetic pulsations, especially in the Pc 3-5 range. Most QPs were observed with magnetic pulsations of identical period in the

Pc 3 range. They have been classified in two categories: either associated (type I or QP1) or not associated (type II or QP2) with magnetic pulsations. This classification has been made by *Kitamura et al.* [1969] and *Sato* [1980].

The most recent classification has been given by *Engebretson et al.* [2004] and is shown in Table 1.1. The last two types are new, and they are actually combinations of QPs and PEs. These emissions have been studied using the data recorded in Antarctica at U.K. (Halley, A80, A81, A84, P2, and P3) and U.S. (Eights and South Pole) stations [e.g. *Ho*, 1973; *Morrison et al.*, 1994; *Smith et al.*, 1998; *Engebretson et al.*, 2004].

### 1.2.2 Triggered emissions

Any ELF-VLF emission that appears to have been initiated or triggered by another event is called a triggered emission [*Helliwell*, 1965]. Triggering sources include whistlers, discrete emissions, signals from ground transmitters (Omega, Siple, etc.),

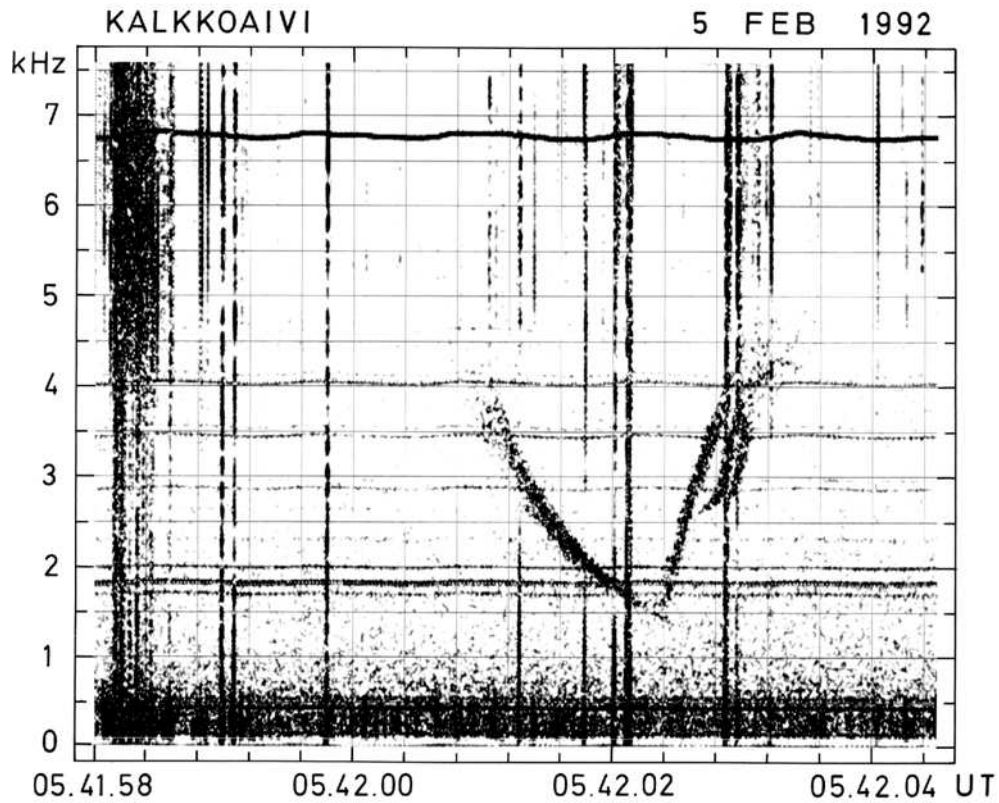


Figure 1.6: Whistler-triggered emission, which triggers a new emission. Near 7 kHz there is a subcarrier of the ULF waveforms recorded by pulsation magnetometer.

and power line harmonic radiation (PLHR). An example of whistler-triggered emission, which triggers another emission is seen in Figure 1.6. The second example shows high-frequency chorus events triggered by whistlers (see Figure 1.7).

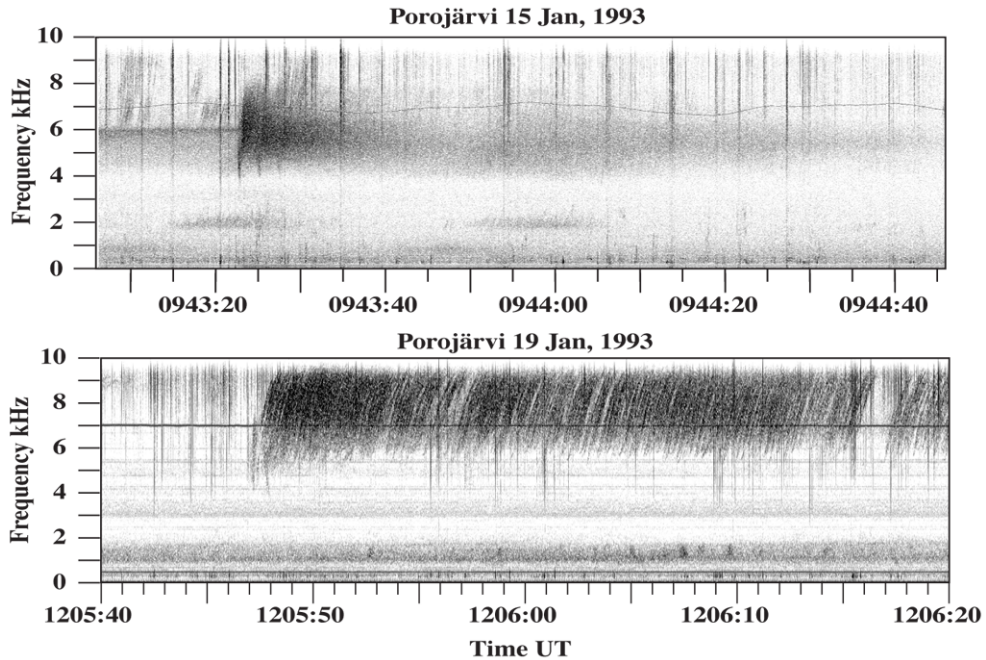


Figure 1.7: Whistler-triggered chorus (WTC) events. Upper WTC is from 15 January 1993 and lower one is from 19 January 1993, both recorded at Porojärvi.

Most triggered emissions follow the apparent source with one exception known as precursor, which precedes the associated whistler [Park and Helliwell, 1977; Paschal, 1990; Chmyrev *et al.*, 1990]. The whistler-mode instability is believed to be responsible for the generation of triggered emissions.

### 1.3 Hiss

The ELF-VLF hiss spectrum resembles that of band-limited noise. It can be identified aurally by a hissing sound. A hiss can last from minutes to even hours, and is then called a ‘steady’ or ‘continuous’ hiss. Occasionally a hiss has variations of the order of a second in amplitude, and is then called an ‘impulsive’ hiss. [Helliwell, 1965] The impulsive hiss is observed in the frequency range extending to several hundred kHz, whereas the continuous hiss is limited to frequencies below  $\approx 30$  kHz. In both types of hiss, the maximum power spectral density is achieved around  $\approx 10$  kHz.

The first direct observation of hiss associated with aurora was made in 1932 in New Hampshire by Burton and Boardman [1933b]. The next observations of hiss related

to aurora were made during the IGY in 1957 by *Ellis* [1957, 1960, 1961], who showed that the fluctuations of hiss intensity are at times correlated with the luminosity of aurora.

### 1.3.1 Auroral hiss

Observed both on the ground and by satellites, auroral hiss is a high latitude ( $\lambda_m \approx 60^\circ$  to  $80^\circ$ ) phenomenon occurring in the frequency range from a few kHz to several hundred kHz in the evening and night hours [*Helliwell*, 1965; *Makita*, 1979; *Sazhin et al.*, 1993]. In satellite observations, auroral hiss often shows a sharp cutoff at the lower hybrid resonance (LHR) frequency [*Gurnett and Frank*, 1972]. A characteristic V-shaped lower boundary of their spectra is also seen in the satellite observations. [*Swift and Kan*, 1975].

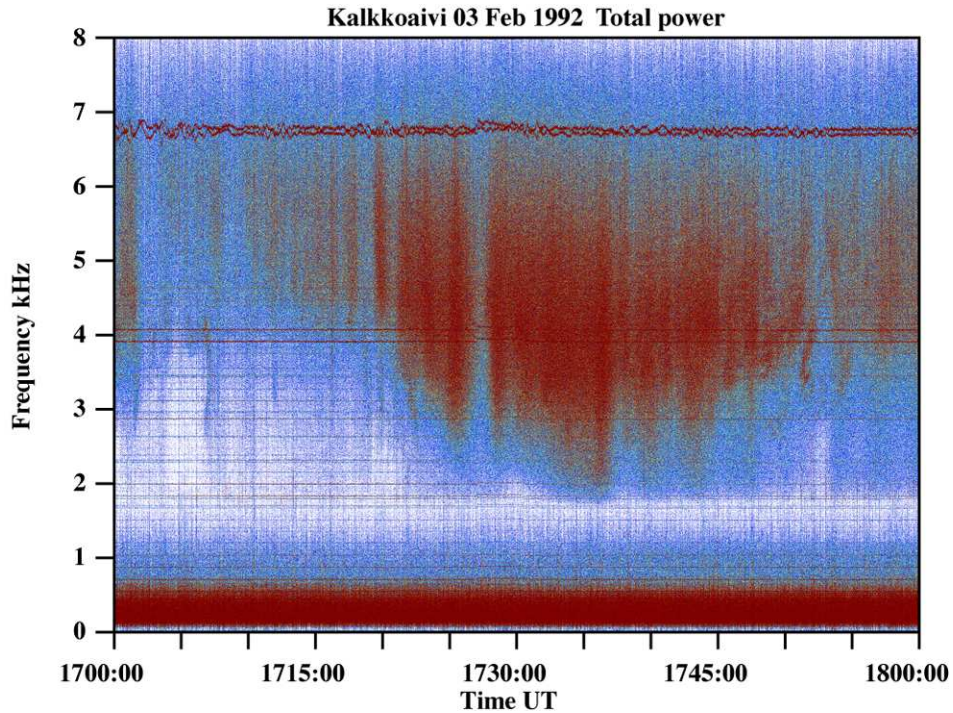


Figure 1.8: Impulsive auroral hiss, which is observed during active auroras near the zenith. This hiss was observed on 03 February 1992 at Kalkkoivi. Near 7 kHz there are two subcarriers of ULF waveforms recorded by two-component pulsation magnetometer.

Satellite measurements have shown that auroral hiss is correlated with low energy (100 eV to 10 keV) inverted-V electron precipitation [*Hoffman and Laaspere*, 1972]. Using ray tracing, *Gurnett et al.* [1983] were able to place a lower limit of 1.7 to 1.9

Earth radii on the generation region of auroral hiss.

Auroral hiss is found to be confined to a very narrow latitudinal extent. There is very little or no correlation between auroral hiss emissions recorded at two stations separated by  $\approx 5^\circ$  in latitude. Most of the auroral hiss (both impulsive and continuous) are observed during the expansion phase of a substorm in the midnight sector [Makita, 1979]. Impulsive hiss (see Figure 1.8) is found to originate in localized regions of bright electron aurorae at the ionospheric height where one finds rapid changes in luminosities and motion, whereas an increase in the continuous hiss is observed when a steady auroral arc is located within a few hundred kilometres of the ground station.

### 1.3.2 Mid-latitude hiss

Mid-latitude hiss peaks near invariant latitudes  $55$  to  $65^\circ$ , and in suitable conditions it can be observed at invariant latitudes from  $20$  to  $70^\circ$ . Its occurrence is related to the plasmopause location [Helliwell, 1965; Hayakawa and Sazhin, 1992]. It usually appears as a band-limited white noise in a 2 to 8 kHz band lasting for an hour or so. During geomagnetically disturbed periods, mid-latitude hiss can last for several hours showing amplitude fluctuations of the order of tens of minutes. The peak amplitude is less than that of the auroral hiss, and it varies relatively little.

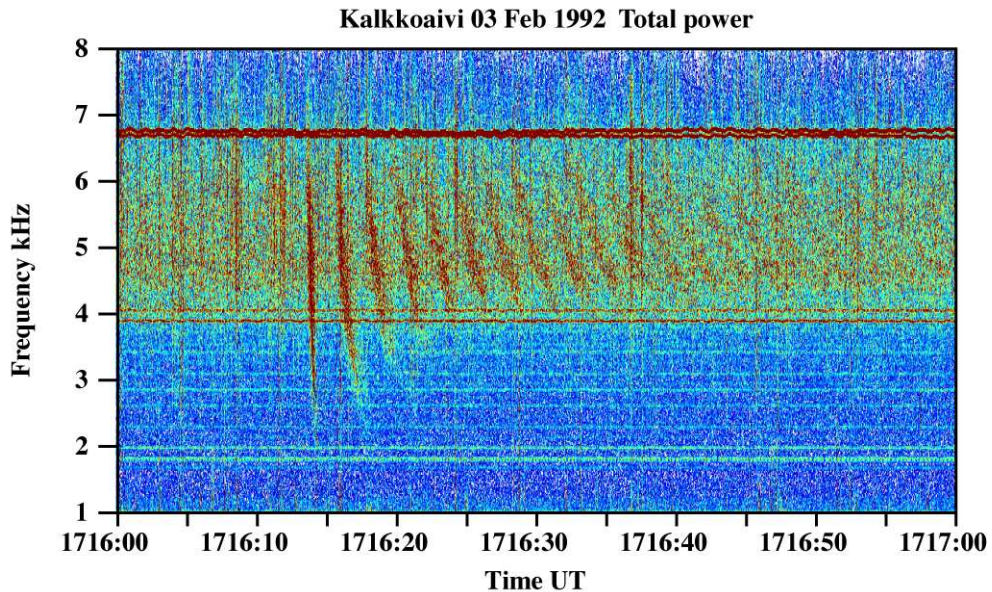


Figure 1.9: An example of a long whistler echo train, which yields band-limited hiss. The event has been observed on 3 February 1992 at Kalkkoivi.

Mid-latitude hiss is frequently accompanied by whistlers and/or chorus emissions echoing in the same path (duct) and amplified in the same frequency band. Actually, Dowden [1971] proposed that a part of the mid-latitude hiss may be generated by

the superposition of highly dispersed, unresolved, overlapping whistlers continuously echoing from one hemisphere to the other along a duct (see Figure 1.9).

Ground-based direction-finding measurements suggest that mid-latitude hiss is generated just inside the plasmopause [Hayakawa *et al.*, 1986]. Electron cyclotron instability of whistler-mode waves is believed to play an important role in the generation or amplification of mid-latitude hiss. Satellite observations show that mid-latitude hiss is often accompanied by chorus and the upper cutoff frequency of the combined band of hiss and chorus is found to be proportional to the equatorial electron gyrofrequency [Dunckel and Helliwell, 1969].

### 1.3.3 Plasmaspheric hiss

Plasmaspheric hiss is a broadband and structureless whistler-mode radiation that is almost always present in the Earth's plasmasphere and is commonly observed by magnetospheric satellites, but not observed on the ground. Sonwalkar and Inan [1988, and references therein] have concluded the following features for plasmaspheric hiss: 1) it is found throughout the plasmasphere and is stronger in the daytime sector compared to the midnight-to-dawn sector, and generally peaks at high latitudes; 2) it often shows a sharp cutoff at the plasmopause for frequencies below  $\approx 1$  kHz, though it is also observed outside the plasmopause at higher frequencies; 3) it is observed in a frequency band from  $\approx 100$  Hz to  $\approx 3$  kHz; 4) the upper cutoff is controlled equatorially while the lower cutoff is controlled locally; and 5) the hiss intensity is correlated with magnetic substorm activity.

Sonwalkar and Inan [1989] have provided evidence that lightning-generated whistlers can generate hiss-like signals and that lightning could be an embryonic source of plasmaspheric hiss. Draganov *et al.* [1992], using ray-tracing simulations, have argued that passive propagation of whistler-mode energy injected into the magnetosphere from lightning discharges may explain the plasmaspheric hiss intensities observed in the magnetosphere. The most recent study by Green *et al.* [2005] shows that their observations strongly support lightning as the dominant source for plasmaspheric hiss.

## 1.4 Power Line Harmonic Radiation – PLHR

Man's influence on his environment does not cover only the vicinity of the Earth, but extends thousands of kilometres into space. It has already been known for four decades that VLF transmitter signals regularly penetrate the ionosphere and travel into the magnetosphere, where they can interact with trapped energetic particles in the Earth's radiation belts. These interactions frequently stimulate ELF-VLF emissions and can precipitate energetic particles into the ionosphere. Furthermore, precipitated particles can stimulate X-ray and optical emissions and can modify the electrical properties of the lower ionosphere. Similarly, power line harmonic radiation (PLHR) enters into the magnetosphere and interacts with particles.

PLHR is a fascinating geophysical phenomenon in the near-Earth space environment that has excited much interest and lively debate during the past 30 years. PLHR lines were first recorded in the 1960s, and in the classic text by Helliwell [1965], they

are visible in many of the figures, although at the time they were not recognised for what they were. It was in 1975 that *Helliwell et al.* [1975] positively identified PLHR lines and postulated that they originated from radiation from terrestrial power line systems. Ground VLF observations at Siple station, Antarctica, and at the conjugate point at Roberval, Quebec, Canada, revealed arrays of spectral lines in the 2 – 6 kHz band. Further analysis showed that such lines must be of magnetospheric origin. Some sets of lines have almost constant spacings of 120 Hz, corresponding to odd harmonics of the Canadian power system. Other magnetospheric lines were found to have variable spacing. Nowadays there is a consensus that magnetospheric lines have their source in terrestrial power line systems and/or heavy industrial plants. ELF-VLF harmonic radiation from power systems penetrates the ionosphere and propagates into the inner magnetosphere, where it is amplified by unstable ambient plasma and may take the form of a self-sustained ELF-VLF emission. Clearly, in order to understand the origin of PLHR and its magnetospheric effects it is necessary to understand the linear and nonlinear dynamics of the interaction between ELF-VLF line radiation and the ambient unstable magnetospheric plasma.

The most overt instance of nonlinear wave particle interaction in the case of PLHR radiation is the triggering of emissions by individual lines. Surprisingly few examples of PLHR TEs (triggered emissions) have been presented in the literature.

There has been much debate in the 1980s concerning the extent to which PLHR contributes to the energy exchange between the magnetosphere and the ionosphere [*Tsurutani and Thorne*, 1981; *Bullough*, 1983]. Emissions and chorus triggered by PLHR could be non-negligible contributors to net precipitated particle fluxes.

Within the plasmasphere, discrete VLF emissions are commonly triggered by externally injected discrete whistler mode waves such as lightning generated whistlers, radiation from power transmission lines and fixed frequency signals from ground-based VLF transmitters, with peak emission intensities reaching values as large as 16 pT [*Bell*, 1985]. During this process, the input waves can be amplified by 30 dB or more. It is commonly believed that the amplification of the input waves and the triggering of emissions take place near the magnetic equator through a gyroresonance interaction between  $\approx 1$ -20 keV energetic electrons and the triggering wave in which the particle pitch angles are altered and free energy is transferred from the particles to the waves [*Helliwell*, 1967; *Matsumoto and Kimura*, 1971; *Omura et al.*, 1991; *Nunn and Smith*, 1996]. Understanding the physical mechanism of the emission process is important since these interactions can directly affect the lifetimes of the resonant electrons.

Most of the electricity generated at power plants is alternating current (AC), as opposed to direct current (DC) produced by batteries. However, there are huge DC cables between, e.g., Finland and Sweden. Those lines are used to transfer electric energy from one country to another without problems of different phases in those countries. In Europe, Asia, most of Africa, and Australia/New Zealand, the electric mains power is at 50 Hz. In North America and in most Central and South American countries as well as in half of Japan, it is at 60 Hz.

The most recent observations made in September-October 2005 in Finland may raise some new plasma physical questions of the relationship between natural chorus emissions and PLHR.

Station	Measurement Locations		
	Geograph. Location	L value	Observations made
Huoneselkä	67.32° N, 26.58° E	5.25	2001-2002
Inari	68.90° N, 27.09° E	5.79	1989-1990
Kalkkoaivi	68.73° N, 22.11° E	5.85	Feb 1992, Oct 1994
Karjala-aapa	67.99° N, 26.12° E	5.44	Mar 1992
Liikkuvankangas	67.51° N, 26.33° E	5.31	1990-1991, 1997-2000
Nutsortonen	67.79° N, 26.26° E	5.37	Sep 1995
Perunkajärvi*	66.78° N, 25.94° E	5.08	Sep 2001 - Jun 2005
Pittiövaara	67.42° N, 26.39° E	5.30	Feb 2004, Sep 2005- *
Pomokaira	67.83° N, 26.10° E	5.37	Oct 1991
Pomokaira	67.83° N, 26.08° E	5.38	Sep 1992
Porojärvi	69.17° N, 21.47° E	6.10	Jan 1993 - Jan 1997
Puolitaival	68.23° N, 23.50° E	5.59	Nov 1991
Siiselkä	67.82° N, 26.08° E	5.47	Sep-Oct 2005

Table 1.2: Locations of ELF-VLF observations in Finland between 1989 and June 2005.  $L$  values are at the altitude of 100 km. The receiver marked \* belong to the British Antarctic Survey (BAS).

## 1.5 Locations of Receivers in Finland

The first ELF-VLF recordings in Finland were made already in autumn 1970 by *Riihimaa* [1972]. In the early 1970s Michael Rycroft from the U.K. made ELF-VLF observations in Sodankylä, but there were no Finnish partners. The second activity occurred in the end of the 1970s when Michael Rycroft, Paul Cannon, and Tauno Turunen made ELF-VLF recordings in Northern Finland and Northern Norway. At that time a very compact battery powered portable ELF-VLF receiver was used. The most important observation was the generation of ELF radio signals in the auroral ionosphere by non-linear demodulation of LF transmissions [*Turunen et al.*, 1980; *Cannon*, 1981].

Coordinates and time of the campaigns between 1989 and 2004 are shown in Table 1.2. Figure 1.10 presents the map of Europe showing magnetic latitudes  $L=4$  and  $L=6$  (heavy lines) at the ground, and the two most important ELF-VLF receiver locations in Finland (POR is Porojärvi and SOD is Sodankylä).  $L$  values in Table 1.2 (at the altitude of 100 km) and in Figure 1.10 (at the ground) are calculated using the International Geomagnetic Reference Field (DGRF/IGRF) models from 1945 to 2005 and the Tsyganenko 2001 model. Near Sodankylä we have had five different locations. Furthermore, photos of receiver stations during different campaigns in 1991–1997 are shown in Figure 1.11 and photos of the equipment inside the stations are in Figure 1.12.

First recordings in the late 1980s and early 1990s were made in Inari and Liikkuvankangas. These observations were related to the Russian Activnyij (Interkosmos-24) satellite. However, no signal from the satellite was received. The receiver was designed for wide-band recordings of natural ELF-VLF waves, too.

In 1991 some small changes were made to the receiver antennas, and the radio link between the antennas and recording unit was replaced with a coaxial cable. This lowered the receiver noise level. This new configuration was tested in February at Liikkuvankangas and in October in Pomokaira. In November ELF-VLF recordings were made during the EISCAT campaign in Puolitaival.

ELF-VLF observations were actively made during the Finnish EISCAT campaign in February 1992 in Kalkkoaivi. The Russian APEX (Active Plasma EXperiments) satellite was launched on 18th December, 1991. The first test operations were made with the satellite just during the Finnish campaign, and some strange signals were received. Several short ELF-VLF recordings were made in Liikkuvankangas in February and March, and a longer campaign was held in the end of March 1992 in Karjala-aapa.

The next generation of ELF-VLF receivers was designed in summer 1992 and the first test campaign was in September at Pomokaira. Antennas were 10-by-10 m squares with 10 turns, which means 1000 m<sup>2</sup> effective area. Also the preamplifiers were totally new. This configuration was successfully used in several campaigns; in January and November 1993 at Porojärvi, in October 1994 at Kalkkoaivi, in November 1995 and in January 1997 at Porojärvi.

Between the January 1997 and the September-October 2005 EISCAT campaigns, ELF-VLF observations have only been made with lighter instrumentation. In September 1997 recordings were made at Nutsortonen during Richard Barr's heating experiments.

In August 1997 the world-wide VLF navigation transmitter chain, Omega, was stopped. That gave a possibility to expand the upper cutoff frequency of the ELF-VLF receiver. Until then the lowest Omega signal (10.2 kHz) was the only reason why wide-band recording had to have low-pass filters at 10 kHz. Also very near to the location of Omega Aldra (66.42° N, 13.14° E) there were problems with the signal strength. Common frequencies transmitted by all Omega stations were 10.2, 11.05, 11 $\frac{1}{3}$ , and 13.6 kHz. Omega Aldra had 12.1 kHz as its unique frequency. Unique frequencies of other Omega stations were 11.8, 12.0, 12.3, 12.8, 12.9, 13.0, and 13.1 kHz.

Some of the recent measurement campaigns have been made at Huoneselkä and at Pittiövaara. At both locations the control signals transmitted along the 20 kV power lines caused too high background disturbance levels.

In September-October 2005 the newest ELF-VLF receiver was used for the first time. The location of the receiver was very good in the sense that the background disturbance level was exceptionally low. That was also the first time when the recording was fully digital. All the data was recorded with 24-bit dynamic resolution and stored onto the hard disk as one-hour files. Every single sample has GPS timing with an accuracy of 0.1  $\mu$ s. High dynamic resolution allowed us to receive all sferics without overflow in the amplifiers. Many interesting observations were made.

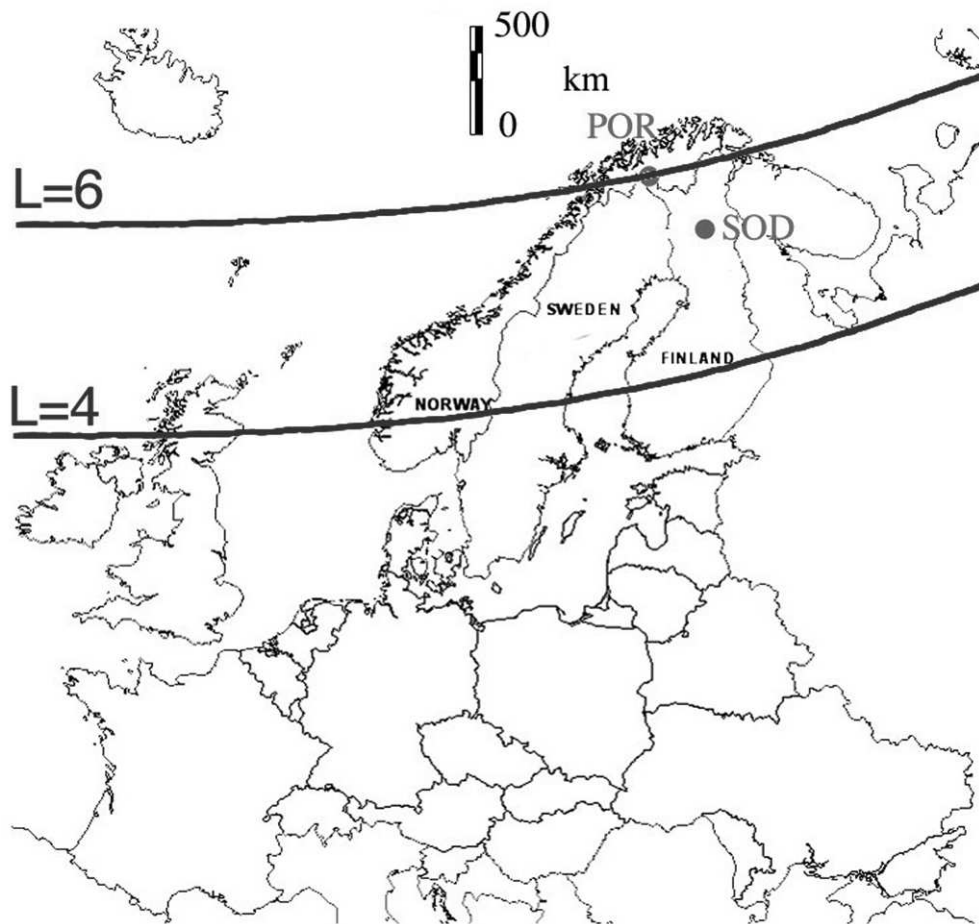


Figure 1.10: The map of Europe showing magnetic latitudes  $L=4$  and  $L=6$  (heavy lines) at the ground, and the two most important ELF-VLF receiver locations in Finland (POR is Porojärvi and SOD is Sodankylä). Near Sodankylä we have used five different locations.

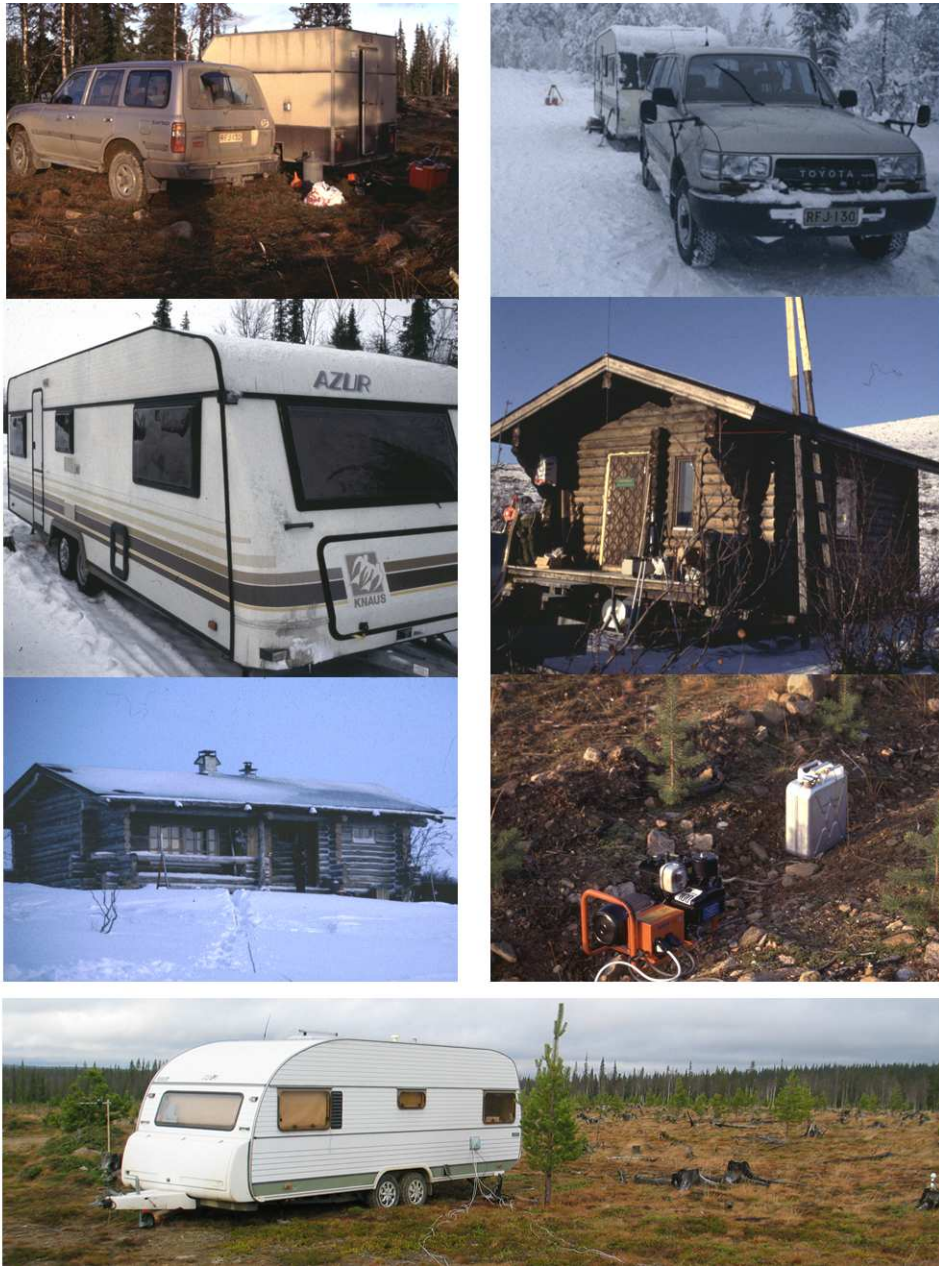


Figure 1.11: Temporary receiver stations during different campaigns in 1991-2005. Sometimes a caravan has been used as a base and sometimes a mountain cottage. Top row: Pomokaira and Puolitaival, second row: Karjala-aapa and Kalkkoaiivi, third row: Porojärvi and the system for generating 230 V AC power, and bottom: Siiselkä with GPS (near right edge) and the Internet connection (left side of the caravan).

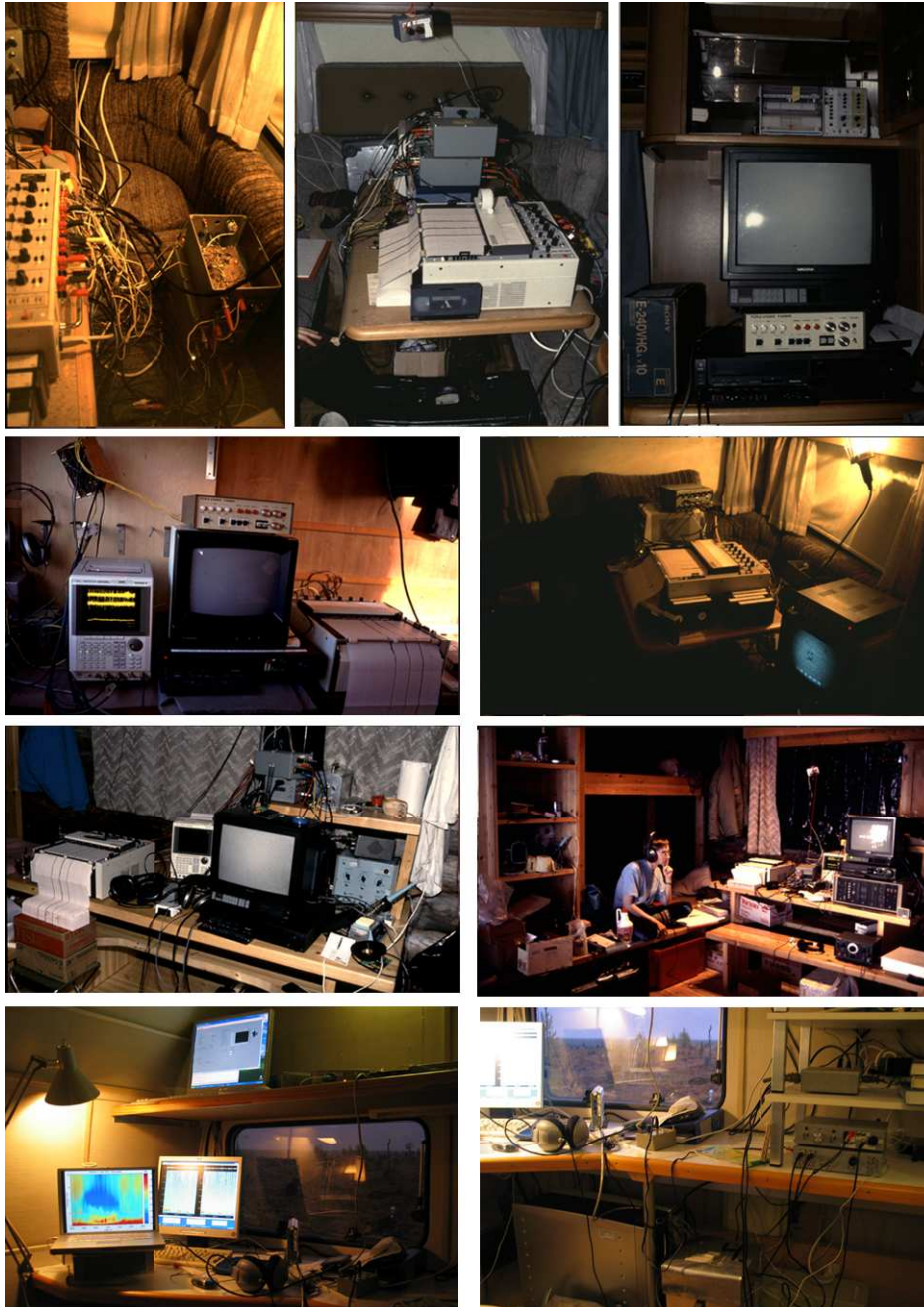


Figure 1.12: Equipment inside receiver stations during different campaigns in 1991-2005. Top row: Karjala-aapa, second row: Pomokaira and Puolitaival, third row: Porojärvi, and bottom row Siiselkä.



## Chapter 2

# Instrumentation

Wideband ELF-VLF observations have been carried out at different locations as shown in Section 1.5 using two vertical  $126 \text{ m}^2$  (“Aktivnyij” aerials) or  $1000 \text{ m}^2$  square loop antennae (called here coaxial cable aerials), signals from which have been amplified by twin low-noise preamplifiers. The receiver was located very far (35 km) from the nearest power line and settlements during most campaigns. Most of the instrumentation can stay outside without additional shelters from wind and rain. The cables between the preamplifiers and the recording part have specifications meeting the climate conditions down to  $-55^\circ\text{C}$ . Only the recording part must be protected against humidity and low temperature.

Locally generated electromagnetic noise is only due to the generator, which is needed for 230 V/50 Hz devices like VHS video tape recorder, auroral TV camera, TV monitor, pen recorder, computers, etc. The sensitivity of the receiver is such that signal amplitudes down to  $\approx 1 \text{ fT}$  can be detected at 5 kHz, which is usually below the natural background noise level. A signal of known intensity, frequency, arrival direction for a source at a given distance to the antennae, is injected from time to time during the campaign for calibration. The calibrator is a circular loop with 15 turns and 1 m diameter. An analog signal generator has been used as a signal source.

ELF-VLF data were recorded on the stereo audio tracks of VHS videotapes. The time code was simultaneously recorded together with auroral TV data on the video track of the same tape. The TV camera provided the TV signal also during daytime for time information. Afterwards, one-hour blocks of ELF-VLF data were digitised in the post processing phase using 16-bit resolution. The instrumental noise level is usually in the 4-6 least significant bits. The timing accuracy is usually  $\pm 0.5 \text{ s}$  due to the user-controlled start of the digitising. If more precise timing is needed, the Omega navigation signal from the Norwegian Aldra station can be used for that purpose for recordings before August 1997. Since September 1997 the RSDN-20 (nicknamed Alpha) transmitter network signals from Russia can be used for precise timing.

Recordings were made continuously throughout every campaign. Only short service breaks occurred usually every 4th day due to generator maintenance, and approximately 1 min gaps three times a day due to change of the tape. Observations during our VLF campaigns in January and November 1993, November 1995, and Jan-

uary 1997 have been made at the same location and with the same instrumentation. Before January 1993, the “Aktivnyij” aerials were used either as orthogonal loops or as a configuration of three antennae integrated per direction, which gave  $\sqrt{3}$ -times better signal-to-noise ratio. Since November 1997 the “Aktivnyij” aerials were used with new amplifiers. In September-October 2005 a new generation of ELF-VLF antennae (“UEV2300” aerials) were used. Their effective area is 2300 m<sup>2</sup>, and they have 2 times 128 turns of 3×3 m<sup>2</sup>.

In September-October 2005 the recording was done digitally with 24-bit dynamic resolution. This allows for a much larger dynamic range of the input signal than before. This larger dynamic range can give some crucial information about the phenomena, which are just above the background noise level or even below that.

Hereafter the term ‘antenna’ refers to the aerial alone, and the term ‘receiver’ means the whole system including the antennae and amplifiers.

## 2.1 Antennae

The antenna is a very important part of the ELF-VLF receiver, because its effective area is directly proportional to the signal from the loop. The features of the antenna affect the design of preamplifiers and main amplifiers as well as filter requirements. A loop antenna is very useful for a very wide frequency range from mHz to high radio frequencies. Detailed descriptions of antennae are given, e.g., in the textbooks of *Watt* [1967] and *Kraus and Marhefka* [2001].

All observations presented in this thesis were made with the square loops shown in Figure 2.2. Both antennas were designed and partly built by Prof. Tauno Turunen.

The frequency range in ELF-VLF applications is often between 0.5 and 10 kHz, the most interesting frequencies are below 3 kHz. The maximum signal level is received between 6 and 9 kHz, which is due to global lightning activity. Before August 1997 the Omega frequencies were almost as strong as lightning signals here in Scandinavia. Nowadays the signal levels of the control signals transmitted in power lines remain just below the lightning signals. These strongest signals are limiting the amplification in the linear receiver system. Unfortunately, the maximum signal level of the lightning can be tens of dB stronger than the desired signals.

### 2.1.1 IGY aerials

The International Geophysical Year from July 1957 to December 1958 motivated also ELF-VLF science. The most common antenna type is the so-called IGY type, which consists of two orthogonal triangular loops with an effective area of approximately 50 m<sup>2</sup>. The antennae were tuned up to 1.6 kHz. The IGY antennae remained a standard for decades. A detailed description has been impossible to find; instead it seems that all single triangular loops are called IGY-type antennae. Figure 2.1 shows such loops at Perunkajärvi near Rovaniemi. This Velox receiver (see *Smith* [1995] for details) belongs to the British Antarctic Survey; it was stopped in June 2005 at Perunkajärvi and reinstalled at Sodankylä in September 2005.



Figure 2.1: The ELF-VLF receiver antenna of IGY type. It has two orthogonal loops suspended from an aluminium mast. This antenna was located at Perunkajärvi, Rovaniemi until June 2005 and is at Pittiövaara, Sodankylä since September 2005, and belongs to BAS. The persons are Dr. Mark Clilverd (left) from BAS and the author of this thesis. (Photo by Thomas Ulich)

### 2.1.2 “Aktivnyij” aerials

In the late 1980s the Sodankylä Geophysical Observatory participated in the Russian Aktivnyij-Active (Intercosmos-24) satellite project. For that purpose a new ELF-VLF receiver was designed and constructed. The base of the antenna was made of  $1.25 \times 1.25 \text{ m}^2$  aluminium tube. There are places for stands on both sides of the antenna as well as handles for carrying. There is a box with power and signal connectors for a preamplifier at the bottom of the antenna. The left photo in Figure 2.2 shows this antenna in operation.

The antenna itself was made from  $0.75 \text{ mm}^2$  copper wire with vinyl insulator. The total length of the wire is 405 m and the number of turns is 81. This gives an effective area of  $126 \text{ m}^2$ . The wiring layout is controlled by two acrylic guides with a hole for each turn for the wire at both sides of every corner of the antenna. Finally the whole aluminium tube was filled up by polyuretan foam in order to avoid damage during transport and to keep the turns separated.



Figure 2.2: The ELF-VLF receiver antennae. The one on the left was used during the Russian Aktivnyij project and during campaigns before January 1993. Different combinations of up to 6 such antennas were used after January 1997. The size of the antenna is  $1.25 \times 1.25 \text{ m}^2$ . Those on the right were used during our campaigns between January 1993 and January 1997. Their size is  $10 \times 10 \text{ m}^2$ , i.e. with 10 turns the effective area is equal to  $1000 \text{ m}^2$ . The left photo shows Prof. Tauno Turunen, who has designed most of the Finnish ELF-VLF receivers.

The antenna does not have centre-tapped output. For balanced use it is made symmetrical using terminal resistance. One end of the coil is grounded to the base in the preamplifier box (single-end) and the other end is connected directly to the input of the preamplifier. There is also a resonance damper circuit. The modern amplifier solutions do not need pre-stage transformers as often used in this kind of receiver. The reason is that the phase shifts of the transformer would be almost impossible to deal with when a phase accuracy of a fraction of a degree is required. This was possible due to a new generation of amplifier circuits. The noise optimising is done at 5 kHz and the total noise is equal to the noise of a  $200 \Omega$  resistor at room temperature.

The resistance of the antenna coil is  $\approx 10 \Omega$  at room temperature, inductance is  $\approx 20 \text{ mH}$ , and ‘free’ resonance about 100 kHz. The grounding of one end decreases the resonance to below 40 kHz. The polyuretan filling brings the resonance down to 28 kHz. The Q value is high, but it was damped down to a value of  $\frac{1}{\sqrt{2}}$  by a parallel RC circuit, which lowers the resonance to 18 kHz. This system prevents almost all long-lasting oscillations at resonance frequency. This also guarantees that the antenna behaves purely inductive below 12 kHz.

The Omega navigation transmitter signal becomes one of the dominant signals,

which affects the dynamics of the receiver. There was no reason to design more effective antennae for these frequencies. However, some changes have been made after August 1997, when the Omega navigation network ceased to operate.

### 2.1.3 Coaxial cable aerials

In 1992 a new type of square loop antennae was designed. The main reason was that the effective area was required to be larger than for the “Aktivnyij” aerials. With the same length ( $\approx 400$  m) of wire it was possible to form  $10 \times 10$  m<sup>2</sup> antenna with 10 turns, i.e. the effective area is equal to 1000 m<sup>2</sup>. This size is near the practical limit for portable antennae.

The sheath of every turn of the coaxial cable was cut at the centre of the upper side of the square loop. The sheaths were connected together at both sides of the cut in order to get a common shield for all of the wire turns. There can be a few similar cuts at different places in the loop. The antenna has centre-tapped output. The output of the antenna and the sheath cut are situated at the opposite side of the loop. The resonance frequency of the antenna is slightly above 20 kHz, the resistance is  $\approx 50$   $\Omega$ , and inductance  $\approx 25$  mH. Similar to the “Aktivnyij” aerials, the antenna behaves purely inductive below 10 kHz.

The loop was suspended from two 12-m high aluminium masts. The masts stood on iron bases with dimensions of  $1 \times 1$  m<sup>2</sup> and were secured by 8 steel cable guys with plastic insulators. They were anchored under the ice of the lake or on the ground. The right photo in Figure 2.2 shows this antenna in operation.

### 2.1.4 UEV2300 aerials

Many new kinds of ELF-VLF phenomena, among others MLR, hiss clouds, and evening time structured hiss bands encouraged us to design a new type of loop antenna (UEV2300 means ULF-ELF-VLF 2300 m<sup>2</sup>). The project started in autumn 2004 and the first observations were made in September-October 2005. The size of the loop is  $3 \times 3$  m<sup>2</sup> with 2 times 128 turns, i.e. the effective area is 2300 m<sup>2</sup>. The total wire length is 3072 m.

The antenna has centre-tapped output, but the antenna is used in single-ended mode. The electric shielding is so good that the differential mode is not needed. The own resonance frequency of the antenna is 3.9 kHz, which is lowered to 1.5 kHz by additional parallel capacitance. The resistance is 14  $\Omega$ , and inductance  $\approx 540$  mH.

The antenna covers the ULF frequencies down to 10 mHz, but the amplifiers and the AD converters limit the lower cutoff at 1 Hz. This allows us to record also Schumann resonances, of which more than ten harmonics have been observed, i.e.  $> 75$  Hz.

## 2.2 Amplifiers

The simplest ELF-VLF receiver consists of only a metal stick as electric antenna and headphones, but such a system is too primitive for research purposes. In order to receive the weakest signals the antenna needs a good amplifier, usually two amplifiers.



Figure 2.3: The UEV2300 ULF-ELF-VLF receiver antennas. The size of the loop is  $3 \times 3 \text{ m}^2$  with 2 times 128 turns, i.e. the effective area is  $2300 \text{ m}^2$ . The person in the photo is Prof. Tauno Turunen.

The preamplifier can be either connected directly to the antenna or to a separate part. Usually the distance between the antenna and the recording unit is of the order of hundreds of metres, and the main purpose of the preamplifier is to keep the signal level high enough against losses in the cable.

The antenna output voltage increases proportionally to the signal frequency (6 dB per octave). Because of that and the fact that the most intense natural signals from lightnings (sferics) occur at the same frequency (ca. 8 kHz), it is reasonable to decrease the signal by 6 dB/octave in the amplifiers.

In both the “Aktivnyij” and the “coaxial cable” receivers, there are two generations of amplifiers: the one used during the time of the Omega transmitters and another thereafter. In the earlier one the amplification of the preamplifier was  $\approx 40 \text{ dB}$ , and it had 15 kHz 5-pole Butterworth low-pass filters. Later 14 kHz 5-pole Chebyshev low-pass filters and 5 kHz 8-to-10-pole Bessel low-pass filters were used, which caused 12 dB damping at 8-10 kHz and 6 dB/octave amplification in the range of 0.5-5 kHz. The preamplifiers used 12 V accumulators as power source.

In the “UEV2300” receiver, the amplifier is DC-coupled to the AD converter input. It contains a preamplifier of 20 dB and 5 kHz 10-pole Bessel low-pass filters with a gain of 30 dB. Cable drivers raise the total amplification to 62 dB. At the main amplifier the signal level is first decreased by 36 dB and then the AD converter drivers finally raise the total gain to 68 dB (from antenna output to AD converter). The attenuation at the line receiver is needed to provide extremely high common mode rejection, which can reject common mode signals up to  $300 \text{ V}_{pp}$ .

The main amplifiers and filters are in separate boxes close to the recording unit.

Freq.	Signal-to-noise ratio (relative to 1V/m wave field)			
	“Aktivnyij”	Coaxial cable	UEV2300	Difference
10 Hz	-	-	<b>109.6 dB</b>	-
200 Hz	<i>112.6 dB</i>	130.2 dB	<b>132.0 dB</b>	19.4 dB
500 Hz	<i>120.2 dB</i>	<b>138.5 dB</b>	134.4 dB	18.3 dB
1000 Hz	<i>125.9 dB</i>	<b>143.6 dB</b>	134.8 dB	17.7 dB
5000 Hz	135.2 dB	<b>151.8 dB</b>	<i>134.3 dB</i>	17.5 dB
10000 Hz	136.9 dB	<b>153.0 dB</b>	<i>132.6 dB</i>	20.4 dB

Table 2.1: S/N ratio for “Aktivnyij”, “coaxial cable”, and “UEV2300” antennas calculated at 6 different frequencies. Bold numbers show the best values and italic numbers are the worst values. The last column gives the difference between the best and the worst values.

The power source can be either 12 V accumulators or the mains.

Table 2.1 shows the S/N ratio for the “Aktivnyij”, “coaxial cable”, and “UEV2300” antennae calculated at 6 different frequencies. Formal S/N ratio was calculated for the antennae at a few frequencies assuming 1 V/m wave field and a bipolar single-ended amplifier having parameters, which are typical for the corresponding amplifier type. The calculation takes into account the voltage and current noise of the amplifier, thermal noise of the termination resistor, feedback resistors, and the antenna resistance. The calculation assumes tuning at 18 kHz, which means operation at the almost purely inductive part of the antenna impedance, except for the UEV2300 antenna, which is tuned at 1500 Hz.

The 1 V/m wave field occurs only in nearby lightning. The field strengths of waves of magnetospheric origin are several orders of magnitude weaker. The “coaxial cable” antenna has the best S/N. The “Aktivnyij” antenna is easy to transport and install. The UEV2300 antenna is heavy and not as good as the “coaxial cable” antenna in S/N except at lowest frequencies. It has the benefit that it covers the frequency band starting from 1 Hz. From the data one can, e.g., detect easily more than ten Schumann resonances. The UEV2300 receiver has two different selectable matching circuitry between the antenna and amplifier. The S/N values are shown for the simple case where the antenna is tuned to 1500 Hz and damped to a Q-value of 0.7. The other mode has -3 dB points at 375 and 6000 Hz. This mode gives several dB better S/N at most of the frequencies, but the lowest frequencies below a few tens of Hz cannot be recorded.

## 2.3 Recording Unit

In the late 1970s the ELF-VLF signals were recorded in Sodankylä by simple C-cassette recorder without the stereo tracks. The main advantages were its weight, which was very light, and its power consumption, which allowed the use of normal batteries. The device was easy to carry even in the pocket. The device had also some disadvantages, like bad stability of the speed of the tape, the short-duration of the

tape, and the sensitivity to temperature changes. However, the tapes could easily be stored and replayed many times without serious damage.

Ten years later, when ELF-VLF waves were recorded during the Russian Aktivnyij project, the main recording unit was a VHS stereo video tape recorder. With half-speed recording it allowed to store 8 hours onto one video tape, and stereo meant that there were two separate audio tracks (and usually even a separate track for mono audio, i.e. 3 separate audio tracks). Until February 1991, only the audio tracks were used for recording. Timing was based on the counter of the video tape recorder.

Since February 1991, also the video signal from an auroral TV camera was recorded simultaneously with two ELF-VLF channels on the same video tape. That allowed us to add a time code from a video timer with 0.01 s time resolution to the TV image. The stability of the timer is better than 1 s/month.

The dynamic range of a VHS video tape recorder is about 90 dB. The amplifiers give a nearly flat frequency response versus signal strength. The peak value of the signal is typically near 8 kHz. The video tape recorder cannot control the dynamics of the signals. In order to record also the instrumental noise level, a considerable part of lightning signals must be allowed to saturate. That causes new problems.

The UEV2300 receiver has been designed for 24-bit digital recording by computers. The signal from both orthogonal loops are digitised by 39062.5 Hz (i.e.  $10^7/256$ ) and saved in the same file as 32-bit words. The lowest 8 bits are used for channel information (0 or 1) and GPS time code. The recording unit is a Windows XP computer with a LabView program. Every file contains one-hour of two-component data. The files start and end 30 min past every hour.

Before AD conversion, the analogue signals are also taken for monitoring. These signals are amplified using the previous generation main amplifier and filter unit, and then the signals can be listened to by headphones and monitored via a realtime 16-bit spectrogram generated by a Windows XP computer with the Gram 12 program (a product of Visualization Software LLC by Richard Horne).

## 2.4 Data Storage

The development of mass memories and hard disks has recently enabled us to make fully digital recordings of ELF-VLF waves. The situation was different only 15 years ago, when the only reasonable medium was a video tape, which can record continuous wide-band signals for 8 hours on two audio channels and on one video channel. The maximum dynamic range of a video tape has been enough for most purposes, but can be improved by  $\approx 20$ -30 dB with new digital technology.

One video tape contains about 4.4 GB ‘raw audio data’ (when using 40 kHz sampling frequency and 16-bit digitising). This is equivalent to the present capacity of a DVD disk, and therefore the digitised data were archived on DVD. Unfortunately, this does not include the video data. One DVD is equal to four hours of new 24-bit ELF-VLF data. Earlier, ELF-VLF data was stored on CDs, which can store one hour of two-component ELF-VLF data with 40 kHz sampling frequency and 16-bits resolution. Unfortunately, nobody can predict how long CDs or DVDs will last physically and for how long readers will be available.

## Chapter 3

# Digital Analysis of ELF-VLF Data

Ground based monitoring of ELF-VLF waves is commonly done by using two orthogonal horizontal loop antennae as detecting sensors. Historically the analysis of the data is often based on different estimates of the power spectrum obtained either by dedicated analogue or digital devices or by computers. Often no other information than the power spectrum is obtained, and often the signal is only partially used, i.e. only one component is used in the processing. Nowadays it is possible to analyse the data in detail even as part of an observatory routine by using fast but still cheap modern computers.

The analysis described below is used for ELF-VLF data in this work, but the method works also at other frequencies recorded similarly. The most important parameter in the analysis is the power spectrum as a function of time, but estimates of the polarisation properties of the wave, i.e. sense of rotation, minor and major axis ratio and orientation of the polarisation ellipse reveal important features of the properties of the detected waves.

The starting point is to define the data from two orthogonal antennae as a complex signal and carry out first a complex Fourier transform of a suitable window of data, which can be from hundreds of points up to millions of points. From the Fourier coefficients one can then estimate the signal power, ellipticity, orientation of the polarisation ellipse, and the sense of rotation. All of this can be done as a function of frequency and time using resolutions, which the stationarity of the process allows. Special filtering of the data is possible in all the obtained parameters.

The signal power can be expressed as a function of frequency and time in different ways including total power, right-hand polarised power, left-hand polarised power, and linearly polarised power. The polarisation ellipse can be described as a sum of linear and circular signals. The physical interpretation is straightforward if at any given frequency and time instant there is clearly one dominating wave having a good signal to noise ratio. In other cases a careful consideration is needed.

Figure 3.1 shows a schematic diagram of the typical experimental arrangement discussed here. A whistler mode wave, which is circularly right-hand polarised, prop-

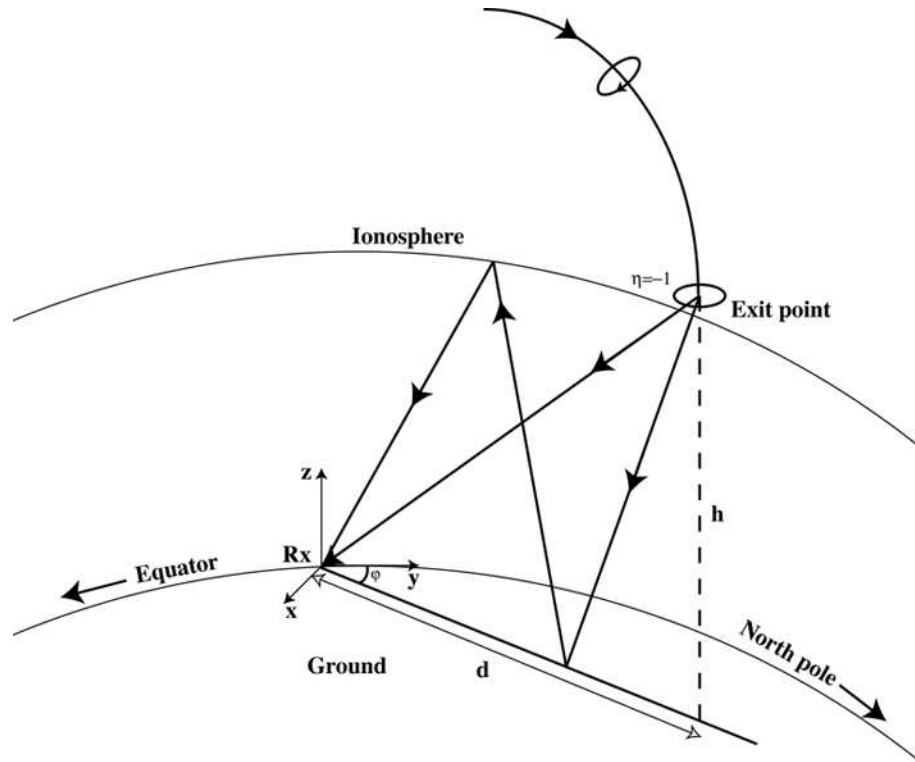


Figure 3.1: Schematic diagram showing the ionospheric exit point of a whistler mode wave, the Earth-ionosphere wave guide and a receiver. The coordinate  $(x, y, z)$  system used in this thesis is also indicated.  $\eta$  is the ellipticity of the polarisation ellipse, and  $\eta = -1$  means right-hand circular polarisation.

agates through the magnetosphere and exits at the lower edge of the ionosphere. The altitude of the exit point is ca. 80 km. From there the wave propagates to the receiver on the ground. The wave field at the receiver can be considered to comprise the summation of either a number of rays or a number of wave-guide modes [Yearby and Smith, 1994].

In the simple case where the receiver is close to the exit point ( $d < h$ ), a single ray is dominant and the polarisation is close to circular with the same sense as the whistler mode wave [e.g. Ohta *et al.*, 1989; Hayakawa *et al.*, 1990].

The ‘ideal’ receiver would contain two antennae for the horizontal magnetic components ( $H_x$  and  $H_y$ ) of the whistler wave and a third for the vertical electric component ( $E_z$ ). The use of the  $E_z$  component makes it possible to derive the signal azimuth without error due to non-linear polarisation by using the method of Okada *et al.* [1977]. It also allows to eliminate the  $180^\circ$  azimuth ambiguity and derive the zenith angle of the received signal. However, this is a more complex system, because the electric

field receivers are much more difficult to calibrate and more susceptible to interference than magnetic field receivers. The remaining field components ( $H_z$ ,  $E_x$  and  $E_y$ ) are not normally used in ground-based receivers, because they have low amplitude near a conducting ground plane [Yearby and Smith, 1994].

*Shimakura et al.* [1986] used the phase difference between the two magnetic components to derive a polarisation parameter. Five years earlier *Hayakawa et al.* [1981] reported on a ‘polarimeter’ which measured the minor to major axis ratio of the polarisation ellipse of the horizontal magnetic components, but did not distinguish left-hand or right-hand polarisation. Furthermore, in both cases measurements were performed in a narrow band.

### 3.1 Analysis Method

The analysis explained here is applied to recordings from two orthogonal sets of antennae. Vertical loops were oriented (magnetically) north-south and east-west. Thus, looking through the loop one faces either the east or the west in the case of the EW loop, and the north or the south for the NS loop. However, the loop detects the magnetic field of the wave, but the wave propagates perpendicular to that, i.e. the EW loop detects the waves arriving from either north or south (or the waves having a NS component of their Poynting vector). The NS loop works accordingly.

The signals were sampled and digitised (to 16-bit or 24-bit precision) and stored on computer disks. A sampling rate of 40 kHz per channel were used, which demands that large amounts of data can be handled and thus the computations must be fast. The computations are based on complex Fast Fourier Transforms using a window length, which gives the desired frequency and time resolution.

Figure 3.2 presents the polarisation ellipse of the ELF-VLF wave received by two horizontal loops, which are set orthogonally to magnetic EW and NS directions. In all computations the signal from the EW antenna is treated as the real part of the complex signal, and the signal from the NS antenna is treated as imaginary part. Therefore, E (east) refers to the positive real axis of the complex coordinate system and N (north) to the positive imaginary axis (Figure 3.2).

*Rietveld et al.* [1987] have presented the ELF-VLF polarisation ellipse for heating-produced waves. Their description is very close to ours, but it differs by the definition of the direction of rotation. We are defining the right-hand polarisation in a way that the wave magnetic field vector rotates clockwise in Figure 3.2, and for the left-hand polarisation the wave magnetic field vector rotates anti-clockwise.

The complex signal  $f(t) = f_1(t) + if_2(t)$  consists of real signals  $f_1$  and  $f_2$  from the two loop antennae. This makes the numerical calculations easier and faster. The Fourier transform  $F(\omega)$  is

$$F(\omega) = \int_{-\infty}^{\infty} f(t)e^{-i\omega t} dt \quad (3.1)$$

and its inverse transform is

$$f(t) = \frac{1}{2\pi} \int_{-\infty}^{\infty} F(\omega) e^{i\omega t} d\omega. \quad (3.2)$$

For any angular frequency one gets two complex Fourier coefficients, one for the negative frequency  $-\omega_k$  and another for the positive frequency  $\omega_k$ . It is convenient to present the coefficients in polar coordinates.

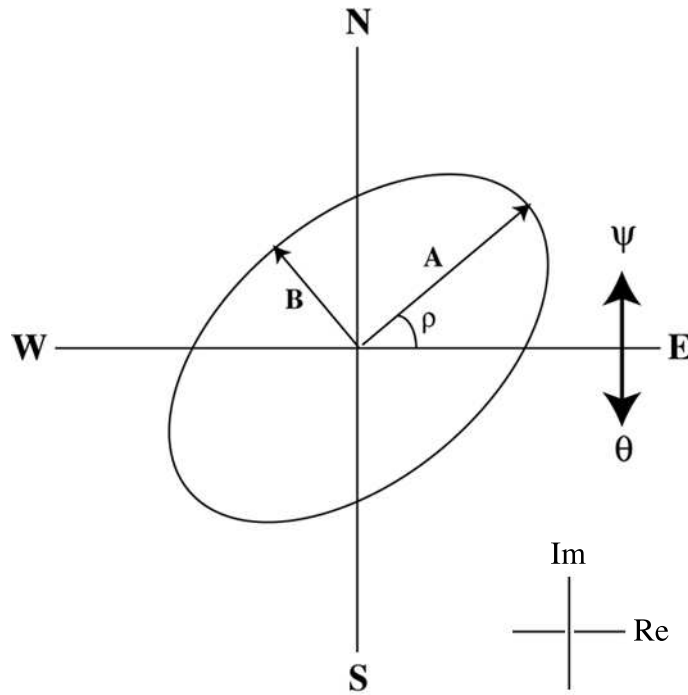


Figure 3.2: The polarisation ellipse of the ELF-VLF wave magnetic field received by two horizontal loops. Parameters are as follows: **A** is semi-major axis, **B** is semi-minor axis,  $\rho$  is orientation angle (i.e. the angle between the real axis and the major axis of the ellipse),  $\psi$  and  $\theta$  are the phase angles of left and right-hand polarised wave components, respectively, and both angles have positive direction as anti-clockwise (i.e.  $\theta$  can be treated as either negative or positive, which causes  $180^\circ$  ambiguity to direction of arrival), N, E, S, and W are the magnetic north, east, south and west, respectively, magnetic field line is pointing into the paper. E and N are also the positive real and imaginary axes, respectively.

$$F(-\omega) = a + ib = r_- e^{i\theta} \quad (3.3)$$

and

$$F(\omega) = u + iv = r_+ e^{i\psi}, \quad (3.4)$$

where  $r_-$  and  $r_+$  are the moduli of the Fourier coefficient and  $\theta$  and  $\psi$  are the phase angles. These two coefficients describe the signal behaviour perfectly at the given angular frequency  $\omega_k$ .

The signal  $S_\omega$  at time  $t$  is described by two terms,

$$S_\omega(t) = r_- e^{i\theta} e^{-i\omega t} + r_+ e^{i\psi} e^{i\omega t} = z_- + z_+, \quad (3.5)$$

where  $S_\omega$  describes an ellipse formed by two oppositely rotating vectors  $z_-$  and  $z_+$  at angular frequency  $\omega$ . They present right and left-hand circular polarisation, which are orthogonal, and therefore all signal polarisations can be presented in the base defined by them. If they lead to elliptic polarisation, the orientation of the major axis is obtained when  $z_-$  and  $z_+$  have the same arguments, i.e.  $\theta - \omega t = \psi + \omega t$ , which gives  $\omega t = (\theta - \psi)/2$ . When this is inserted in  $S_\omega(t)$ , the result is

$$\begin{aligned} S_\omega(t) &= r_- \exp \left[ i \left( \theta - \frac{\theta - \psi}{2} \right) \right] + r_+ \exp \left[ i \left( \psi + \frac{\theta - \psi}{2} \right) \right] \\ &= (r_- + r_+) \exp \left[ i \left( \frac{\theta + \psi}{2} \right) \right] \end{aligned} \quad (3.6)$$

Hence the angle between the real axis and the major axis of the ellipse is  $\rho = (\theta + \psi)/2$ .

The semi-major axis  $A$  is the sum

$$A = r_+ + r_- \quad (3.7)$$

and correspondingly the semi-minor axis  $B$  of the ellipse is

$$B = |r_+ - r_-|. \quad (3.8)$$

The sense of rotation  $K$  is obtained by

$$K = \text{sign}(r_+ - r_-). \quad (3.9)$$

Negative values of  $K$  mean right-handed rotation (R-polarisation) and positive values correspond to left-handed rotation (L-polarisation).

The ellipticity  $\varepsilon$  is given by

$$\varepsilon = (r_+ - r_-)/(r_+ + r_-) \quad (3.10)$$

and it has values from  $-1$  (right circular) to  $0$  (totally linear polarisation) and  $+1$ , which means left circular polarisation. Thus the sign gives the sense of rotation.

The total signal is  $S_\omega(t) = z_+ + z_-$ , and it can be written either as

$$S_\omega(t) = r_+ [e^{i(\psi + \omega t)} + e^{i(\theta - \omega t)}] + (r_- - r_+) e^{i(\theta - \omega t)} \quad (3.11)$$

or

$$S_\omega(t) = r_- [e^{i(\psi+\omega t)} + e^{i(\theta-\omega t)}] + (r_+ - r_-) e^{i(\psi+\omega t)}. \quad (3.12)$$

In both cases the total signal is presented as a sum of signals with linear and circular polarisations. Although the two divisions are different, the power of the signal with circular polarisation is

$$P_{cir} = (r_+ - r_-)^2, \quad (3.13)$$

total power is

$$P_{tot} = r_+^2 + r_-^2, \quad (3.14)$$

and linear power is

$$P_{lin} = P_{tot} - P_{cir} = r_+^2 + r_-^2 - (r_+ - r_-)^2 = 2r_+r_-. \quad (3.15)$$

## 3.2 Digital Analysis

Analogue data must be digitised before it can be analysed by computer. Usually an ELF-VLF recording system uses analogue audio or video tapes, on which the data is stored. Digitising is an important phase of the data analysis and can cause timing errors.

If the ELF-VLF data is stored onto DAT tape, it is already in digital form. Similarly, the newest recordings were made directly by computers, which makes the analysis procedure easier and especially the timing accuracy becomes much better than in the old system, because earlier the timing information was multiplexed into the video image, and the triggering of the start was usually set manually, which meant an inaccuracy of  $\approx 0.5$  s.

When the complex data  $f(t)$  is digitised to a sequence of numbers  $f_j$  with sampling interval  $\Delta$ , i.e. the sampling times are  $t_j = j\Delta$ , where  $j = 0, 1, 2, \dots, N-1$ , the discrete Fourier transform  $F_k$  is

$$F_k = \sum_{j=0}^{N-1} f_j e^{-2\pi i k j / N} = \sum_{j=0}^{N-1} f_j e^{-i\omega_k t_j}, \quad (3.16)$$

where  $f_j$  are digitised data points and  $N$  is the number of the complex samples. The inverse transform is

$$f_j = \frac{1}{N} \sum_{k=0}^{N-1} F_k e^{2\pi i k j / N} = \frac{1}{N} \sum_{k=0}^{N-1} F_k e^{i\omega_k t_j}. \quad (3.17)$$

Hence  $2\pi j k / N = \omega_k t_j$  so that

$$\omega_k = \frac{2\pi j k / N}{j\Delta} = \frac{2\pi k}{N\Delta}. \quad (3.18)$$

In the following the analysis is limited to the surrounding of  $\omega_n$  by setting all the other Fourier coefficients to zero and denoting angular frequency  $\omega_n$  simply by  $\omega$ .

Similarly to continuous signals the ratio of minor and major axes is obtained from Equation 3.10 and the power of the signal is obtained from Equations 3.13-3.15.

In order to get well-behaving Fourier coefficients, a suitable window function is used. If we only measure the signal for a short time, the FFT works as if the data were periodic for all time. If not quite an integral number of cycles fit into the total duration of the measurement, the end of one signal segment does not connect smoothly with the beginning of the next - the assumed signal is similar to the actual signal, but has little ‘glitches’ at regular intervals.

The glitches can be reduced by shaping the signal so that its ends match more smoothly. Since we cannot assume anything about the signal, we need a way to make any signal’s ends connect smoothly to each other when repeated. The easiest way to make sure the ends of a signal match is to force them to be zero at the ends: that way, their value is necessarily the same. Mathematically, a window function has the property that its value and all its derivatives are zero at the ends.

Multiplying by a window function (called ‘windowing’) suppresses glitches and thereby avoids the broadening of the frequency spectrum due to glitches. Windowing can narrow the spectrum and make it closer to what was expected.

There are lots of different window functions, but Kaiser windows [*Kaiser*, 1974] having beta-parameters between 4 and 10 are used in our ELF-VLF analysis. The Kaiser window function is unique in that its shape is variable. A variable parameter defines the shape, so the Kaiser window is able to match precisely the attenuation one requires without overperforming. The Kaiser (or sometimes called Kaiser-Bessel) window is a well-behaving window function, which gives a good power estimate, and successive power estimates correlate little even with 50 % overlapping, when the beta-parameter is higher than 6. This window is available in many software packages. A beta-parameter equal to 1 gives a rectangular window, and beta-parameters higher than 10 do not improve the window any more in practical solutions.

These computations are done at every angular frequency. Thereafter one can apply special filtering, e.g. basic time and/or frequency domain averaging (low pass filtering). An example of more complicated filtering is limiting the polarisation ellipse within a given angular interval. This selects signals coming from a given horizontal angle of arrival but with 180 degrees ambiguity. It is also possible to limit the analysis to such signals, which simultaneously are strong, have a polarisation ellipse axis ratio within given limits and have a given sense of rotation.

There are clearly numerous other possibilities, too, and many of them have turned out to be very useful. In the case of the orientation of the main axis, i.e. the horizontal angle of arrival, one has to apply filters for values around  $0^\circ=360^\circ$  carefully. Another, similar case is the ratio of minor and major axis, when the signal has nearly linear polarisation ( $\varepsilon \approx 0$ ). Then the noise level can easily alter the sense of rotation. However, these optional filter possibilities are not applied in this thesis.

The parameters given by the described analysis are mostly presented in frequency-time plots, usually as colour surface plots.

When using orthogonal sensors, the physical interpretation is simple only for those cases where the signal comes from a single source. When multiple processes contribute to the data and none of them is clearly dominating, the physical interpretation of the result must be done on a case-by-case basis and obtaining a meaningful result may

turn out to be impossible.

### 3.3 Examples of Analyzed ELF-VLF Data

#### 3.3.1 Quick-look plots

The large amount of digital ELF-VLF data per time unit means that we can usually analyse only a very short interval of time, which is sufficient for studying individual discrete emissions or whistlers. For quick-look purposes, one often needs plots covering up to one day of observations in order to see the overall activity. This requires a powerful computer and large hard disk capacity.

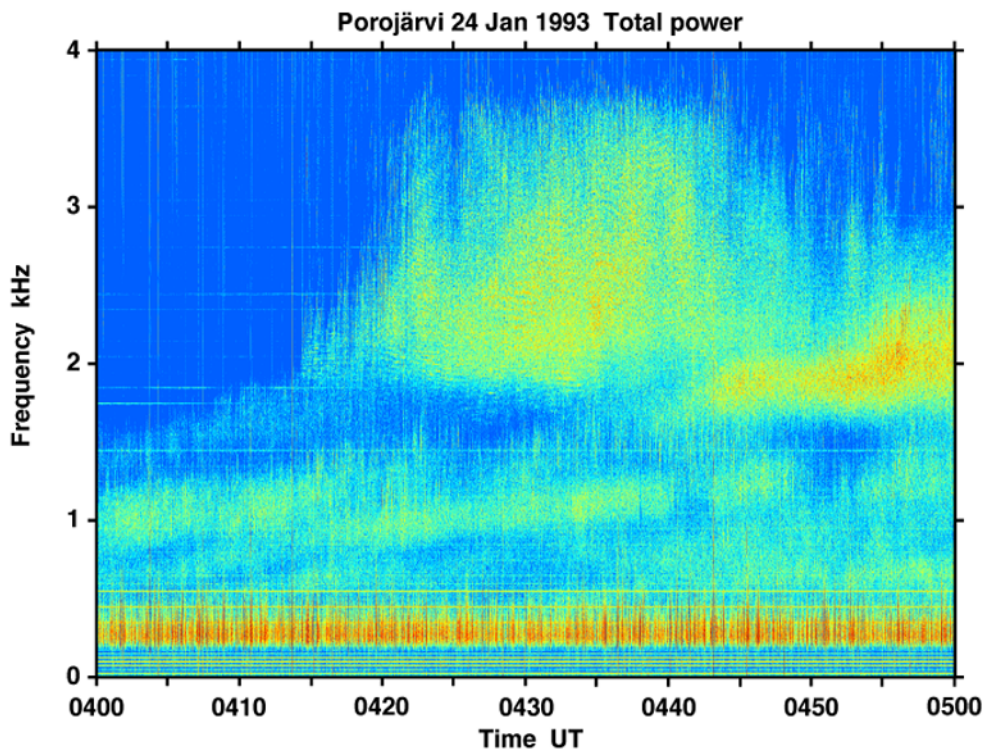


Figure 3.3: Example of a one-hour quick-look plot of data recorded on 24 January 1993 at Porojärvi. The event above 1.5 kHz is studied in more detail in Chapter 5, which presents the MLR (Magnetospheric Line Radiation) phenomenon. Below 1.5 kHz the chorus related to the auroral pulsations is seen.

The basic quick-look plot contains one hour of wide-band data. We have made two separate sets of plots; one with frequency range of 0–4 kHz (in some cases 0–5 kHz), shown in Figure 3.3, and another with frequency range of 0–8 kHz (in some

cases 0–10 kHz), shown in Figure 3.4. The narrower frequency range has been used to find typical chorus and hiss activity, while the wide-band plots are for high-frequency emissions and auroral hiss events. Figure 3.3 presents one morning hour on 24 January 1993 in frequency range of 0–4 kHz. There the ‘main’ event is MLR (Magnetospheric Line Radiation) above 1.5 kHz, and the part below 2 kHz is a chorus event related to auroral pulsations. Figure 3.4 presents a different kind of VLF phenomenon, which is related to the aurora, too. There were more than 10 auroral hiss bursts within one hour on 27 January 1993. Auroral hiss bursts have relatively short durations and therefore one-hour quick-look plots are very useful to detect them.

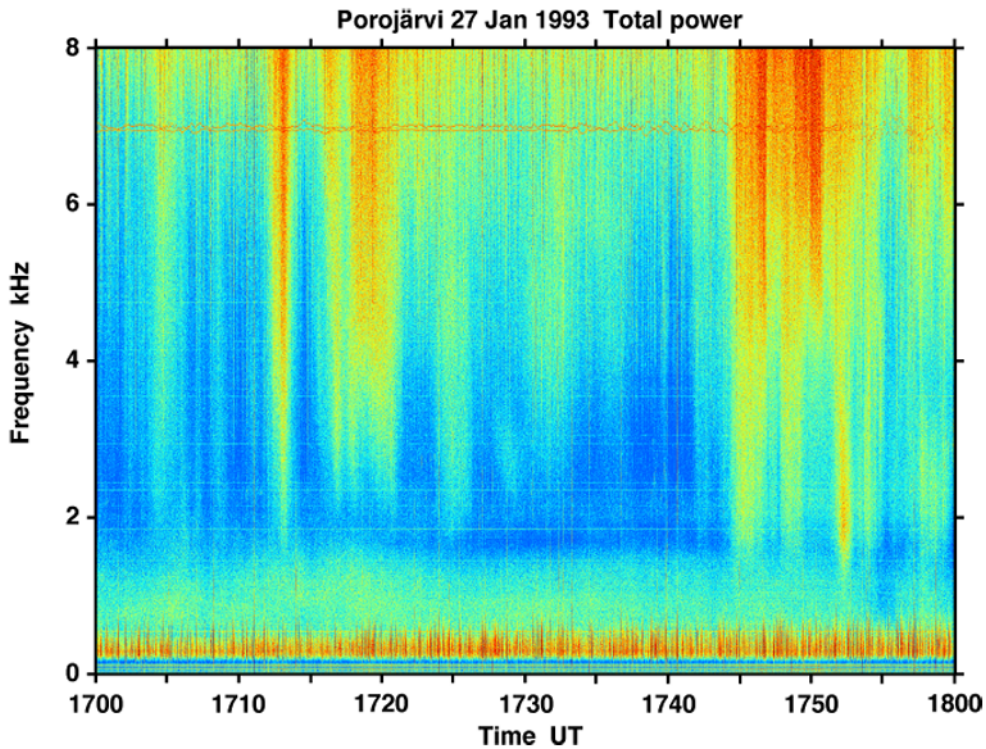


Figure 3.4: Example of a one-hour quick-look plot of data recorded on 27 January 1993 at Porojärvi. There are several auroral hiss bursts, which are most intense at 8 kHz. The two waveforms near 7 kHz are multiplexed into the ELF-VLF data from a two-component pulsation magnetometer.

In order to make a plot with reasonable file size and minimal loss of general information, only 4096 point FFT windows with 96 point overlapping, and integration over 10 spectra have been used, i.e. the time resolution of this analysis is 1 second. However, the compression of the plot causes loss of time resolution, and events like whistlers and single emissions will be merged into the background. However, all phe-

nomena, whose duration is longer than 10 seconds, can be seen in the plots.

Wider frequency plots contain mostly sferics, whose intensity maximum occurs around 8 kHz. This makes event finding very difficult, but it is still possible assuming all sferics are linearly polarised. Other events are usually elliptically polarised, and they can be identified from plots of circularly polarised power. Some examples of high-frequency phenomena are given in Chapter 6 (narrow band hiss events) and Chapter 10 (hiss clouds). Also whistler-triggered chorus events often occur above 5 kHz.

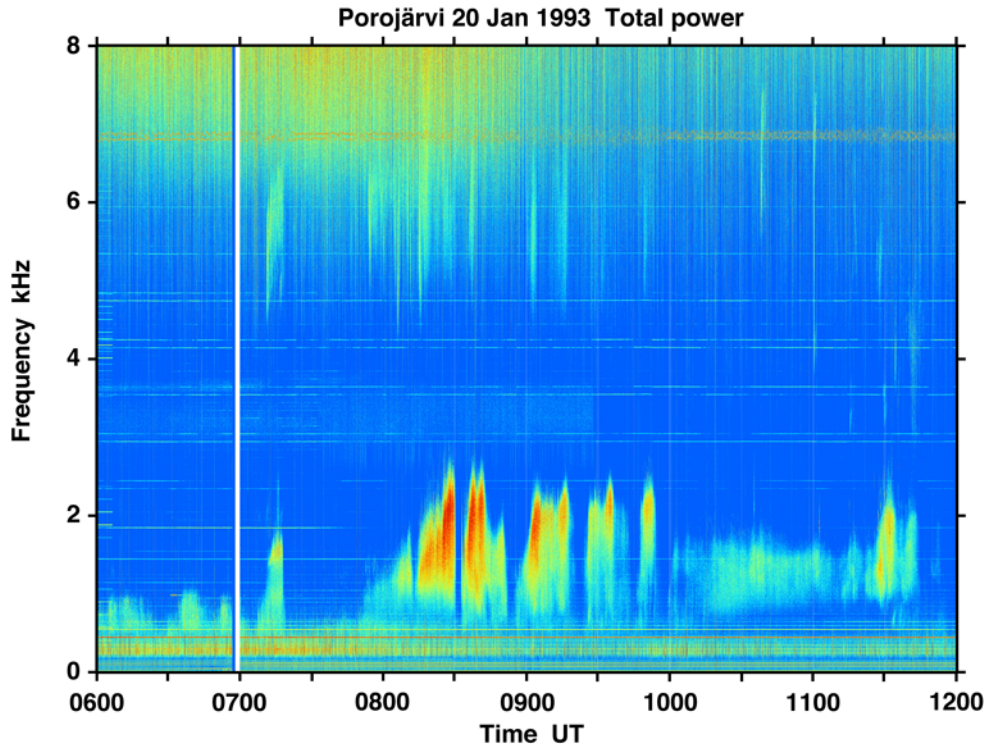


Figure 3.5: Example of a 6-hour quick-look plot of data recorded on 20 January 1993 at Porojärvi. There are chorus bursts between 0800 UT and 1200 UT. Some high-frequency emission bursts can also be seen above 4.5 kHz. This event has been studied more carefully in Chapter 8. The narrow white bar just before 0700 UT is a data gap due to change of the recording video tape.

Even if one-hour plots cover a very long interval compared to so-called synoptic (1 min every 15 min) recordings, they are too short to study, e.g., temporal behaviour of morning chorus or MLR events. One-hour plots are not enough to be able to determine, e.g., hiss clouds, because their duration can be up to 10 hours. They are usually so weak that it is very difficult to separate them from background noise, but plots with longer time intervals can make the events visible in the dynamic spectrum.

For aforementioned reasons we have made 6-hour and 12-hour plots. They are

combinations of 6 or 12 one-hour plots, with the time axes re-scaled by factors of  $\frac{1}{6}$  and  $\frac{1}{12}$ , respectively. Even if the time resolution of the analysis result is still 1 second, the re-scaling causes the effective time resolution to decrease also by these scaling factors, i.e. the resulting time resolution will be 1 and 2 minutes, respectively. Examples of these time-compressed plots are shown in Figures 3.5 and 3.6.

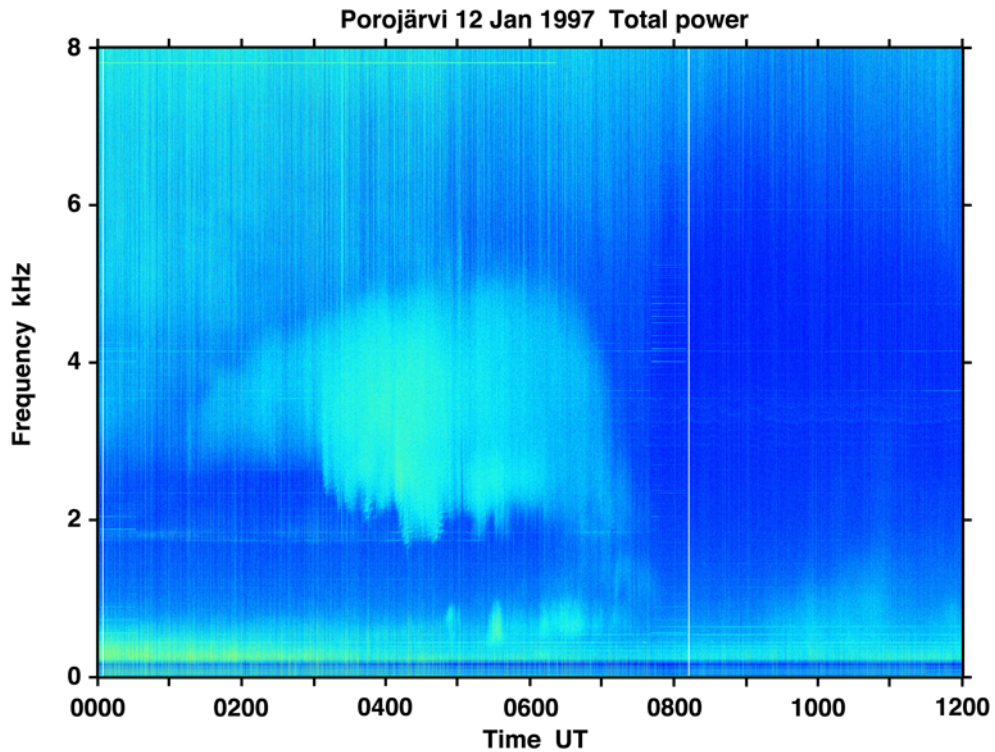


Figure 3.6: Example of a 12-hour quick-look plot of data recorded on 12 January 1997 at Porojärvi. There is a hiss cloud, which occurs between 0100 UT and 0800 UT. This phenomenon has been investigated in detail in Chapter 10. The narrow white bars just after 0000 UT and 0800 UT are short data gaps due to change of the recording video tape. The colour scale has been the same in data analysis of all campaigns, and in January 1997 the recorded signal level was much lower than earlier. This explains why, e.g., sferics seem to be so weak.

Both examples are ELF-VLF events which cannot be observed by 1-minute recordings every 15 minutes. For instance, interesting gaps among the chorus activation could be missed, or short-duration high-frequency emission bursts will not be seen by 1-minute samples: Figure 3.5 shows that the low-frequency chorus starting just before 0800 UT continues until 1145 UT, and even the last chorus burst at about 1130 UT seems to belong to the same group.

The hiss cloud presented in Figure 3.6 lasts 7 hours, which means that even 6-

hour plots are too short to show the whole event. This phenomenon is most probably introduced for the first time in this thesis. The intensity of the hiss clouds is mostly such that they can hardly be detected in 1-hour plots and much less so in 1-min plots. They usually occur in the (early) morning hours, when the sferics are still intense due to less absorption in night-time than daytime.

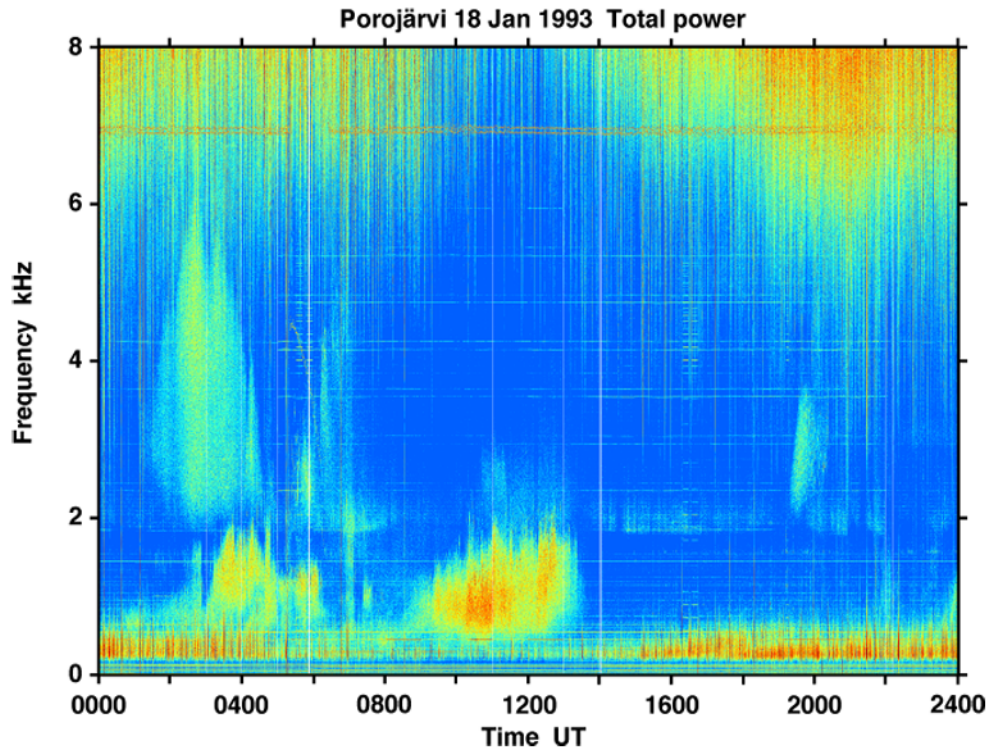


Figure 3.7: Example of a 24-hour quick-look plot of data recorded on 18 January 1993 at Porojärvi. There is a hiss cloud, which occurs between 0100 UT and 0500 UT, and two chorus events from 0200 UT to 0630 UT and from 0900 UT to 1400 UT. In the evening a MLR event is seen between 1920 UT and 2053 UT. This phenomenon is investigated in Chapter 5.

A 24-hour plot is useful when diurnal activity is studied. It also allows to see certain large-scale events and is useful for finding similar events in many days of observation. An example is given in Figure 3.7. There are many ELF-VLF phenomena seen in one plot. The first event is a hiss cloud in the frequency range of 2–6 kHz, a bit later a chorus related to pulsating aurora appears in the range of 0.5–2 kHz, and then between 0900 UT and 1400 UT there is a morning chorus event below 3 kHz. A MLR event starts 1920 UT and it ends abruptly at the time of an auroral hiss burst at 2053 UT. There are more auroral hiss bursts after 2100 UT, but their durations are so short that they are hardly seen in this plot.

### 3.3.2 Detailed plots

As explained in Section 3.1, several output parameters can be obtained simultaneously. The main result file contains total power obtained by equation 3.14. Most of the figures shown in this thesis are total power plots. In certain cases other plots are shown: linear power (equation 3.15) plots can be used to study phenomena, which are purely linearly polarised, e.g. sferics, PLHR (mostly), and signals arriving from close to the radio horizon. On the contrary, purely circular (equation 3.13) power plots are reasonable, when linearly polarised waves should be excluded.

Additional information can be acquired from ellipticity or sense of rotation (equation 3.9) plots, as well as from the horizontal direction angle of wave arrival. According to the magneto-ionic theory the whistler-mode waves are always right-hand polarised. However, the analysis of ELF-VLF data presented in this thesis show also left-hand polarised waves, which are presented in Chapters 4 and 5. Furthermore, there are a couple of reports about left-hand polarisation in certain whistlers [*Ohta et al.*, 1989; *Yearby and Smith*, 1994], and a few theoretical papers [*Lundin*, 1979, 1983, 1985; *Lundin and Krafft*, 2002].

The first analysis package for complex ELF-VLF data was developed at SGO in the summer of 1996. It was based on LabView programs, which were used to calculate complex FFTs (total, right-hand circular, left-hand circular, and linear powers), horizontal angle of arrival, and ellipticity. At that time LabView (versions 3.x–5.x) could not produce colour plots, which required the use of Matlab software for plotting. On the other hand, old Matlab versions could not be used to calculate complex FFTs.

Nowadays only Matlab (versions 7.x onwards) is used for calculations and plotting. Furthermore, the speed and capacity of computers have increased so much that it is easy to make one-hour plots in reasonable time. The new analysis package produces total, right-hand circular, and left-hand circular power plots as well as horizontal angle of arrival plots ( $0^\circ$ - $180^\circ$  counter-clockwise starting from North), axis ratio of polarisation ellipse (value 1.0 means pure circular polarisation without sense of rotation and 0.0 means purely linear polarisation), and sense of rotation (shows just right and left-hand signals regardless the ellipticity of polarisation ellipse).

Figure 3.8 is an example of total, right, and left polarisation plots, axis ratio of polarisation ellipse plot, sense of rotation plot, and horizontal angle of arrival plot. It presents a strong chorus event observed between 1200 UT and 1300 UT on 19 January 1993 at Porojärvi. The total power plot shows strong chorus, especially after 1240 UT, and PLHR lines between 2.9 kHz and 3.5 kHz, as well as sferics above 3 kHz. The right-hand circular power plot contains only signals having ‘correct’ polarisation, i.e. chorus. The left-hand circular polarisation plot should be empty according to magneto-ionic theory, but it contains PLHR around 3 kHz, some chorus, and some sferics. The appearance of chorus and sferics can be explained by saturation of the receiver, and also by the fact that linear polarisation can be described as a sum of right and left-hand polarisations. However, most of the sferics are linearly polarised, which is seen on the lack of them in the circular polarisation plot.

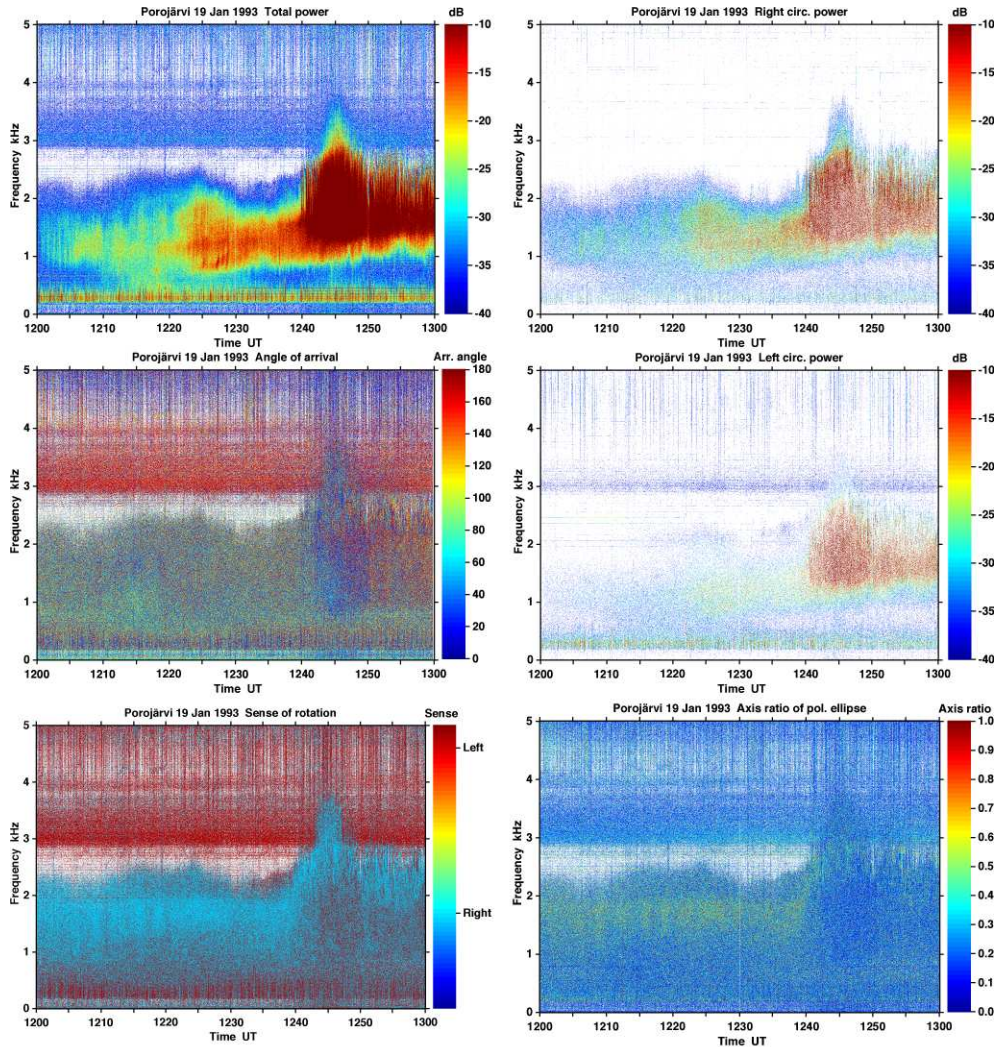


Figure 3.8: Example of a 1-hour quick-look plot (0–5 kHz) of data recorded on 19 January 1993 at Porojärvi. There is a normal chorus event, which is right-hand polarised. The top left panel presents total power, the top right panel shows right-hand polarised power, the middle left panel shows horizontal angle of arrival, the middle right panel depicts left-hand polarised power, the bottom left panel shows axis ratio of polarisation ellipse, and the bottom right panel presents the sense of polarisation.

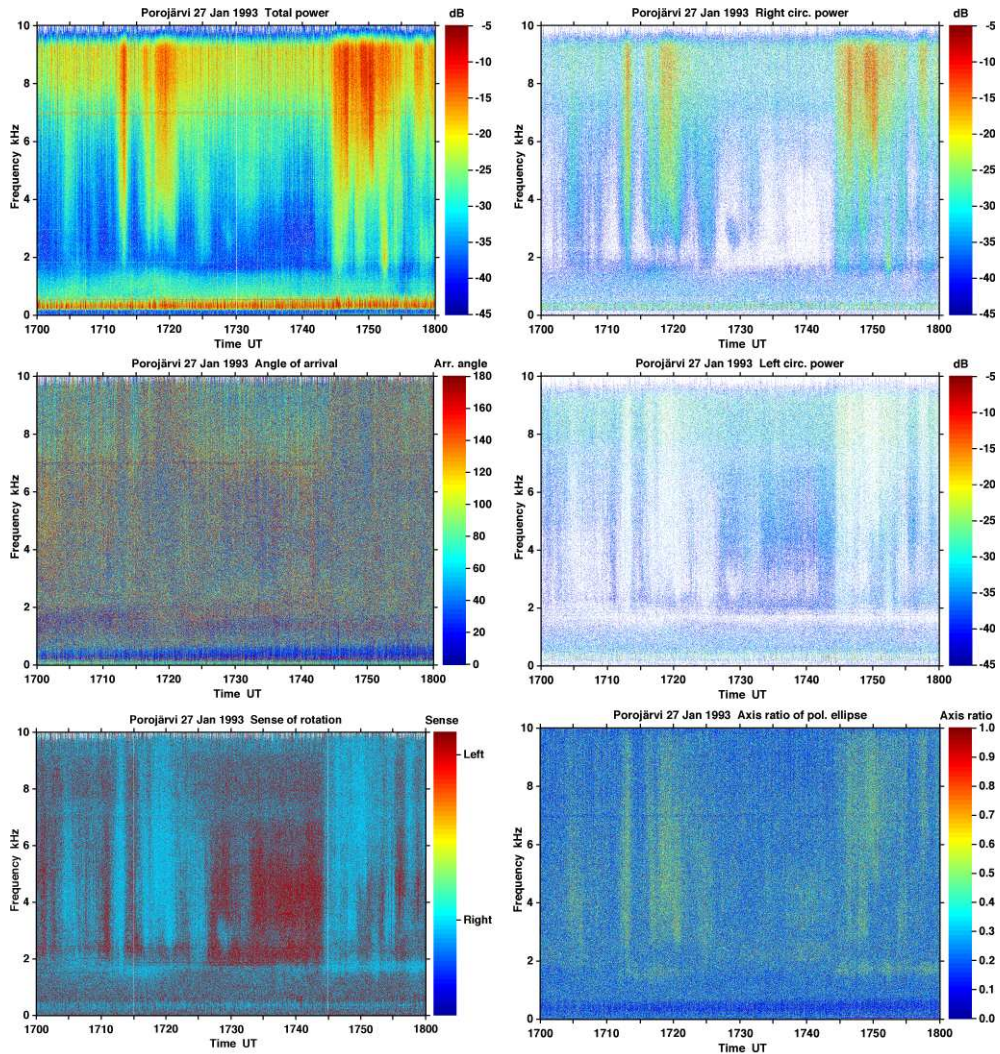


Figure 3.9: Example of a 1-hour quick-look plot (0–10 kHz) of data recorded on 27 January 1993 at Porojärvi. There are many normal auroral hiss events, which are right-hand polarised. The top left panel presents total power, the top right panel shows right-hand polarised power, the middle left panel shows horizontal angle of arrival, the middle right panel depicts left-hand polarised power, the bottom left panel shows the axis ratio of polarisation ellipse, and the bottom right panel presents the sense of polarisation.

The sense of rotation plot presents practically the same signals as total power, but the colour code separates right and left-hand polarisations (blue is right-hand and red is left-hand). In principle, if there are purely linear signals, they should be yellow, but so far they have been too weak or too rare to be seen in the plots.

The horizontal angle of arrival plot shows that PLHR-related signals arrived either from between S and SW or from between N and NE. The strongest chorus came mostly from either N or S. The weaker chorus, which is mainly hiss, appears to come from all directions. The same is valid for sferics. The axis ratio of the polarisation ellipse shows that all signals arrived far from the zenith, because there are no yellow and red colours. Only waves arriving from close to zenith have polarisation ellipses, which are almost circles.

The second example in Figure 3.9 presents one-hour plots containing mostly auroral hiss on 27 January 1993 at Porojärvi. There are nine hiss bursts in the frequency range of 1-10 kHz. These bursts are right-hand circularly polarised, and they are arriving from near the zenith, which can be seen from the plot of the axis ratio of the polarisation ellipse. The strongest bursts reach the axis ratio of  $\approx 0.6$ . Now the plot of horizontal angle of arrival does not give any reasonable information, which agrees with wave arrival from near zenith. When the wave arrives from overhead, a very small movement of the ionospheric exit point changes dramatically the horizontal component of angle of arrival.

The white colour seen in many plots, here and afterwards, means that the signal level is below a certain threshold value, which is usually the same as the lowest dB value (dark blue) in the total power plot.

More examples of detailed analyses can be found in Chapters 4, 5, and 11.

## Chapter 4

# Power Line Harmonic Radiation

Radiation from power lines at high harmonics of the fundamental 50 or 60 Hz has long been accepted as an electromagnetic compatibility (EMC) problem especially in industrial areas. This radiation, which is called Power Line Harmonic Radiation (PLHR), also reaches large parts of the lower magnetosphere. Although weak, PLHR is a coherent signal, which continuously leaks into and interacts with the magnetospheric plasma. Frequently, these signals are amplified and either trigger or interact with other magnetospheric emissions, as routinely seen in ground-based observations. Actually, PLHR can play a catalytic role when boosting other weak signals over the threshold of triggering and stimulate strong emissions.

Usually, people believe that the effects of man-made activity are confined only to the Earth's surface and atmosphere. However, there are no man-made effects caused by radio waves on surface and atmosphere, but all radio waves (from, e.g., radio transmitters and PLHR) propagate through the ionosphere to the magnetosphere. Satellites have shown that electromagnetic signals from VLF transmitters and power lines routinely travel to beyond  $4 R_E$  [Heyborne, 1966; Lurette, 1983; Parrot, 1995].

Ground-based studies show that both transmitter signals and PLHR interact with energetic particles in the magnetosphere and trigger strong emissions [e.g. Helliwell, 1975; Helliwell *et al.*, 1975; Park and Helliwell, 1978; Nunn *et al.*, 1999]. Lurette [1983] estimated that, if magnetospheric wave activity can be affected by PLHR from a certain area, global power grids could play an important role in the dynamics and wave activity in the magnetosphere and ionosphere. This, however, is disputed by Thorne and Tsurutani [1979, 1981], Tsurutani *et al.* [1979], and Tsurutani and Thorne [1981], who maintain that PLHR has a negligible effect on the radiation belts. Similar opinions have been presented also, e.g., in the URSI General Assembly in Toronto in 1999 (presentation by *D.L. Jones*, 1999, and discussions afterwards). Today there are several observations supporting both ways of thinking.

However, man-made signals in the magnetosphere can have a direct economic impact on science and technology. Firstly, PLHR is frequently amplified by 30 dB in wave-particle interactions [Helliwell, 1975] and can trigger strong emissions [Park

and Chang, 1978]. Although PLHR may be too weak to scatter many particles, the emissions it triggers are frequently quite strong and can result in significant particle precipitation [Lurette, 1983]. Secondly, amplified waves and triggered emissions increase the background noise level of the radio frequency in the magnetosphere and under certain circumstances increase the background noise level of the radio frequency in the atmosphere. This additional noise makes experiment design for magnetospheric study more complicated, and it degrades VLF communication links and interferes with ground-based experiments.

## 4.1 History of PLHR Observations

By the 1960s it was already known that VLF transmitter signals penetrate into the ionosphere, interact with energetic particles in the magnetosphere and trigger strong emissions [Heyborne, 1966; Helliwell, 1975]. The history of studies of PLHR is impressive and vast beginning with Helliwell *et al.* [1975], and leading to a special issue of *Space Science Reviews* in 1983. Excellent ground-based observations of PLHR have been obtained from the magnetically conjugate pair of receivers at Siple, Antarctica and Roberval, Quebec, Canada [Helliwell *et al.*, 1975; Park and Helliwell, 1981; Park *et al.*, 1983]. These papers report a frequent occurrence of magnetospherically propagated harmonic signals with separations of about 120 Hz. Such harmonics most probably originate from the Canadian power system. These lines in the power spectra are often offset from exact harmonics of the 50 or 60 Hz lines by up to 20 Hz, and individual lines can show significant spectral broadening of this order. Some arrays of lines with separations of  $\approx 20$  Hz are observed. These are most likely sidebands due to the nonlinear sideband instability [Nunn, 1986].

Park [1977] showed that the strongest waves emerging from the magnetosphere between L shells of 3 and 7 during recovery phases of magnetic storms and during isolated substorms are often emissions stimulated by PLHR. The data of Park and Helliwell [1978] consist of PLHR-triggered emissions in the range of 1–8 kHz, and show that triggered activity reaches a maximum around local noon. Park and Miller [1979] studied chorus emissions in the 2–4 kHz range recorded at Siple in 1974 and 1975. The measured wave intensity showed a distinct minimum on Sunday compared to the rest of the week. This minimum was confined to the dawn-afternoon local time sector where chorus intensity had a diurnal maximum. The authors suggested that most of the chorus activity is triggered by PLHR, and that the Sunday minimum is the result of reduced industrial power consumption on Sunday.

Lurette *et al.* [1979] showed that the starting frequencies of measurable chorus emissions occurred within  $\pm 2$  Hz of PLHR spectral lines. It is not known if PLHR actually triggered the emissions or just controlled the starting frequencies.

Ground data from the conjugate pair of receivers at Halley Bay, Antarctica and St Anthony, Newfoundland showed rather different characteristics from Siple observations, probably because the PLHR input from the ground was different [Matthews and Yearby, 1981; Yearby *et al.*, 1981]: Newfoundland employs a mix of 50 and 60 Hz power systems. Yearby and coworkers found spectral line separations to be rather variable, in the range of 50–90 Hz, and individual lines had considerable bandwidths

of up to 20 Hz. They also noted ‘sideband’ substructures with characteristic spacing of 20 Hz. The observed time distribution of PLHR events had an occurrence peak in the local afternoon, and a noted minimum on Sundays. Most events occurred at times of low magnetic activity.

Some interesting measurements have been made in Newfoundland by *Yearby et al.* [1983]. They measured the VLF wave amplitude spectra at different distances from power lines and deduced the unbalanced currents in the lines (of the order of mA). The calculated total radiated power was only  $\approx 1 \mu\text{W}$ .

*Lurette* [1983] examined some theoretical aspects of wave-guide propagation. If the signal is launched tangentially to the Earth, it is clear that direct signals are confined to a radius of 1000 km from the source, when the bottom of the ionosphere is assumed to be at the altitude of 90 km. Beyond this distance, propagating waves must be reflected at least once by the ionosphere. Within 1000 km from the source, the signals at the bottom side of the ionosphere are the sum of a direct ray and many reflected rays. The lower boundary, which is either sea-water or soil, influences the total attenuation rate of wave-guide signals. The high conductivity of sea-water (ca. 4.5 S/m) reflects almost all of the incident signal, i.e. attenuation is small. Since soil is less conductive ( $10^{-4}$  to  $10^{-2}$  S/m), the reflection coefficient of this medium ranges from 0.6 to 1.0, depending on the angle of incidence. When the reflection coefficient is low (propagation over soil), the attenuation is high.

In conjunction with ground data extensive satellite observations of PLHR are available. Generally observations in space tend to confirm the PLHR characteristics observed on the ground, but care in interpreting the data has to be taken due to Doppler shifts and the fact that a satellite may be observing leakage from a duct (same as a whistler duct, see Chapter 1, Section 1.1) some distance away. *Bell et al.* [1982] reported on PLHR observations on the ISEE1 satellite. PLHR was observed in only about 5% of the orbits.

A very extensive study of PLHR observations made by the OGO-4 satellite showed that PLHR presumably generated by coastal sources can propagate to distances greater than 2000 km over sea-water, but radiation from land-locked sources tends to be confined to the immediate vicinity of the source [*Lurette*, 1983]. OGO-4 observations revealed that the harmonic radiation tends to be the highest near mining operations. Most of the equipment used in both open pit and underground mines is powered by electric motors. Silicon-controlled rectifiers are frequently used to regulate the speed of the motors. This distorts the power waveform and generates a spectrum of harmonics. Some mines rectify the AC power to provide DC, e.g. for trains.

Observations from the Ariel 3 and Ariel 4 satellites showed that PLHR was most conspicuous at quiet times when  $K_p < 2$ . The geographical distribution was concentrated over North America and to a lesser extent over Europe. In a paper of considerable interest, *Rodger et al.* [1995] reported on PLHR observed on the ISIS 1 and 2 satellites over New Zealand. Two distinct types of PLHR were observed. One of these, so-called ‘‘tram lines’’ (TLs), consisted of lines with narrow bandwidth, with zero drift, and close to harmonics of 50 or 60 Hz. TLs clearly have their origin in power distribution systems. The other kind of PLHR were called magnetospheric lines (MLs), characterized by broader bandwidth, and no obvious correlation between line frequencies and multiples of 50/60 Hz. MLs were observed normally to drift in

frequency at rates of up to 40 Hz/min. The drift was more often upwards though downward drifts were noted. Since ML frequencies no longer correspond to those of the supposed terrestrial source, they would appear to be decoupled from that source and thus self-sustaining. It is not clear what role terrestrial PLHR radiation plays in either initiating MLs or in sustaining them.

A very good overall review of man-made influences on the magnetosphere has been written by *Parrot and Zaslavski* [1996].

## 4.2 Nonlinear Effects

Clearly, since the terrestrial input signal is often fairly weak, the ELF-VLF signal injected into the magnetosphere must be amplified as a result of electron cyclotron resonance instability. The signal will also be repeatedly amplified while executing multiple reflections between hemispheres. In situations where the linear growth rate is high, PLHR may be amplified to levels  $> 2$  pT at which nonlinear trapping may occur in the equatorial region, and wave phenomena commonly associated with nonlinear wave-particle interaction will appear.

In the literature examples of nonlinear phenomena in PLHR are common. Most observations of magnetospheric lines reveal spectral broadening [*Helliwell et al.*, 1975; *Park and Helliwell*, 1981; *Matthews and Yearby*, 1981; *Yearby et al.*, 1981; *Park et al.*, 1983]. ‘Extra’ sidebands with separations of  $\approx 20$  Hz are also commonly noted.

Most of the observational papers report PLHR-triggered emissions. Risers are most common, but fallers and hooks also occur. However, none of the papers present good individual examples of triggered emissions. *Helliwell et al.* [1975] reported bursts of emissions which merge to form something like a single chorus element, which is then repeated at the 2-hop wave bounce period.

Weak spectral lines with separations of 50 or 100 Hz were transmitted from Siple, Antarctica, to simulate PLHR [*Park and Chang*, 1978; *Park et al.*, 1983]. Input wave intensities were only about 0.1 pT, but strong lines were observed at Roberval, Quebec, Canada, with spectral broadening and triggered emissions. It seemed that the frequencies at which strong magnetospheric lines were excited, did not depend upon the transmitted power, but rather on ambient plasma conditions. *Helliwell et al.* [1975] observed that chorus and periodic emissions are often associated with PLHR. Furthermore, the lower onset frequency of the chorus sometimes is remarkably constant, suggesting triggering at the lower edge by a PLHR line.

## 4.3 Theoretical Background

Neutral-grounded power lines can be viewed as large vertical loop antennae driven by harmonic currents. For frequencies small compared to the resonant frequency, PLHR-generated fields are proportional to the area of the loop, which depends on the harmonic frequency, soil conductivity, and line length. High voltage ( $V > 70$  kV) lines carry an overhead shield wire that is grounded at each tower [*Lurette*, 1983]. Three high voltage systems (110 kV, 220 kV, and 400 kV) are in use in Finland. All of them are grounded at each tower. Therefore, in Finland 20 kV lines are the main source

of PLHR; their grounding distance can be from several tens of kilometres to hundred kilometres. [*J. Elovaara, Fingrid Oyj, private communication, 2005*].

For high voltage lines, the neutral currents enter the Earth, usually travel a short distance, enter the shield wire ground, and are returned along the shield wire. This system forms only a relatively small loop antenna, and therefore PLHR should be quite weak. Any conductor near a grounded power line reduces the effective area of the vertical loop antenna and the subsequent radiation.

It is very difficult to say exactly, how effective a radiator is a certain power line, because the loop size is strongly dependent on the properties of the ground where the return current flows. Some estimate can be obtained if the skin depth is known [*Lurette, 1983*]. However, all recordings presented in this thesis were made further than 10 km from the nearest power line, and the most probable source of PLHR observed during our campaigns is much further away. Detailed theoretical presentations of power line models can be found in the papers of *Lurette [1983]* and *Bullough [1995]*.

A very comprehensive review of the characteristics of the radiating source is provided by *Kikuchi [1983]*. The trans-ionospheric injection of the weak PLHR signal into the magnetosphere was dealt with by *Molchanov et al. [1991]*. PLHR must be considerably amplified to be an observable phenomenon. Observations by *Helliwell [1983]* give a figure of about 30 dB for the integrated linear growth along a field line at  $L=4$  for a ducted, parallel propagating whistler. The idea of *Helliwell [1983]* was well supported by numerical simulations by *Nunn [1993]* and *Nunn et al. [1997]*, which required linear equatorial growth rates of more than 60 dB/s. If the ionospheric reflection loss does not exceed the integrated growth (about 23 dB), then it is possible that PLHR induction lines could be a self-sustaining emission, but it is not clear, if PLHR is always a ducted phenomenon.

When PLHR equatorial amplitudes reach levels of  $\approx 2$  pT (at  $L=4$ ), in the case of a continuous wave (CW) or band-limited ELF-VLF wave, electron cyclotron resonance trapping occurs, and the wave-particle interaction process becomes nonlinear [*Nunn et al., 1999*]. Nonlinear trapping dynamics and the consequences for field evolution are fairly well understood, and discussed theoretically and numerically by *Karpman et al. [1974]*, *Omura and Matsumoto [1982]*, *Bespalov and Trakhtengerts [1986]*, *Nunn [1990]*, *Trakhtengerts [1995]*, and *Trakhtengerts et al. [1996]*.

A major theoretical problem with PLHR is the slow drift of the lines either upward or downward at rates of 20 Hz/min. If spectral broadening occurs only on the upper side of the line, then this would explain a slow upward drift of frequency of radiation repeatedly crossing the equator. Another theoretical and numerical approach was presented by *Shklyar et al. [1992]*. The authors examined theoretically and numerically the problem of a CW pulse making a single passage of the equator at nonlinear frequency shifts. They found numerically a small upwards frequency shift of 1 Hz, which was theoretically predicted. Repeated equatorial transits should result in slow upward drifts of the order observed. Both of these theoretical approaches cannot explain observed PLHR drifting downwards in frequency.

Line drift immediately causes further theoretical problems, since the PLHR will become effectively decoupled from its terrestrial source. Magnetospheric lines with variable or non-harmonic spacings should then constitute a self-sustaining phenomenon. In this case what determines the spacings of MLs?

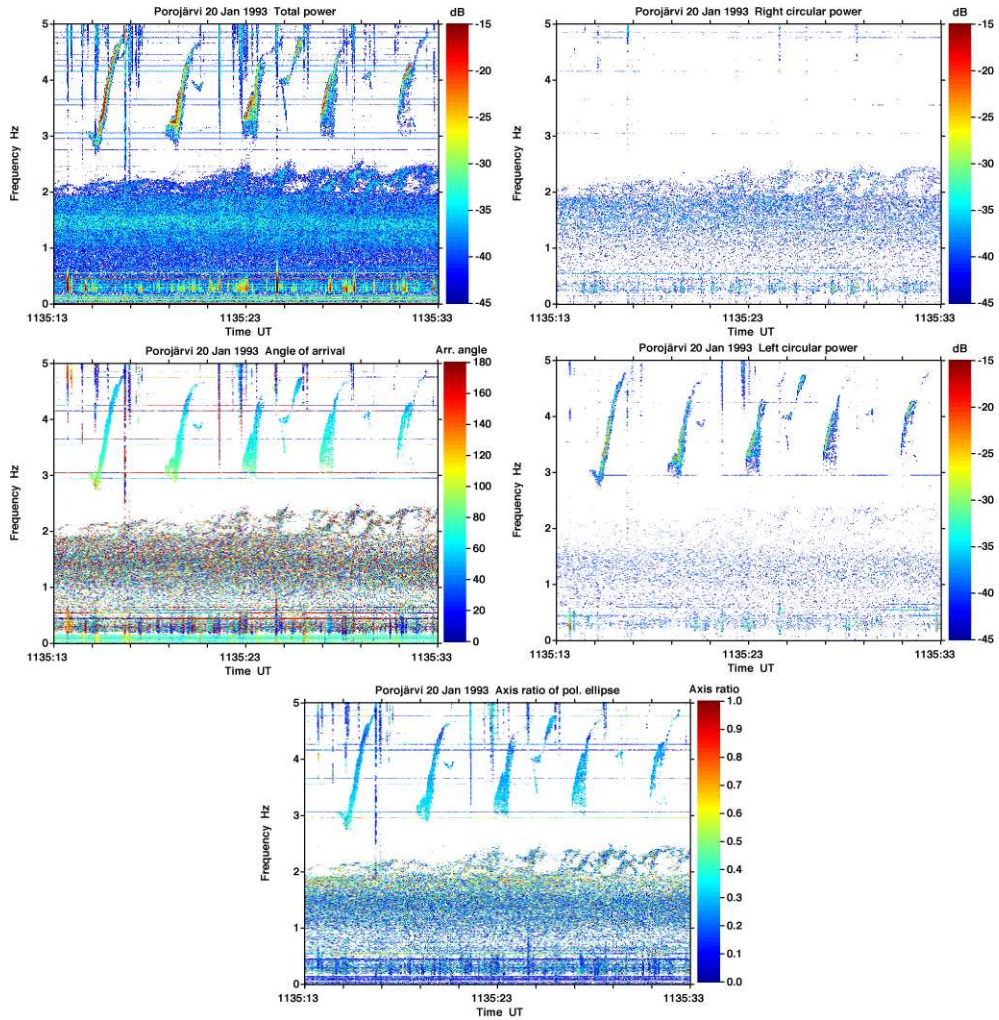


Figure 4.1: Strong rising frequency emissions triggered by a pair of prominent lines at 2950/3050 Hz. The periodicity, 4 seconds, is the 2-hop wave period, and the broadening of each emission is due to the 2-hop echo of the previous one. The top left panel shows total power, the top right and middle right panels present right and left circular polarised power, respectively. Horizontal angle of arrival is shown in the middle left panel, and the bottom panel shows the axis ratio of polarisation ellipse.

## 4.4 Observations of PLHR TEs

The data from Porojärvi is rich in PLHR events, especially in triggered emissions (TE). This appears to be partly due to the strong PLHR radiation by the Scandinavian power systems. The other factor is the apparently high ionospheric reflectivity, which is evident through the appearance of strongly echoing VLF events.

The magnetospherically propagated PLHR observed at Porojärvi must, of course, originate from the northern hemisphere, since the area conjugate to Porojärvi is located in the Southern Ocean between South Africa and Australia.

A full set of PLHR lines in the band of 2–5 kHz are often observed. In Finland the power system is 220V/3 phase. At heavy industrial plants the conversion to DC power is done using 12 pulse bridges. This results in strong harmonics being radiated at frequencies of

$$f = 50(cp \pm 1)\text{Hz}, \quad p = 12, \quad c = 1, 2, 3, 4 \dots \quad (4.1)$$

Therefore prominent pairs of lines obvious in the data are at 550/650, 1150/1250, 1750/1850, 2350/2450, 2950/3050, 3550/3650 and 4150/4250 Hz etc. The lines observed at Porojärvi are ‘tramlines’, with constant frequency of separation of 100 Hz locked to the terrestrial source.

Figure 4.1 shows a set of strong PLHR lines, with prominent risers triggered from the PLHR doublet at 2950/3050 Hz at 1335:15 UT. Note, that PLHR is normally a weak feature, and these results show PLHR of surprising strength. It appears to be the upper line which triggers the risers. The frequency gradients are consistently in the region of +1.0 kHz/s. The first riser exhibits an initial falling frequency segment which goes down to 2800 Hz, where it seems to ‘reflect’ off a weak PLHR line. The risers have a marked periodicity which is the 2-hop wave bounce time (which is the same as the bouncing time of electrons between the hemispheres along a certain L shell). The spectral broadening obvious in the latter emissions may be due to reflected wave energy from the previous event.

Interestingly, a weak narrow band faller is triggered off a line near 3.9 kHz at 1135:20 UT. Polarisation analysis shows that both PLHR lines and emissions consist of a large linearly polarised component and a prominent left-hand circularly polarised component, while the right-hand component is missing entirely. In accordance with *Yearby and Smith* [1994], this suggests that the duct exit point is far away from Porojärvi. The same conclusion can be drawn from the plot of the axis ratio of the polarisation ellipse in Figure 4.1. The triggering PLHR is also seen only in the panel which shows left hand polarised power. There is even an amplitude modulation, which has quite the same periodicity as the TEs. Similar results for polarisation apply to all following examples in Figures 4.2, 4.3, and 4.4. With the Porojärvi data it is not possible to localise exactly the source or duct exit point for the VLF signals observed, which would require multiple receiving sites.

Direction finding from the orthogonal magnetic loops gives an ambiguous bearing for the power line at 3050 Hz of either north or south, and bearing for the triggered emissions of NW or SE.

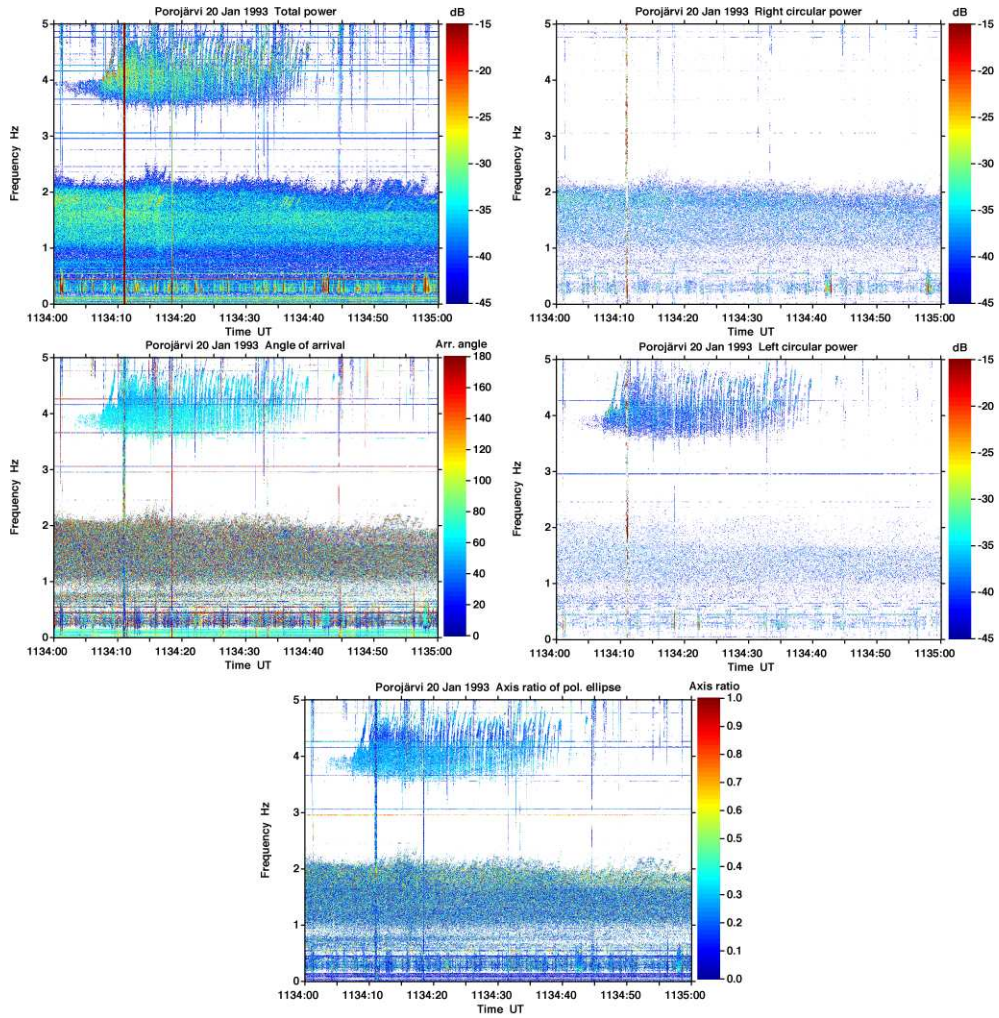


Figure 4.2: Numerous emissions triggered by pairs of PLHR at 600 Hz intervals. The doublet 3550/3650 Hz triggers short risers or even a chorus. The 3.5-5.5 kHz band contains numerous steep triggered risers. The top left panel shows total power, the top right and middle right panels present right and left circular polarised power, respectively. The horizontal angle of arrival is shown in the middle left panel, and the bottom panel shows the axis ratio of the polarisation ellipse.

Since the emissions rise to nearly 5 kHz and the equatorial electron gyro-frequency at Porojärvi would be in the region of 4 kHz it may be assumed that the duct exit point for the TEs is SE of Porojärvi, as seen in a plot of horizontal angle of arrival in Figure 4.1. The angle of arrival seems to change with frequency. This is probably due to the exit point moving with frequency, which has been studied theoretically by *Strangeways* [1981] and empirically by *Yearby and Smith* [1994] to lead to angle of arrival changes. Below 3 kHz the angle of arrival is about  $90^\circ$  (W or E) and near 5 kHz the angle is about  $45^\circ$  (NW or SE). It should be noted that PLHR signals themselves arrived from different directions than TEs. Furthermore, for ducted ELF-VLF signals to be seen on the ground it requires that signals propagated inside the plasmapause, which also points to a southern source.

Figure 4.2 shows some rather different features. There is no clear trigger, but a weak narrow band hiss, which gradually strengthens, appeared at 1134:00 UT. About 7 s later it seemed to trigger rising tones with  $\approx 0.5$  s repetition periods. The lower cutoff frequency was controlled by the strong doublet at 3550/3650 Hz. The upper cutoff was also controlled by a doublet at 4750/4850 Hz. However, the controlling PLHR is not seen in the panel of left-hand polarised power. At 1134:11 UT there is a strong spheric, which might also affect the risers.

Polarisation features are quite similar to the event in Figure 4.1, as well as the horizontal angle of arrival. Here the chorus and PLHR seem to arrive from the same direction. It should be noted that this event occurred about one minute before the event of Figure 4.1, but it has no features of the 2-hop wave bounce time.

Figure 4.3 also shows a profusion of risers triggered in the 3.5-5.5 kHz band. These risers are very steep, particularly around 3.5 kHz, and seem to show a whistler-like dispersion. It seems likely that the relevant ducts for this data example are located at a low L value ( $L < 4$ ), which would give a whistler nose frequency above 4.5 kHz and cause risers below this frequency to be steepened by dispersive propagation to the ground. The doublet 4150/4250 Hz seems to trigger a chorus-like emission consisting of a tangle of slow risers with upper cutoff at about 5100 Hz. Here only a 20 s long example of the event is shown, whose total duration was more than 5 min.

In this event PLHR is right-hand polarised, except at 2950 Hz, which seem to control the lower cutoff frequency of TEs. All triggered emissions are left-hand polarised, although they are not far from the linear polarisation. This can be seen in the plot of the axis ratio of the polarisation ellipse, where most ratios are below 0.4.

Small downward hook emissions are triggered off the lines at 3050 Hz and 3650 Hz. An interesting feature is the lengthy powerful faller at 1143:18 UT, which penetrates the hiss band, and turns upwards from 1250 Hz to be recaptured by the triggering line at 2950 Hz. The hiss band is most likely associated with another duct or L value, and will thus not degrade the nonlinear wave-particle interaction process. Emissions below 3.5 kHz come from a direction of ENE, around 4 kHz the bearing is more SSE, and emissions above 5 kHz come from due south.

The faller at 1143:18 UT is actually a hook, which has quite different features from other emissions in this example. Even if the trigger seem to be the same 3050 Hz line, which plays a very important role for other emissions, its horizontal angle of arrival is almost perpendicular to other emissions below 3.5 kHz.

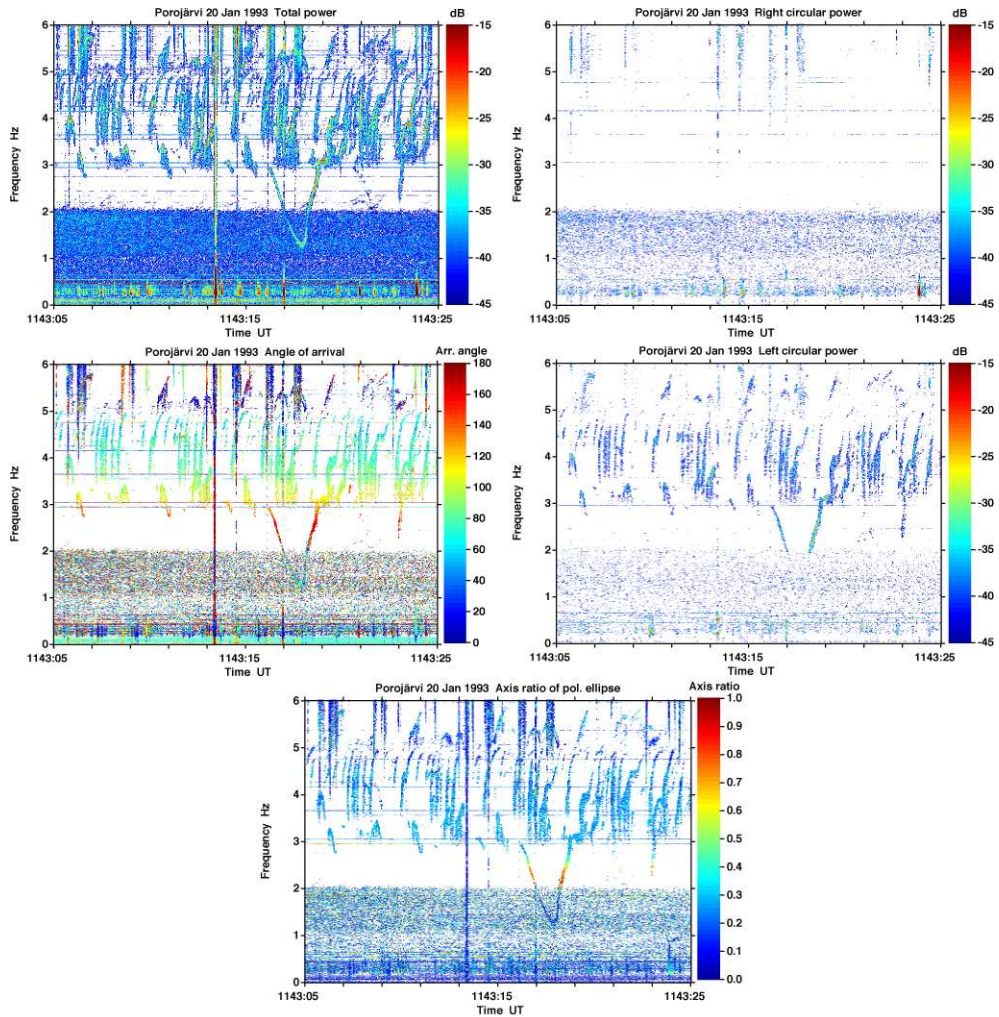


Figure 4.3: An example of PLHR-triggered risers and hooks observed at 1143 UT on 20 January 1993 at Porojärvi. Numerous emissions are triggered by pairs of PLHR at 600 Hz intervals. The doublet 2950/3050 Hz triggers short hooks and a pronounced slow upward hook. The 3.5-5.5 kHz band contains numerous steep triggered risers. Note the very prominent hook below 3 kHz.

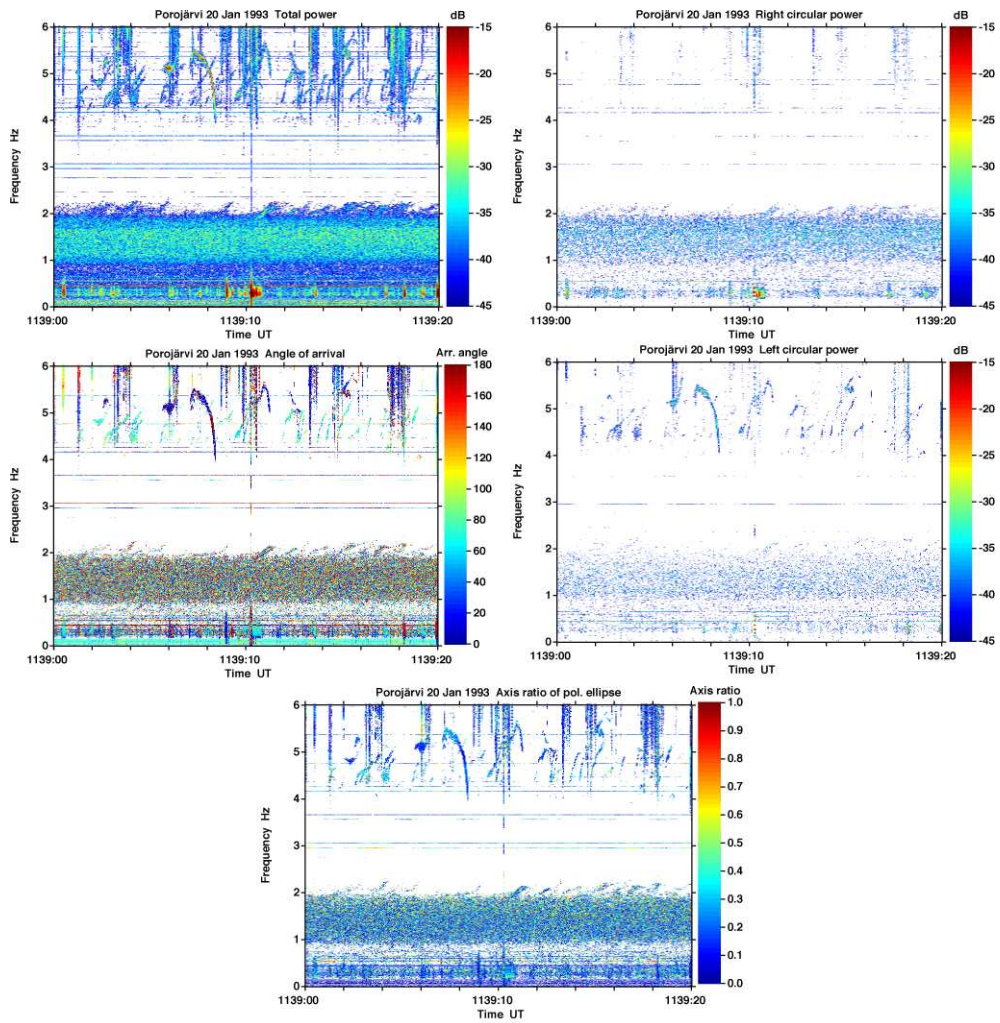


Figure 4.4: A variety of discrete PLHR-triggered emissions in the band 4-6 kHz at 1139 UT on 20 January 1993 observed at Porojärvi. Risers predominate, but there are a number of fallers and downward hooks.

The part of the hook above the hiss band has left-hand polarisation, while the part inside the hiss band has linear polarisation. In principle, this lower part could be thought of being overlapped by hiss emission, but the hook is much more intense than the hiss.

When looking at the axis ratio of the polarisation ellipse, it appears that the hook has a ratio of 0.6 or more at frequencies of 2-3 kHz. This means that a certain part of the hook has nearly circular polarisation, and thus, comes from near the zenith.

Figure 4.4 shows scattered emissions triggered by lines in the 4.5-6.0 kHz band. Risers predominate, but there are some fallers and a few downward hooks. The most prominent feature is the strong slow faller at 1139:07 UT, which is triggered at 5350 Hz and descends to 4.0 kHz in about 2 s.

However, the risers change their horizontal angle of arrival with frequency, but the strong faller retains its angle of arrival between 5.5 and 4.0 kHz. All these emissions appear to come from a southerly or SE direction. One interesting feature is that the most probable trigger of risers (4250 Hz line) has right-hand polarisation, although all emissions appear only in left-hand polarisation.

One nonlinear phenomenon is ‘capture’: a riser triggered by the lower hiss band is temporarily captured by the 2 lines at 2950/3050 Hz. The emissions below 3.5 kHz appear to have a bearing of ESE, while the higher frequency emissions at 4 kHz come from a SSE direction. The event occurred at 1141 UT and is not shown here.

## 4.5 Special Features of PLHR

In the northern parts of Norway, Sweden, Finland and Russia (Kola Peninsula) a lot of electric power is produced, consumed and transferred at L values between 4 and 7. The conjugate areas (Indian Ocean) are, as a source region, practically empty. Similar situations, but at lower L values, can be found, e.g., on the west coast of the USA (Seattle), India, and New Zealand.

The nominal frequency of local AC power line systems may vary a little (within an allowed tolerance, which is  $\pm 0.1$  Hz in Scandinavia). The harmonics may, as a consequence, deviate in frequency from the nominal value by, e.g.,  $\pm 5$  Hz (frequency dependent). The frequency difference of two neighbouring lines is approximately the nominal frequency. Although the frequency of PLHR varies approximately 0.2%, i.e.  $\pm 0.1$  Hz at 50 Hz, some ELF-VLF transmitter signals are much more accurate.

An example is given in Figure 4.5, where the harmonics of the Russian ELF transmitter *Zevs* (69° N, 33° E, NE of Murmansk, Kola Peninsula) are shown for 20 January 1993 at 0541-0551 UT and 0558-0600 UT. The transmitted frequency of *Zevs* is 82 Hz, and it has been observed as far away as at the Arrival Heights base in Antarctic (78° S, 167° W). In the early 1990s, there was no frequency modulation observed in ELF-VLF data recorded in Finland.

In this particular case, although the location of the source is known (see Figure 4.6), the horizontal angle of arrival depicts a variety of angles, showing mostly S and SE directions. The plots of the circular polarisations show very little power at the frequencies of the transmitter harmonics. Furthermore, the axis ratio of the polarisation ellipse shows the signals being almost linearly polarised.

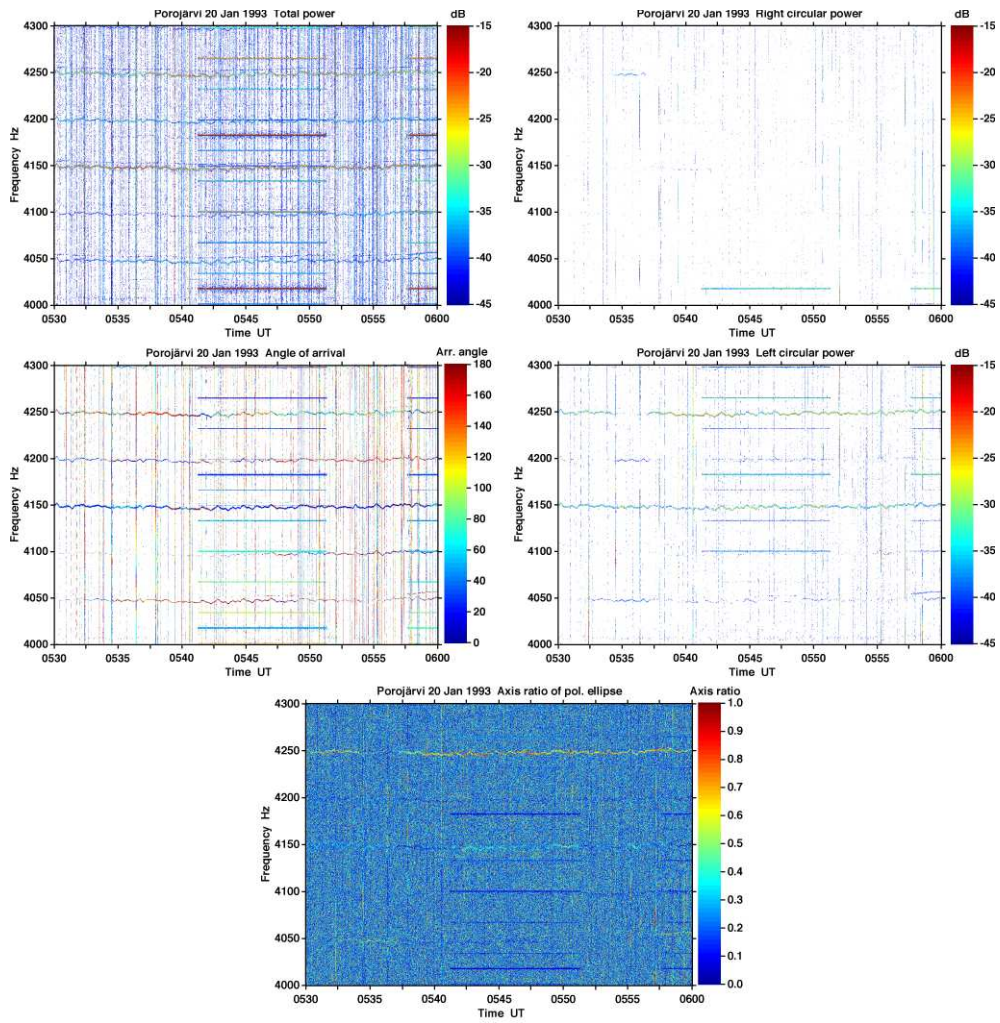


Figure 4.5: Frequency-time-power diagram of a few power line harmonics and signals created by the Russian 82 Hz ELF-transmitter Zevs showing that the recording system does not create the variation seen in PLHR.

The accuracy of the 82 Hz harmonics must be due to crystal-controlled frequency stabilisation or based on an atomic clock. These harmonics were observed during the campaigns in January 1993, November 1993, October 1994, and September-October 2005, but in November 1995 they were not observed. The harmonics, with a new modulation, appeared during our campaign in January 1997. Then Zevs was making use of a carrier with minimum shift keying, MSK. This type of transmission mode is in use by nearly all modern submarine-communication VLF-band transmitter facilities. The frequency shifts within the narrow frequency range from 81 Hz to 83.3 Hz, i.e. the carrier shifts only 2.3 Hz.

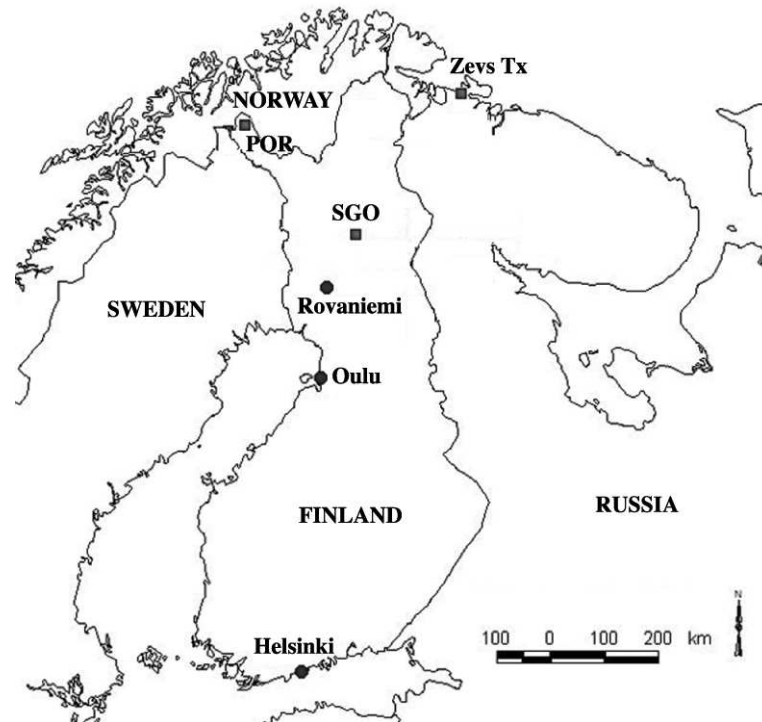


Figure 4.6: A map showing the locations of the Porojärvi ELF-VLF receiver, the Russian Zevs transmitter, SGO, and a few Finnish towns.

The transmitter consists of two swept-frequency generators and two parallel horizontal grounded feedlines, each about 60 km long, which forms a long horizontal electric dipole, oriented in an approximate east/west (EW) direction. The generators provide 200-300 A currents in the feedlines, in the frequency range from 20 Hz to 250 Hz. The actual antenna is the Earth itself. By building the antenna at a location with a poor effective conductivity of the ground, and by grounding the ends of the feedline, the signal is forced deep down into the Earth, making the Earth itself the effective radiating element.

The reasons why we were detecting the harmonics of 82 Hz at Porojärvi are more

likely the distance to Zevs (about 400 km) and the fact that the Zevs' antenna construction is producing lots of harmonics.

The carrier frequency is shifted from the normal carrier frequency of 82 Hz down to 81.6 Hz and then up to 82.7 Hz prior to the message. This is most likely the message waiting call function. The message itself consists of several frequencies between 81 Hz and 83.3 Hz.

The Russian Zevs transmitter has also been used for geophysical research, e.g. the Earth Crust Research Institute from St. Petersburg and the Geological Institute of the Kola Science Centre have used it for electromagnetic sounding and monitoring the Earth's crust at frequencies of 31-166 Hz in 1994. Later the Zevs transmitter has been used in various research projects with its nominal frequencies.

The (strong) power line control signals at some frequencies seem to follow the frequency variation of neighbouring PLHR (see Figure 4.7). These control signals are used for the remote control of tariff changes and clocks. The frequencies transmitted along the 20 kV power lines are mainly 3025 Hz and 4825 Hz. When the electricity meters are read remotely, also 3275 Hz and 4575 Hz are transmitted (not used in northernmost Finland). Due to the fact that the electricity meters are not immediately ready to receive the control signals, they must be transmitted several times within about half an hour. There are so-called wake-up signals before the main signal as well as confirmation signals afterwards.

The busiest times are around 0700 LT and 2200 LT, which corresponds to 0500 UT (0400 UT, summer time) and 2000 UT (1900 UT), respectively. Always both frequencies (3025 and 4825 Hz) with the same 'message' are transmitted by every transformer station. The average distance between the transformer stations is about 60 km. Therefore, one ELF-VLF receiver will receive the control signals transmitted by several stations. Signals of different origin can be distinguished by the angle of arrival.

Figure 4.7 presents a control signal at 4825 Hz on 17 February 2004 observed at Pittiövaara near the observatory. The total duration of the signals was almost 20 min, and they nearly saturated the receiver 16 times for 18 s. They had a tiny component of right-hand polarisation, but mostly they were linearly polarised, whereas the PLHR at 4850 and 4950 Hz were strongly circularly polarised. The horizontal angle of arrival shows different direction for control signals from PLHR. Of course, it should be considered that the signal level might be too high, and the saturation may cause wrong results.

There is another interesting feature in Figure 4.7, which covers 30 min of data in the frequency range of 4750 to 5000 Hz. Namely, the PLHR is linearly decreasing in frequency approximately by 10 Hz in 30 min. There are also a few harmonics of Zevs transmitter signals at 0700-0704 UT, as well as at 0727-0730 UT. They all seem to come from E-NE.

In the Nordic countries the power line systems are often phase locked, but this does not guarantee a constant frequency at any instant in time. Thus many parts of our sky can be illuminated by "independent" PLHR signals, which do not have the same frequency. Thus frequency differences of, e.g., 47, 50, 53 Hz as well as 3 and 6 Hz can be present in the same "whistler-mode propagation" duct around the same PLHR frequency simply because of source properties. More complicated possibilities are easy to imagine.

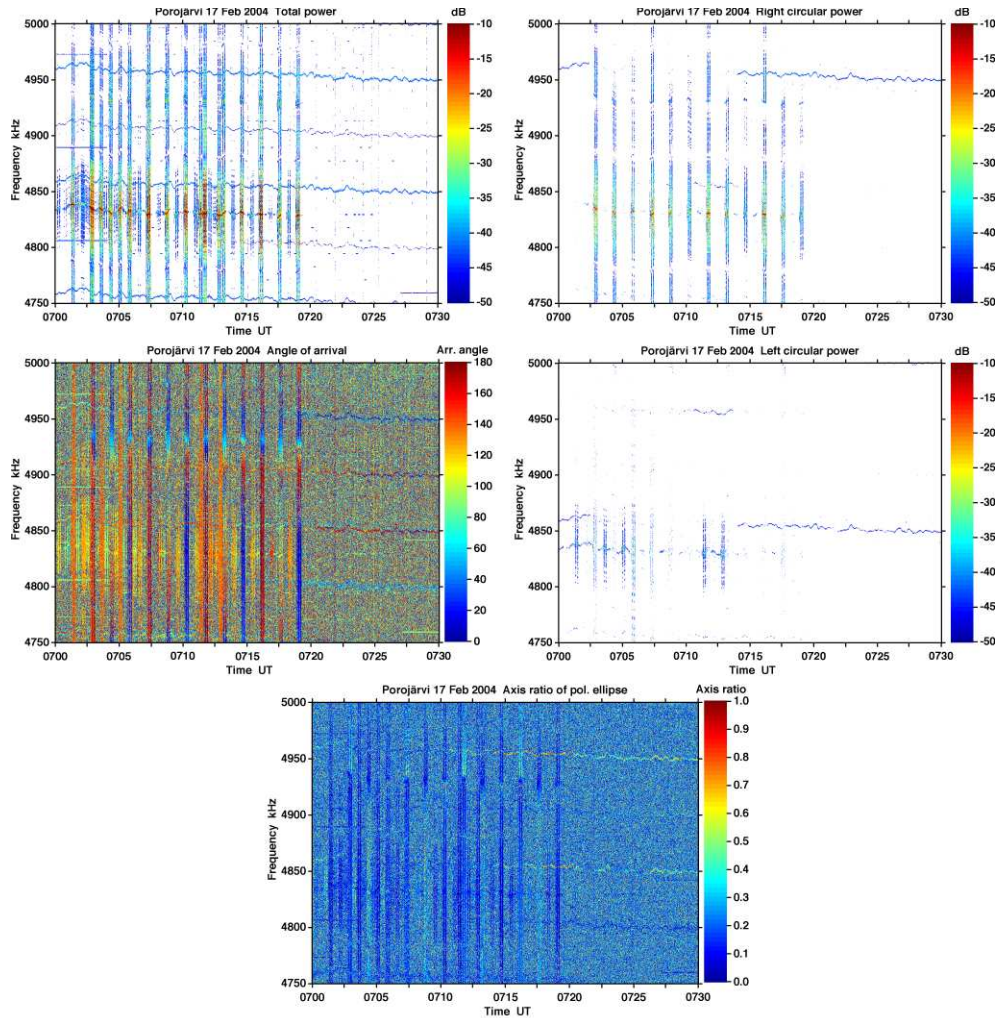


Figure 4.7: Very high order of power line harmonics of 50 Hz measured in a very noisy place. The nominal and measured frequency can deviate by more than 10 Hz. Vertical bars are caused by power line control system signals using phase modulation. The carrier seems to follow the PLHR frequency variation.

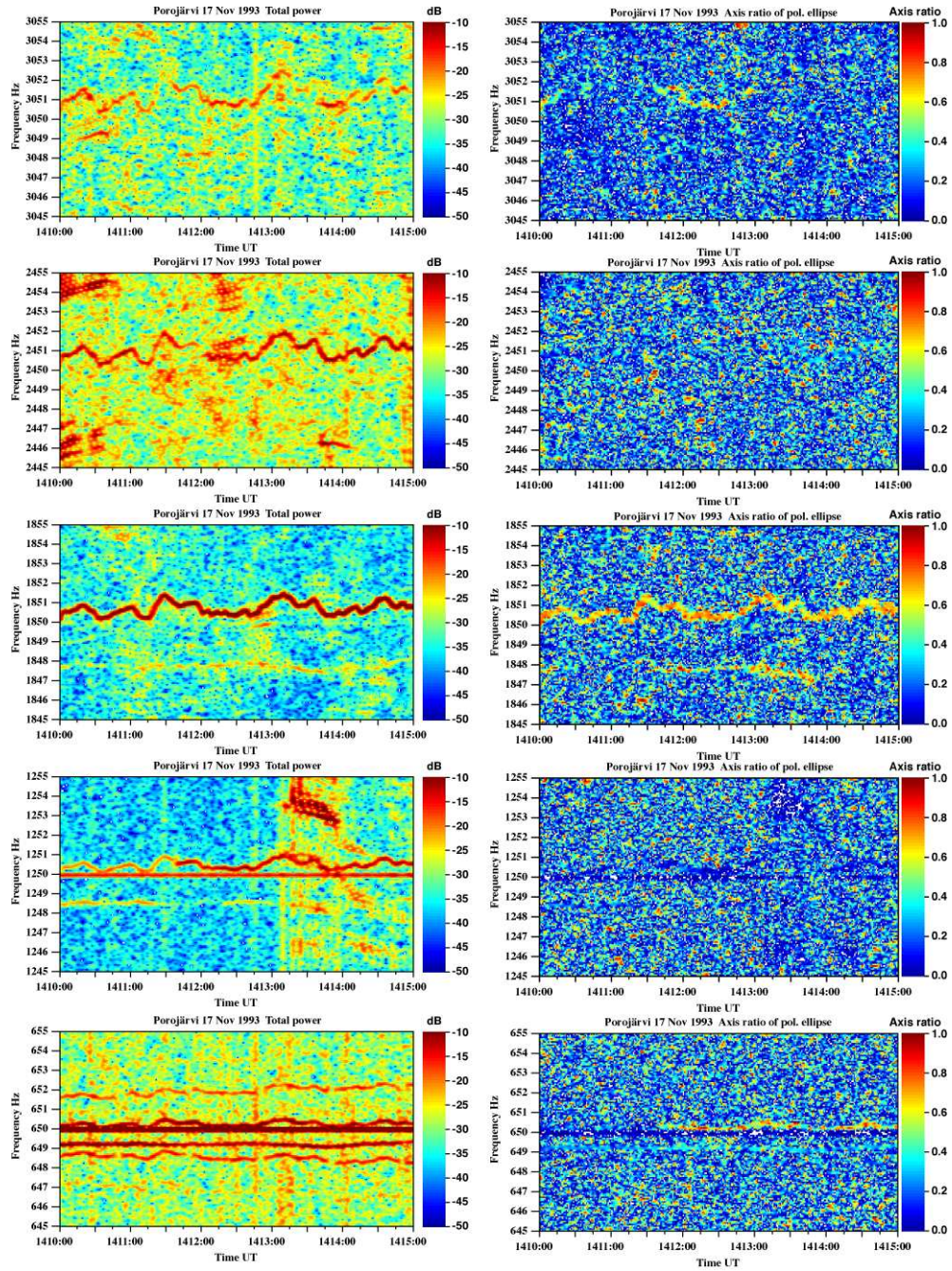


Figure 4.8: Five PLHR at 650, 1250, 1850, 2450, and 3050 Hz were observed on 17 November 1993 at Porojärvi. These PLHR frequencies are the upper ones of the doublets. The left panels are total power plots and the right panels present the axis ratios of the polarisation ellipses. Especially the lines at 650, 1250, and 1850 Hz were accompanied by weaker lines with separation of a couple of Hz. Sometimes these ‘side lines’ have the same frequency behaviour as the main line (bottom left panel), but often they are varying differently (other panels). Sources at different frequencies are probably in Finland, Sweden and Norway.

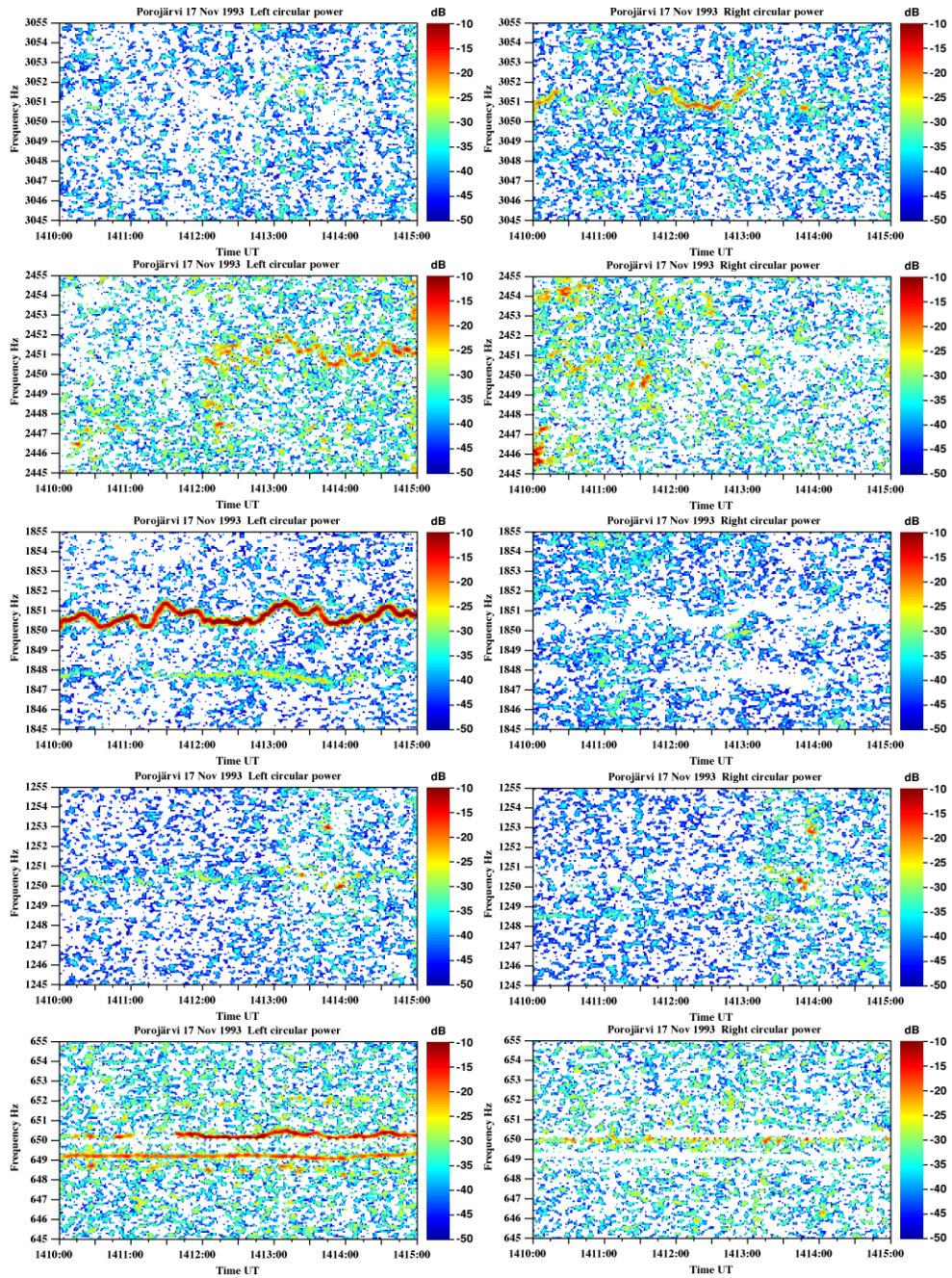


Figure 4.9: Same event as in Figure 4.8, but here the left panels show the left-hand circular power, and the right panels show the right-hand circular power. See the difference of the polarisation at different frequencies.

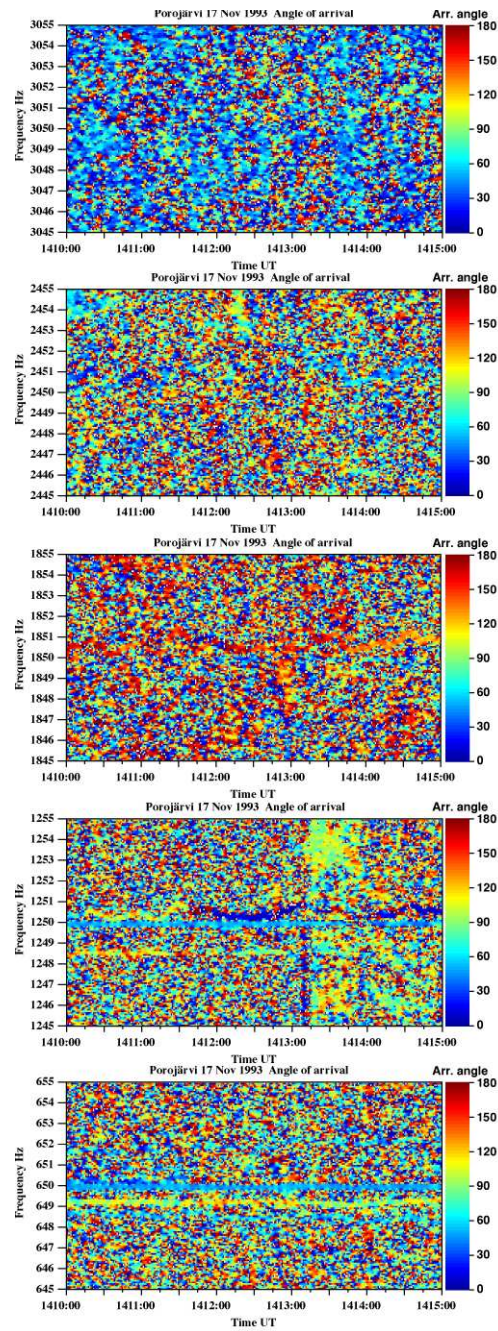


Figure 4.10: Same event as in Figures 4.8 and 4.9, but here the horizontal angles of arrival are shown. See the difference of the angles of different ‘side lines’.

Figures 4.8–4.10 show five PLHR frequencies at 650, 1250, 1850, 2450, and 3050 Hz, observed at 1410–1415 UT on 17 November 1993 at Porojärvi. These PLHR frequencies are the upper ones of the doublets (see Equation 4.1). The frequency of the ‘main’ harmonics varies by about 1%, i.e. the fundamental frequency varies in the range of  $50 \pm 0.5$  Hz. However, the lines at 650, 1250, and 1850 Hz were accompanied by weaker ‘side lines’ with separations of a couple of Hz. Sometimes these ‘side lines’ have the same frequency behaviour as the main line (see the panel of 650 Hz), but often they vary differently (see other panels). Sources at different frequencies are probably in Finland, Sweden and Norway.

The left panels in Figure 4.8 show total power plots and the right panels present the axis ratio of the polarisation ellipses. Figure 4.9 shows the right-hand and the left-hand circular powers. There is a difference of the polarisation at different frequencies, e.g. 650, 1850, and 2450 Hz are left-hand polarised, while 3050 Hz is right-hand polarised. The horizontal angles of arrival are presented in Figure 4.10. There are some interesting features, like the 1850 Hz line changes the angle from S to W, and the ‘side lines’ of 1250 Hz and 650 Hz have a remarkable difference in the angles (from N to W).

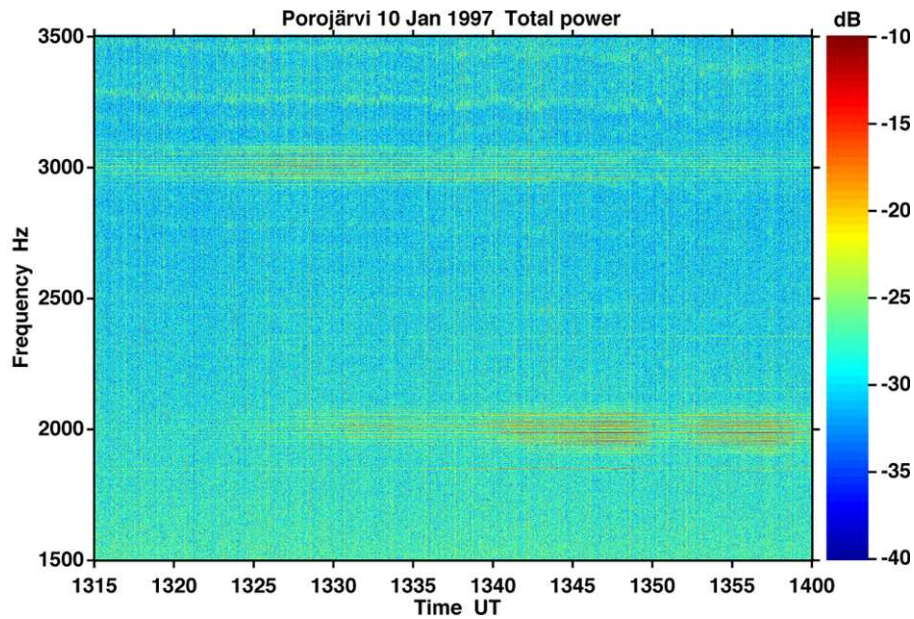


Figure 4.11: Peculiar bands with a bunch of lines were observed around 2000 Hz and 3000 Hz at 1315–1400 UT on 10 January 1997 at Porojärvi. The whole event lasted for 9.5 hours, from about 1130 UT to about 2100 UT.

The lines with exact frequencies of 650 Hz and 1250 Hz are strange, because there are no lines with exact frequencies at 1850, 2450, and 3050 Hz. These lines are linearly polarised, but their source is unknown.

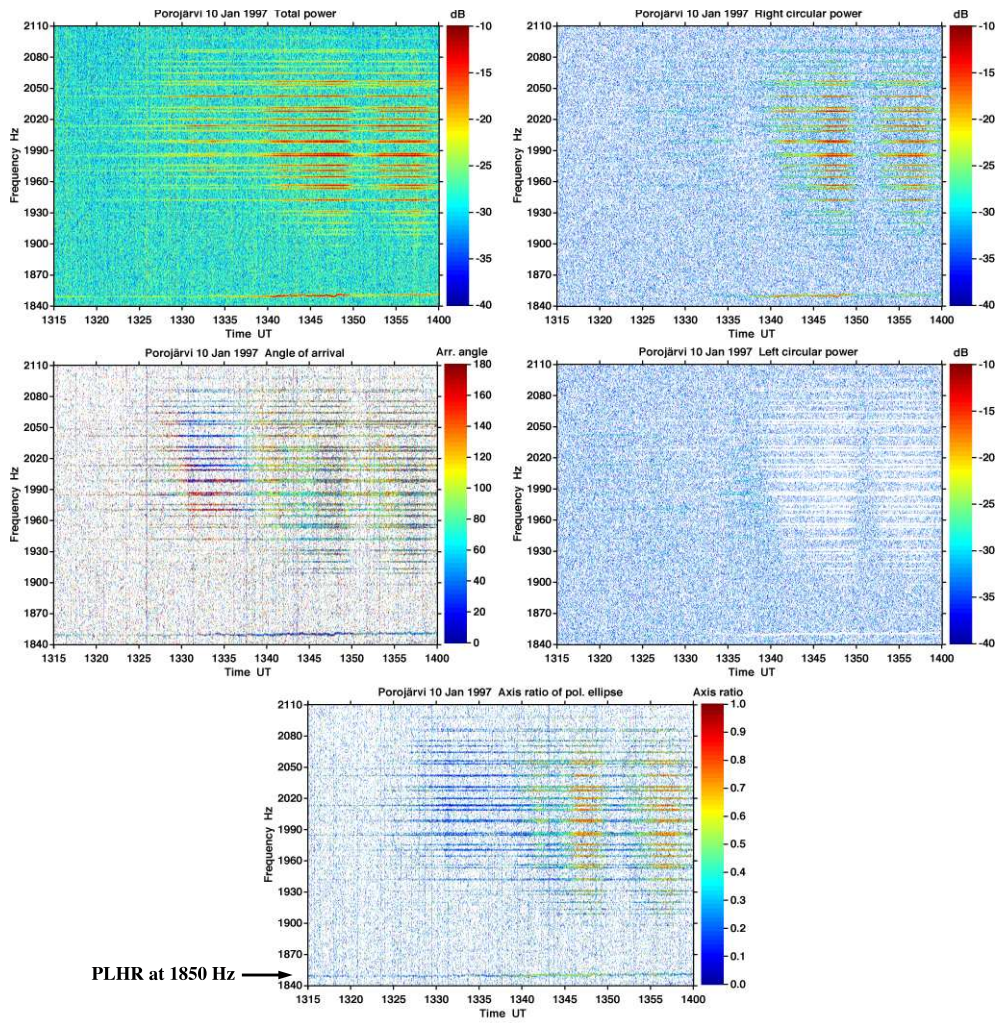


Figure 4.12: Magnification from Figure 4.11: fine structure of the lines around 2000 Hz. Note the PLHR at 1850 Hz. The prominent line structure is more stable in frequency than the PLHR.

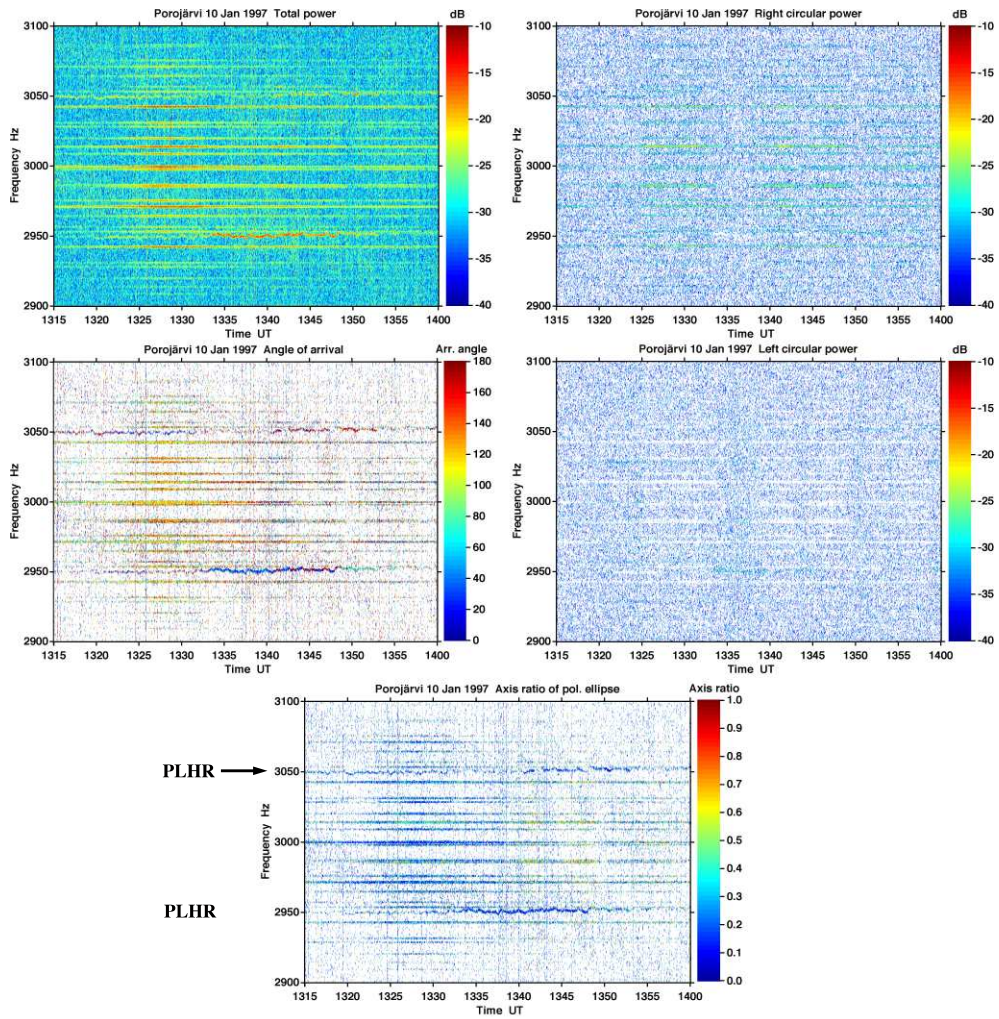


Figure 4.13: Magnification from Figure 4.11: fine structure of the lines around 3000 Hz. Note PLHR lines at 2950 and 3050 Hz. The variation of PLHR frequencies excludes a direct relation between PLHR and ‘straight lines’.

Figure 4.11 shows an example of two peculiar bands with a bunch of lines around 2000 Hz and 3000 Hz observed at 1315-1400 UT on 10 January 1997 at Porojärvi. These bands started at about 1130 UT (around 3 kHz) and at about 1205 UT (around 2 kHz). The event ended at about 2100 UT. The upper band ended already at 1900 UT. The lower band was stronger for most of the time. The intensity of both bands grew first gradually, but it varied between the threshold of detection and the strongest signal of that time interval. Usually the intensification occurred at different time in these bands.

Fine structures are seen in Figures 4.12 and 4.13. There were three intensification at 1331-1335 UT, 1340-1350 UT, and 1353-1359 UT in the frequency band of 1900-2060 Hz. The second intensification occurred also in the PLHR line at 1850 Hz. The ‘straight lines’ were not equally spaced, on the average there were 30 lines between 1900 Hz and 2100 Hz. All lines were right-hand or linearly polarised. The angle of arrival showed that signals came from all directions. However, all lines in a bunch changed their direction of arrival simultaneously, which suggests a moving source.

Figure 4.13 presents frequencies of 2900-3100 Hz. There was one intensification at 1325-1333 UT. One doublet at 2950/3050 Hz is also visible. There were 27 lines between 2900 Hz and 3100 Hz. The lines were mostly linearly polarised with a weak right-hand part. The horizontal angle of arrival shows strongly western direction at the time of the most intense signals. In this case, the PLHR doublet came from a different direction compared to the ‘straight lines’.

Similar bands occurred also on 11 January 1997 at 0320-0325 UT and 1410-1430 UT. It seems that there was no other ELF-VLF activity during these times.

Many questions remain unanswered. For instance, maybe it was a transmitted signal either within the power line system or independent from it? Was it some local disturbance? A physical interpretation seems not to be straightforward at all.

#### 4.5.1 Spectra of PLHR

The detailed high-resolution spectra around a single PLHR line may show very complicated features with a lot of individual separate lines. One reason is the continuous frequency and amplitude variation of a single power line harmonic signal or a group of power line harmonics from separate sources. Also the effects created by an AD conversion of a very low level signal, possible effects of nonlinearities in the measuring process etc. must be considered.

The upper panels in Figures 4.14, 4.15, and 4.16 show the power spectra in the frequency range of 0-6000 Hz, while the lower panels and Figure 4.17 show power spectra in the frequency range of 4000-4300 Hz, 4000-5000 Hz, or 4449-4551 Hz.

Figure 4.14 shows the PLHR power spectrum, which was observed on 20 January 1993 at about 0545 UT at Porojärvi. The spectrum was integrated over one minute in order to reduce the background noise. The upper panel presents the whole frequency range up to 6000 Hz with a spectral resolution of 0.61 Hz. Most of the intense lines were Zevs transmitter signals (see the Section 4.5 and Figure 4.5). The lower panel presents the same frequency range as shown in Figure 4.5. Black arrows show PLHR frequencies at 4050, 4100, 4150, 4200, and 4250 Hz. The peaks of 4018, 4100, 4182, and 4264 Hz came from the Zevs transmitter, i.e. they are harmonics of 82 Hz.

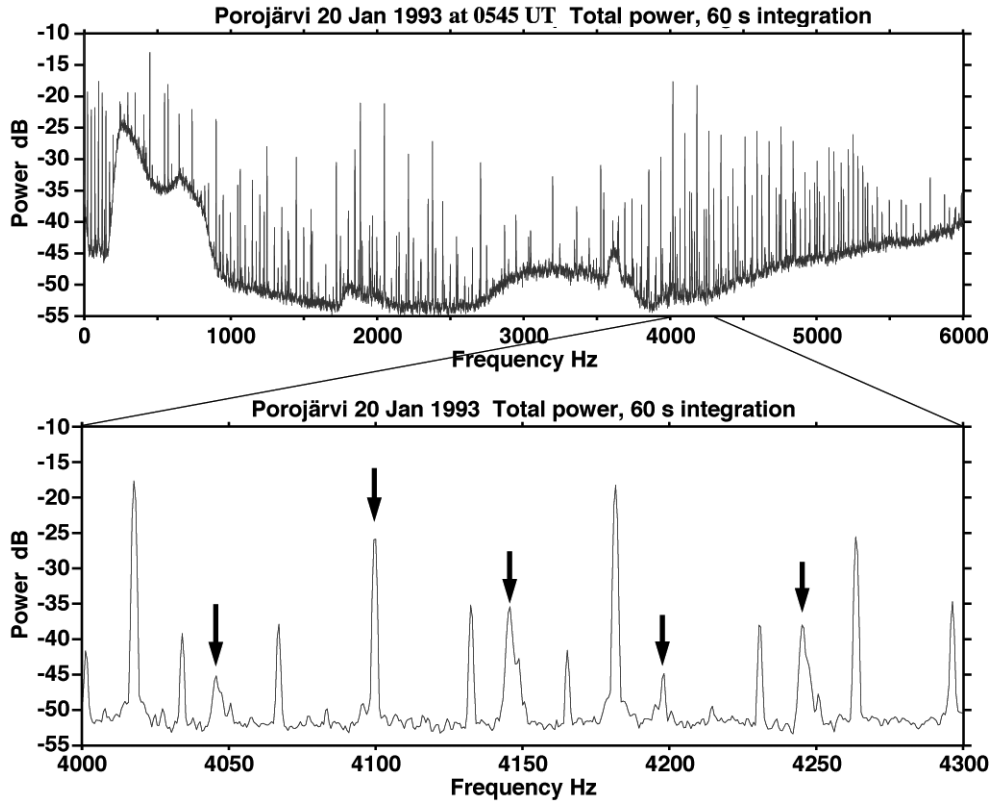


Figure 4.14: PLHR power spectrum on 20 January 1993 was observed at about 0545 UT at Porojärvi. The spectrum was integrated over one minute. The upper panel shows the frequency range of 0-6000 Hz with a spectral resolution of 0.61 Hz. Most of the intense lines were Zevs transmitter signals. The lower panel presents the same frequency range as shown in Figure 4.5. Black arrows show PLHR frequencies at 4050, 4100, 4150, 4200, and 4250 Hz. The peaks of 4018, 4100, 4182, and 4264 Hz came from the Zevs transmitter.

Figure 4.15 presents the PLHR power spectrum, which was observed on 7 January 1997 at about 1640 UT at Porojärvi. The spectrum was integrated over one minute. The upper panel shows the frequency range of 0-6000 Hz with a spectral resolution of 0.61 Hz. The lower panel presents the frequency range of 4000-5000 Hz, which is mostly contaminated by the Zevs message transmission for which frequencies between 81.0 Hz and 83.3 Hz were used. The PLHR lines are hardly seen.

Sometimes, we really see plasma physical processes, i.e. the PLHR has entered the near space and the wave returns with signatures from those processes. Figures 4.5-4.13 show a lot of spectral lines in the ELF-VLF band. The lines seem sometimes to have “mysterious” relations to PLHR frequencies. The reason is that PLHR originated from different countries or they were not PLHR.

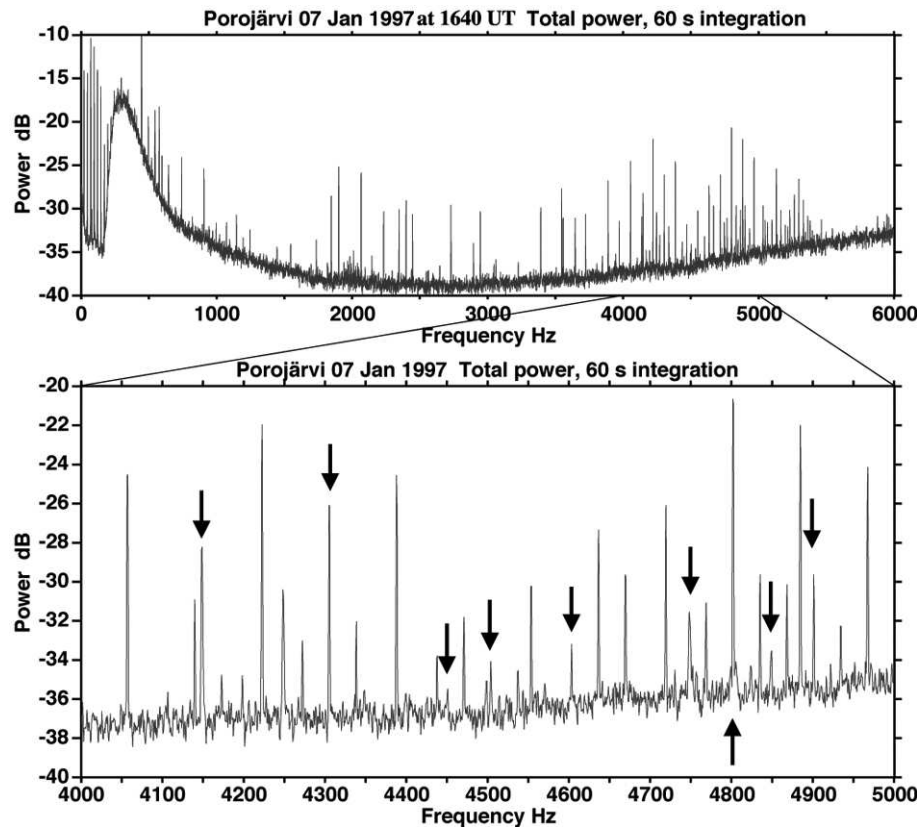


Figure 4.15: PLHR power spectrum on 7 January 1997 was observed at about 1640 UT at Porojärvi. The analysis parameters are the same as in Figure 4.14. The lower panel presents the frequency range of 4000-5000 Hz. The PLHR lines are hardly seen, but black arrows show PLHR frequencies at 4150, 4300, 4450, 4500, 4600, 4750, 4800, 4850, and 4900 Hz. The strongest peaks are due to the Zevs transmitter sending a the message for which frequencies between 81.0 Hz and 83.3 Hz were used.

Figure 4.16 is the same as Figure 4.15, but the spectrum was integrated over ten minutes. Thus the peaks of the Zevs transmitter are much weaker, because one transmission frequency was used only for a very short time compared to the integration time of 600 s. Also PLHR lines are weaker, but wider due to frequency variation during integration time (see, e.g., Figures 4.8-4.10). On the other hand, the number of the peaks is much higher than in the previous Figures 4.14 and 4.15.

During magnetically quiet periods like on 7 January 1997, the number of detected PLHR lines as well as the Zevs transmitter signals was very high. In night-time the number of lines is much smaller due to stronger sferics above 2 kHz. A similar situation is met during magnetically disturbed time, when other ELF-VLF events are stronger and they can mask PLHR lines in the spectrum.

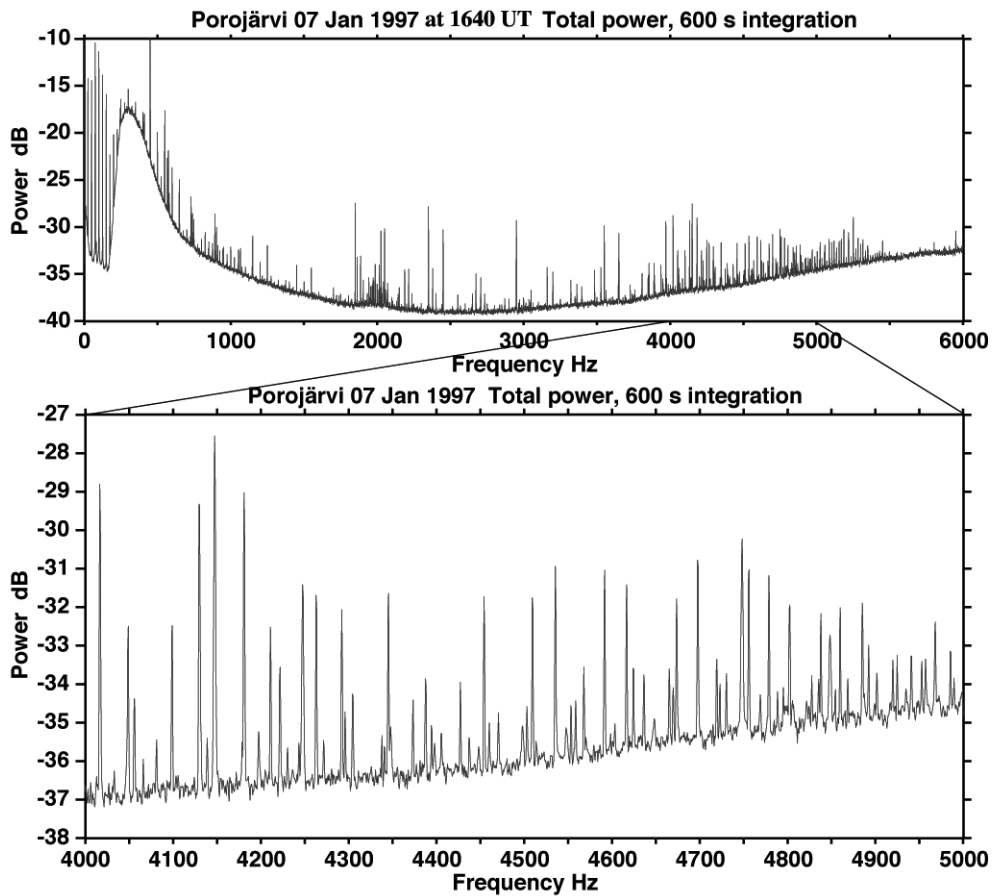


Figure 4.16: Same as in Figure 4.15, but the spectra were integrated over ten minutes. Now the peaks are much weaker, because each frequency of the Zevs transmitter was used only for a very short time compared to the integration time. On the other hand, the number of the peaks is much higher than in Figure 4.15. Long integration makes also all PLHR lines detectable.

Of course, sometimes magnetic activity can enhance PLHR events. A few of such enhanced PLHR events (EPE) were observed during the September-October 2005 campaign. They certainly require more investigation, before we can understand them properly.

Figure 4.17 presents one case, where PLHR peaks were very weak, but spread by several Hz. The stronger peaks are the harmonics of the Zevs transmitter, e.g. 4455 Hz is equal to  $55 \times 81$  Hz, 4510 Hz is equal to  $55 \times 82$  Hz, and 4536 Hz is equal to  $56 \times 81$  Hz. The transmitter signals were much more monochromatic than PLHR lines.

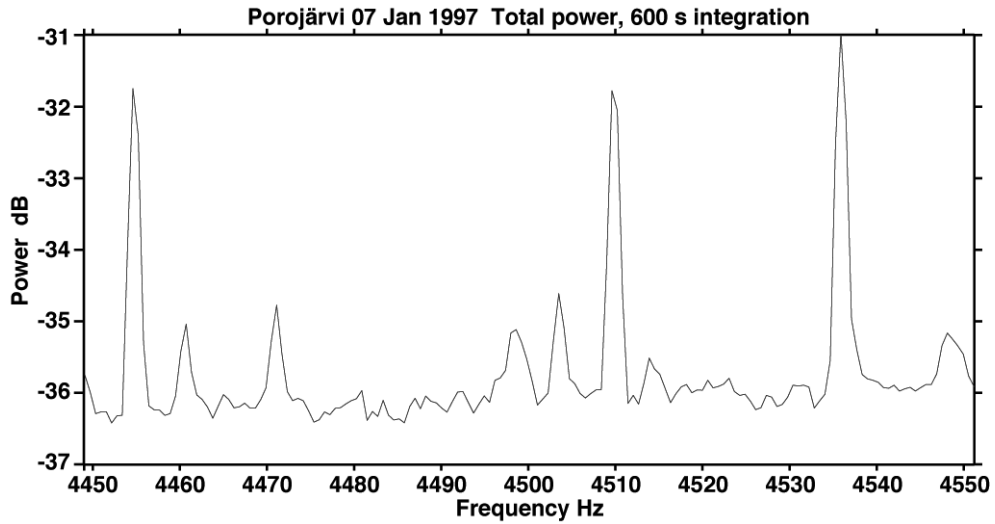


Figure 4.17: Same as in Figure 4.16, but showing the frequency band of 4449-4551 Hz. PLHR lines were very weak, but spread by several Hz. The stronger peaks are the harmonics of the Zevs transmitter, e.g. 4455 Hz is equal to  $55 \times 81$  Hz, 4510 Hz is equal to  $55 \times 82$  Hz, and 4536 Hz is equal to  $56 \times 81$  Hz. The transmitter signals were much more monochromatic than PLHR lines.

## 4.6 Discussion

The studies of PLHR have an impressive history beginning with *Helliwell et al.* [1975]. However, there are many interesting but still unknown features related to PLHR. Figures 4.1-4.4 depict PLHR-triggered emissions, which clearly show a left-hand polarisation. This feature has not been published except for conference presentations. There is no comprehensive theoretical explanation for such behaviour, yet, although a few studies of left-hand polarised ELF-VLF waves exist [*Lundin*, 1979, 1983, 1985; *Yearby and Smith*, 1994; *Lundin and Krafft*, 2002].

By left-hand polarisation we mean that the horizontal component of the wave field vector  $\mathbf{B}$  rotates clockwise when looking towards the source. This definition of the sense of polarisation is relative to the downward vertical at the receiver, i.e. it is defined with respect to the direction of the magnetic field, and is therefore opposite in the southern hemisphere.

According to the magneto-ionic theory, the left-hand mode cannot propagate in the magnetosphere in whistler-mode, but obviously the emissions in Figure 4.1 have bounced between the hemispheres. This supports the idea that the propagation in the magnetosphere is right-handed but some kind of conversion of the propagation mode, e.g., in the ionosphere or during the propagation from the ionospheric exit point to the receiver causes the change of the polarisation, as *Yearby and Smith* [1994] proposed.

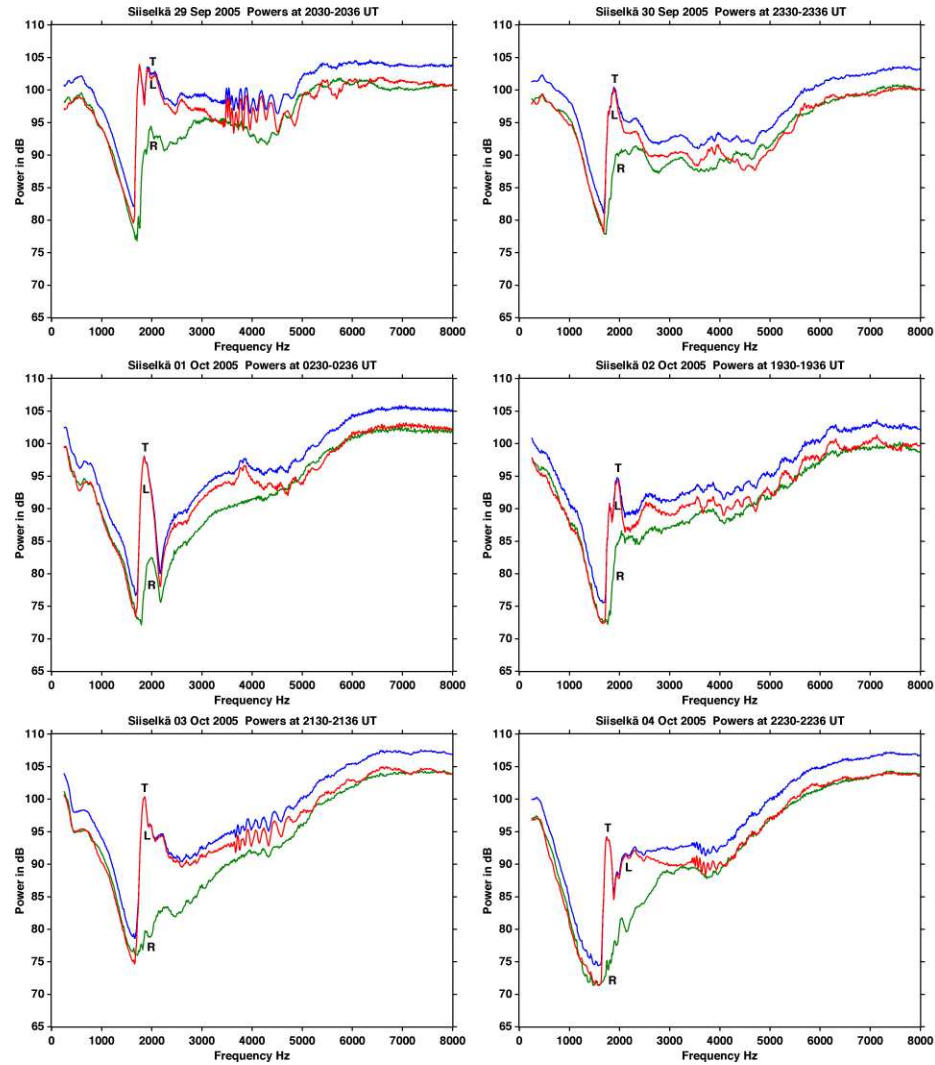


Figure 4.18: Integrated power over 6 minutes from 6 different nights observed during the September-October 2005 campaign. All spectra present night-time sferics. T, L, and R mean total (blue curve), left-hand (red curve), and right-hand (green curve) powers, respectively. The cutoff of mode 1 of sferics propagation is near 2 kHz. The enhanced peak just above the cutoff is most probably due to tweaks. Interestingly, the frequencies between the cutoff and  $\approx 5$  kHz show left-hand polarisation. Note that L and R mean the elliptically left-hand and right-hand polarised part of the total power, i.e. they include also linear power ( $T=L+R$ ).

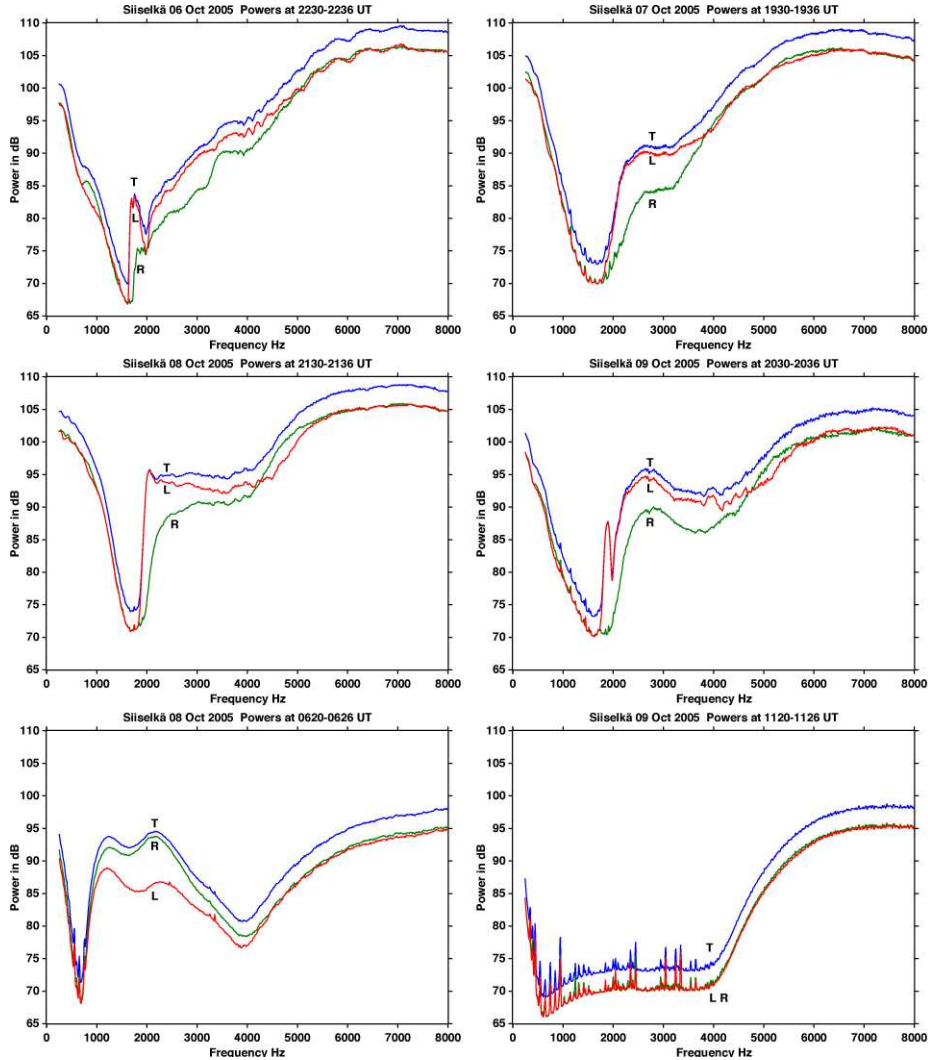


Figure 4.19: Four additional nights showing similar features as in Figure 4.18. The lowest left panel shows an example of morning chorus, which is clearly right-hand polarised. The lowest right panel shows a daytime quiet example, which is purely linear polarised, which is seen from left-hand and right-hand powers, which are equally intense. Note that L and R mean the elliptically left-hand and right-hand polarised part of the total power, i.e. they include also linear power ( $T=L+R$ ).

The response of the Earth-ionosphere wave-guide for the sources covering a wide area can be tested by using sferics. The sferic waveforms radiated from lightning and received at long distances from the source stroke contain a great deal of information about the state of the ionosphere along the propagation path. *Cummer* [1997] has developed techniques to use sferic observations to determine the characteristics of the ionosphere and lightning.

During the September-October 2005 campaign, the UEV2300 receiver was not saturated by sferics. That allows us to investigate the polarisation behaviour over a wide frequency band. Figures 4.18 and 4.19 show a series of night-time observations of sferics, which have propagated in the Earth-ionosphere wave-guide over a long distance. There are the cutoff of mode 1 (or  $TE_1$  or  $TM_1$  mode) of sferics propagation near 1.7 kHz [see *Volland*, 1995, for details] and the enhanced peak just above cutoff is most probably due to tweaks.

Interestingly, the frequencies between the cutoff ( $\approx 1.7$  kHz) and  $\approx 5$  kHz show left-hand polarisation, but at higher frequencies the polarisation is linear. Just above the cutoff the sferics are almost circularly left-hand polarised and they become more elliptical with the increasing frequency. Usually they have been supposed to be linearly polarised regardless of the frequency. It might be so that this is the very first observation of the polarisation of sferics.

As seen in Figures 4.18 and 4.19 the effect is not marginal, but the difference between L and R polarisation can be more than 20 dB. It should be noted that the vertical scale shows the power in dB, which means that -3.16 dB is equal to a factor of 0.5. If both L and R powers are 3.16 dB below total power ( $L=0.5T$  and  $R=0.5T$ ), the wave must be linearly polarised. In other words, always  $T=L+R$ .

The imbalance between L and R polarisation is significant up to  $\approx 5$  kHz. This covers the whole frequency range, where left-handed PLHR-triggered emissions were observed. If the polarisation of the PLHR-triggered emissions is produced by propagation in the Earth-ionosphere wave-guide, an immediate question arises: how are non PLHR-triggered waves influenced by this propagation? The chorus observed at  $L \approx 5$  occurs mainly below the mode 1 cutoff, where only the mode 0 (or TEM or  $TE_0$  or  $TM_0$  mode) can propagate.

Chorus is related to geomagnetic activity and particle precipitation, which means that the lower ionosphere is disturbed. Figure 4.3 shows one peculiar hook, which was very strong and covered the frequency range of 1.2-3.0 kHz. Its polarisation was left-handed down to 1.8 kHz and below that the polarisation was linear, while the continuous hiss band below 2 kHz was right-handed.

The strength of the hook was very steady in the whole frequency range. The axis ratio of the polarisation ellipse had very low values between 1.2 and 1.8 kHz, which supports the linear polarisation. The axis ratio increased suddenly to close to unity at the frequency of 2.1 kHz, and above that the polarisation became elliptic. The behaviour of the hook was consistent with sferics shown in Figures 4.18-4.19. Similar features can be found in Figures 4.8-4.9 where the 1850-Hz PLHR line was almost circularly left-hand polarised.

An assumption that the wave would be left-hand polarised already above the ionospheric exit point is difficult and unlikely. So far, no left-hand polarised ELF-VLF waves were observed by satellite. If the mode conversion from the right-hand to

the left-hand polarisation occurs in the Earth-ionosphere wave-guide, it is easier to understand, e.g., the behaviour of the polarisation of the above-mentioned hook.

All sferics have encountered several reflections both on the ground and in the ionosphere. After several reflections different polarisation modes encounter selective losses and the left-hand polarisation becomes dominant as seen at the receiver on the ground. The possible loss mechanisms do not include only absorption, but part of the wave energy may leak into the ionosphere and then to the magnetosphere.

*Shimakura et al.* [1986] studied a linear relationship between the polarisation and dispersion of whistlers recorded at a mid-latitude station Moshiri (L=1.59) in Japan. They found nearly circular polarisation for whistlers with the ionospheric exit point near the station, and nearly linear polarisation for whistlers with propagating paths far from the station. They did not report whistlers with left-hand polarisation.

*Ohta et al.* [1989] studied low latitude whistlers received at Yamaoka Observatory (L=1.22) in Japan. Also they did not report left-hand polarisation.

The main conclusions of *Yearby and Smith* [1994] are that the left-hand polarisation could be due to the whistler exit point position changing with frequency, and some whistlers having the exit points well to the north or south of the receiver were nearly right-hand circular polarised. The first result is based on a ray tracing programme by *Strangeways* [1980], and a theoretical study of *Strangeways and Rycroft* [1980]. The ray tracing results shown in Figure 8 of *Yearby and Smith* [1994] allow for left-hand polarisation at several frequencies but cannot explain our observations shown in Figure 4.1, because the frequency range having left-hand polarisation was 2.7-5.0 kHz, and all parameters repeated similarly within five emissions.

However, the angle of arrival is changing with frequency in our observations, which supports the conclusions of *Yearby and Smith* [1994]. The sharp edge at  $\approx 1.7$  kHz cannot be explained by their results. Their explanation of the left-hand polarisation and our versatile observations must be studied more carefully in the future.

Recently *Ando et al.* [2002] studied theoretically the penetration of PLHR into the ionosphere. They showed that 1) the effect of the radiation is limited in a relatively narrow region below the cutoff frequency of the guided mode in the Earth-ionosphere waveguide, while the region affected by the power line radiation becomes much wider if the guided modes exist, 2) the radiated fields are directed almost horizontally, and 3) the altitude distribution of EM fields changes at the ion gyrofrequency.

*Lundin and Krafft* [2002] proposed that the ion sense of polarisation can appear in the interference pattern of two plane waves even when both of them are right-hand polarised. Moreover, the electric and magnetic wave field components can reveal opposite senses of polarisation at the same receiver location.

PLHR-like signals can also be used for testing the receiver. Different kinds of transmitter signals, e.g. the Russian Zevs, prove the stability of the tape speed of the video recorder. The increased use of the power line control signals causes more and more difficulties to the ELF-VLF observations. Nowadays all 20 kV power lines in Finland are 'full' of these signals about 20% of the time.

PLHR seems to vary in frequency quite a lot as seen in Figures 4.8-4.10. This feature, of course, can be seen only when using at least  $2^{16}$  (=65536)-point FFT, because otherwise the frequency resolution is not high enough. Sometimes several differently behaving PLHR lines were observed, which can be explained by different

source locations, like Finland, Sweden, Norway, or Russia. The harmonics appear to be the prominent pairs of lines, whose frequencies are obtained by Equation 4.1.

A very special event is shown in Figures 4.11-4.13. This 9-hour event is the only of its kind, which has been observed during our ELF-VLF campaigns so far, except for a couple of short intervals on the following day. At the moment, there is neither an explanation nor a hint of what the source of the long duration bunched lines could be. In September-October 2005 some sudden enhancements of PLHR activity were observed. However, they lasted usually only from some tens of seconds to a few minutes. Such enhancements are much easier to understand by external trigger.

PLHR has a structure and it varies in frequency and amplitude. Several lines at slightly different frequencies can be simultaneously present at any time. The intensity of different lines can change quite individually. The lines deviating by, e.g., about 10 Hz from the nominal frequency are seen quite systematically. Those may be of magnetospheric origin. The assumption that PLHR is about a monochromatic line at the nominal frequency is certainly not true. Thus even the man-made part of the phenomenon is complicated.

## 4.7 Conclusions

The left-hand polarisation of the PLHR-triggered emissions is due to the mode conversion from the right-hand to the left-hand polarisation in the Earth-ionosphere waveguide. This causes that all night-time sferics between  $\approx 1.7$  kHz and  $\approx 5$  kHz are left-hand polarised starting from almost pure circular polarisation just above  $\approx 1.7$  kHz, changing to elliptic polarisation, and ending at linear polarisation above  $\approx 5$  kHz.

Our results extend the explanation of the left-hand polarised ELF-VLF waves in comparison with observational results of *Yearby and Smith* [1994] and theoretical simulations of *Strangeways and Rycroft* [1980]. There might also be some latitudinal effect, because the left-handed waves are observed more frequently at high latitudes.

The ‘wrong’ polarisation was observed in PLHR-triggered emissions and in PLHR lines, but natural emissions and whistlers did not show left-hand polarisation. The results by *Yearby and Smith* [1994] are reasonable, and they can very likely be included in the mechanism proposed above. A theoretical explanation for the mode conversion in the Earth-ionosphere wave-guide is required in the future. Furthermore, diurnal and seasonal behaviour should be studied carefully.

PLHR-like signals are also used for testing the receiver. Different kinds of transmitter signals, e.g. from the Russian Zevs, prove the stability of the tape speed of the video recorder. The power line control signals in 20 kV power lines cause more difficulties to the ELF-VLF observations. However, they do not seem to propagate over long distances, because during the September-October 2005 campaign they were not observed at all. Maybe it is worth investigating their possible penetration through the ionosphere to the magnetosphere.

Numerous examples are found, which propose the generation of natural emissions having evident relation to PLHR, but making a final conclusion is difficult. Certainly, the PLHR and related phenomena are not yet fully understood.

## Chapter 5

# Magnetospheric Line Radiation

Magnetospheric line radiation (MLR) was reported for the first time by *Helliwell et al.* [1975], where it was visible in many of the figures, although at the time it was not recognised for what it was. The recordings were made in the 1960s and 70s at Siple, Antarctica and Roberval, Quebec. The authors observed thick magnetospheric lines in the frequency range of 2-5 kHz. The main spacing was roughly 120 Hz, but also fine structures with spacing of 20-30 Hz were observed. Often those lines were fairly constant in frequency but sometimes they drifted up or down in frequency at rates of up to 50 Hz/min. Note, that power line harmonic radiation was not discovered before the mid-1970s by *Helliwell et al.* [1975] and *Park and Helliwell* [1978].

In his Ph.D. thesis, *Yearby* [1982] studied MLR events observed during 1977-80 at Halley, Antarctica. At that time the analysis techniques were based on mostly analogue filters, leading to rather low frequency resolution, typically of the order of 10 Hz. MLR was defined to have a bandwidth of about 30 Hz or more. *Yearby* [1982] presented many features of MLR, like frequency behaviour, spacing, diurnal occurrence, and relation to preceding magnetic activity.

The satellites S3-3, ISEE-1, SCATHA, AUREOL-3, and ISIS made observations of magnetospheric line radiation. These observations were reported by *Koons et al.* [1978], *Bell et al.* [1982], *Koons* [1985], *Parrot* [1995], and *Rodger et al.* [1995]. *Rodger et al.* [1995] found no marked correlation between the diurnal occurrence of MLR and either the load of power grids or its rate of change. Their observations were related to  $K_p$  values of less than 4, the most common  $K_p$  being 3.

*Rodger et al.* [1999, 2000a,b] studied ground-based observations extensively. *Rodger et al.* [1999] found the MLR occurrence rate to be about 7% in the first 2 weeks of June 1995 at Halley, which is considerably more than suggested by observations during the late 1970s. The frequency of the MLR events had a range of 550 Hz to 4400 Hz with a mean value of 2310 Hz. The observed bandwidths of the individual MLR lines were 30 Hz. The MLR drift rates varied from -125 to +230 Hz min<sup>-1</sup>. There were almost equally many upward and downward drifts. The frequency spacing in the Halley data showed a wide range of values, mostly from 40 to 80 Hz, but spacing did not

seem to be fixed to 50 or 60 Hz PLHR. The distribution of MLR line spacings had a roughly exponential form in the range 50-500 Hz suggesting a different mechanism for MLR and PLHR. *Rodger et al.* [1999] made a large number of observations of MLR rms (root-mean-square) field amplitudes getting the mean amplitude of 11.5 fT when the amplitude range was from 1.5 to 103.5 fT. This is of the order of 10-100 times weaker than a typical whistler received on the ground but very similar to amplitudes of man-made transmissions, which have propagated through the ionosphere and magnetosphere.

*Rodger et al.* [2000a] have studied temporal properties of MLR in Halley data. Case studies indicate that single lines tend to be made up of multiple (2-3) lines with widths of 5-10 Hz with smaller spacings (<10 Hz). They observed that MLR growth rates are considerably smaller than those of other ELF-VLF emissions. The difference is up to 4 orders of magnitude, i.e.  $\approx 0.1-0.2 \text{ dB s}^{-1}$  for MLR and  $25-2000 \text{ dB s}^{-1}$  for other ELF-VLF emissions. The diurnal occurrence of MLR had two maxima at  $\approx 0400 \text{ LT}$  and  $\approx 1700 \text{ LT}$ . The morning peak in diurnal occurrence was probably due to association with a combination of chorus and mid-latitude hiss, while the later peak was due to mid-latitude hiss only. MLR occurrence rates can vary greatly within a given month. The highest rate was  $\approx 8\%$  (June, Antarctic winter) and the lowest was  $0.3\%$  (December, Antarctic summer). There was no dependence of MLR occurrence rates upon the instantaneous levels of geomagnetic activity. The average duration of a typical MLR event at Halley was  $\approx 30 \text{ min}$ .

*Rodger et al.* [2000b] studied whether MLR is man-made. Their conclusions were that the expected load pattern in the conjugate hemisphere and the diurnal variation of MLR occurrence did not correlate. Observed directions of MLRs had the same ratio as natural activity, but PLHR should be highly asymmetric. There was no evidence of a Sunday, weekend, or other 7-day cycle in the MLR occurrence.

There are a lot of other ELF-VLF waves in the magnetosphere. Signals of VLF transmitters propagate in space. Sferics from lightnings generate whistlers. ELF-VLF waves spontaneously generated in the magnetosphere can take many different forms. All these waves experience wave-particle interaction and thereby affect each other. Many of these waves can also trigger new wave phenomena in these complicated wave-particle interaction processes.

The MLR events reported in this thesis were observed at high latitudes in Northern Finland at  $L=6.1$ . These events were recorded during our ELF-VLF campaigns in January and November 1993, November 1995, and January 1997. Nowadays computers are much more powerful than, e.g., ten years ago. At that time it was not possible to analyse several minutes or hours of wide-band ELF-VLF data on a routine basis. Our recordings contain 24 hours of wide-band (0-10 kHz) data per day during campaigns with a duration of a couple of weeks. Here I will show the development and fine structure of MLR events.

## 5.1 Analysis of Five Events

Quick look plots were produced for all data by using FFT-based spectral analysis with about 5 Hz spectral resolution from 0 to 8 kHz and 1 s time resolution. The analysis

procedure is explained in Chapter 3.

The quick-look plots covering 24 hours reveal sometimes extended diffuse events usually at frequencies between 1 and at most 6 kHz. The spectral coverage may be more than one octave band. Sometimes banded structures appear at constant frequencies, but the bands may also shift in frequency with time in timescales of minutes. These events may last for hours. They are seen only when there are no strong magnetic disturbances. High-resolution analyses of the events show, that they are MLR events. In a detailed analysis, better than 1 Hz spectral resolution can be used and properties of the received polarisation can be studied.

Five events are analysed in detail in this thesis. MLR events are not yet well enough understood to define precisely what they are. The number of analysed phenomena published in the literature is very small and theoretical explanations are unclear. One of the goals of this work is to describe the features, which we have seen in our data. We consider events to be MLR, if they contain clear discrete narrow band structures lasting from minutes to hours, which do not belong to any known ELF-VLF phenomenon. Thus it may well be that the events contain features created by different physical processes and thus in the future, when the processes are clearly identified and understood, it may happen that these events will have to be reclassified.

Altogether we have identified and analysed in detail 31 MLR events from our data collected in four 2-week measurement campaigns. The total duration of MLR events is about 48 hours. The total duration of analysed VLF data is 1096 hours. The average probability for MLR event is about 4.4%. MLR events usually last several tens of minutes and the longest so far lasted for 5 hours 55 minutes and appeared in the frequency range from 2 to 8 kHz, i.e. two octaves. One of the events covered a frequency range of 0.2-1 kHz, which is more than two octaves. Only 7 out of 31 events occurred in the afternoon or evening, while all others were observed in the morning hours. So far we have not identified any event during magnetically high activity.

**Event 1.** The event on 17 November 1993 contains the basic features of MLR events. The overall features of the event are presented in Figure 5.1. The measurement was done at Porojärvi, at L=6.1. The event occurred in the afternoon and lasted for more than two hours. The general magnetic activity was very low, the magnetic variation was locally of the order of 20 nT during the event. These are typical features for all events.

The resolution of the dynamic power spectra in Figure 5.1 does not allow the recognition of all MLR features, but at some frequencies and time periods one can identify a fine structure where numerous narrow frequency bands are active and have about the same time variation. One can quite easily see, that the event is neither a high-latitude chorus event nor an auroral zone hiss event. It is clearly not an event related to whistlers or whistler-triggered emissions. One does not see indications of usual PLHR-triggered emissions either. Therefore, it is an MLR event.

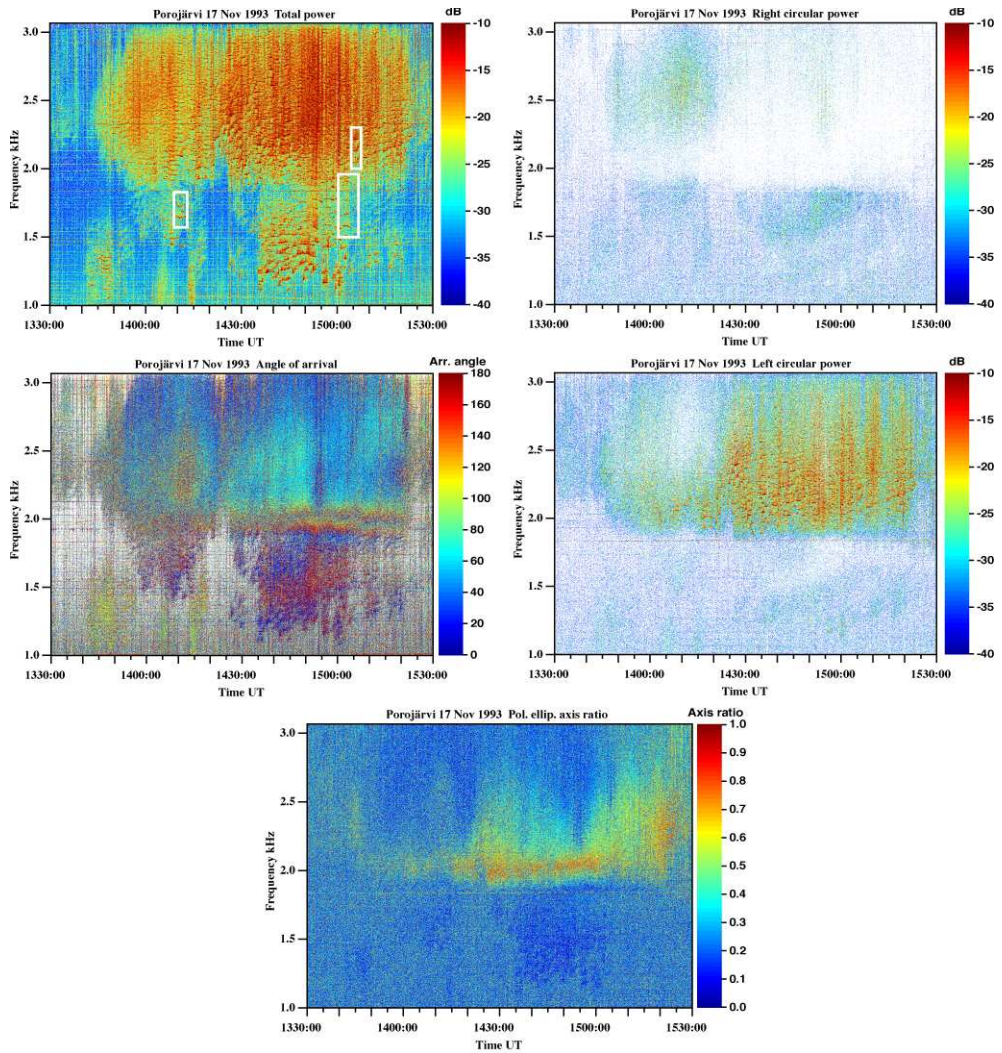


Figure 5.1: Magnetospheric line radiation at Porojärvi on 17 November 1993, at 1330–1530 UT. Frequency range is 1.0–3.0 kHz. The left-top panel shows total power, the left-middle panel shows the horizontal angle of arrival, the right-top panel shows right-hand circularly polarised power, the right-middle panel shows left-hand circularly polarised power, and the bottom panel presents the axis ratio of the polarisation ellipse (‘0’ means purely linearly polarised wave and ‘1’ means purely circularly polarised wave). A very interesting feature of this event is that most of the time MLR is left-handed, which contradicts whistler-mode propagation theory. Also the axis ratio of the polarisation ellipse seems to reach high values during the strongest signals. White rectangles are enlarged in Figures 5.2, 5.3, and 5.4.

The signal level varies from the threshold of detection to the maximum level, which is quite similar to typical chorus emissions. The dynamic range is large in this event, but very often the signal level in these events is low.

The middle-left panel in Figure 5.1, showing angle of arrival in colour code, shows that the emissions do not come from a single source: there are separate sources active simultaneously at different times and frequencies. When the conditions are suitable for a MLR event, several sources can exist in the recording horizon and the same source can emit roughly from the same apparent direction for up to tens of minutes.

A quite surprising result is seen in the panels showing separately right and left-handed polarised power in Figure 5.1. In this thesis we describe total power at any given frequency as sum of linear polarisation and a circular polarisation with the sense of rotation (see Chapter 3). When purely linear polarised power is removed, the result shows that the event is to a large extent left-hand polarised, but not completely: there are some frequency-time intervals showing also weak right-hand polarised power. Comparison with total power shows that those weak signals must be very nearly linearly polarised and thus the determination may be quite inaccurate. In any case the major part of the power is left-hand polarised. This is never seen in our ‘natural’ data, e.g., in chorus, hiss, whistlers or whistler triggered emissions, which always behave according to whistler mode propagation theory.

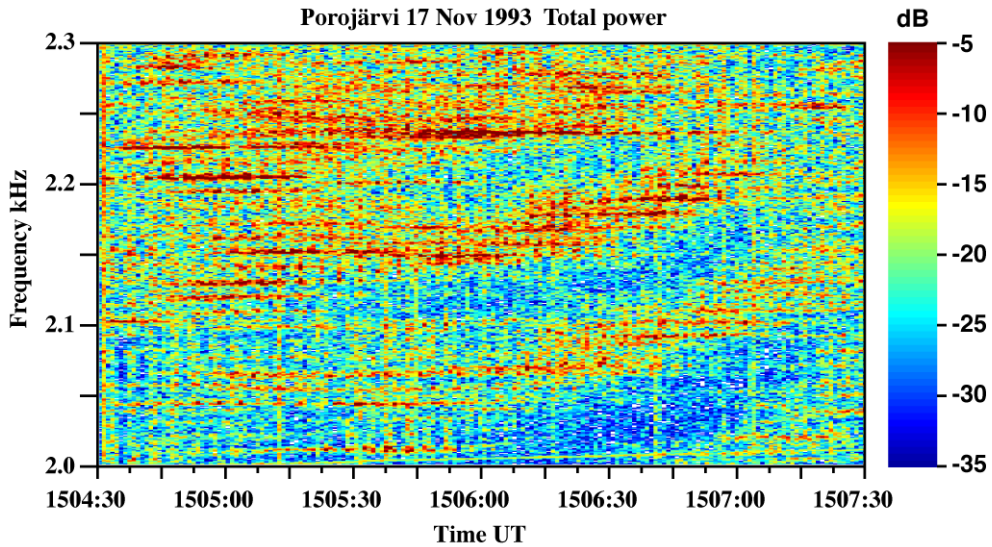


Figure 5.2: Fine structure from the upper-left panel of Figure 5.1. Large amount of emissions have durations of some tens of seconds, and their centre frequency is almost constant in time, bandwidth is a few Hz and there are signatures of amplitude modulation having periods of a few seconds.

MLR events are, however, mostly left-hand polarised, but there are right-hand or mixed mode polarised cases. The only other ELF-VLF phenomenon showing left-

hand polarisation seems to be PLHR-triggered emissions, which have been discussed in Chapter 4.

Another interesting feature is the horizontal angle of arrival, which seems to vary quite a lot in Figure 5.1. Of course, there is a  $180^\circ$  ambiguity due to the lack of the third antenna in the receiver. That means any colour can come also from the opposite direction,  $90^\circ=270^\circ$  etc., which causes problems in interpreting certain features. However, there are frequencies near 2 kHz, which are nearly circularly polarised (seen in the bottom panel). These signals arrived almost from zenith, which causes very large variation in horizontal angle of arrival. It is impossible to determine the correct horizontal angle of arrival for a wave coming from zenith.

The last panel in Figure 5.1 presents the axis ratio of the polarisation ellipse. The value '0' means purely linear polarisation and '1' means purely circular polarisation. Values in between indicate the wave being more or less elliptically polarised. On the other hand, only the waves coming from zenith are observed as pure circularly polarised waves. The further from the zenith the wave has come (i.e. the ionospheric exit point is far from the receiver) the more linearly polarised it is at the receiver.

The combination of two panels in Figure 5.1 gives better information about the scale of the event. When combining the horizontal angle of arrival and the axis ratio of the polarisation ellipse, the spatial scale becomes more realistic. Frequencies near 2 kHz arrive from near zenith while other frequencies arrive from horizontally much further away. Therefore, the ionospheric 'source' is not a point, but a very wide area.

Figure 5.2 shows a dynamic spectrum covering 300 Hz in frequency around 2.15 kHz and 3 minutes of time around 1506 UT. This figure shows that the structure seen in Figure 5.1 is formed by a large amount of emissions having durations of some tens of seconds. Their centre frequency is almost constant in time, bandwidth is a few Hertz, and there are signatures of amplitude modulations having periods of a few seconds. The emissions have quite regular spacing in frequency, which is of the order of 10-15 Hz. The spacing has been presented in Section 5.2 by histograms of the spectral lines of the emissions.

The emissions start and stop at different times in such a systematic way that together they form the typical MLR pattern seen in dynamic spectra covering wide frequency bands and long times. In Figure 5.1 these same emissions form low resolution patterns seen as bands of enhanced power covering about 50 Hz in frequency and drifting upwards at a rate of a little more than 1 Hz/s. Finally one can notice in Figure 5.2 that outside the narrow band emissions there are a background hiss-like emission and possible weak discrete lines just near the detection threshold.

More details on those discrete narrow band emissions are seen in Figures 5.3 and 5.4. They show bands of 250 Hz around 1725 Hz covering 4 minutes around 1411 UT and 1453 UT, respectively. There are at least two groups of MLR lines. Three lines, which slowly decrease in time on the left side of Figure 5.3 having about 72 Hz separation and a few lines keeping almost constant frequency and having quite exactly 50 Hz spacing.

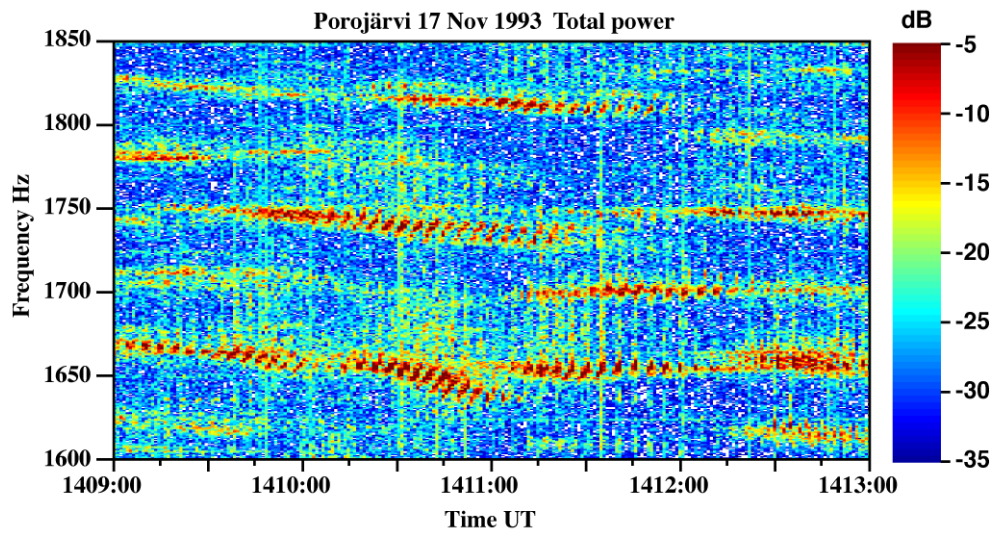


Figure 5.3: Fine structure from the upper-left panel of Figure 5.1. There are at least two groups of MLR lines. Lines, which slowly decrease in time, and lines, which keep almost constant frequency.

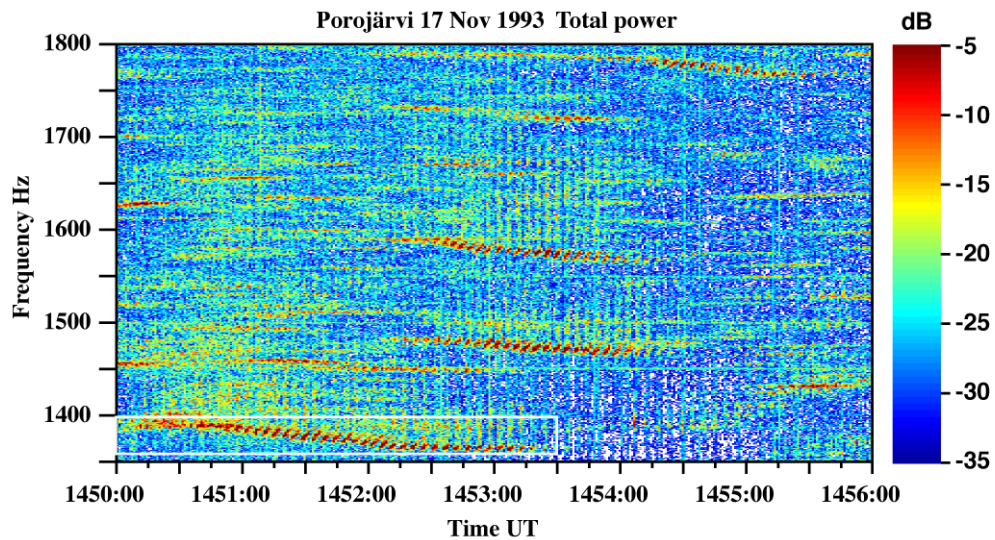


Figure 5.4: Another fine structure from the upper-left panel of Figure 5.1, having similar features as in Figure 5.3. The white rectangle is enlarged in Figure 5.5.

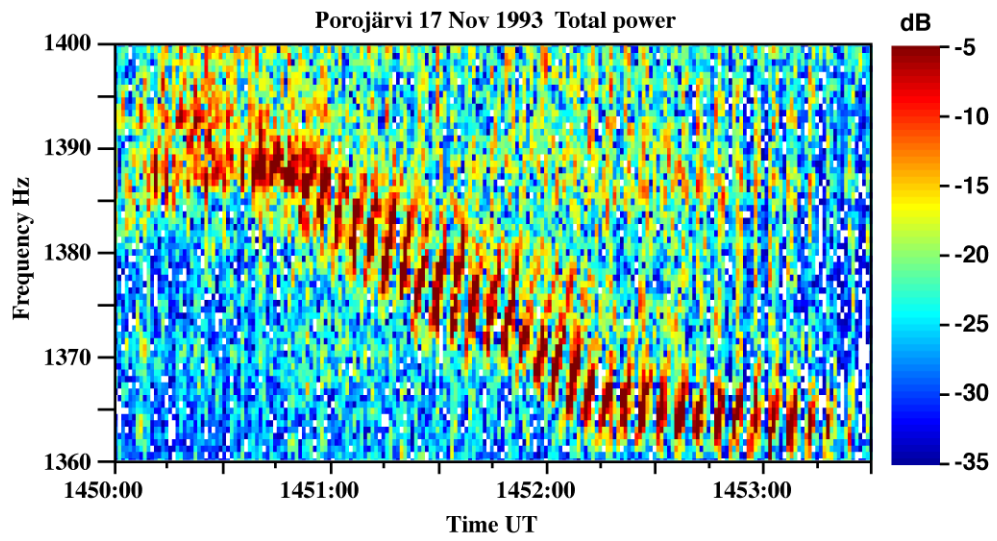


Figure 5.5: Fine structure from Figure 5.4. A clear modulation is seen in one MLR line.

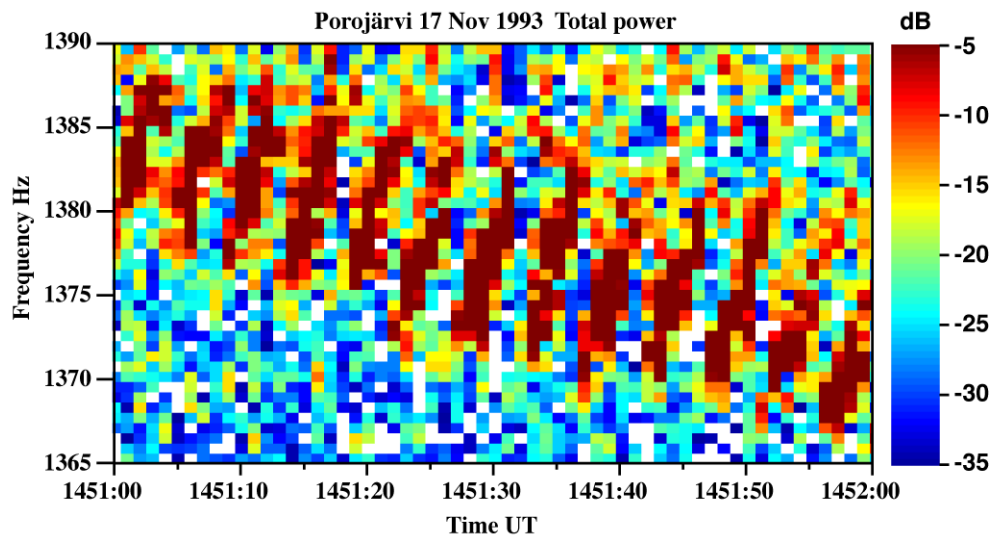


Figure 5.6: Fine structure from Figure 5.5. The modulation has a periodicity of  $\approx 4$  s and there are rising components.

Strong lines have a pronounced common feature: periodic amplitude and frequency modulation (see Figures 5.5 and 5.6). The modulation is in strong cases on-off modulation with a period of 4-6 s. Within every modulation period there is also a systematic frequency modulation. The frequency sweeps linearly upwards by a few Hz with a rate of 3 Hz/s. This modulation is not always seen as nicely as in the given example, but some signatures of it are often seen in individual MLR lines.

A quite similar amplitude modulation is seen in Figure 2 of *Rodger et al.* [2000b], but they did not comment on it at all. It would be interesting to analyse this event again using a much longer FFT, and see if it shows similar fine structures as the MLR observations from Finland.

**Event 2.** The event on 15 January 1997 starting at about 0320 UT contains quasi-periodic emissions with the features of MLR events. The overall features of the event are presented in Figure 5.7. The measurement was made at Porojärvi. The event occurred in the morning and lasted for more than two hours.

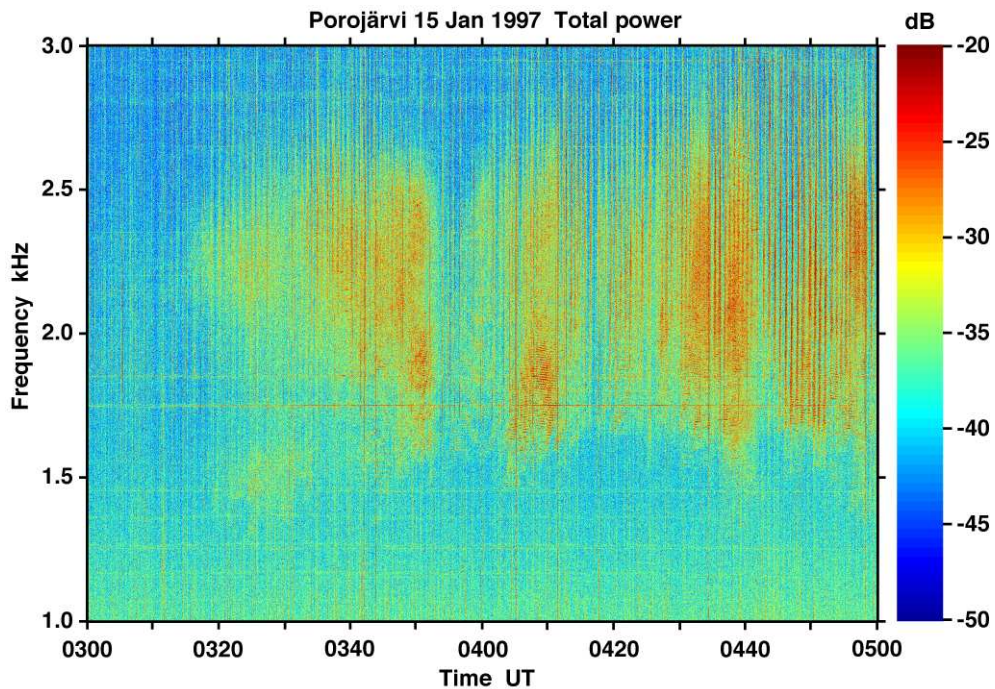


Figure 5.7: Two-hour plot of Event 2. Magnetospheric line radiation at Porojärvi on 15 January 1997, at 0300–0500 UT. Frequency range is 1-3 kHz. The whole event consists of quasi-periodic emission bursts with periods of  $\approx 50$  seconds. ‘Normal’ MLR structures are only seen around 0400 UT, and MLR fine structures appear everywhere (see Figures 5.8 and 5.9). Unfortunately, the campaign ended at 0500 UT, and the duration of this event is unknown.

Abbrev.	Name	Geogr. lat.	Geogr. long.	CGM lat.	CGM long.	L value
NAL	Ny Alesund	78.79° N	11.95° E	75.25	112.08	-
LYR	Longyearbyen	78.20° N	15.82° E	75.12	113.00	15.8
SOR	Sørøya	70.54° N	22.22° E	67.34	106.17	6.9
TRO	Tromsø	69.66° N	18.94° E	66.64	102.90	6.5
AND	Andenes	69.30° N	16.03° E	66.45	100.37	6.4
MAS	Masi	69.46° N	23.70° E	66.18	106.42	6.3
KIL	Kilpisjärvi	69.02° N	20.79° E	65.88	103.79	6.1
LEK	Leknes	68.13° N	13.54° E	65.40	97.50	5.9
ABK	Abisko	68.35° N	18.82° E	65.30	101.75	5.8
IVA	Ivalo	68.56° N	27.29° E	65.10	108.57	5.8
MUO	Muonio	68.02° N	23.53° E	64.72	105.22	5.6
LOZ	Lovozero	67.97° N	35.08° E	64.23	114.49	5.4
SOD	Sodankylä	67.37° N	26.63° E	63.92	107.26	5.3
PEL	Pello	66.90° N	24.08° E	63.55	104.92	5.1
RVK	Rørvik	64.94° N	10.98° E	62.23	93.31	4.7
OUJ	Oulujärvi	64.52° N	27.23° E	60.99	106.14	4.3
DOB	Dombas	62.07° N	09.11° E	59.29	90.20	3.9
HAN	Hankasalmi	62.30° N	26.65° E	58.71	104.61	3.8
UPS	Uppsala	59.90° N	17.35° E	56.51	95.84	3.3
NUR	Nurmijärvi	60.50° N	24.65° E	56.89	102.18	3.4
TAR	Tartu	58.26° N	26.46° E	54.47	102.89	3.0

Table 5.1: IMAGE magnetometer stations, their geographic and magnetic coordinates, and L values.

The general magnetic activity was very low, the magnetic variation was locally of the order of 10 nT during the event. However, at the same time strong Pc 5 pulsations occurred at the northernmost stations of the IMAGE magnetometer network (see Table 5.1), but the period of Pc 5 did not match the period of the QP emissions.

There was a dominant fine structure of  $8\frac{1}{3}$  Hz spacing seen in Figures 5.8 and 5.9. This frequency was 50/6 Hz, i.e. the sixth subharmonic of 50 Hz. Also an ‘original’ MLR feature was seen after 0409 UT in Figure 5.8, where the rising structures had a frequency drift of 125 Hz/min. These fine structures could only be detected with long FFTs (e.g.  $2^{16}=65536$  points). This differed quite a lot from the analysis presented in the paper by *Rodger et al.* [2000a]. They used only  $2^{10}$  (=1024)-point FFT, which gave 12.5 Hz frequency resolution in common cases, and 2.5 Hz resolution in the frequency translated cases, where they shifted the  $\approx 4$  kHz MLR lines into the band of 0-1 kHz.

This event was different from Event 1 in many ways, e.g. it occurred in the early morning instead of in the afternoon, there were natural quasi-periodic emissions simultaneously instead of ‘empty’ sky, and the fine structure had only one dominant spacing ( $8\frac{1}{3}$  Hz). One noticeable feature was the occurrence of vertical structures produced by quasi-periodic emissions. During these quasi-periodic emissions the horizontal signals seemed to almost vanish.

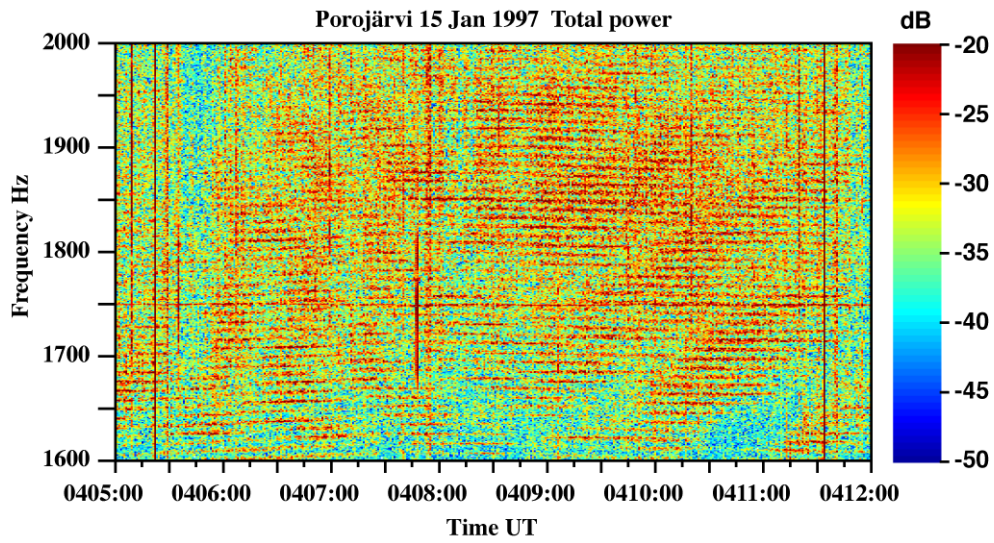


Figure 5.8: Fine structure of Event 2 at 0405–0412 UT. Quasi-horizontal structures are only seen with long FFTs ( $2^{16}=65536$  points). After 0409 UT also ‘original’ MLR features exist with an upward drift of 125 Hz/min.

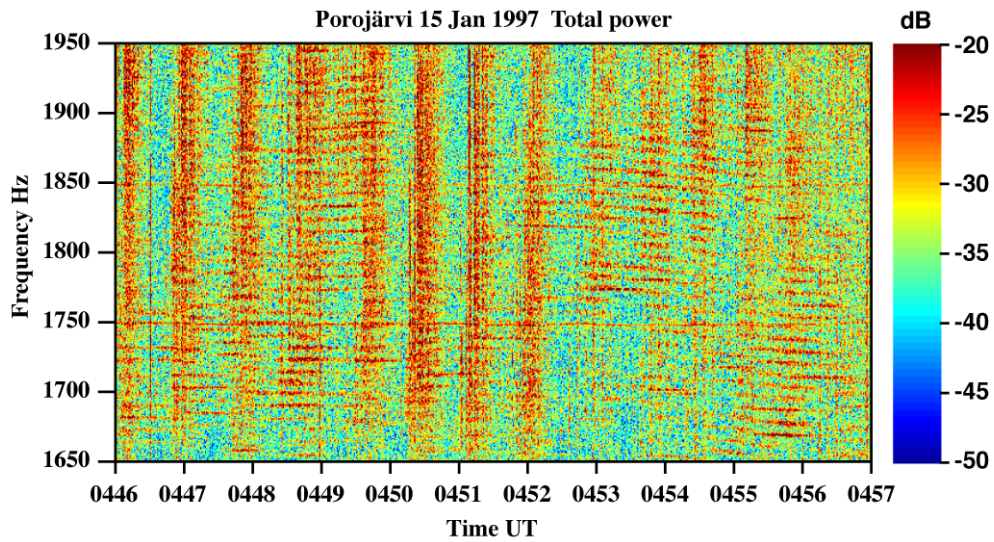


Figure 5.9: Fine structure of Event 2 at 0446–0457 UT. There are 36 horizontal signals within 300 Hz with spacing of  $8\frac{1}{3}$  Hz ( $\Delta f=0.61$  Hz). Vertical structures are bursts of quasi-periodic emissions.

Only total power was shown in Figure 5.7, because the event was mostly linearly polarised at the receiver and did not have a left-handed component. Also the values of the axis ratio of the polarisation ellipse were close to zero.

The emissions had quite regular spacing in frequency, which was  $<10$  Hz. The spacing is presented in Section 5.2 by histograms. Also a comparison of the events will be shown there.

This event was, so far, the only one, where there were simultaneous quasi-periodic emissions. The following event (Event 3) occurred together with natural but PLHR-triggered emissions.

Unfortunately, the campaign in January 1997 ended on 15 January just at 0500 UT, so the duration of this event is unknown. There were no other observations, which could give information about the end of the event. However, quasi-periodic emissions usually last quite a long time, which could mean that Event 2 continued for several hours after the end of the campaign.

**Event 3.** The event on 24 January 1993 occurred at 0410-0700 UT in the frequency range of 1.5-4.1 kHz. Here we discuss only the interval of 0410-0450 UT (Figure 5.10), because it was the most interesting. The event occurred in the morning and lasted for approximately 3 hours. In the beginning of the event, the natural background consisted of discrete emissions. The general magnetic activity was again very low. The magnetic field variation was only of the order of 10 nT during the event. Strong Pc 5 magnetic pulsations occurred almost at all IMAGE magnetometer stations between PEL and SOR (see Table 5.1). This MLR event did not contain any structure with a period similar to that of Pc 5 frequencies.

There were a few spacing frequencies in this event. Most of the time the spacing was close to 50 Hz. The second common spacing frequency was approximately 14 Hz, which is difficult to correlate to, e.g., 50 Hz power line harmonics. During shorter intervals also subharmonics of 50 Hz occurred, e.g. 33.3 Hz ( $\frac{2}{3}$  of 50 Hz), 10 Hz ( $\frac{1}{5}$  of 50 Hz), 5.55 Hz ( $\frac{1}{9}$  of 50 Hz).

There was a clear right-hand polarised part without MLR features below 2.1 kHz after 0442 UT. It was as intense as the MLR at maximum. Its horizontal angle of arrival did not differ dramatically from that of MLR.

Figure 5.11 presents temporal fine structures at 0421:40–0422:10 UT of Figure 5.10. A relatively short FFT of  $2^{13}=8192$  points was used to get better time resolution. This causes a lower frequency resolution. There were strong discrete emission bursts with a periodicity of  $\approx 6$  s. The actual shape of discrete emissions is seen in the middle-left panel. They resembled very much PLHR-triggered emissions above 3 kHz, while the main MLR features were between 1.75 and 3 kHz. The emissions being only left-hand polarised could be explained by PLHR triggering. The emissions arrived most probably from south and close to the zenith, which is seen in the axis ratio of the polarisation ellipse.

There is a very sharp lower cutoff at 1850 Hz, which is often seen in our recordings. The top of the emission bursts contained PLHR-triggered discrete emissions. The seed seems to be the 3050-Hz PLHR line. The 3650-Hz line looks like some kind of upper limit of the emissions.

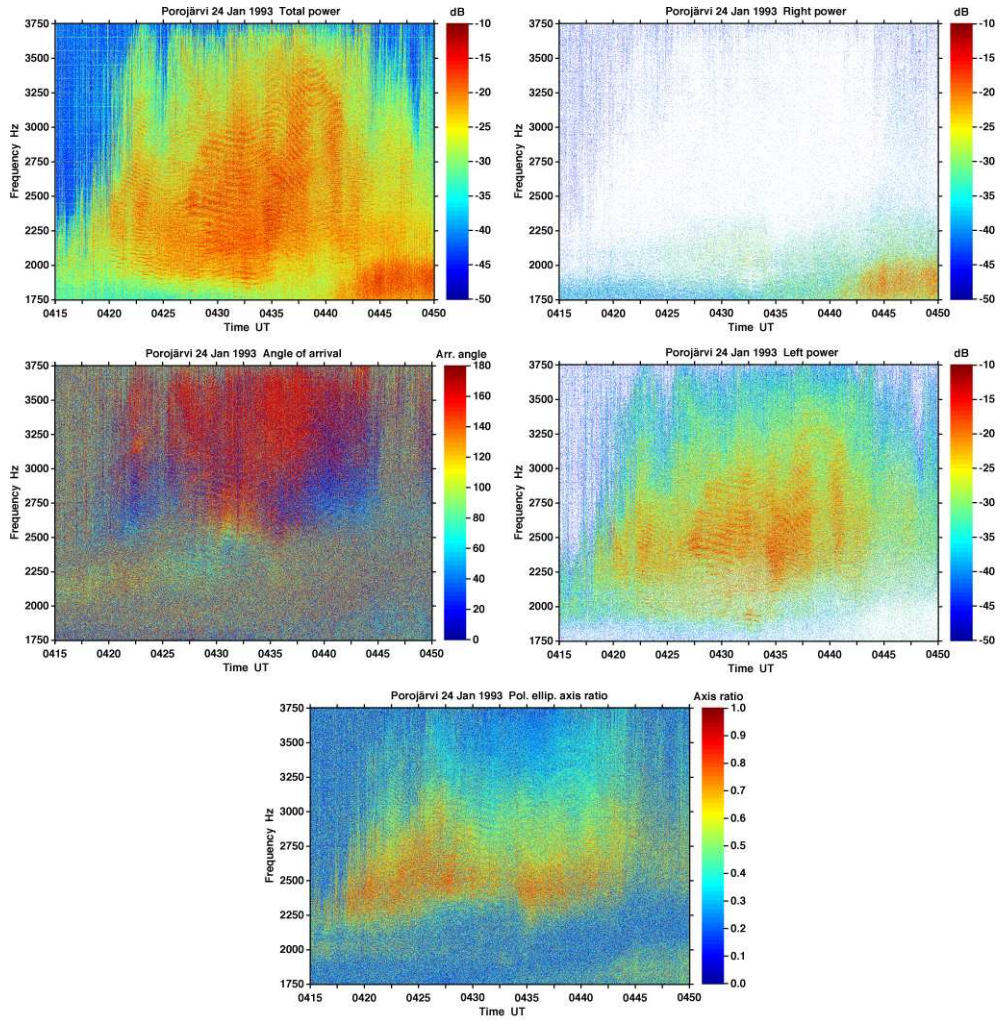


Figure 5.10: Magnetospheric line radiation at Porojärvi on 24 January 1993, at 0415–0450 UT. The upper-left panel shows total power, the upper-right panel shows right-hand circular power, the middle-left panel shows the horizontal angle of arrival, the middle-right panel shows left-hand circular power, and the bottom panel presents the axis ratio of the polarisation ellipse. Notice the absence of right-hand circular polarised power above 2 kHz. However, the axis ratio of the polarisation ellipse shows that the major part of the MLR event is almost circularly polarised.

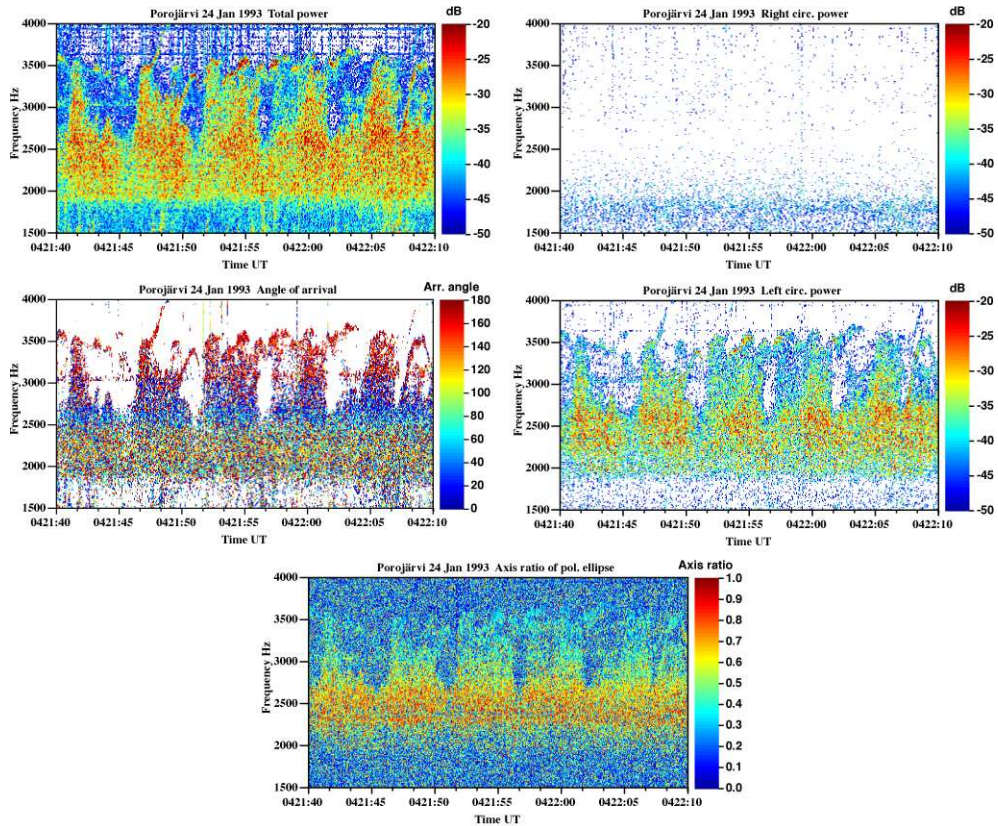


Figure 5.11: A fine structure of the magnetospheric line radiation at Porojärvi on 24 January 1993, at 0421:40–0422:10 UT. There are discrete emissions, which resemble PLHR-triggered emissions. Also the polarisation feature supports the idea of a triggering source.

**Event 4.** The event on 18 January 1993 occurred at 1917–2053 UT in the frequency range of 1.8–3.1 kHz. This is the only case which occurred in the evening and it lasted for about one hour and a half. There was no natural activity just before this MLR event. There was no obvious trigger or initial frequency, but the event started at 1917 UT at about 2.2 kHz. Its upper cutoff frequency increased gradually from 2.2 kHz to about 3.7 kHz within 25 minutes. After that it decreased to 3.2 kHz within 15 minutes. Simultaneously with the change of the upper cutoff frequency, the lower cutoff frequency decreased first to 2 kHz and then after 1945 UT further to 1.8 kHz, where it stayed until the end of the event. The polarisation of the event divides it into two frequency ranges: above 2.6 kHz the event was right-hand polarised, and below 2.6 kHz it was left-hand polarised. Auroral hiss bursts were seen at 2005–2100 UT in the right-hand polarisation, and a burst at 2053 UT stopped the MLR event.

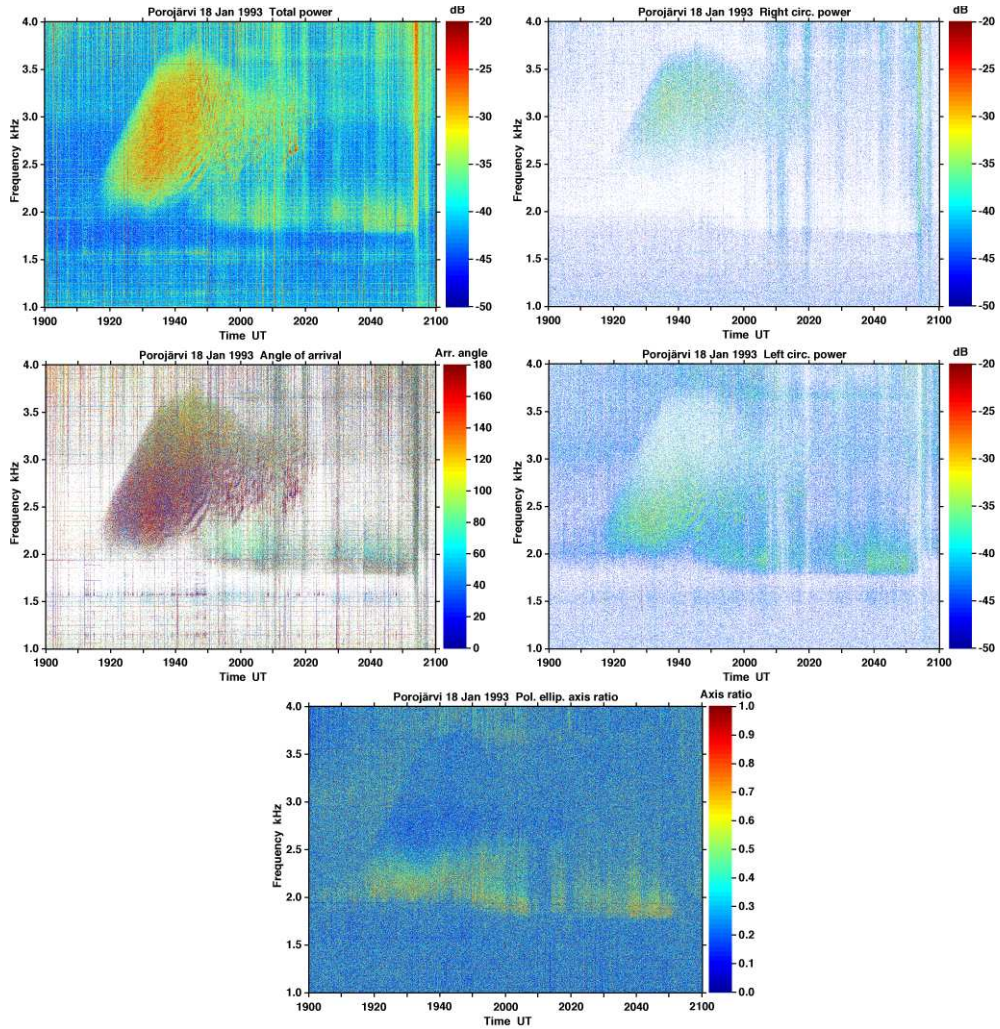


Figure 5.12: Magnetospheric line radiation at Porojärvi on 18 January 1993, at 1917–2053 UT. The upper-left panel shows total power, the upper-right panel shows right-hand circular power, the middle-left panel shows the horizontal angle of arrival, the middle-right panel shows left-hand circular power, and the bottom panel presents the axis ratio of the polarisation ellipse.

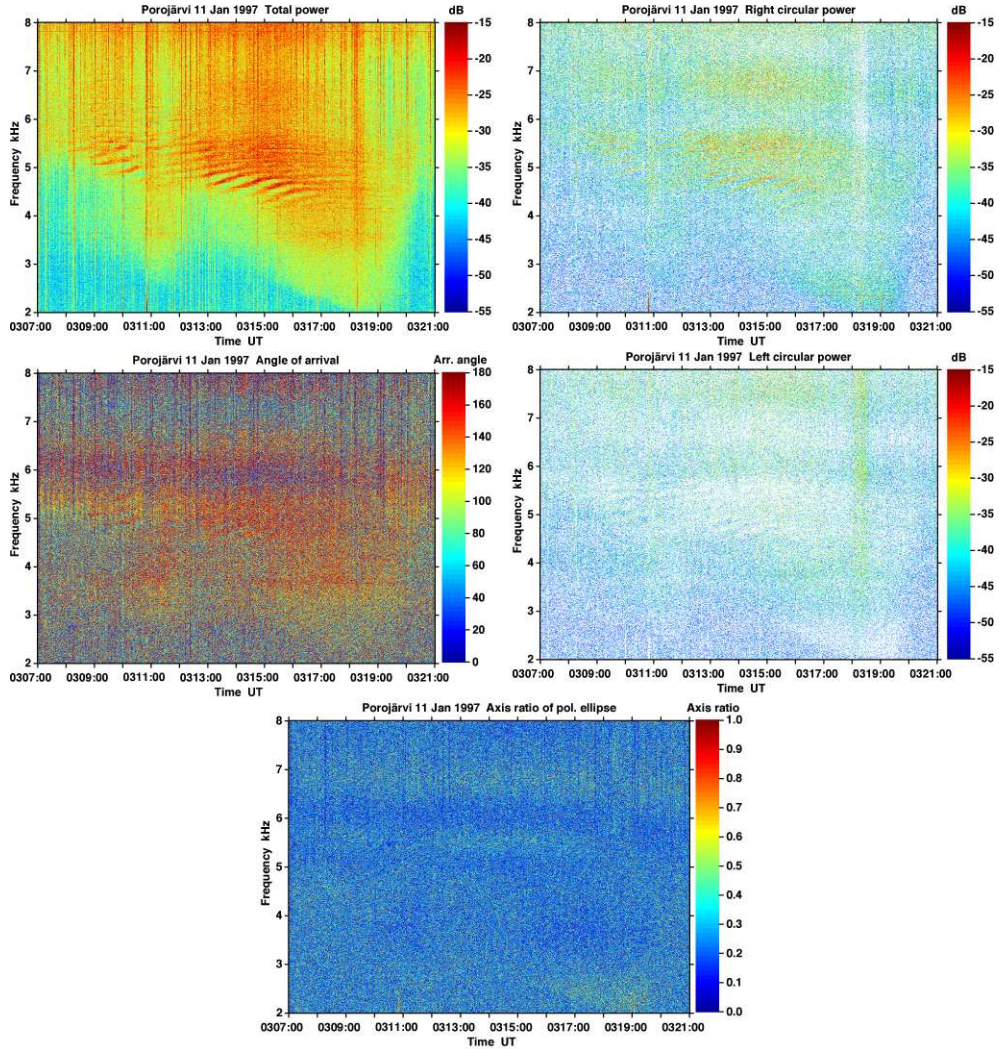


Figure 5.13: Magnetospheric line radiation at Porojärvi on 11 January 1997, at 0307–0321 UT. The upper-left panel shows total power, the upper-right panel shows right-hand circular power, the middle-left panel shows the horizontal angle of arrival, the middle-right panel shows left-hand circular power, and the bottom panel presents the axis ratio of the polarisation ellipse. This event was almost purely linearly polarised. Only frequencies above 4.5 kHz showed right-hand circular polarisation. Also the axis ratio supported the conclusion of the linear polarisation.

**Event 5.** The event shown in Figure 5.13 occurred at 0307-0321 UT on 11 January 1997 in the frequency range of 2-6 kHz. It is a small detail of a MLR event, which began at 0035 UT and lasted for about 6 hours. In general, the MLR structures appeared mostly above 5 kHz, except at the time shown in Figure 5.13 and at 0420-0550 UT, when the MLR was concentrated between 2 and 4 kHz. After 0550 UT the MLR rose back to above 5 kHz. Most of the time the MLR structures occurred as about 10-minute long weak bursts typically 30-40 minutes apart.

The strongest MLR features seemed to be related to hiss bursts, which resemble an auroral hiss. Unfortunately, this morning was so cloudy that it was not possible to get any information from auroral cameras in Finland.

The detail of the event shown in Figure 5.13 is extremely interesting. The background event is a clear auroral hiss event covering a wide range of frequencies and the MLR features are seen as apparent modulation of the auroral hiss burst between 4 and 6 kHz, which is really a small part of the frequency range of the auroral hiss. The process seems to create minima and maxima, which then form the MLR lines. Auroral hiss originates at low altitudes in the magnetosphere, far from the equator, where chorus signals are generated [*Santolik and Gurnett, 2002*]. If the process creating MLR can modulate auroral hiss, then it has to be also a low altitude process above the ionosphere in the same region where processes generating hiss take place.

Another interesting feature is that every line has a sharp start at some PLHR frequency, e.g., the MLR lines starting before 0311 UT were related to the frequencies of 4650, 4750, 4850, 5050, 5350 and 5850 Hz, while the lines beginning after 0312 UT were related to 4150, 4250, 4450, 4500, 4600, and 4750 Hz. This proposes that the lines originally are related to PLHR.

The MLR lines drift in frequency with time. Event 5 shows very steep upward drifts at the beginning of each line. The drift varied from +137 to +264 Hz/min being mostly greater than +200 Hz/min. These observations are in agreement with the highest values observed by *Rodger et al. [1999]*.

## 5.2 Frequency Spacing

From all 31 available events five special cases (Events 1-5) were selected. The selection criteria were that the event was strong and showed evident features of MLR events. Total durations of those selected intervals for analysis were about 2 hours. The basic data selection was based on data covering the whole measured ELF-VLF frequency range.

In order to determine the frequency spacing, several short intervals were selected. The selection criterion was that the MLR lines should stay at constant frequencies during the selected period. The duration of the selected intervals varied between 10 and 450 seconds in time and between 1000 and 3200 Hz in frequency. In all cases the major part of the events occurred below 3 kHz.

The MLR events are generally very weak and, if there was no additional 'natural' activity, even at best they were not much above the noise level of the receivers and the recording system, which was based on VHS-hifi videotapes. In the standard analysis there are difficulties in getting sufficient dynamic range, because the data

contain sferics, which have a peak power at around 8 kHz. The peak amplitudes of sferics limit the maximum possible gain before AD-conversion. In order to get maximal dynamic range for the events below 3.1 kHz, the original analogue data was further filtered by a 11-pole analogue low-pass Chebyshev filter with 3.1 kHz corner frequencies. The filtered data allowed for higher gains of the order of 12 dB before the 16-bit AD-conversion.

The spectrum analysis was based on complex FFT of 65536 samples using 25536 samples overlap in the analysis. The frequency interval becomes 0.61 Hz and the frequency resolution is 1.22 Hz. The analysed frequency range of the events was between 1 kHz and 3.1 kHz.

The obtained power spectra were integrated over the selected period, during which the event had constant behaviour. In the next phase, normalized autocorrelation functions for every integrated spectrum were produced. The lags were then computed as a function of frequency shift. The frequency spacings were studied by defining the maxima of these autocorrelation functions. In one event, frequency maxima of up to 55 Hz are defined, and up to 110 Hz in other events. For all selected MLR events about 30 integrated independent periods were studied in this way. Finally, all maxima of each event were plotted as a histogram to find possible systematic features in frequency spacing in the events. The frequency resolution of the histograms is 1 Hz.

Event 1 occurred on 17 November 1993 at 1330-1530 UT in the frequency range of 1 kHz to 3 kHz. 28 spectra integrated over 60-300 s were analysed. The resulting histogram is shown in the upper panel of Figure 5.14.

There was one dominant peak at 10.0 Hz. The sub-harmonics at 12.5, 16.67, and 33.33 Hz were not related to any significant peak, while the sub-harmonics at 25.0 and 37.5 Hz were close to the peaks in the frequency spacing. This event contained also many amplitude modulated MLR lines as seen in Figures 5.3 and 5.4. The frequency spacing was about 100 Hz in those cases. All amplitude modulated lines remained stable in frequency or they were drifting slightly towards lower frequencies.

Event 4 occurred on 18 January 1993 at 1917-2053 UT in the frequency range of 1.8 kHz to 3.1 kHz. Between 1920 and 2020 UT altogether 34 spectra integrated over 60-300 s were analysed. The resulting histogram is shown in the lower panel of Figure 5.14. A sub-harmonic at 12.5 Hz was the highest peak after the peak of 50 Hz, and about one third of the integrated spectra had frequency spacings down to 5 Hz. In other cases, it is difficult to say whether the sub-harmonics were related to the frequency spacing.

There are no clear maxima at any spacing frequency in events 1 and 4. All those showing sub-harmonics of 50 Hz are somewhat equally re-presented in the histograms. The only remarkable feature is that there are a number of observed spacing frequencies below 15 Hz.

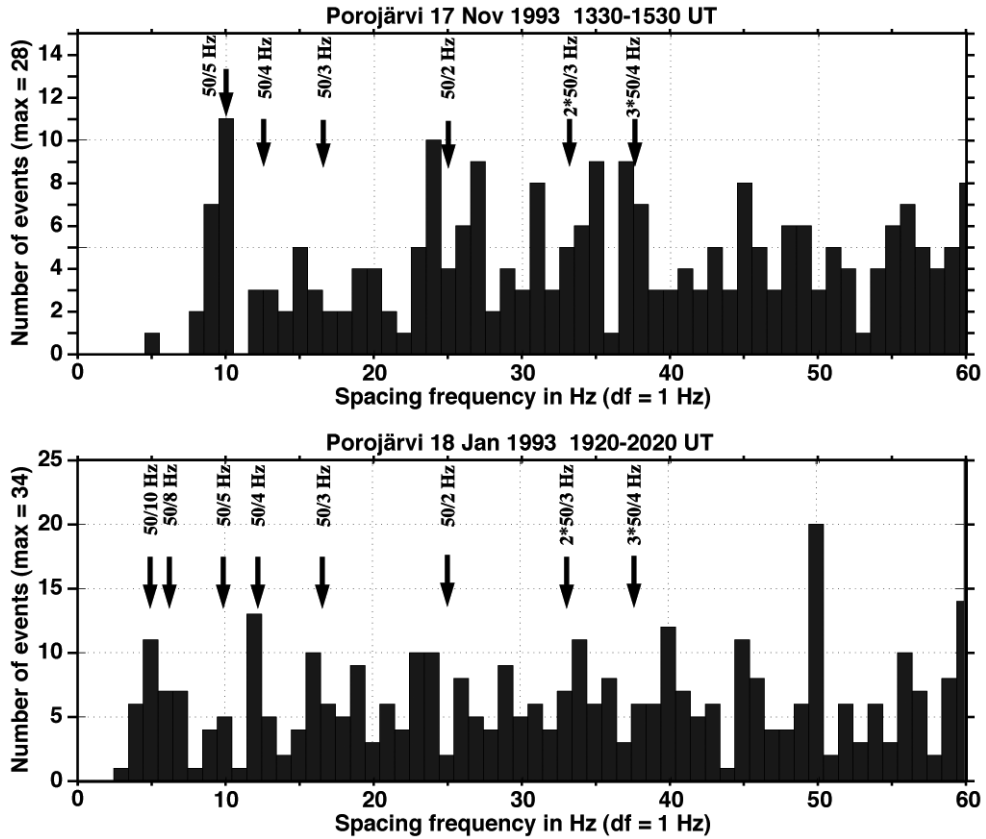


Figure 5.14: Frequency spacing of two MLR events (17 November 1993 and 18 January 1993) presented as histograms. Certain sub-harmonics of 50 Hz are marked by arrows. Their frequencies are  $50/10$  Hz,  $50/8$  Hz,  $50/5$  Hz,  $50/4$  Hz,  $50/3$  Hz,  $50/2$  Hz,  $2 \times 50/3$  Hz, and  $3 \times 50/4$  Hz, i.e. 6.25 Hz, 10.0 Hz, 12.5 Hz, 16.67 Hz, 25.0 Hz, 33.33 Hz, and 37.5 Hz. On 17 November 1993 there was one dominant peak at 10.0 Hz, and on 18 January 1993 a sub-harmonic at 12.5 Hz was the highest peak after the peak of 50 Hz.

Event 2 occurred on 15 January 1997 at 0300-0500 UT in the frequency range of 1.25 kHz to 3.0 kHz. Altogether 34 spectra integrated over 10-450 s were analysed. The resulting histogram is shown in Figure 5.15. The frequency spacing had prominent peaks in this MLR event. Many sub-harmonics were closely related to these peaks, although most of the peaks differed by about -1 Hz from the sub-harmonics.

The highest peak is at 8.54 Hz, which is 0.31 Hz above 8.33 Hz ( $=50/6$  Hz) or 1.46 Hz below 10.0 Hz ( $=50/5$  Hz). Remembering that  $\Delta f=0.61$  Hz, the 8.33 Hz sub-harmonic is more probable. Actually, the sixth sub-harmonic of 50 Hz is also obtained as  $0.5 \times 16\frac{2}{3}$  Hz, which would be related to Swedish railways.

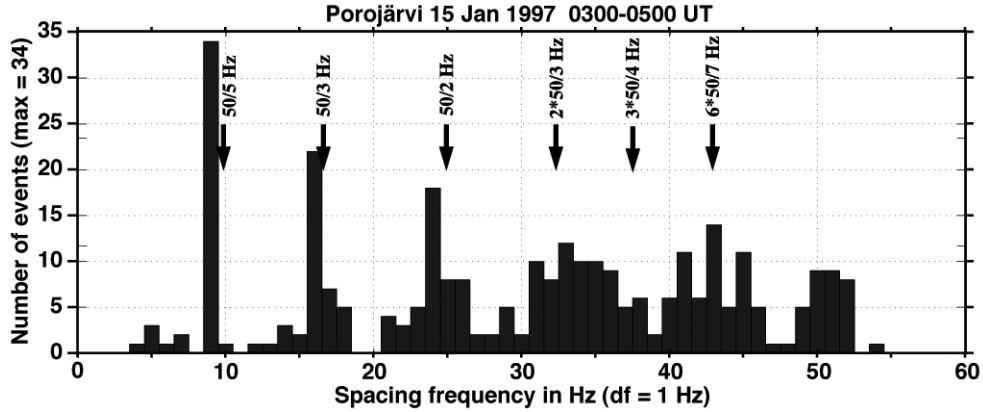


Figure 5.15: Frequency spacing of a MLR event (15 January 1997) presented as a histogram. Certain sub-harmonics of 50 Hz are marked by arrows. Their frequencies are  $50/5$  Hz,  $50/3$  Hz,  $50/2$  Hz,  $2 \times 50/3$  Hz,  $3 \times 50/4$  Hz, and  $6 \times 50/7$  Hz, i.e. 10.0 Hz, 16.67 Hz, 25.0 Hz, 33.33 Hz, 37.5 Hz, and 42.86 Hz. The frequency spacing has prominent peaks in this MLR event. Many sub-harmonics were closely related to these peaks.

Events 2 and 3 (on 24 January 1993) were similar in the sense that they both occurred together with discrete emissions and QP emissions. A possible relationship between the emissions and the frequency spacing of the MLR lines is still unknown.

There were numerous different frequency spacings among all 31 MLR events observed during our ELF-VLF campaigns. However, the frequency separations were fixed for a long time in each event, regardless of the frequency or the frequency drift of the event. There were some events with at least two different frequency spacings and drifting rates simultaneously (see, e.g., Figures 5.3 and 5.4). Especially Figure 5.4 depicts slowly downward drifting, intense MLR lines at the time when most of the lines had either a constant frequency or their frequencies increased.

*Rodger et al.* [1999] observed a small number of events with a modulation in addition to the overall drift. One interesting question was presented by *Rodger et al.* [1995, 1999, 2000a,b]: Is MLR man-made? They stated that MLR does not have a significant influence on geospace as viewed from Halley. However, they concentrated on looking only for the frequency spacing of 50 and 60 Hz, but they did not study the sub-harmonics of 50 and 60 Hz at all.

The FFT analysis was undertaken using  $2^{15}$ - $2^{17}$ -point complex transforms of the ELF-VLF data for this thesis. Those transforms led to 0.61, 0.31 and 0.15 Hz frequency resolution in the 0-10 kHz range, respectively. These values are significantly

different from  $2^{10}$  (=1024)-point transforms and 12.5 Hz resolution used by *Rodger et al.* [1999, 2000a].

### 5.3 Statistics of 31 Events

The total number of observed MLR events during 1993–1997 is 31, which represents 4.4 % of all of our ELF-VLF recordings during those years. The magnetic activity was in almost all MLR cases very low (below 50 nT during MLR), except in two cases, when MLR occurred close to an auroral substorm. These parameters agreed well with *Rodger et al.* [1999, 2000a].

The parameters of all 31 MLR events have been summarised in Table 5.2. Durations varied between 15 min and 6 hours. The events were observed practically in the whole frequency range of the receiver, except the highest frequencies of 8.0-10.0 kHz, which were contaminated by sferics.  $K_p$  values of the MLR observations were mostly very low, except on 11 January 1997 when they reached the level of 5<sub>-</sub>. One column shows the magnetic Pc 5 pulsation activity at high latitudes, and the last column indicated when the MLR event had fine structure.

Surprisingly, often there were magnetic Pc 5 pulsations at high latitudes ( $>68^\circ$  N). Table 5.2 clearly shows that magnetic Pc 5 pulsations were observed simultaneously with all MLR events. The periods of magnetic pulsations varied between 190 and 600 s, which corresponds to the definition of Pc 5 pulsations.

There are two main categories of Pc 5 pulsations: compressional and toroidal Pc 5 [see, e.g., *Anderson, 1994*]. Compressional Pc 5 waves, found on the nightside towards the flanks of the magnetosphere, are the dominant pulsations occurring at  $L > 8$ . The compressional (along magnetic field) perturbation of the wave is often accompanied by a comparable radial perturbation; the amplitudes of the oscillations are typically large with periods of 150 to 600 seconds (i.e. frequencies of 2-7 mHz).

Azimuthally polarised toroidal Pc 5 pulsations are thought to be fundamental mode toroidal field line resonances (FLR) with a magnetic node at the equator. They are considered to be a separate phenomenon from multi-harmonics because of the difference in occurrence distribution: toroidal Pc 5 are found close to the flanks of the magnetosphere either both at dawn and dusk (as derived from some ground based studies), or only at dawn side (as derived from satellite measurements) [see, e.g., *Anderson, 1994*, and references therein].

*Manninen et al.* [2002] studied the high-latitude long period geomagnetic pulsations excited during the first hours (0430–0830 UT) of the magnetic cloud impact on 10 January 1997. They found similar Pc 5 range modulations in both ELF-VLF and riometer data. The two days following the 10 January 1997 were ‘MLR days’, but the 10 January 1997 was not.

The MLR events studied in this thesis occurred mostly during the early morning and morning hours (19 out of 31); only one event occurred during the late evening hours.

Date	Start UT	End UT	Dur. min	Freq. kHz	$K_p$	Pc 5 activity	Fine structure
16 Jan 1993	1020	1130	70	3.0–6.0	1	yes	no
18 Jan 1993	0110	0430	200	2.0–6.0	2, 3 <sub>-</sub>	yes	no
	0530	0630	60	1.0–4.5	3 <sub>-</sub>	yes	no
	1917	2053	96	2.0–4.0	3 <sub>-</sub>	yes	yes
19 Jan 1993	1130	1145	15	1.0–2.0	4 <sub>-</sub>	yes	no
	1300	1330	30	1.0–7.0	2 <sub>+</sub>	yes	no
21 Jan 1993	0130	0520	230	3.0–6.0	2 <sub>+</sub> , 3 <sub>+</sub>	yes	no
	0920	1005	45	3.5–5.0	2 <sub>-</sub>	yes	no
22 Jan 1993	0515	0530	15	2.0–3.0	2 <sub>-</sub>	yes	no
	1335	1350	15	1.5–5.0	1	yes	no
24 Jan 1993	0400	0830	270	1.5–6.0	2 <sub>+</sub>	yes	yes
25 Jan 1993	1050	1120	30	0.5–2.5	3	yes	no
26 Jan 1993	1200	1400	120	0.5–2.0	3 <sub>+</sub>	yes	no
29 Jan 1993	0610	0810	120	0.5–2.0	1 <sub>+</sub>	yes	no
11 Nov 1993	0140	0213	33	2.0–5.0	3	yes	no
	0420	0500	40	3.5–6.0	3	yes	no
	0830	0850	20	2.0–5.0	3	yes	no
12 Nov 1993	0500	0540	40	0.2–1.0	3 <sub>+</sub>	yes	no
	0850	1030	100	1.0–2.5	2 <sub>-</sub>	yes	no
17 Nov 1993	1340	1550	130	1.0–4.0	0	yes	yes
17 Nov 1995	0210	0250	40	0.5–1.5	3 <sub>+</sub>	yes	no
19 Nov 1995	1140	1200	20	3.0–5.0	1	yes	yes
20 Nov 1995	1300	1600	180	2.0–5.0	0 <sub>+</sub>	yes	no
22 Nov 1995	0140	0200	20	2.0–4.0	1 <sub>+</sub>	yes	no
24 Nov 1995	0400	0530	90	0.5–1.5	0	yes	no
07 Jan 1997	0440	0500	20	2.0–4.0	4	yes	no
11 Jan 1997	0035	0630	355	2.0–8.0	5 <sub>-</sub> , 4	yes	no
12 Jan 1997	0100	0630	330	2.0–5.0	2 <sub>-</sub> , 2	yes	no
14 Jan 1997	0200	0230	30	2.0–4.5	1 <sub>-</sub>	yes	no
	0530	0600	30	1.0–3.0	1 <sub>-</sub>	yes	no
15 Jan 1997	0300	0500	120+	1.0–3.0	1 <sub>-</sub>	yes	yes

Table 5.2: Parameters of 31 MLR events observed during campaigns in January 1993, November 1993, October 1994, November 1995, and January 1997.

## 5.4 Discussion

MLR structures appeared mostly with some background activity. There were few events, which occurred in the ‘empty sky’ and only a few events appeared during intense ELF-VLF activity.

There are a few differences in our data compared to the data mostly published in the papers referred to in this chapter. First, the MLR events analysed above were measured at exceptionally high L values of 6.1 compared to the data from locations in Antarctica like Halley (L= 4.3), Sanae (L=4.1), and Siple (L=4.1), which are used in ground-based studies related to MLR. Our measurement sites are thus mostly poleward from the plasmopause or, during magnetically very quiet times, near it.

The second difference is that the conjugate areas of our observation sites do not have any source of PLHR. Thus, if the events presented in this thesis were related to PLHR, then necessarily they were related to PLHR having their source on the same hemisphere than the measurement site. In the longitude sector of Finland there are among mines and big factories several towns and a lot of electric power stations near or well above  $L \approx 6$ .

The power systems operate with 50 Hz in Northern Europe, but there is an interesting possibility for another type of source, too. The Swedish railway operates at 16.7 Hz (=50/3 Hz) and the distance from the measurement site to the railway is less than 200 km. The main traffic on that railway is due to trains transporting iron ore from Kiruna in Northern Sweden to Narvik at the Norwegian coast.

The altitude change of the railway between Kiruna and Narvik is remarkable. It starts from 385 m above sea level at Kiruna, rises up to 1000 m a.s.l. at the Norwegian border, and finally drops down to 10 m at Narvik. This altitude profile means huge needs of electric power, when a train carrying about 4200 tonnes of iron ore goes from Kiruna to Narvik. There are 11-13 trains every day making their 167 km run.

This potential source of high-latitude PLHR having identifiable harmonic structure extends to L values of  $\approx 7$ . Therefore, it is interesting to look for evidence of harmonics of 16.7 Hz in MLR events. We do not have evidence that direct harmonic radiation from the railway is above the detection threshold of our ELF-VLF receiver. This special kind of potential source is another difference compared to data from other stations used earlier in MLR research.

There is evidence, that PLHR creates other events. For example PLHR-triggered discrete emissions are quite common in the data and are studied, e.g., by *Nunn et al.* [1999] and in Chapter 4 of this thesis. Another question is whether the MLR events studied above are related to PLHR. There was no weekday/weekend effect in our MLR observations, which is consistent with *Rodger et al.* [2000b]. Neither *Karinen et al.* [2002] did find a weekend effect in magnetic activity during the years 1868-2000, who studied the behaviour of  $aa$  and  $A_p$  indices.

The lack of sources in the conjugate area is perhaps not very important. If PLHR from the northern hemisphere enters the magnetosphere, finds a duct and becomes amplified by wave-particle interactions, then the reflected wave from the southern hemisphere may be stronger than the original injection from the northern hemisphere. In Event 1 we clearly see a periodic amplitude modulation of about 4-6 s in practically all discrete lines forming the event. The period is likely the two-hop whistler propaga-

tion time at that frequency and for that duct. Within every modulation period there is also a systematic frequency modulation. The frequency sweeps linearly upwards by a few Hz with a rate of 3 Hz/s. It may well be that the modulated discrete lines are echoing wave packets at relatively constant and narrow frequency. However, any dispersion was not observed in the frequency range of 1.0-3.0 kHz.

The direction of arrival has been estimated by measuring the orientation of the main axis of the polarisation ellipse. A 180° ambiguity exists and the method does not work if several sources are active at the same frequency at the same time. However, even this information is sometimes very good.

The horizontal angle of arrival shows that several lines come sometimes from the same direction and continue for longer duration. Evidently they propagate using the same, stable duct. It also shows that the event can contain several active propagation ducts because different groups of lines have different apparent directions of arrival. This is important when trying to measure the frequency separation of discrete lines. It is not physically justified to measure the difference of discrete lines if they clearly come from different ducts. It is interesting to mention that even if propagation ducts clearly exist, there are usually no whistlers. We never found a single whistler in our data observed on the ground while a MLR event has been active.

The main characteristic features related to the events are summarised here:

- 1 The MLR events appear mostly during low magnetic activity ( $K_p = 0 - 2_+$ ), only three events occurred during  $K_p \geq 4_-$ .
- 2 Most of the events occurred simultaneously with natural chorus or hiss activity.
- 3 There were magnetic Pc 5 pulsations observed at high-latitude stations during all MLR events.
- 4 The frequency range of the events varied from 0.2-1.0 kHz to 2.0-8.0 kHz.
- 5 The duration of the events varied between 15 min and 6 hours.
- 6 The horizontal angle of arrival varied with frequency, but a certain direction could be stable for hours.
- 7 More than 60% of the events occurred during the early morning and morning hours, only one event was observed in the late evening.
- 8 Several events showed left-hand polarisation, but also pure linear events were found. Some events were related to PLHR-triggered emissions.
- 9 Five events had fine structure, which consisted of discrete narrow lines with spacing down to 5 Hz when using  $2^{15}$ - $2^{17}$ -point complex Fourier transforms having Nyquist frequency at 20 kHz.
- 10 At least one event showed a clear periodic amplitude modulation of about 4-6 s. Within the modulation period there was also a systematic frequency modulation, and the frequency swept upwards with a rate of 3 Hz/s (see Figures 5.5-5.6).
- 11 The frequency drifts could be different between neighbouring MLR lines (see, e.g., Figures 5.3 and 5.4).
- 12 There was no clear trigger, but in Event 5 the lines start at PLHR frequencies shown in Figure 5.13 where the process seems to modulate auroral hiss.

The events can last for several hours, during which propagation from different directions was observed. The source of that kind of event cannot be localised in space. The process can cover wide areas, which are much wider than the ELF-VLF horizon of the ground-based ELF-VLF station.

The distribution of the power level in MLR events appears to decrease smoothly to the instrumental detection limit, which is controlled by the noise of the receiver system. In this work, a special post filtering was used in order to raise the gain in the post processing to a level high enough to study the weakest MLR lines. In general, the signal level is low and this is equivalent to the earlier finding of *Rodger et al.* [1999] that the growth rate is low.

All the presented data has been measured using our “coaxial cable” antenna. Provided that the external noise does not control the detection threshold one can formally obtain 3 dB S/N ratio for waves having an amplitude of 0.37 fT at 1 kHz using 1 Hz noise bandwidth. At higher frequencies the S/N ratio is even better. The used bandwidth of the analysis is often slightly below 1 Hz and we can certainly detect waves having amplitudes well below 1 fT under good environmental conditions.

The connection of MLR to PLHR has been under discussion for many years [e.g., *Rodger et al.*, 1995, 1999, 2000a,b]. The strongest evidence is in Event 5, where the MLR structures start from power line harmonics but then move rapidly to other frequencies. Also Event 2, where the lines are separated by  $8\frac{1}{3}$  Hz, indicates that there probably is a connection to PLHR. The frequency spacing shown in Figure 5.15 shows clearly the power line relation. This kind of study is, however, difficult because several sources are often seen at the site simultaneously. As it was shown in Chapter 4, PLHR lines can vary several Hz within a few minutes. If MLR lines are related to PLHR lines they could have similar variation in frequency spacing. Checking the differences in frequency spacing in a situation when the signals from several sources overlap each other is not meaningful and careful consideration is needed.

If the MLR process really acted together with the auroral hiss event shown in Figure 5.13, then it must be a low altitude process, at least in that case. It is not at all clear at how low altitude it can exist.

The magnetic activity is mostly low when MLR events occur but it does not need to be extremely low. As seen from Table 5.2, the events can also occur under the conditions when an auroral hiss event takes place. The occurrence of magnetic Pc 5 pulsations at the time of MLR events might as well be coincidental.

The polarisation of MLR events tends to be left-handed when received on the ground, but also right-hand polarisations occur. As mentioned earlier, within the accuracy, which can be obtained in a single station measurement, only PLHR-triggered emissions and MLR events show left-hand polarisation. Chorus, auroral hiss, whistlers and whistler-triggered emissions are never left-handed in our data.

The outer structure of MLR is easiest to explain by interference in the wave-guide and thus could be a consequence of multi-hop propagation from a phase coherent source. This mechanism could also explain Event 5 where an auroral hiss was modulated. Thus, the outer structure is simply a moving interference pattern on the ground. The frequency of the inner structure is almost constant. It changes but at much lower rate than the apparent frequency change of the outer band structure. The events show a large amount of nearby spectral lines at regular intervals lasting for tens

of minutes.

The inner structure, where the bandwidth of the lines is  $\approx 1$  Hz and a lot of lines appear at about regular frequency intervals, is really problematic. It is difficult to understand how freely drifting energetic particle population could maintain suitable constant characteristics for such a long time. More information could be obtained from multi-station observations.

Items 3-11 are new features compared to earlier MLR studies [*Helliwell et al.*, 1975; *Koons et al.*, 1978; *Bell et al.*, 1982; *Koons*, 1985; *Parrot*, 1995; *Rodger et al.*, 1995, 1999, 2000a,b]. The main reasons are the differences in data analysis, e.g. FFT analysis are done using  $2^5$ - $2^7$  times longer transforms.

## 5.5 Conclusions

The MLR events are most likely produced during very quiet geomagnetic conditions at low altitudes over wide spatial areas, initially triggered by PLHR, but then moving away from the PLHR frequencies and becoming self-sustaining. Our new observations suggest that MLR contains, simultaneously, fast and slow processes, which are completely locked to one another. Such MLR is made up of many narrow band rising elements existing in an “envelope” that slowly changes in frequency but guides the small bandwidth fast elements.

At the same time, evidence for wave-energy coupling is also present in our new observation that all MLR events are accompanied by Pc 5 magnetic pulsations.

We have narrowed down the source region for MLR, and provided an evidence that it is, initially, triggered by PLHR. It is clearly a complex and finely balanced plasma wave process occurring on multiple time scales, but both self-sustaining and self-stabilising. On the basis of our observations low-level PLHR can act as the “seed” for MLR, after which multiple wave processes occurring in MLR decouple from PLHR. As such, the dominant energy source is unlikely to be PLHR, which probably explains the earlier results of *Rodger et al.* [1995, 1999, 2000a,b].

The fact that many MLR events were left-hand polarised may be explained by the mode conversion in the Earth-ionosphere wave-guide, as proposed in the case of PLHR-triggered emissions. In all cases when the MLR event showed the left-hand components, and as seen in Figures 5.1, 5.10, 5.11, and 5.12, the polarisation and the angle of arrival of the MLR event changed dramatically at about 2 kHz. The polarisation was almost circularly left-handed near 2 kHz and at higher frequencies it was elliptically left-handed until above 5 kHz it became purely linear.

Some MLR events had periodic amplitude and frequency modulation. The amplitude modulation had periods of 4-6 s, while the frequency swept linearly upwards with a rate of 3 Hz/s. The clearest modulation occurred in Event 1. There was no significant difference in the modulation periods at different frequencies. Neither the polarisation change affected the modulation.

The explanation of new features require theoretical studies as well as numerical simulations in the future. Also more orientation to the propagation of sferics and the spatial and temporal properties of the Earth-ionosphere wave-guide is required.

## Chapter 6

# Bursts of Very Narrow Band VLF hiss

Hiss-type ELF-VLF emissions appear mostly during auroral substorm onset and morning chorus. They are explained usually by Cerenkov radiation from the charged particles [e.g., *Ellis*, 1957; *Maggs*, 1976, 1978; *Yamamoto*, 1979] whilst discrete emissions are interpreted as being generated via cyclotron resonance [e.g., *Kennel and Petschek*, 1966; *Helliwell*, 1967; *Coroniti and Kennel*, 1970]. However, sometimes it seems that hiss and discrete emissions are connected.

The generation mechanism of plasmaspheric hiss has been studied by *Cornilleau-Wehrlin et al.* [1993]. They found three frequency ranges of wave spectrum maxima at  $\approx 0.4$ ,  $\approx 0.9$  and  $\approx 1.8$  kHz, which is expected because the plasmaspheric hiss occurs at low frequencies.

*Francis et al.* [1983] have studied abnormally high frequency, discrete VLF emissions and noticed that the groups of risers display a 4 min periodicity in occurrence. They observed also constant frequency tones and banded hiss around 7 kHz. Those events were explained to be originated in power line harmonic radiation as discussed by *Matthews and Yearby* [1981]. However, magnetospheric line emissions normally occur around 3 kHz [*Park and Helliwell*, 1978].

Narrow band 5 kHz hisses were observed by ISIS satellites between December 1976 and January 1983 [*Ondoh et al.*, 1981; *Ondoh*, 1993]. The hisses were found typically between invariant latitudes of about  $55^\circ$  and  $65^\circ$  under geomagnetically quiet conditions. The bandwidth varied from a few hundreds of Hz to a few kHz. *Ondoh* [1993] concluded that the narrow band hiss is completely different from electrostatic LHR hiss, but more likely it is plasmopause hiss.

The most recent Cluster satellite observations of narrow band hisses were reported by *Masson et al.* [2004]. These observations have been made in the immediate vicinity of the plasmopause. The hiss always corresponded to invariant latitudes from  $50^\circ$  to  $67^\circ$ .

*Coroniti and Kennel* [1970] presented a theory for interaction between VLF turbulence and magnetic micropulsations, which is a possible mechanism to produce modulated VLF emissions.

## 6.1 ULF Bursts

There are eight different types of hydromagnetic (HM) emissions introduced in detail by *Fukunishi et al.* [1981]. Their classification is based on frequency-time spectra of HM emissions. One of the classes is called HM emission burst, which seems to be somehow related to ELF-VLF observations in Finland (see also Chapter 8). In general, the HM emission bursts occur successively at irregular intervals of 10-30 min. These bursts differ from PiB (Pi burst) pulsations by their diurnal occurrence; PiB pulsations are observed at night closely associated with substorm activity, while the HM emission bursts occur in the daytime with a good correlation to the SI (sudden impulse)-like disturbances [*Hirasawa, 1980*]. Therefore, it is likely that these emissions are excited by a compression of the magnetosphere. However, a HM emission burst is quite a rare phenomenon, as *Fukunishi et al.* [1981] showed in their study over a 25-month period. Occurrence probability was only 4-5 %.

Unfortunately, on 25 January 1993 the nearest possible pulsation magnetometer at Kilpisjärvi had a malfunction. Instead of Kilpisjärvi data we have presented Ivalo (68.55° N, 27.28° E, L=5.7) pulsation magnetometer data. Ivalo is situated about 0.8° south of Kilpisjärvi in invariant magnetic latitude, but nearly 5° east in invariant magnetic longitude. The distance between these stations is 260 km.

The morning of 25 January 1993 was magnetically rather quiet. The  $K_p$  index varied between 1- and 3, and the local K index values at Sodankylä were between 0 and 2 during the first half of the day. The local activity was lowest during the early morning hours. HM emission bursts appeared at about 0700 UT lasting to about 1300 UT with two short gaps at 0940-1000 UT and 1120-1140 UT. In the beginning of the event these HM emissions occurred simultaneously with narrow band hisses. The initial frequency of HM emission bursts was about 0.5 Hz.

Within half an hour the frequency band of magnetic pulsations expanded in the range of 0.3-1.2 Hz. The first occurrence interval was at 0700-0940 UT. During that time the frequency of the intensity maxima of the pulsations increased from 0.5 Hz up to 0.8 Hz. The upper cutoff frequency of the bursts varied from 0.5 Hz to 1.2 Hz having a gradual tendency of frequency increase. During the first interval the repetition period of the bursts was about 30 minutes.

After a gap at 0940-1000 UT, the second pulsation occurrence period was between 1000 UT and 1120 UT. The frequency of maximum intensity increased again from 0.5 Hz to 0.8 Hz, while the upper cutoff frequency started to increase from 0.7 Hz reaching the maximum of 1.2 Hz at 1115 UT. The second gap was probably caused by sudden impulse (SI) in the magnetic field at 1116 UT. However, the third activation of HM emissions occurred at 1140 UT. The upper cutoff frequency started from 0.8 Hz and increased only to 1.0 Hz until 1200 UT, when the event started to diminish.

## 6.2 Observations

Figure 6.1 shows a time-compressed 6-hour plot (0600-1200 UT). The most prominent feature is a low-frequency chorus, whose frequency increases until 0940 UT. Within 4 hours the upper cutoff frequency of the chorus doubles. One interesting feature seen

easily in the 6-hour plot is that the intensity of the low-frequency chorus decreases approximately at the time when the narrow band hiss events start above 6 kHz (the latter is seen clearer in Figures 6.2 and 6.3).

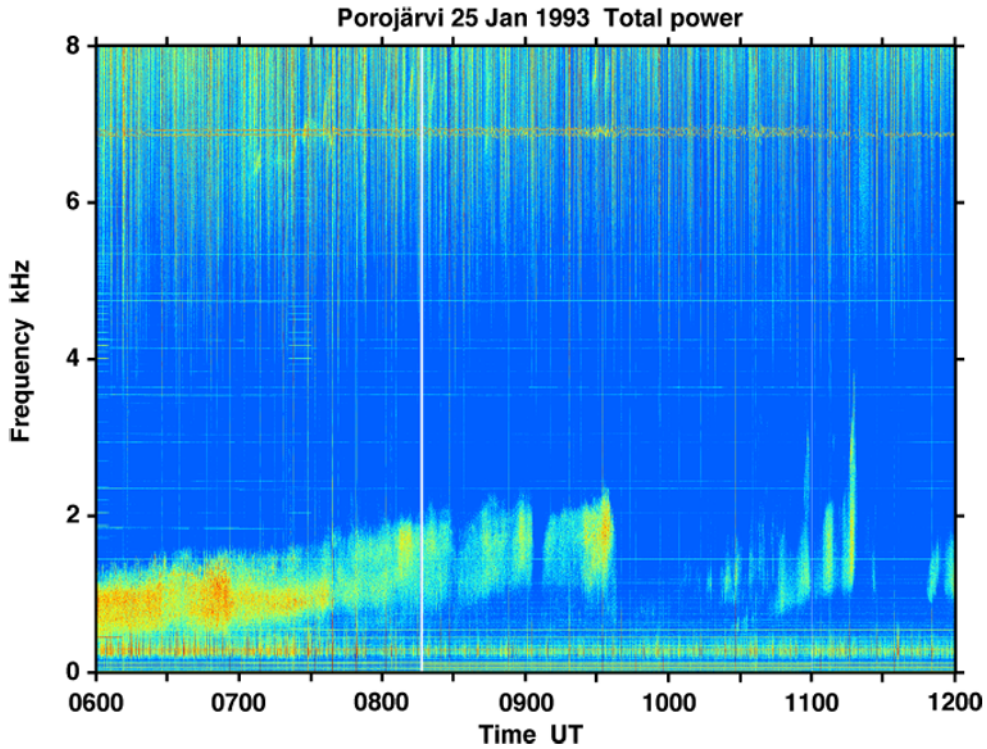


Figure 6.1: A 6-hour quick-look plot of narrow band hiss events observed between 0700 UT and 0940 UT at Porojärvi on 25 January 1993. The narrow band hiss events are very weakly seen above 6 kHz (they are seen clearer in Figures 6.2 and 6.3). The two waveforms near 7 kHz are multiplexed into the ELF-VLF data from a two-component pulsation magnetometer.

In total, 17 separate narrow band hiss bursts in the frequency range of 6-9 kHz were observed in 0700-0937 UT on 25 January 1993 (see Figures 6.2 and 6.3). Quite often the hiss events were modulated by a short-period pulsation with about 5 s period. They seem to be occurring at the same time as the HM (hydromagnetic) emission bursts, as seen in Figure 6.5, although a one-to-one correlation has not been found.

When one narrow band hiss (seen in the second panel of Figure 6.2) was investigated in detail, an amplitude modulation was observed. Such example is shown in Figure 6.4, where the upper panel displays the intensity of one event after 0800 UT. There is a clear modulation during the intensification. The lower panel gives the power spectrum with a prominent peak at 0.28 Hz.

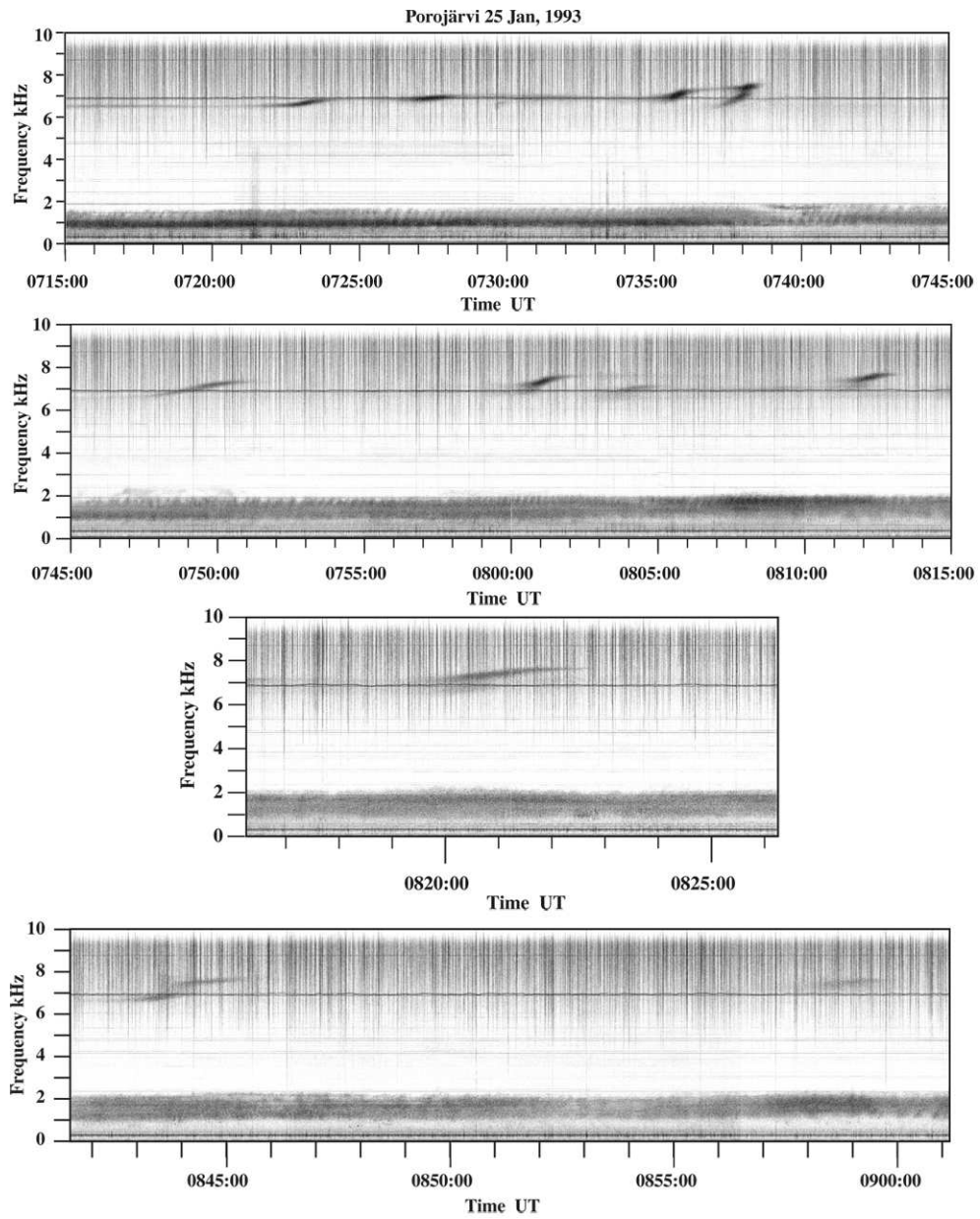


Figure 6.2: The high-frequency narrow band hiss events. There are altogether 14 events at 0715-0745 UT (top panel), at 0745-0815 UT (second panel), at 0816-0826 UT (third panel), and at 0841-0901 UT (bottom panel). Typical features, like increasing centre frequency and intensification at every  $\approx 10$  min, can be seen.

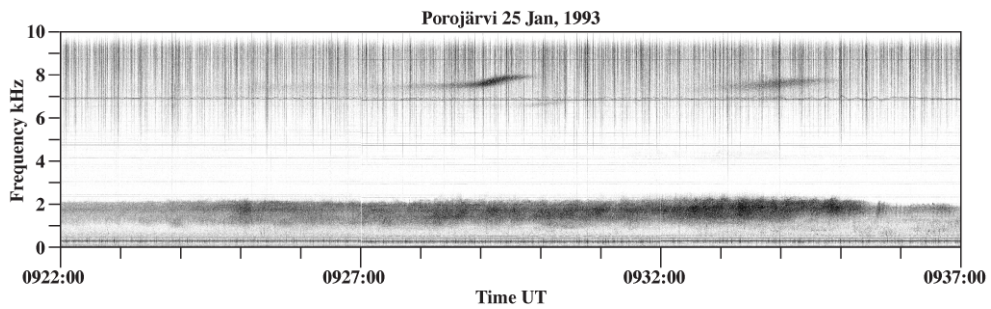


Figure 6.3: Same as in Figure 6.2, but at 0922-0937 UT. Three events are seen.

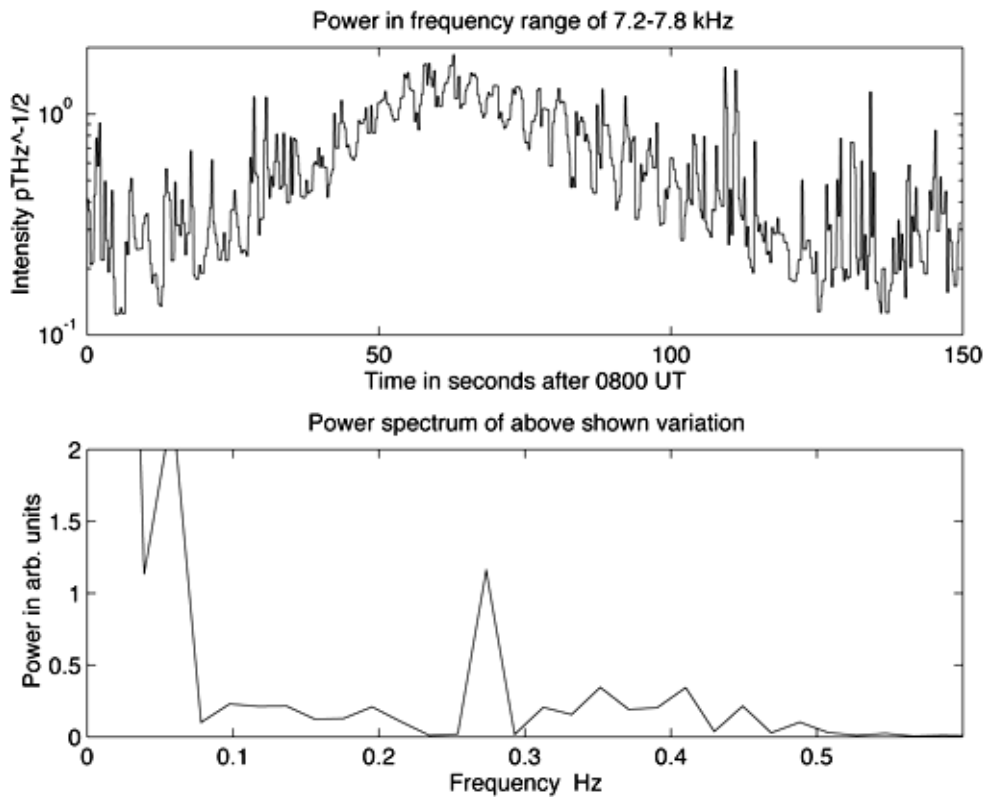


Figure 6.4: Amplitude modulation inside the narrow hiss event (upper panel). The power spectrum (lower panel) shows a clear peak at frequency of  $0.27 \pm 0.02$  Hz.

However, 0.28 Hz is well below the lower cutoff frequency of pulsation bursts simultaneously observed by induction coil magnetometer. Therefore, magnetic pulsations cannot directly explain the amplitude modulation.

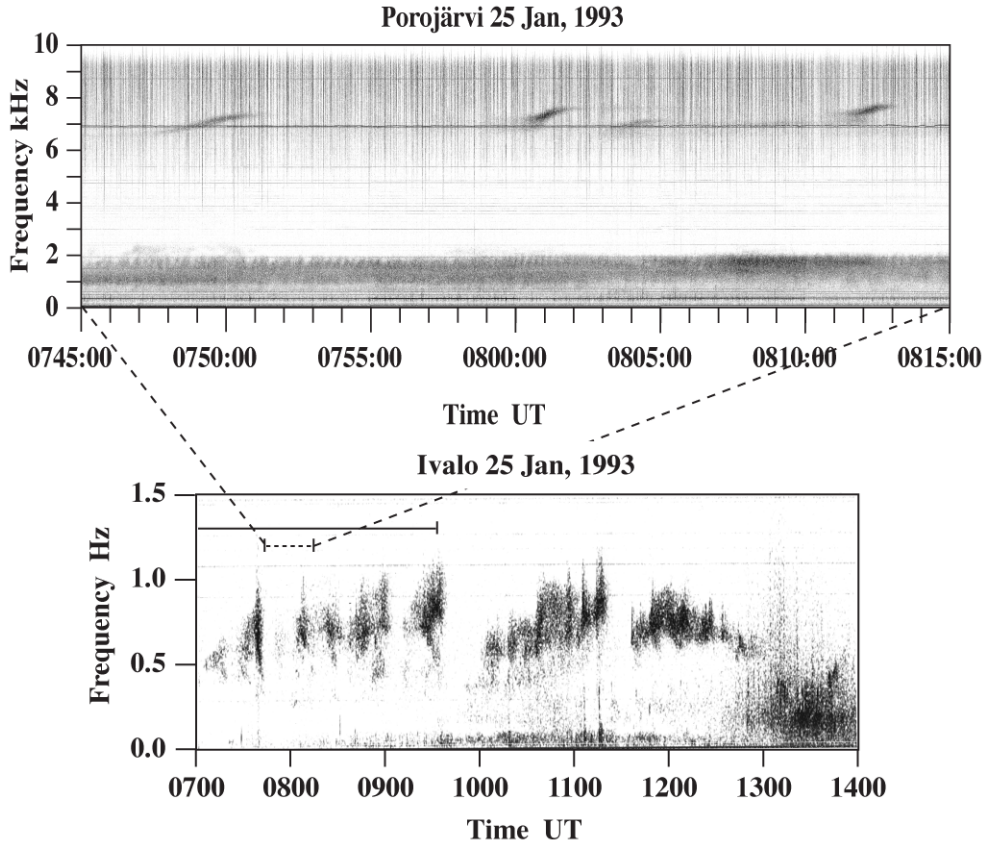


Figure 6.5: High-frequency narrow band hiss events observed at Porojärvi on 25 January 1993 (upper panel). Magnetic pulsation recordings were made at Ivalo (lower panel).

A low frequency chorus exists in the frequency band of 0.6-1.3 kHz at 0700-0750 UT. The mean frequency increases slowly from 0.8 kHz up to 1.0 kHz during that time. After 0750 UT the chorus was divided into two bands. The lower band was around 1 kHz and the upper band around 1.5 kHz. After 0805 UT the upper chorus band was activated and the mean frequency increased from about 1.5 kHz up to 1.8 kHz within one hour. Simultaneously the lower band disappeared.

When the high-frequency narrow band hisses disappeared totally for 15 minutes at 0825-0840 UT, also the low-frequency chorus became weaker. Reactivation started at 0840 UT and at 0903 UT all VLF emissions disappeared completely for 6 minutes. The last group of events appeared at 0909-0937 UT.

There are 10 characteristic features related to all of these narrow band hiss bursts. 1) The narrow band hisses appear together with the HM emission bursts. 2) The intensity of the narrow band hiss increases very slowly. During several minutes the intensity is just above the level of the background noise. 3) The frequency remains very stable when the intensity is low. 4) A sudden increase of the frequency of about 0.5 kHz occurs within 2-3 minutes. Then the event disappears. 5) Simultaneously with frequency increase, the intensity increases more than 10 dB. 6) The next event appears when the previous one has disappeared. The intensity of a starting event is just above the background noise level. 7) The mean frequency increases 0.3-0.5 kHz between events. 8) The repetition period of intensity maxima is roughly 10 minutes. 9) Also 0-2 kHz band has similar increase in the upper and the lower cutoff frequencies. 10) There is no obvious trigger, which causes the events.

Figure 6.5 presents four narrow hiss events (upper panel) and magnetic pulsations (lower panel) in the frequency range of 0-1.5 Hz recorded at Ivalo. The increase of the upper cutoff frequency of the magnetic pulsation bursts is consistent with ELF-VLF chorus and narrow band hisses. There is a gap of half an hour after 0940 UT, when no pulsations were observed. A new group of bursts occurred between 1010 and 1130 UT, which coincidences with a chorus activation, but no narrow band hisses were recorded. Again, the low-frequency hiss band had a similar increase in the upper and lower cutoff frequencies as earlier events.

### 6.3 Discussion and Conclusions

The narrow band hiss or line emission observed by *Francis et al.* [1983] had a frequency of 7 kHz and a duration of over 2 min. When a 100 Hz band filter was used for auto-correlation, the event showed a period of 1.98 seconds. *Francis et al.* [1983] explained the period as the two-hop echo time for the waves. Nevertheless, they did not mention the frequency drift or the frequency steps, which are visible in their Figure 4 [*Francis et al.*, 1983].

There are, however, many differences between observations made by *Francis et al.* [1983] and observations in Finland. Finnish observations show neither high-frequency discrete emissions, nor whistlers. The frequencies of the narrow band hisses and the low-frequency chorus behave quite the same in the sense that an increase occurs at the same time and with the same gradient. *Francis et al.* [1983] did not consider a chorus below 4 kHz at all, because semi-automated whistler analyses found the bearings to be different from that of the high-frequency emissions. Unfortunately, there is no information about the activity of the magnetic pulsations.

Another study by *Koons et al.* [1974] describes high-frequency narrow band events, but they are related to Doppler shifts of signals from the Transportable Very-Low-Frequency (TVLF) transmitter. They used 13.275 kHz as a carrier frequency, which was 100 % amplitude modulated by 0.5 Hz.

*Masson et al.* [2004] have found the following characteristics of the mid-latitude hiss events observed by four Cluster spacecrafts: 1) they occurred between 2 and 10 kHz, always below the electron gyrofrequency and the plasmafrequency but above the LHR; 2) they are 1-2 kHz wide; 3) they are banded in frequency; 4) they are right-hand

elliptically polarised electromagnetic waves; 5) they are escaping from the equator; 6) they are structure less, 7) rising tones and whistlers are sometimes embedded within; 8) they are lasting from a few minutes to an hour, always corresponding to invariant latitudes from  $50^\circ$  to  $67^\circ$ , and they are not MLT dependent.

The mid-latitude hiss events have similarities with a narrow band plasmopause hiss observed by the ISIS 1 and ISIS 2 satellites [Ondoh *et al.*, 1981; Ondoh, 1993]. In the paper by Ondoh [1993], similarity between ISIS and ground-based observations at Syowa station, Antarctica suggest that this hiss is electromagnetic, propagating in the whistler mode.

There are ten characteristic features related to all events summarised here:

- 1 The narrow band hisses appear together with the HM emission bursts.
- 2 The intensity of the narrow band hiss increases very slowly. During several minutes the intensity is just above the level of the background noise.
- 3 The frequency remains very stable when intensity is low.
- 4 A sudden increase of the frequency of about 0.5 kHz occurs within 2-3 minutes. Then the event disappears.
- 5 Simultaneously with the frequency increase the intensity increases more than 10 dB.
- 6 The next event appears when the previous one has disappeared. The intensity of a starting event is just above the background noise level.
- 7 The mean frequency increases 0.3-0.5 kHz between events.
- 8 The repetition period of intensity maxima is roughly 10 minutes.
- 9 Also the 0-2 kHz band has similar increase in the upper and the lower cutoff frequencies.
- 10 There is no trigger, which causes the events.

There are some overall features (like frequency band, polarisation, structureless) in our observations that resemble observations by Masson *et al.* [2004], but detailed characteristics (e.g., bandwidth, intensity maxima, relation to low-frequency chorus) seemed to be different.

The electron gyrofrequency at the equator at  $L=6.15$  is about 4 kHz, which means that our narrow band hisses were most likely originated from mid-latitudes, as long as the generation mechanism is the gyroresonance mechanism. The repetition period (10 min) of intensity maxima is too long to be explained by any Pc-type magnetic pulsation, but the HM emission bursts can have such a periodicity. However, observations by Fukunishi *et al.* [1981] were made at Syowa station ( $L=6$ ), which corresponds to the location of Porojärvi, but since the narrow band hisses have more mid-latitude origin, their relation to HM emission bursts is questionable.

Previous studies of narrow band hiss events [Ondoh *et al.*, 1981; Ondoh, 1993; Masson *et al.*, 2004] have shown that these events are electromagnetic but there might be some mode transfer process from electrostatic wave to electromagnetic wave that allows LHR hiss, being electrostatic, to propagate to the ground. LHR hiss is often observed in the mid-latitude topside ionosphere [Ondoh, 1993].

## Chapter 7

# Whistlers and Auroral Substorm

In this chapter 860 whistlers observed at Liikkuvankangas ( $67.51^\circ$  N,  $26.33^\circ$  E,  $L=5.18$ ) near Sodankylä in Northern Finland have been analysed covering the period from 2000 UT to 0024 UT on February 14-15, 1991. The magnetic activity was moderately high ( $K_p$  varied between  $2_+$  and  $4_-$ ) and two substorm onsets occurred at about 2214 UT and 2340 UT. The night was exceptional in the sense that the amount of whistlers recorded was very high. There are usually only a few whistlers at  $L>5$ .

A comparison has been made on the relative locations of auroral forms and active whistler ducts. The analysis was done using the diffuse equilibrium model given by *Park* [1972]. This method gives, e.g., the  $L$  values of the whistler paths and the equatorial electron density inside the whistler ducts. The whistler ducts were detected between  $L=2.4-4$  but they were clustered near a well-defined boundary between  $L=3.5-3.9$  during the studied period. The measured equatorial electron densities at the whistler duct boundary are of the order of  $400 \text{ cm}^{-3}$ , which proposes that the boundary was at or just inside the plasmapause.

The auroral forms were all the time located at higher  $L$  values than any of the detected whistlers. During the period between 2200 UT and 2340 UT the movements of the whistler duct boundary were related to the movements of the equatorward boundary of the auroral illumination. The substorms themselves do not seem to alter the plasmapause position in any remarkable way although tiny movements are clearly detectable.

### 7.1 Properties of Whistlers in Earlier Studies

Whistlers are an interesting wave phenomenon, because they connect ground level thunderstorms and magnetospheric phenomena. Lightning discharges on the ground radiate electromagnetic waves in a wide frequency range. Some wave energy from the Earth-ionosphere waveguide can penetrate through the ionosphere to the magnetosphere, where the whistler-mode waves travel through different magnetospheric

plasma populations. When travelling through plasma the whistler waves are dispersed depending on the plasma properties and they get their well known spectral forms [see e.g. *Helliwell*, 1965].

Whistlers propagating in the magnetosphere also interact with energetic particles. In these wave-particle interactions whistler waves can be amplified and pitch-angle diffusion can trigger electron precipitation into the ionosphere. This precipitation can produce, e.g., auroral emissions, X-rays and enhanced ionization [e.g. *Chang and Inan*, 1983a,b; *Doolittle and Carpenter*, 1983; *Rycroft*, 1991]. Whistlers can also trigger other interesting ELF-VLF phenomena like chorus and hiss-type emissions.

For a long time, it was thought that whistlers propagate in the magnetosphere in field-aligned tubes of enhanced electron density, so-called whistler ducts, and that most of the whistlers observed on the ground are ducted whistlers [*Helliwell*, 1965]. Another propagation mode is unducted propagation and usually whistlers propagating in the unducted mode are not observed on the ground because these waves are reflected upward above the ionosphere at the lower hybrid frequency [*Edgar*, 1976; *Kimura*, 1985]. Unducted propagation is thought to be the most common mode in the magnetosphere.

According to *Thomson and Dowden* [1977] as well as *Thomson* [1977], unducted pro-longitudinal (PL) whistlers can be occasionally observed also on the ground and are more interesting, because they allow to study the plasmasphere more widely than normal ducted whistlers. It is not possible to determine if the whistlers are ducted or if they are PL whistlers based on ground-based measurements only: additional satellite measurements are required.

Some experimental evidence for the existence of whistler ducts was found in satellite measurements. *Angerami* [1970] deduced from OGO-3 satellite data that in the duct the plasma density is enhanced by typically 6-22% only rarely exceeding 33%. The L shell thickness of the ducts was in the range of 220-450 km in the equatorial region and 15-27 km at ionospheric heights. At the equator the separation between single ducts was found to be 110-1140 km and at ionospheric heights 6-73 km in north-south direction. The width of the duct in longitude was estimated to be 4°.

*Mosier* [1976] found evidence of field-aligned enhancements of ionization measured by the RAE-1 satellite near L=2. The enhancement factor was up to 45% and the duct diameter a few hundreds of kilometres. During times of local sunset at low latitudes high enhancements of over 100% have been found [*Hayakawa and Iwai*, 1975]. *Ondoh* [1976] deduced from the satellite data the latitudinal variation of the duct dimension. At middle latitudes the dimension was around 10-40 km. The duct dimension was found to decrease with decreasing geomagnetic latitude.

The exit point of the whistler duct in the ionosphere was found to be at altitudes from a few hundreds of kilometres up to a few thousands of kilometres [*Bernhardt and Park*, 1977; *Thomson and Dowden*, 1977, 1978; *Tixier et al.*, 1984]. Theories for the formation of the whistler ducts and whistler wave propagation in the duct have been proposed, e.g., by *Park and Helliwell* [1971], *Thomson* [1978], *Walker* [1978a,b], *Lester and Smith* [1980], and *Hayakawa and Ohta* [1992].

Whistlers make it possible to study many magnetospheric plasma properties, because they contain a lot of information on the magnetospheric plasmas through which they propagate. For example, the plasmopause was first discovered by ground-based

whistler measurements [Carpenter, 1963]. After that the whistlers became the basic tool for plasmasphere and plasmopause studies. The structure of the plasmasphere can be effectively studied by ground-based whistler measurements. The location of the plasmopause and its variations with magnetic activity and time can be estimated from whistler observations [e.g. Carpenter, 1966; Angerami and Carpenter, 1966; Sagredo and Bullough, 1973; Turunen and Oksman, 1979]. The plasmopause is usually located at  $L=3-6$  depending on magnetic activity and local time.

In the equatorial region the electron density of the plasmasphere deduced from whistler measurements was found to be in good agreement with satellite measurements [Carpenter *et al.*, 1981]. Furthermore, by ground-based whistler measurements it is possible to estimate the east-west electric fields in the equatorial region of the magnetosphere [e.g. Bernard, 1973; Sagredo *et al.*, 1973; Block and Carpenter, 1974; Park, 1978, 1982; Sazhin *et al.*, 1992]. Moreover, some estimates of the electron temperatures in the magnetosphere can be obtained by studies of whistlers [review by Sazhin *et al.*, 1992, 1990].

## 7.2 Whistler Analysis

All selected whistlers were analysed by using the methods by Park [1972] and Tarcsai [1975]. By these methods it is possible to estimate several parameters: the nose frequency, the dispersion during the propagation along the path, the nose delay, the gyro-frequency of electrons in the equatorial plane, the  $L$  value of the whistler duct, the equatorial electron density in the whistler duct, the electron density in the ionosphere at 1000 km altitude, and the total number of electrons within the whistler path.

The models by Park [1972, 1982] are based on the derivation of whistler-wave travel time. The travel time was found to be proportional to the equatorial electron density and to the function which describes the variation of the electron density along the magnetic field line, inversely proportional to the wave frequency, and to the equatorial electron gyro-frequency [see Equation 2.1 in Park, 1972]. The function of the variation of the electron density can be solved by considering either the diffusive equilibrium model (DE model) or the collisionless model (R-4 model). Here the diffusive equilibrium model has been chosen, because all whistlers propagated inside the plasmopause. It can be deduced from the level of the magnetic activity, the location of auroral forms, and the  $L$  values of the whistlers obtained from the analysis.

Both models describe the electron distribution along the magnetic field line at 1000 km altitude. In the diffusive equilibrium model the ion concentration is usually supposed to be 90 % of  $O^+$ , 2 % of  $He^+$  and 8 % of  $H^+$ . The diffusive equilibrium model is useful when the electron densities are of the order of  $100 \text{ cm}^{-3}$  or more in the duct [Angerami and Carpenter, 1966], this condition is met inside the plasmasphere. The collisionless model is more useful outside the plasmopause where electron densities in the duct are smaller of the order of  $1-10 \text{ cm}^{-3}$ . The differences between these two models have been described by Angerami and Carpenter [1966].

Empirical formulas for the calculation of the whistler parameters mentioned previously as well as their error estimates were derived by Park [1972]. Moreover, Park took the ionospheric and wave-guide effects to the whistler wave propagation into ac-

count. The basic parameters in the equations by *Park* [1972] are the nose frequency and the group delay time of the whistler. In most of the cases one or both of these two parameters cannot be determined from the measured spectrograms. In this case these parameters can be extrapolated from the spectrograms by different methods. Here the least squares fitting method by *Tarcsai* [1975] has been used.

All whistlers were analysed by using a signal analyser and the best time-frequency pairs were taken into account for curve fitting. The frequency points were chosen within the frequency range of 2750 Hz to 6000 Hz in frequency steps of 250 Hz.

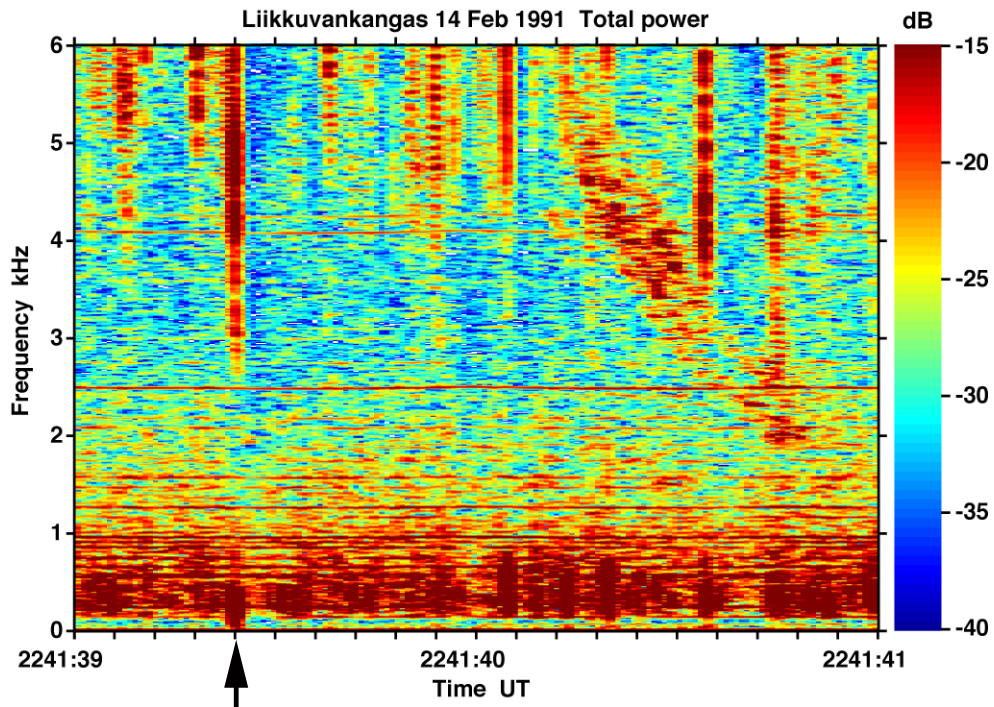


Figure 7.1: An example of the whistler recorded on 14 February 1991 at 2241:40 UT. The causative sferic is shown by an arrow at the bottom.

## 7.3 Observations

### 7.3.1 Whistlers and magnetic activity

An example of a whistler recorded on 14 February 1991 at 2241:40 UT is shown in Figure 7.1. The causative sferic of the whistler is shown by an arrow at the bottom. The extrapolated nose frequency for the whistler is 6784 Hz and the group delay time (the time between nose of the whistler and the sferic) is 1.1 s. This whistler propagated along the L shell of 3.63.

All the whistlers received on that evening and night were single, discrete type whistlers. No multi-component whistlers were observed. This is unfortunate because from this data set it is not possible to estimate the cross-L motions of the individual whistler ducts and thus to determine, e.g., the equatorial electric field and the exact location of the plasmopause.

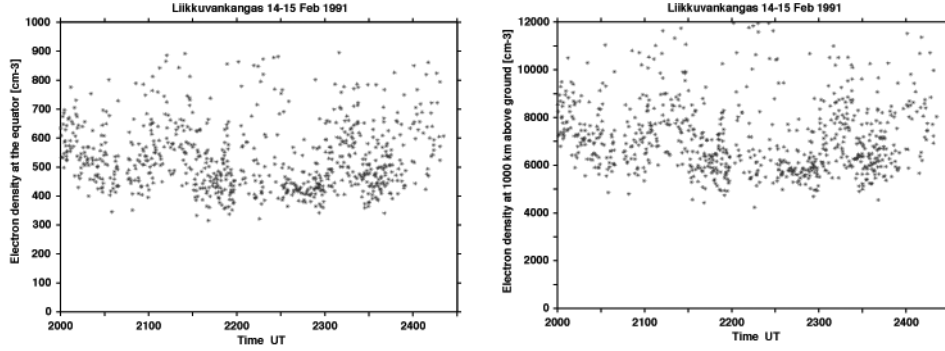


Figure 7.2: Electron densities at the equator and at 1000 km above ground obtained from analysis of 860 whistlers.

The  $K_p$  index during 1800-2100 UT and 2100-0000 UT on 14 February was  $2_+$  and  $3_-$ , respectively. On 15 February 0000-0300 UT the  $K_p$  index was  $4_-$ . A crude estimate for the location of the plasmopause ( $L_{pp}$ ) as a function of magnetic activity can be obtained by the formula

$$L_{pp} = 5.7 - 0.46 \cdot K_{pmax}, \quad (7.1)$$

where  $K_{pmax}$  is the maximum  $K_p$  value in the preceding 12 hours [Carpenter and Park, 1973]. According to this the plasmopause was located approximately at the L value of 4.0-4.4 during the studied period.

The whistler ducts were detected at L values between 2.4 and 4.0, but they were clustered near a well-defined boundary within  $L = 3.5-3.9$  (see Figure 7.3). These values are inside the calculated plasmopause position. The equatorial electron densities in whistler ducts vary between  $400 \text{ cm}^{-3}$  and  $700 \text{ cm}^{-3}$ , which are typical values inside the plasmasphere. These results indicate that most whistler ducts were inside the plasmasphere or very near the plasmopause, which has been shown to be a good VLF wave-guide [Inan and Bell, 1977].

### 7.3.2 Auroral activity

The comparison between auroral motions and the whistler ducts together with magnetic field variations is shown in Figure 7.4. The L values of the equatorward boundary of the auroral forms were estimated from TV images. The variation of the L values of the whistler ducts was obtained as 5 min averages. The variations of the magnetic field were measured at Sodankylä about 20 km from the VLF station. The lower panel of

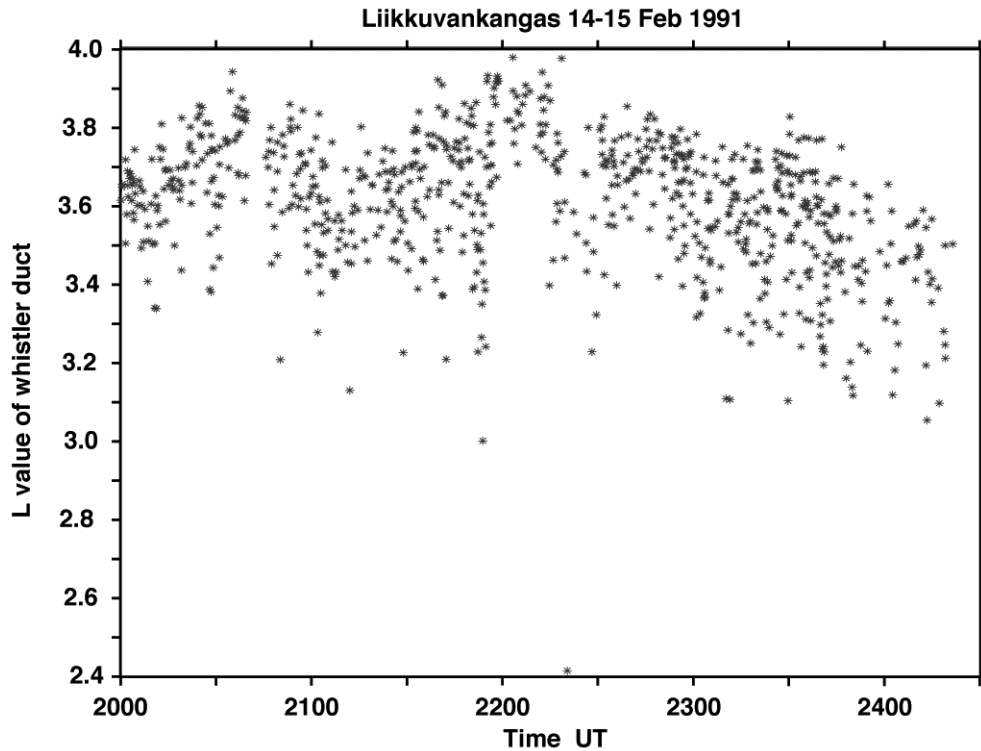


Figure 7.3: The  $L$  values of 860 whistlers are plotted versus time. There is a clear cluster of the whistler ducts in  $L$  range of 3.5–3.9.

Figure 7.4 presents the magnetic pulsations in the frequency range of 0–1.6 Hz. Clear substorm related Pi pulsations are seen at about 2215 UT and at about 2245 UT. The auroral activity started at about 1800 UT and a few weak arcs appeared in the north. At 1930 UT those arcs passed our station and they continued to move southward. The magnetic X component decreased slowly until 2214 UT when a tiny, short-lived disturbance occurred. Until then the equatorward southern boundary of the aurora moved slowly southward but during the magnetic disturbance at 2214 UT a clear rapid equatorward motion took place followed by movement back in a way we have not been able to define exactly. A similar auroral event was studied by *Safargaleev et al.* [1996], but they did not analysed ELF-VLF data at all. They have shown that the plasma depletion was observed only on the poleward edge of an auroral arc.

After that disturbance the equatorward movement continued in quite a similar way as earlier until a clear substorm onset at 2340 UT caused active aurora and made the determination of the border impossible from the available recordings.

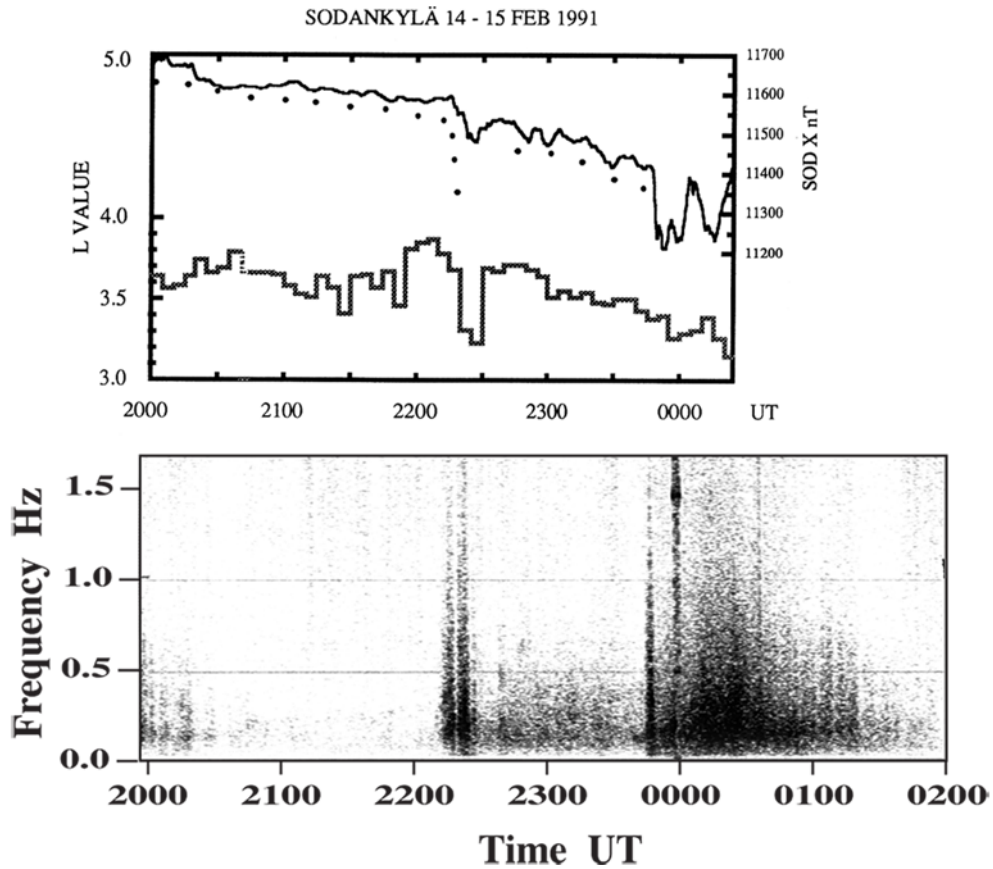


Figure 7.4: The upper panel shows the L value of the whistler boundary (lowest curve), the magnetic field X component (uppermost curve), and the equatorward boundary of the observable auroral illumination as determined from auroral TV pictures (dots) between 2000 and 0024 UT. The lower panel shows the ULF spectrum in the frequency range of 0–1.6 Hz. Clear substorm related Pi pulsations are seen at about 2215 UT and at about 2245 UT.

Before 2140 UT the whistler duct boundary was located around  $L=3.7$  showing small excursions without any recognisable connection with the magnetic excursions and auroral boundary. Around 2200 UT the duct boundary moved poleward to  $L=3.9$  from where it moved rapidly equatorward to  $L=3.3$  at the same time as the tiny magnetic disturbance and related equatorward movement of auroras took place. Even the value of the relative movements seems to be the same.

At 2230 UT the whistler duct boundary moved rapidly back to about  $L=3.7$  from where it moved slowly equatorward reaching  $L=3.2$  at 0024 UT. The clear substorm having its onset at 2340 UT caused barely noticeable equatorward movement of the whistler duct boundary. Between 2230 UT and 2340 UT the auroral border and the

whistler duct boundary had a very similar trend in their movement. After 2340 UT we have not been able to define the auroral border.

## 7.4 Discussion and Conclusions

The measured whistler duct boundary was located around  $L=3.5-3.9$ , which seems to be just inside the plasmopause. When compared to the equatorward boundary of the auroral forms, the whistler duct boundary was always located at lower  $L$  values. The relative movements between whistler duct boundary and auroral forms were quite unrelated except between 2214 UT and 2340 UT, i.e. from the first tiny magnetic disturbance to the onset of the substorm when the movements seem to be in fact closely related. The substorm itself at 2340 UT did not have any remarkable effects in the whistler duct boundary movements. If our whistler duct boundary reflects the movements of the plasmopause then only at about 2214-2340 UT the movements of the border of the auroral forms and plasmopause were coupled together.

The whistler activity on 14-15 February 1991 was exceptionally high. From the ELF-VLF recordings the 860 strongest whistlers were selected for the analysis, the total amount of the observed whistlers was even higher. At the auroral zone an auroral substorm is a very natural phenomenon. Similarly, the whistler rate can occasionally be very high, but very seldom these have been observed simultaneously. Obviously, the second substorm at 2340 UT occurred too far from the receiver in order to observe whistlers having ducts at the longitude of the substorm.

The analysis shows that under suitable conditions, whistlers can be used to study even the details of processes near the plasmopause during magnetic events. On the other hand such conditions are only rarely met.

## Chapter 8

# Chorus and ULF Bursts

Many authors have shown that ELF-VLF and ULF waves correlate with each other [e.g. *Sato*, 1980; *Sato and Kokubun*, 1980; *Sato and Fukunishi*, 1981; *Sato and Kokubun*, 1981]. However, these authors have found correlation only between ELF-VLF emissions and Pc 3-4 magnetic pulsations. Figure 8.1 shows an event, where there is a relation between low-frequency chorus and HM (hydromagnetic) emission bursts. These HM emission bursts are quite a rare phenomenon as mentioned in Chapter 6. Their occurrence is concentrated around magnetic local noon, and their frequency range is fairly wide at  $\approx 0.1$ – $2.0$  Hz [*Fukunishi et al.*, 1981].

### 8.1 HM Emission Bursts

HM emission bursts were observed on 20 January 1993 between 0800 UT and 1000 UT. Unfortunately, the nearest pulsation magnetometer at Kilpisjärvi had a malfunction on that day. Instead of Kilpisjärvi data, we have presented Ivalo ( $68.55^\circ$  N,  $27.28^\circ$  E,  $L=5.7$ ) pulsation magnetometer data. Ivalo is situated about  $0.8^\circ$  south of Kilpisjärvi in invariant magnetic latitude, but nearly  $5^\circ$  east in invariant magnetic longitude. The distance between Porojärvi and Ivalo is 260 km.

The time of observations is consistent with the definition given by *Fukunishi et al.* [1981]. Also the frequency range is the same as in their observations. There were 11 bursts during two hours. The bursts, which were most intense, had also the highest upper cutoff frequency reaching 1.4 Hz at maximum. Otherwise the upper cutoff frequency varied between 1.0 and 1.4 Hz. The lower cutoff frequency was not as simple to determine due to increasing low-frequency noise.

In the beginning of the event, bursts showed some features of dispersive HM emissions or dispersive irregular HM emissions. Possibly the event was a combination of all the HM emission types mentioned above.

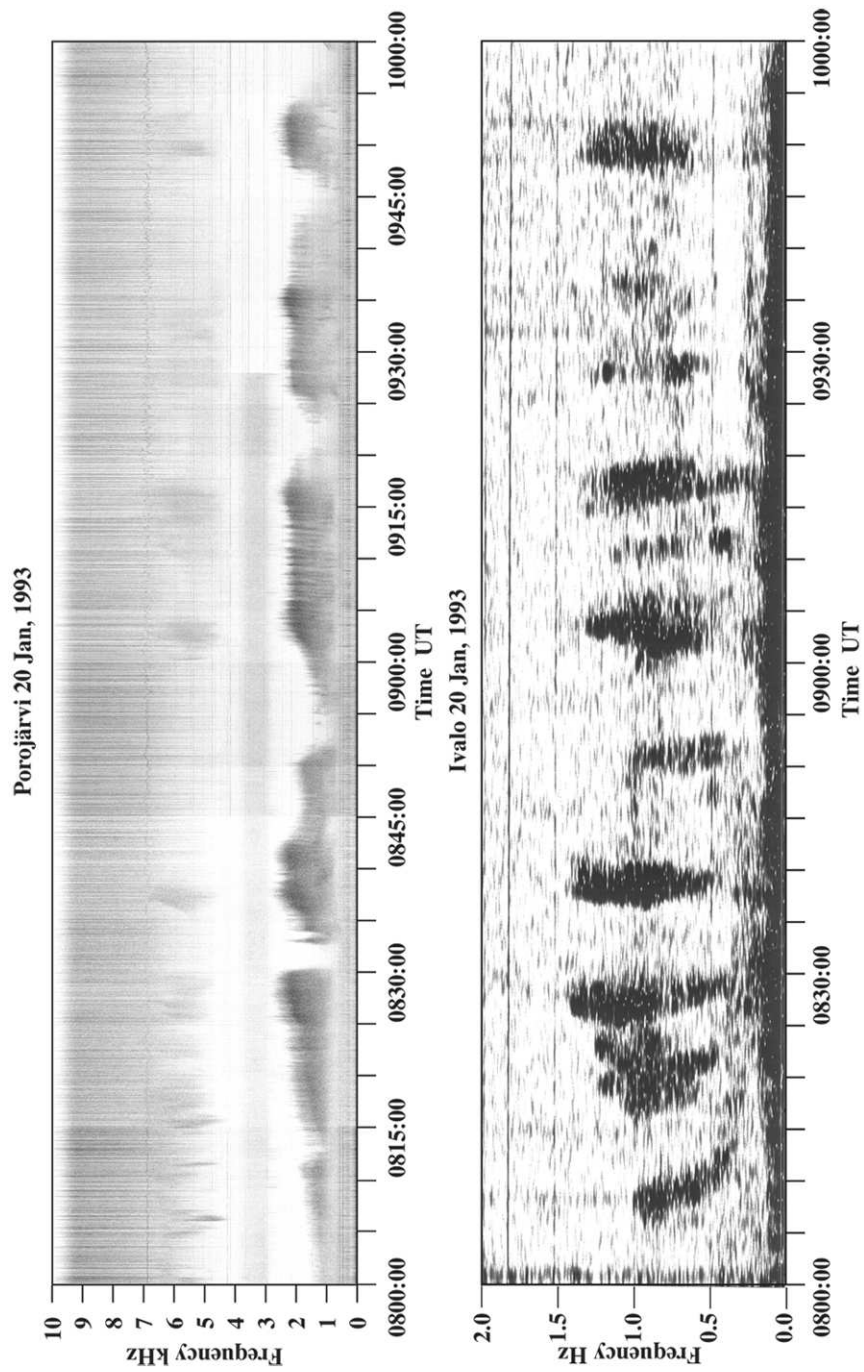


Figure 8.1: The upper cutoff frequency of the ELF-VLF chorus below 3 kHz in the top panel shows clear correlation with the upper cutoff frequency of the ULF bursts in the bottom panel. The ratio between cutoff frequencies is  $1921.2 \pm 170.3$ , which is close to the mass ratio of protons to electrons (see text for details).

## 8.2 ELF-VLF Frequencies <3 kHz

Already before 0600 UT there was weak morning chorus, which disappeared at about 0720 UT. A chorus intensification occurred at 0711-0718 UT, when simultaneously a high-frequency chorus burst occurred (see Figures 8.2 and 8.3). After half an hour of silence, the morning chorus started again at 0750 UT. The upper cutoff frequency increased from 1 kHz to 2.7 kHz within one hour. It stayed above 2 kHz until at 1000 UT the chorus weakened abruptly. There were several gaps during the chorus roughly every 15 minutes. The gaps might be due to short-lived sharp decreases in the magnetic field (in all components).

Individual discrete emissions inside the chorus bursts reached the upper cutoff frequency of 3 kHz, but the significant cutoff frequency of the chorus remained below 2.7 kHz. The lower cutoff frequency was about 1 kHz before 0815 UT and after that it decreased down to 0.75 kHz. One possible reason for the 750 Hz cutoff frequency might be the 15<sup>th</sup> harmonics of 50 Hz.

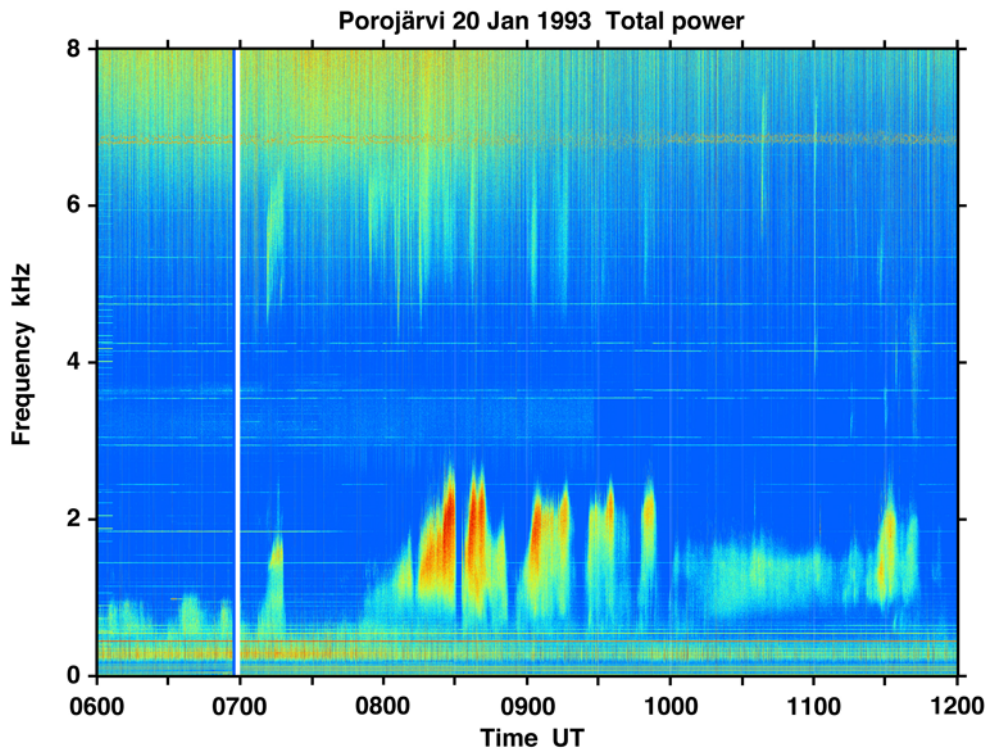


Figure 8.2: A 6-hour quick-look plot with 0–8 kHz range recorded on 20 January 1993 at Porojärvi. There are chorus bursts between 0800 UT and 1200 UT. Some high-frequency emission bursts are above 4.5 kHz. The narrow white line just before 0700 UT is a data gap due to the change of the recording video tape. This is the same as Figure 3.5 in Section 3.3.

The intensity of the chorus increased together with the upper cutoff frequency approaching a maximum at 0828 UT. After a 3-minute gap, the intensity stayed at the same level until 0842 UT, when both intensity and upper cutoff frequency began to decrease. The next gap started at 0852 UT and it, too, lasted 3 minutes. The next intensity maximum occurred at 0904 UT. Now the chorus remained at that level until 0917 UT, when the third gap occurred. At 0920 UT the chorus returned back to the previous level, and it stayed there till 0943 UT, when the last gap started. The last intensification occurred at 0947-0958 UT.

### 8.2.1 Relation between upper cutoff frequencies

The upper cutoff frequency of ELF-VLF chorus varied between 1 kHz and 2.7 kHz, while the upper cutoff frequency of simultaneously occurring HM emission bursts varied between 1.0 Hz and 1.5 Hz. At the time of an individual HM emission burst, the ratio between cutoff frequencies can be calculated. Due to the frequency resolution of the ULF spectrum the uncertainty is  $\pm 5\%$ . In ELF-VLF chorus the upper cutoff frequency can be chosen either at the highest frequencies of individual discrete emissions or at the mean of the highest chorus frequency. This causes about 10% uncertainty. Taking into account both inaccuracies the ratio is  $1921.2 \pm 170.3$ . Interestingly the result is close to the mass ratio of protons to electrons ( $\approx 1840$ ).

It is also the ratio between the gyrofrequencies of an electron and a proton at the same location inside the magnetosphere. If we suppose the HM emission bursts were generated in a proton-cyclotron process in the magnetosphere, then the generation region both for the ELF-VLF chorus and the HM emission bursts was the same. But if we suppose the bursts were generated in another ion-cyclotron process, then the generation regions must be at different places in the magnetosphere.

Local frequency maxima in ELF-VLF chorus occurred at the time of HM emission bursts. Between the maxima the upper cutoff frequency of ELF-VLF chorus decreased by 0.1-0.2 kHz.

## 8.3 VLF Frequencies at 3-4 kHz

The storm sudden commencement (SSC) at 1021 UT or the sudden impulse (SI) at 1146 UT on 19 January 1993 initiated a weak hiss band between the doublets of 2950 and 3650 Hz. This weak band was not affected by any change in other ELF-VLF bands. However, this band did not stay stable, but sometimes it consisted of a bunch of harmonics and sometimes it was a pure hiss. There were randomly occurring spikes below the lower part of the hiss band after 0730 UT (see Figures 8.2 and 8.3).

Suddenly, all activity, except PLHR, between 3 and 4 kHz stopped at 0928 UT. There was no remarkable reason for this in geophysical parameters, like in magnetic field variation, in ionospheric absorption, or in the solar wind.

The discrete emissions after 1115 UT seen in Figure 8.2 were PLHR-triggered emissions, and they were studied in detail in Chapter 4. However, the earlier events during this morning were not directly triggered by PLHR.

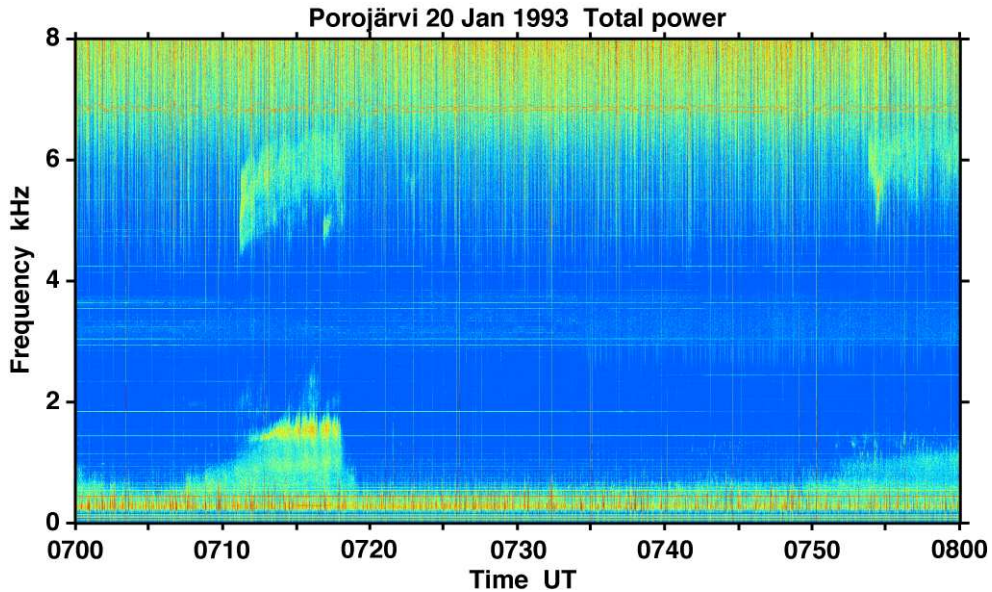


Figure 8.3: A 1-hour quick-look plot of data recorded on 20 January 1993 at Porojärvi. There were two chorus bursts starting at 0711 UT and at 0754 UT in the frequency range of 4.5-7.0 kHz. Both bursts lasted 7 min.

## 8.4 VLF Frequencies >4 kHz

Figure 8.3 shows a 1-hour quick-look plot with 0–8 kHz frequency range at 0700–0800 UT. The first chorus burst above 4.5 kHz started at 0711 UT and it lasted for 7 minutes. It consisted of discrete emissions, and it had an amplitude modulation with  $\approx 60$  s period.

The mean frequency of the chorus burst increased by 800 Hz (from 5.2 kHz to 6.0 kHz). The next burst occurred above 5 kHz at 0754–0801 UT. After 0800 UT all chorus bursts at the frequency range of 4.5–7.0 kHz occurred simultaneously with intense HM emission bursts. There were two HM emission bursts, which were not accompanied by chorus bursts above 4.5 kHz (at 0850 and 0935 UT).

The events after 0754 UT were more likely discrete emissions instead of chorus bursts. They usually had an intense part with a duration of less than one minute, and otherwise the emissions were much weaker. After 0910 UT these events resembled a hiss without clear discrete emissions.

### 8.4.1 Relation between intensities

Discrete emissions and hiss appeared above 4.5 kHz only at the time of intense HM emission bursts. There were no emissions or hiss at 0850 UT or at 0935 UT. Events above 4.5 kHz were not related to the frequency of the HM emission bursts.

There is one interesting feature between events below 3 kHz and above 4.5 kHz. Namely, the higher frequency events seemed to lead the lower frequency ones. This can especially be seen at 0837 and 0902 UT in Figure 8.1. A similar conclusion could also be made about the event at 0711 UT in Figure 8.3.

The time difference between the maximum intensities of low-frequency ELF-VLF chorus and HM emission bursts was about 100 s, while the time difference in the case of the 4.5 kHz events above was even 200 s. In both cases the ELF-VLF waves led the HM emission bursts. This delay can be explained partly by the difference in propagation velocities between Alfvén and ELF-VLF waves, but it is difficult to find a reason for the delay of 200 s.

## 8.5 Discussion and Conclusions

Usually, the relation between ULF and ELF-VLF waves is seen as an amplitude modulation, i.e. ELF-VLF chorus is modulated by Pc 3-4 magnetic pulsations with a modulation period of 15 to 150 s. There are several studies related to this interaction [see *Sato*, 1980; *Sato and Kokubun*, 1980; *Sato and Fukunishi*, 1981; *Sato and Kokubun*, 1981; *Manninen et al.*, 1994; *Morrison et al.*, 1994; *Sazhin and Hayakawa*, 1994; *Alford et al.*, 1996; *Smith et al.*, 1998; *Engebretson et al.*, 2004]. Nevertheless, none of them reports any relation between the upper cutoff frequencies of ULF and ELF-VLF waves.

The most common wave-particle interaction for ELF-VLF waves is the cyclotron resonance between the wave and the electrons propagating in the opposite direction. For instance, *Pasmanik et al.* [1998] have developed a theoretical model, which is very useful for the explanation of the main features of energetic electron fluxes observed aboard low-altitude satellites as the energetic electrons drift into a region of enhanced plasma density and precipitate from the outer radiation belt. This model describes the cyclotron wave-particle interactions during magnetic storms. Unfortunately, this theory is not taking into account the ions. However, already *Ginzburg* [1961] proposed the cyclotron resonance between the ELF-VLF wave and the proton beam propagating in same direction. Thereafter *Kimura* [1961] made detailed calculations of the interaction.

*Neufeld and Wright* [1964] showed theoretically that an interaction between a proton beam and a whistler-mode wave can occur, when the velocity of a proton beam equals the group velocity of a wave. There are two velocities, which leads to frequencies of  $\omega_1 = \frac{1}{2}\omega_{He}$  and  $\omega_2 = 2\omega_{Hi}$ . *Gendrin* [1965] proposed that the interaction occurs in a wide frequency range around  $\omega_1$  and  $\omega_2$ .

Some newer studies of the interaction between the whistler-mode waves and the proton beams were made by *Akimoto and Winske* [1989] and *Kozyra et al.* [1994].

The above mentioned reports show that the interaction is possible, but they cannot explain the observed ratio between the upper cutoff frequencies, which is close to the gyrofrequency ratio of electrons to protons at the same location in the magnetosphere. So far, the event shown in this thesis is the only observed event of its kind.

## Chapter 9

# ELF-VLF and Auroral Emissions Related to Pc 3

Regular magnetic pulsations with periods of about 30-40 s (Pc 3) sometimes exhibit a one-to-one correlation with quasi-periodic VLF emissions. This shows that the hydromagnetic wave can modulate the local parameters in space strongly enough that suitable conditions for particle interaction are formed. A phase delay of about half a wavelength is usually seen between quasi-periodic VLF emissions and ULF waves on the ground, because of the difference in propagation velocity of the waves [e.g. *Sato, 1980*]. Wave-particle interaction should cause particle precipitation, which, in turn, should cause detectable optical emissions.

Pc 3 waves are believed to be generated in the solar wind outside the magnetosphere by solar wind protons. The waves propagate into the magnetosphere and can be detected also on the ground. The periods are of the order of 30-40 seconds and at least on the ground the waveform is quite regular and monochromatic. The period seems to be well related to the solar wind speed and it has been found that  $f(\text{mHz}) \approx 6B$  (nT), where  $B$  is the magnetic flux density of the IMF [*Troitskaya et al., 1971, 1972; Guglielmi et al., 1973*]. *Engebretson et al.* [1986] showed that this relationship also holds for some of the high-latitude pulsations.

Near and inside the plasmasphere these waves give rise to a set of other phenomena. One is the generation of quasi-periodic VLF waves [*Carson et al., 1965; Sato and Kokubun, 1980; Sato and Fukunishi, 1981; Sato and Kokubun, 1981*]. This is seen as periodically changing intensity and spectral structures of various hiss and chorus components at least in the frequency band of a few hundred Hz to a few kHz. The observed time delays between the wave phases of Pc 3 waves and the periodic variation of VLF waves indicate, that the region where the modulation takes place is somewhere in the equatorial zone near the plasmopause or in plasmasphere.

If the explanation is true, that the magnetic waves are originally generated outside the magnetopause [*Troitskaya et al., 1972*], then necessarily the magnetic wave is the source wave and the behaviour of the VLF waves is only a modulation caused by the magnetic wave. The growth of VLF waves gets the energy from the energetic particles in wave-particle interactions and as a result precipitation of particles to

the atmosphere is possible. The precipitation of electrons having energies of tens or hundreds of keV can be detected on the ground by measurements of the D-layer absorption of HF waves, e.g., by riometers. Precipitation of low-energy electrons is often observed in optical emissions from E- and lower F-layer altitudes.

*Engbretson et al.* [1994a,b] have studied similar events as presented in this thesis, but they did not have wide-band ELF-VLF recordings.

## 9.1 Observations

We have made simultaneous recordings of optical emissions, VLF emissions and magnetic pulsations at Porojärvi in Northern Finland ( $L=6.1$ ) in January 1993. Optical emissions were recorded by a simple wide angle photometer based on a silicon photo diode without any filters. It has a wide ( $\approx 45^\circ$ ) field of view and it is sensitive from about 500 to 1050 nm. The magnetic pulsations were measured by a 2-component induction coil magnetometer. The VLF recordings were made by “coaxial cable” receiver. For absorption measurements we have used our nearby riometer stations at Kevo, Kilpisjärvi and Ivalo.

On 15 January 1993 in the late morning hours at about 0551 UT, a strong Pc 3 event occurred and continued for several hours. The pulsation event was strong with peak-to-peak amplitudes temporarily in excess of 15 nT. Pulsations were structured changing often in amplitude in time scales of a few minutes or tens of minutes. During most of the time a one-to-one correlation was found between quasi-periodic VLF events and Pc 3 pulsations (Figure 9.1). The magnetic pulsations had a lag of about 40 s with VLF chorus variation. This is in agreement with the difference of the propagation velocity between ULF and VLF waves if the interaction is assumed to take place at the equatorial region.

Optical pulsations were seen for the first time at about 0600 UT. These pulsations clearly correlated with Pc 3 and there is no doubt that those two phenomena were closely coupled. The recording of optical pulsation stopped at 0722 UT (0922 LT), when the rising sun finally caused the detector amplifier to saturate. Perfect correlation between VLF waves, optical emissions and pulsations was temporarily seen after sunrise. This was possible due to the photometer, which is sensitive in UV range, too.

An example of the magnetic and optical pulsations is shown in Figure 9.2 for a period just before the detector system saturated. The intensity variation is small but several times stronger than necessary in order to be detectable. Figure 9.2 was made by computer processing of the penrecorder traces. It is interesting to note that during all of the period during which the correlation was found, the ambient light level was so high that the usual photomultiplier-based systems could not be used.

There are several riometer stations in Northern Finland, but none of them showed indication of pulsating absorption. We have studied riometer data from Kevo, Kilpisjärvi and Ivalo in detail. There was actually not any kind of absorption during our event.

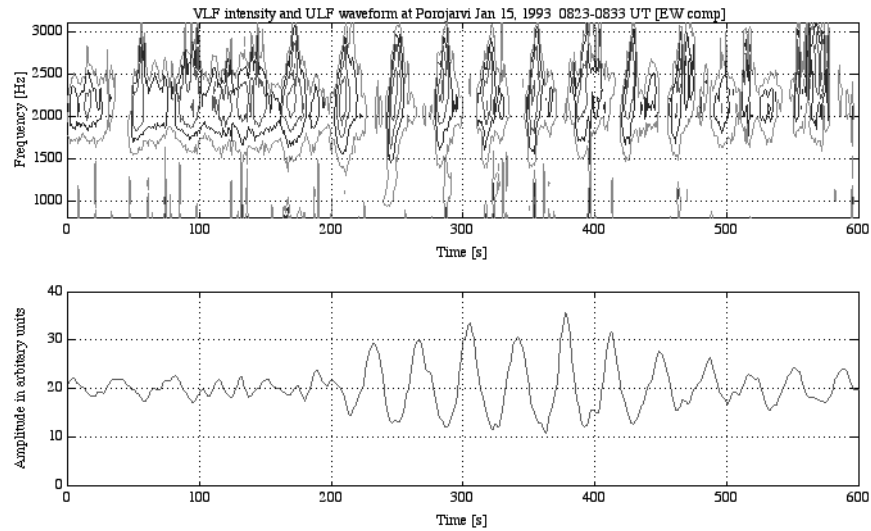


Figure 9.1: Intensity variation of ELF-VLF chorus bursts in the frequency range of 0.1–3.1 kHz at 0823–0833 UT are shown as a contour plot in the upper panel and the EW component of the magnetic field variation with arbitrary units is shown in the lower panel. Both ELF-VLF and the magnetic pulsations were observed at Porojärvi on 15 January 1993. [From *Manninen et al.*, 1994]

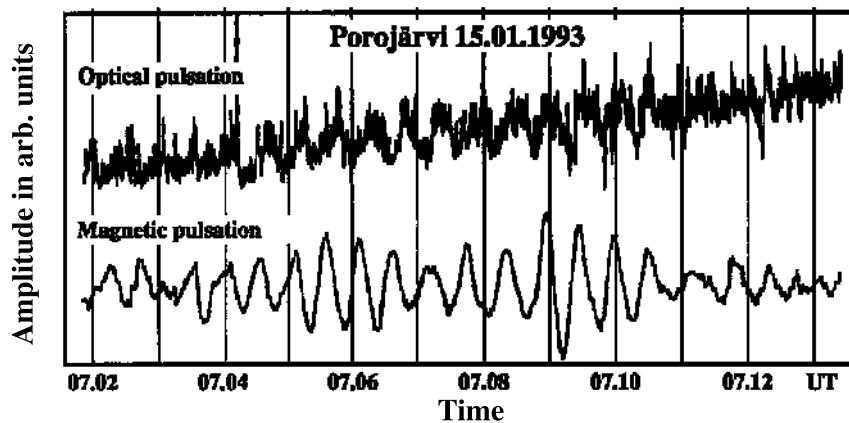


Figure 9.2: Simultaneous optical and magnetic pulsations measured at Porojärvi between 0702 UT and 0713 UT. The clearest correlation can be found during the time interval of 0704–0711 UT. The amplitude scales of both recordings are in arbitrary units. [From *Manninen et al.*, 1994]

## 9.2 Discussion and Conclusions

A clear correlation between optical and magnetic Pc 3 pulsations was found during an event where Pc 3 correlated most of time perfectly with periodic ELF-VLF emissions. No indication of pulsating absorption was observed.

In summary it seems that Pc 3 waves caused modulations of VLF waves, which, in turn, caused periodic intensity variations of low-energy (perhaps from hundreds of eV to some keV) precipitating electrons in the late morning hours. Within the detectability of the available instruments it did not cause periodic variation of precipitation of high energy electrons above 10 keV.

There was ELF-VLF observations made at Lovozero (67.97° N, 35.08° E, L=5.4) in Kola Peninsula, Russia. They recorded narrow bands of ELF-VLF waves and magnetic pulsations simultaneously. The best correlation between periodic ELF-VLF emissions and Pc 3 pulsations appeared a couple of hours earlier than at Porojärvi, which is in agreement with the difference of MLT. So, it seems that the best correlation occurred when the generation region of the ELF-VLF waves were at the magnetic meridian of the station.

## Chapter 10

# Hiss Clouds

The phenomenon, which certainly requires continuous wide-band observations, is the morning-side ‘hiss cloud’. It usually lasts for several hours and covers the frequency band of 2–6 kHz. Altogether 15 hiss clouds were observed during our campaigns. A 1-hour plot covers too short a time interval to recognise a hiss cloud. The events were observed during our campaigns on six days in January 1993, one day in November 1993, two days in November 1995, and four days in January 1997. This kind of observations have not been reported earlier, possibly due to the lack of continuous wide-band recordings.

At any given instant it is difficult to recognise from the data because it does not essentially differ from the noise of the receiver system. The occurrence frequency is a few percent of the time. When it appears it lasts for hours and covers a wide frequency band of the order of an octave or more. It seems to be present especially in midwinter conditions. It seems to be present simultaneously with diffuse aurora existing after some auroral activity and when the auroral luminosity is moving towards the pole.

### 10.1 Observations

The hiss cloud starts during the early morning hours usually at frequencies of 2–3 kHz. Then its upper cutoff frequency increases several kHz within a couple of hours. Simultaneously the lower cutoff frequency decreases gradually down to 1–2 kHz. The duration varies from 3 hours to 11 hours, and the maximum intensity of the cloud occurs around the middle of the time interval of the event, which is also the time of the widest frequency coverage.

There seems to be neither trigger of the hiss cloud nor preceding ELF-VLF activity. The lower cutoff frequency is often limited to a certain frequency, which can be a power-line harmonic. For example, in Figures 10.1, 10.4, 10.5, and 10.8 this is the PLHR doublet at 1750/1850 Hz. However, during the September-October 2005 campaign it was observed that the night-time Earth-ionosphere wave-guide cutoff can vary a few hundreds of Hz within a couple of hours, and very often it had frequencies of PLHR.

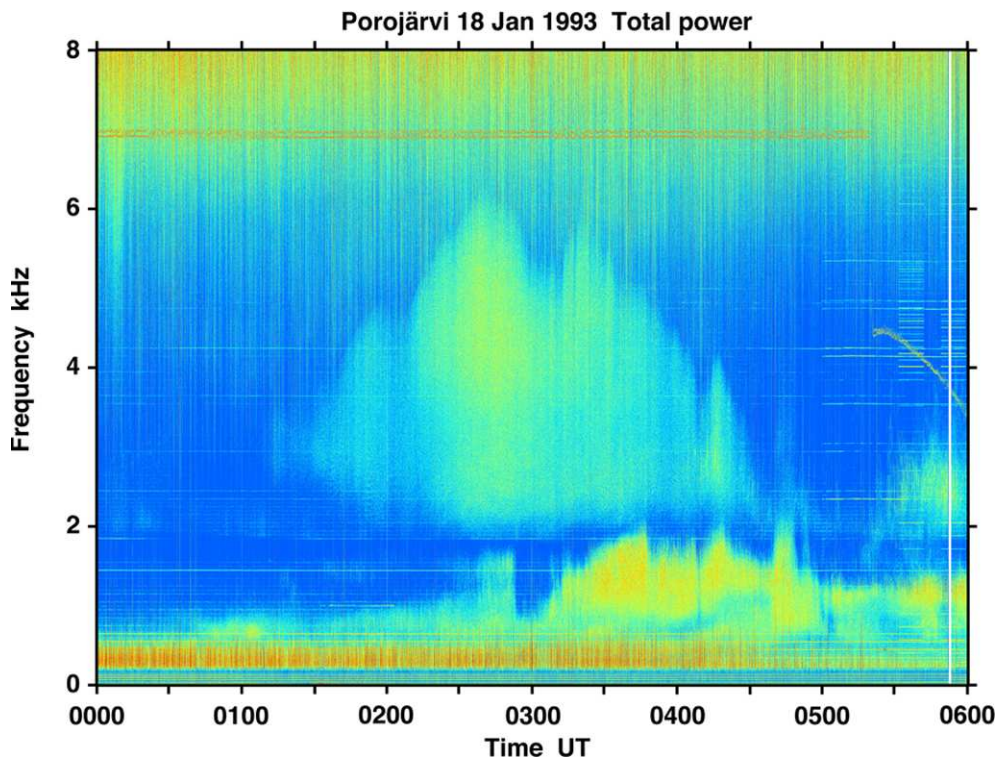


Figure 10.1: A hiss cloud was observed on 18 January 1993 at 0100-0440 UT. The initial frequency was  $\approx 3$  kHz. The cloud reached the widest frequency range of 1.85-6.1 kHz at about 0240 UT, which was the time of maximum intensity. The lower cutoff frequency was limited by a PLHR doublet at 1750/1850 Hz.

Figure 10.1 presents one of the best examples of the hiss clouds. It was observed on 18 January 1993 at 0100-0440 UT between the frequencies of 1850 and 6000 Hz. The initial frequency was at  $\approx 3$  kHz. The cloud reached the uppermost frequency of 6 kHz about at 0240 UT, which was the time of the maximum intensity. There were four enhancements, at 0155, 0240, 0320, and 0420 UT, when both the upper cutoff frequency and the intensity increased. During the strongest enhancement (at 0240 UT) also low frequency chorus suddenly rose to 1.7 kHz, and it abruptly stopped at 0255 UT.

The hiss cloud is nearly symmetrical in time. This can be due to a situation where the ionospheric exit point is first located far to the east of the receiver and then passes the receiver moving towards the west. However, the nature of the events is such that it is impossible to determine the horizontal angle of arrival using the analysis described in Chapter 3. The reason is that a hiss cloud is a relatively weak noise-like phenomenon, which requires usually several minutes of data in order to separate it from background noise. The 16-bit resolution used does not allow us to do it. The

horizontal angles obtained in hiss cloud analysis show mostly random values.

The lower cutoff frequency showed an interesting feature at 0315 UT, when a low-frequency chorus appeared below 2 kHz. When the frequency of the chorus increased close to 2 kHz, the lower cutoff frequency of the hiss cloud increased, too. There was a frequency gap between the chorus and the hiss cloud until the hiss cloud ended at 0440 UT. The width of the gap between the cutoff frequencies remained almost constant, although the cutoff frequencies themselves varied.

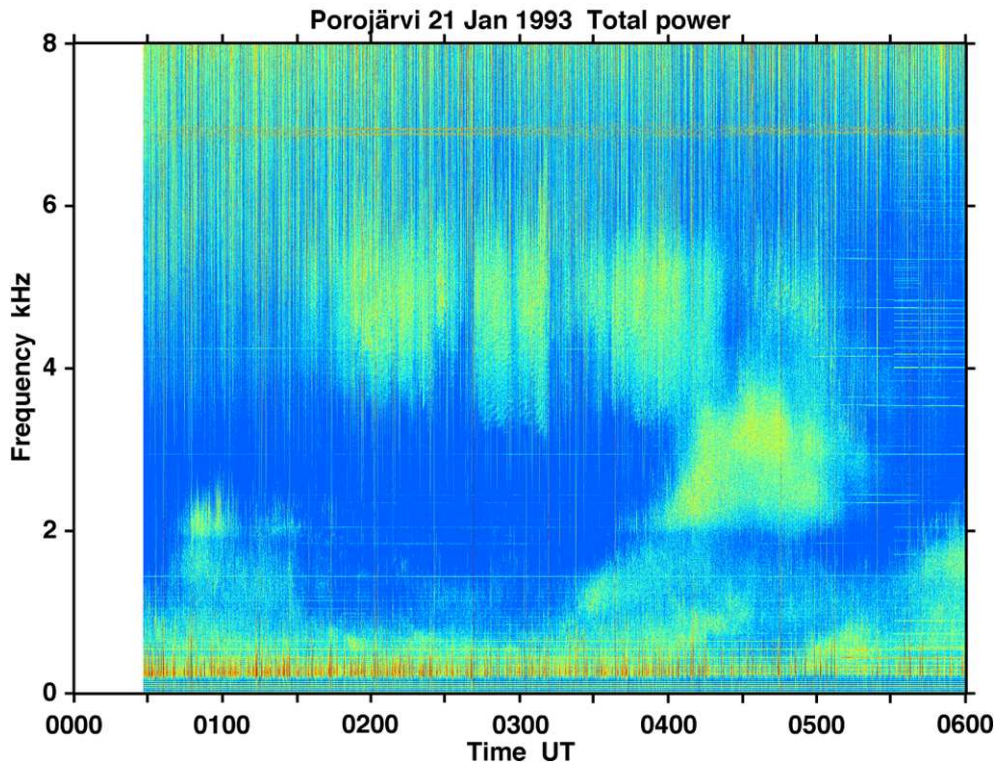


Figure 10.2: On 21 January 1993 a hiss cloud was certainly observed at 0330-0530 UT between 2 and 5 kHz. However, it may have started already at 0130 UT and obscured by a long MLR event which might or might not have contained hiss. The initial frequency was  $\approx 2$  kHz at 0330 UT. The cloud reached the uppermost frequency of 5 kHz at about 0500 UT, which was the time of maximum intensity. The lower cutoff frequency was  $\approx 2$  kHz. A data gap in the beginning of the plot was due to generator maintenance.

Figure 10.2 shows a hiss cloud observed on 21 January 1993 at 0130-0530 UT or only at 0330-0530 UT. This uncertainty is due to a long MLR event, which might contain hiss or not. Certainly, a hiss cloud was observed at 0330-0530 UT between 2 and 5 kHz. The initial frequency was  $\approx 2$  kHz. The cloud reached the uppermost frequency of 5 kHz at about 0500 UT, which was the time of the maximum intensity.

The lower cutoff frequency was  $\approx 2$  kHz. A data gap of half an hour before 0030 UT was due to generator maintenance.

However, it might also be so that the hiss cloud really started at 0130 UT, because most of MLR events occurred simultaneously with natural chorus or hiss activity, as mentioned in Chapter 5.

One usual feature of a hiss cloud is that there is no other ELF-VLF activity at the beginning of the cloud. This is seen in Figures 10.2, 10.4, and 10.6–10.8. Nevertheless, a morning chorus or hiss often appeared around the middle of the time interval of a hiss cloud.

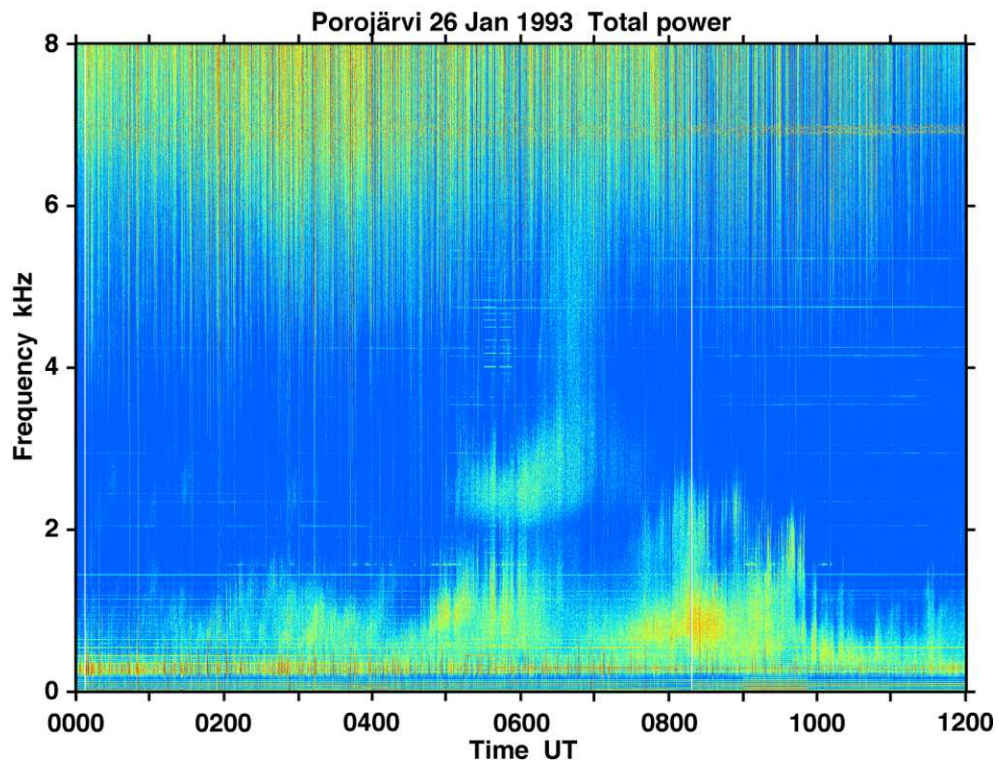


Figure 10.3: A hiss cloud was observed on 26 January 1993 at 0500–0700 UT. The initial frequency was  $\approx 2.5$  kHz. The cloud reached the uppermost frequency of 6 kHz at about 0645 UT, which was 30 min or so later than the time of the maximum intensity.

One of the shortest hiss clouds occurred on 26 January 1993 at 0500–0700 UT. Figure 10.3 shows that the initial frequency was  $\approx 2.5$  kHz. The cloud reached the uppermost frequency of 6 kHz at about 0645 UT, which was 30 min or so later than the time of maximum intensity. This event differed from usual hiss clouds due to quite strong simultaneous ELF activity, which seems to have been discrete emissions.

A very long hiss cloud was observed on 10–11 November 1993 at 2300–0550 UT,

which is seen in Figure 10.4. This was the only event, which started already in the previous evening. The initial frequency was  $\approx 2$  kHz. The cloud reached the uppermost frequency of 7 kHz at about 0430 UT, which was the time of maximum intensity.

Note that the lower cutoff frequency was strongly controlled by a PLHR doublet at 1750/1850 Hz, until at about 0335 UT, when the lower cutoff frequency sharply increased to the frequency of a higher PLHR doublet at 3550/3650 Hz. Simultaneously a lower frequency chorus started and its upper cutoff frequency increased to 1850 Hz. The frequency gap between the low-frequency chorus and the hiss cloud behaved similarly to Figure 10.1.

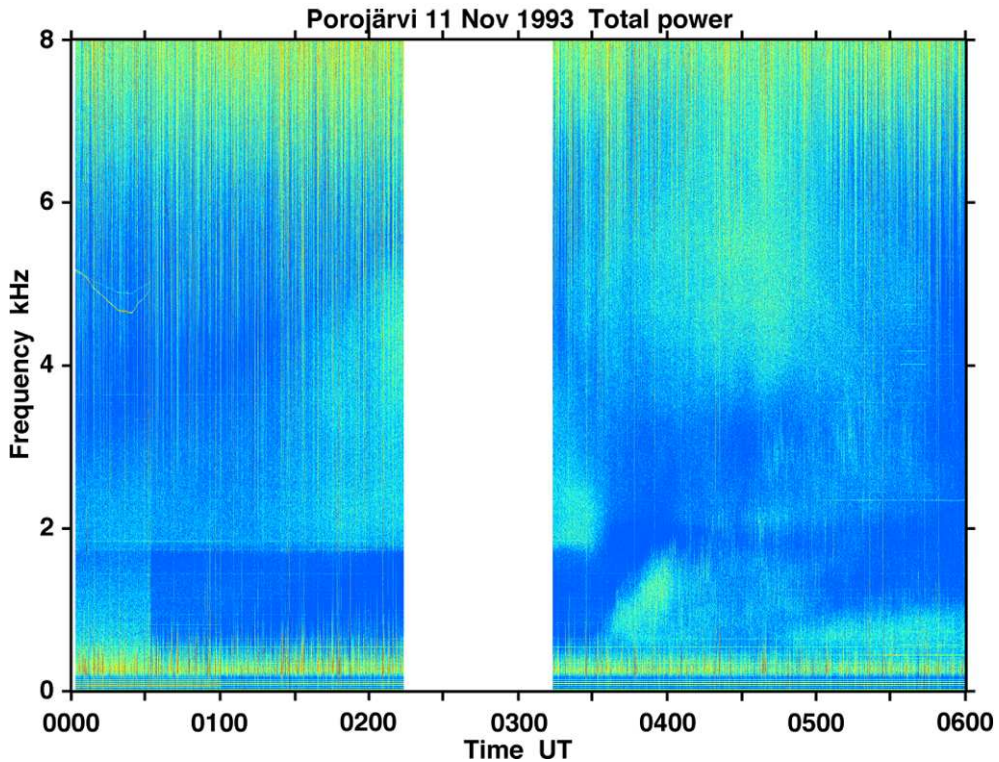


Figure 10.4: A hiss cloud event occurred on 10-11 November 1993 at 2300-0550 UT. There was one main cloud from 2300 to 0335 UT, another cloud between 3.5 and 7 kHz started at about 0315 UT and two other ‘clouds’ were below 4 kHz after 0400 UT. Note that the lower cutoff frequency was strongly controlled by a PLHR doublet at 1750/1850 Hz, until at about 0335 UT. Simultaneously a low-frequency chorus started. A weak cloud consisting mostly discrete emissions occurred between 2 and 4 kHz. A one hour gap in the observations at 0215-0315 UT was due to generator maintenance.

Unfortunately, there was a one hour gap in the observations at 0215-0315 UT due to generator maintenance. However, the main development of the event can be appreciated in spite of the gap. Probably the first intensification and a local

maximum of the upper cutoff frequency occurred during the gap, but obviously the highest maximum of the upper cutoff frequency of the entire event was observed at 0430 UT.

There were three separate ‘clouds’ after 0400 UT: the lowest one was a chorus below 2 kHz; the middle one was the weakest and it occurred in the range of 2-4 kHz; and the uppermost one belonged to the main hiss cloud. Both the middle and the uppermost cloud ended at 0550 UT.

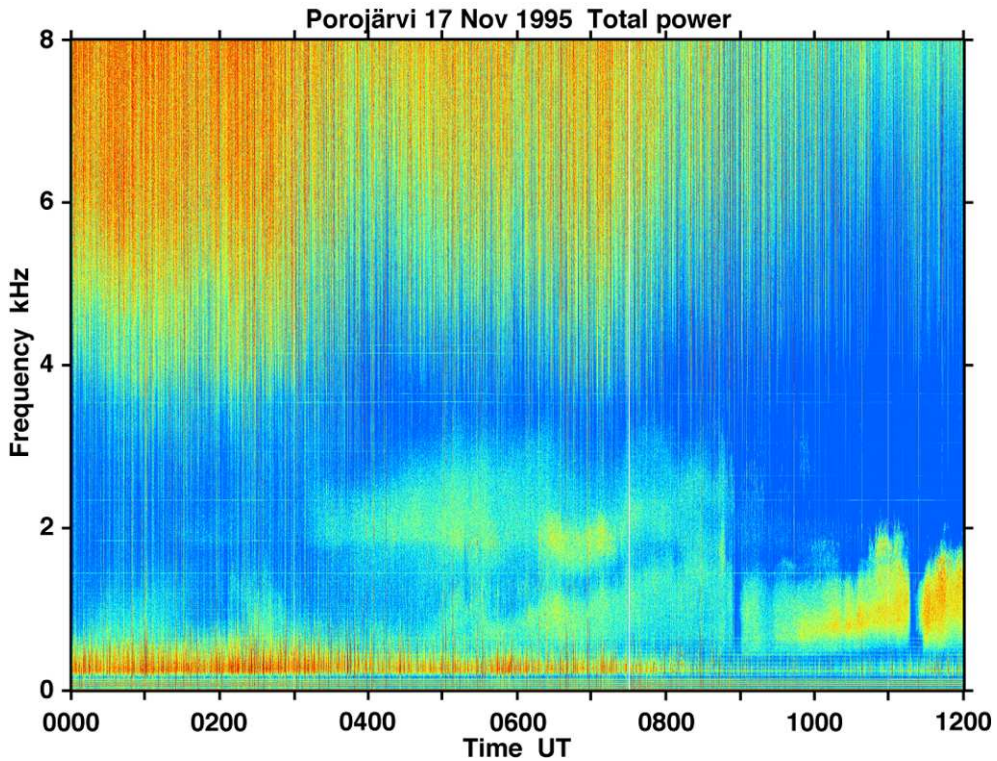


Figure 10.5: A hiss cloud was observed on 17 November 1995 at 0100-0500 UT. The initial frequency was  $\approx 2$  kHz. The cloud reached the uppermost frequency of 3.5 kHz three times about at 0530, 0630, and 0750 UT. The lower cutoff frequency was partly controlled by a PLHR doublet at 1750/1850 Hz, and partly it decreased down to 1.5 kHz. The hiss cloud faded away at 0900 UT.

Figure 10.5 presents a hiss cloud, which was observed on 17 November 1995 at 0100-0500 UT. This event was the narrowest in frequency, because its range was only 1.5-3.5 kHz. The initial frequency was  $\approx 2$  kHz. For two hours from the start the event was very weak. The hiss intensity was barely above the background noise level. At about 0310 UT the hiss cloud became stronger and simultaneously it spread between two PLHR doublets (1750/1850 and 2350/2450 Hz). The upper cutoff frequency started to increase at 0400 UT.

The cloud reached the uppermost frequency of 3.5 kHz three times at about 0530, 0630, and 0750 UT, of which the second was the time of maximum intensity.

The lower cutoff frequency was partly controlled by a PLHR doublet at 1750/1850 Hz, and partly it decreased down to 1.5 kHz. About at 0500 UT a low-frequency chorus started and it continued till 2000 UT. During the hiss cloud there was a frequency gap of 0.2-0.3 kHz between the chorus and the hiss cloud. This hiss cloud faded away at 0900 UT, when there was a short gap in the lower chorus band. It is not obvious, what the reason of the short gap was.

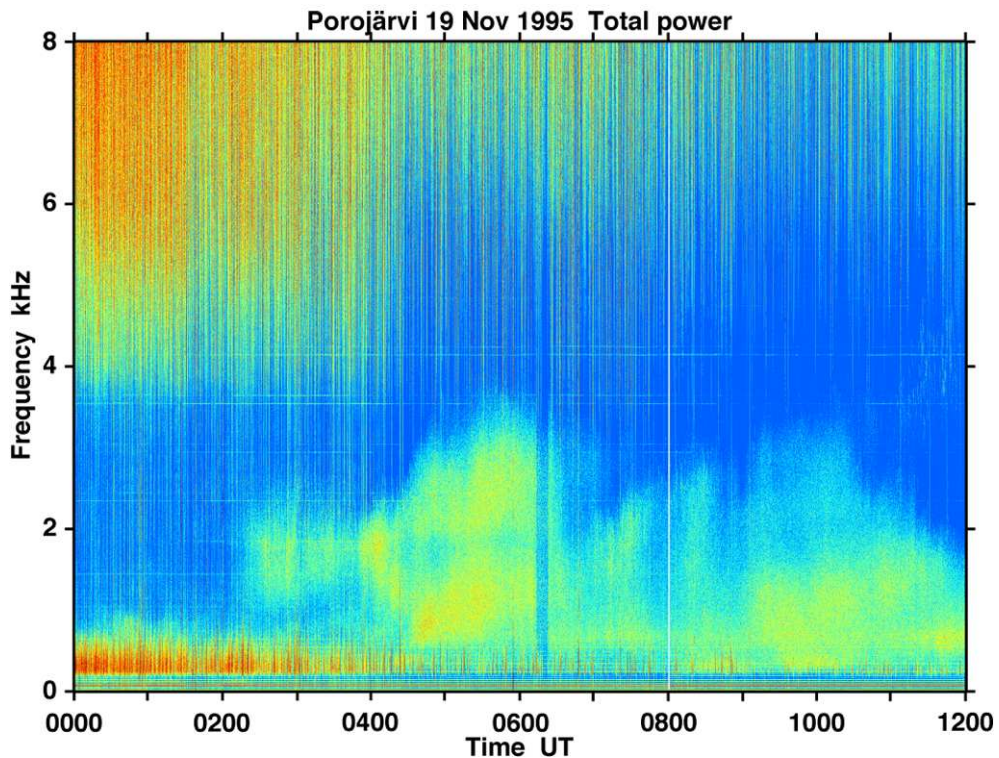


Figure 10.6: A hiss cloud was observed on 19 November 1995 at 0210-1300 UT. The initial frequency was either at  $\approx 1.25$  kHz or at  $\approx 1.85$  kHz. The cloud reached the uppermost frequency of 3.65 kHz about at 0600 UT. The lower cutoff frequency seemed to be uncontrolled. About at 0430 UT a lower frequency chorus event started and it continued after 1200 UT.

The longest event was observed on 19 November 1995 at 0210-1300 UT. The whole cloud stayed below 4 kHz, and it contained also some discrete emissions. The initial frequency was either  $\approx 1.25$  kHz or  $\approx 1.85$  kHz. The cloud reached the uppermost frequency of 3.65 kHz at about 0600 UT. The lower cutoff frequency seemed to be uncontrolled. At about 0430 UT a lower frequency chorus event started and continued until after 1800 UT.

Figure 10.6 shows how difficult it is to separate hiss cloud and low-frequency chorus. The first deduction would be that the hiss cloud ended at about 0700 UT, but a hiss continued till 1300 UT. After that only a chorus remained below 2 kHz.

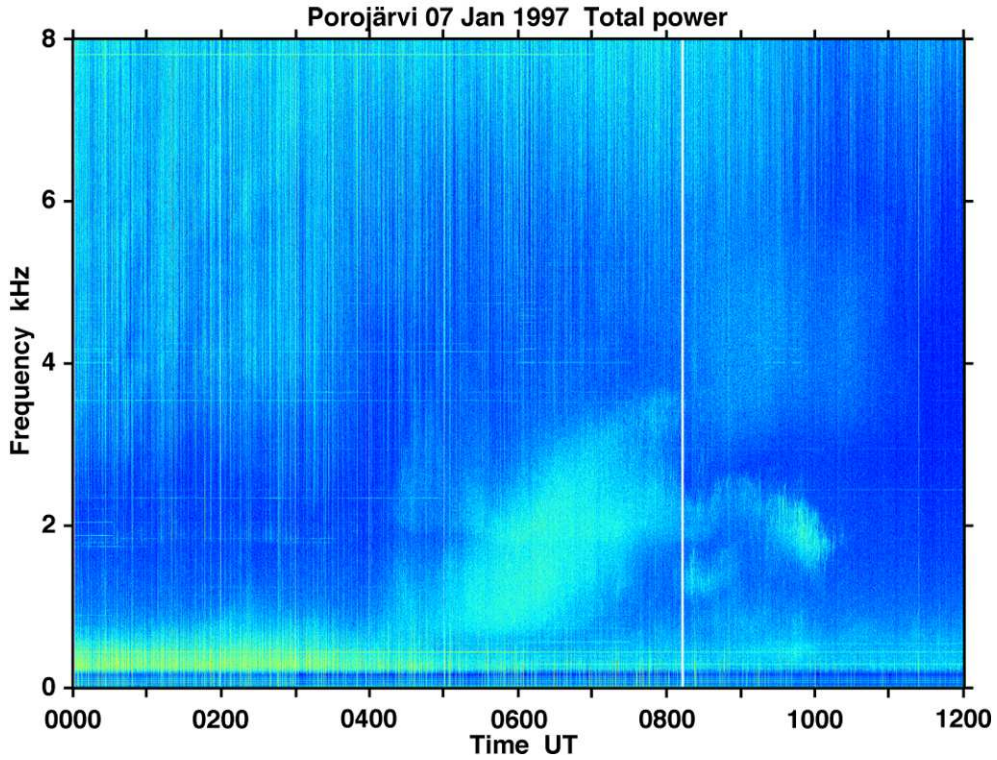


Figure 10.7: Two hiss clouds were observed on 7 January 1997 at 0400-1120 UT. The first one had no clear initial frequency. Somehow the hiss cloud started at  $\approx 0.6$  kHz. The lower cutoff frequency started to increase at 0630 UT. A weaker hiss cloud occurred in the frequency range of 3-6 kHz at 0815-1115 UT.

Figure 10.7 shows two different kinds of hiss clouds, which were observed on 7 January 1997 at 0400-1120 UT. The first hiss cloud (at 0400-0800 UT) had, in some sense, three different branches. The first one had no clear initial frequency, but somehow the hiss cloud started at  $\approx 0.6$  kHz. This was the only event, which had that low starting frequency. It also meant that the lower cutoff frequency did not become lower, but it increased after 0630 UT.

The second branch started about at 0415 UT, and it had quite a clear initial frequency at 2.05 kHz. Its lower cutoff frequency had a minimum of 1.9 kHz at 0440 UT. At 0540 UT this second branch merged into the first one. The third branch turned to the chorus event after 0755 UT.

The first cloud reached the uppermost frequency of 3.65 kHz about at 0800 UT. The lower cutoff frequency started to increase at 0630 UT from 0.6 kHz to its maximum

of  $\approx 2$  kHz at 0800 UT.

A weaker, but more typical hiss cloud occurred at 0815-1120 UT. Its upper cutoff frequency reached its maximum of 6 kHz at 0900 UT and the lower cutoff frequency was above 2.95 kHz during the event.

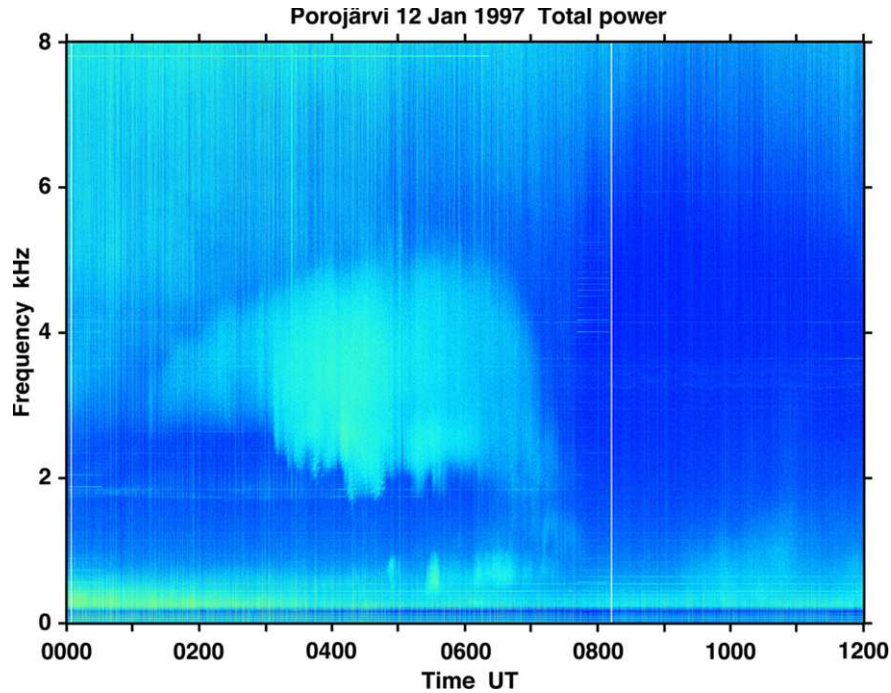


Figure 10.8: A strong hiss cloud was observed on 12 January 1997 at 0100-0740 UT. Its initial frequency was at  $\approx 3$  kHz. The cloud reached the uppermost frequency of 5 kHz about at 0530 UT. The lower cutoff frequency was controlled by a PLHR doublet at 1750/1850 Hz.

One of the strongest hiss clouds (Figure 10.8) was observed on 12 January 1997 at 0100-0740 UT. The initial frequency was between 2.65 kHz and 3.5 kHz. The upper cutoff frequency increased gradually until at 0530 UT, when the cloud reached the uppermost frequency of 5 kHz. After that the event faded away within two hours.

The lower cutoff frequency stayed at 2.65 kHz until 0305 UT, when it gradually started to decrease by jumping from a 50 Hz harmonic to the next lower harmonic. The lowest lower cutoff frequency was controlled by a PLHR doublet at 1750/1850 Hz. During these jumps the lower part of the hiss cloud showed some MLR structure. The weak chorus bursts below 1 kHz at 0450-0505 UT and at 0525-0540 UT did not seem to affect the hiss cloud.

## 10.2 Relations to Other Parameters

The hiss clouds listed in Table 10.1 seemed to be independent of other parameters, but that is not true. When comparing with the MLR events it can be found that the hiss clouds occurred on the same days as the MLR events (compare Tables 10.1 and 5.2 in Section 5.3). The exact times were mostly different, because the hiss clouds occurred during early morning hours, while the MLR events were more common a few hours later. Altogether 12 days contained both types of the events.

Only one hiss cloud day was lacking the MLR, i.e. on 10 January 1997 only a hiss cloud was observed. Nevertheless, on that day there were peculiar bands with a bunch of lines from 1130 UT to about 2100 UT (see Figure 4.11 in Section 4.5).

The fact that the hiss clouds appeared on same days as the MLR events means that the magnetic activity was usually very low and Pc 5 pulsations were observed at high latitudes.

When studying the auroral observations made at the time of hiss clouds, it was found that always when the sky was clear, also auroral activity existed. It is also very probable that there was aurora during cloudy nights, because the magnetic activity preceding the hiss clouds was suitable for aurora.

Last column in Table 10.1 shows magnetic  $K_p$  indices during the hiss clouds.

Date	Start UT	End UT	Dur. Min	LCO kHz	UCO kHz	MLR obs.	Aurora obs.	$K_p$
18 Jan 1993	0100	0440	220	1.85	6.1	yes	cloudy	2, 3 <sub>-</sub>
19 Jan 1993	0100	0500	240	1.85	6.0	yes	yes	4, 3 <sub>+</sub>
21 Jan 1993	0130	0520	230	1.85	6.0	yes	cloudy	2 <sub>+</sub> , 3 <sub>+</sub>
	0330	0520	110	1.85	4.0	yes	cloudy	3 <sub>+</sub>
22 Jan 1993	0000	0530	330	1.85	6.5	yes	cloudy	1 <sub>-</sub> , 2 <sub>-</sub>
24 Jan 1993	0530	0830	180	3.0	6.0	yes	yes	2 <sub>+</sub> , 2 <sub>+</sub>
26 Jan 1993	0500	0700	120	2.1	7.0	yes	yes	4 <sub>-</sub> , 4 <sub>-</sub>
11 Nov 1993	2300*	0550	410	1.85	7.0	yes	yes	3, 3
	0720	1050	210	2.3	5.3	yes	daytime	3, 2
17 Nov 1995	0300	0850	350	1.5	3.5	yes	yes	2 <sub>+</sub> , 2 <sub>-</sub>
19 Nov 1995	0200	1300	660	0.5	3.7	yes	yes	3 <sub>-</sub> , 3 <sub>-</sub>
7 Jan 1997	0400	1030	390	0.7	7.0	yes	yes	4, 2
10 Jan 1997	0330	0630	180	1.85	7.0	no	yes	5 <sub>-</sub> , 6
12 Jan 1997	0100	0740	400	1.85	5.5	yes	yes	2 <sub>-</sub> , 2
14 Jan 1997	0400	0800	240	1.85	3.2	yes	yes	1 <sub>-</sub> , 1 <sub>+</sub>

Table 10.1: Hiss clouds observed during campaigns in January 1993, November 1993, November 1995, and January 1997. Parameters like start and end times, the minimum of lower cutoff frequency (LCO) and the maximum of the upper cutoff frequency (UCO) are shown. One column shows the MLR activity on the same day, next column presents the auroral activity during the cloud, and the last column gives  $K_p$  values during the cloud. (\* means that the time belongs to the previous day.)

## 10.3 Discussion

The hiss cloud is one of the widest-scale ELF-VLF phenomena, because it covers the frequency range of several kHz and its duration can be as long as 11 hours (on 19 November 1995). Sometimes it is difficult to determine exactly the upper cutoff frequency, because above 5-6 kHz the sferics are the most intense signals, and therefore they can mask weaker phenomena.

The total duration of the observed hiss clouds was about 71 hours, which means 6.5% of 1096 hours of wide-band recordings during our ELF-VLF campaigns between January 1993 and January 1997. If the occurrence rate is calculated based on observation days, then we have observed the hiss clouds on 14 days out of 58 analysed days between January 1993 and January 1997, i.e. the rate was 24.1%.

It is not obvious that it is PLHR that controls the cutoff, but they are the ionospheric propagation modes. This supports the idea that hiss clouds have the ionospheric exit point very far from the receiver.

The hiss clouds seem to be present especially in midwinter conditions (hiss clouds were observed neither during the October 1994 nor the September-October 2005 campaign). They occurred simultaneously with poleward moving diffuse aurora after active aurora. The magnetic activity was mostly moderate during hiss clouds, which is quite obvious after auroral substorm events. If the hiss clouds are related to aurora they are more likely generated near or at the same regions as auroral hiss.

The low frequency chorus exists often during or near the end of the hiss cloud, but it seems that there is no direct connection between them. Plasmaspheric hiss has too low upper cutoff frequency (usually 2-3 kHz) compared to hiss clouds. Also mid-latitude hiss would be a candidate for hiss clouds, but according to *Hayakawa and Sazhin* [1992] the mid-latitude hiss has higher frequencies (from 3 to 8 kHz) than hiss clouds, whose lower cutoff is usually between 1 and 2 kHz. On the other hand, steady mid-latitude hiss shows a local time variation, peaking around 0500 and 2200 LT. In Finland 0500 LT is 0300 UT during winter, i.e. the peak agrees well with intensity maxima of hiss clouds. However, further studies are needed.

Although the MLR events occurred more likely during quiet magnetic conditions, there was a tendency to have both hiss clouds and MLR events on the same day. Actually half of the hiss cloud events occurred simultaneously with MLR events, which means that both phenomena appear in similar geophysical conditions. However, the nature of these two phenomena is different, but if they are connected the interaction should occur relatively close to the topside ionosphere. Proving this idea certainly requires some morning-side satellite observations at auroral latitudes.

Because the polarisation of the hiss clouds was not studied in this thesis, it should be done in the future. The lower cutoff frequencies of the hiss clouds were very close to certain PLHR frequencies (e.g. 1850 Hz), but there is also another cutoff, which may provide a more reasonable explanation. It is the Earth-ionosphere wave-guide cutoff for waves propagating over long distances in the wave-guide. Also the durations of the hiss clouds support the idea that the phenomenon cannot be localised. In that time scale the ionospheric and plasmaspheric drifts change the plasma inside the receiver "horizon" several times.

## 10.4 Conclusion

The hiss clouds are most likely observed during quiet or moderate geomagnetic conditions over wide spatial areas. Most of the observed hiss clouds occurred in the morning hours during the recovery phase of the auroral activity, when diffuse aurora still exists. The duration (2-11 hours) and wide frequency range (0.5-7.0 kHz) separate the hiss clouds from other hiss-types.

The lower cutoff frequency of 1.85 kHz may be related to PLHR, but more likely it is due to the cutoff in the Earth-ionosphere wave-guide. The latter supports the idea that the hiss clouds propagated long distances in the wave-guide.

The hiss clouds and MLR events tend to occur on the same days. If they are connected, the interaction should occur relatively close to the topside ionosphere. Proving this idea certainly requires some morning-side satellite observations at auroral latitudes. The phenomenon must be studied more carefully in the future.

## Chapter 11

# Some Unusual ELF-VLF events

Two very unusual ELF-VLF phenomena are introduced in this chapter. The first one is new and requires continuous wide-band ELF-VLF recordings as the hiss clouds. The banded hiss is an evening sector event, which is shown here only briefly, because the phenomenon is under investigation by our INTAS team. We have collected here some preliminary ideas.

The second phenomenon is a real mystery, because it has been observed only on a few days in 1992. They were always observed near the pass of the Russian Apex satellite.

### 11.1 Banded VLF Hiss

A weak, banded VLF hiss event from 2 kHz to 9 kHz was observed at Liikkuvankangas ( $L=5.18$ ) from 1910 to 2000 UT (i.e. 22.10 to 23.00 LT) on 26 November 1997. Between 3.5 and 6 kHz the band separation was about 0.5 kHz, and this varied in a complex way (as evident from Figure 11.1). The bands appeared as minima in the total power; they were about 0.1 kHz wide. From 3.5 to 6 kHz the right-hand power (whistler mode) in the hiss band exceeded the left-hand power, whereas between 2 and 3.5 kHz and above 6 kHz the left-hand power was greater than the right-hand power. The minima of the total power coincided with minima of the left-hand power. A similar event was observed at the same time on the next day.

Geomagnetically, 26 November 1997 was quiet, with a weak positive bay occurring from 19 to 20 UT, indicating a weak (30 nT) auroral electrojet nearby. Strong Pc 1 pulsation activity (narrow band, at 0.8 Hz) occurring throughout the day indicated significant proton fluxes in the magnetosphere. These Pc 1 pulsations stopped abruptly at 19 UT. From 19 to 20 UT, broadband (0 to 1 Hz) activity was recorded; linearly polarised, this was due to fluctuations of an overhead electrojet. No significant riometer absorption was noted at Sodankylä on that day.

When we checked all our quick-look plots, we found many similar events observed

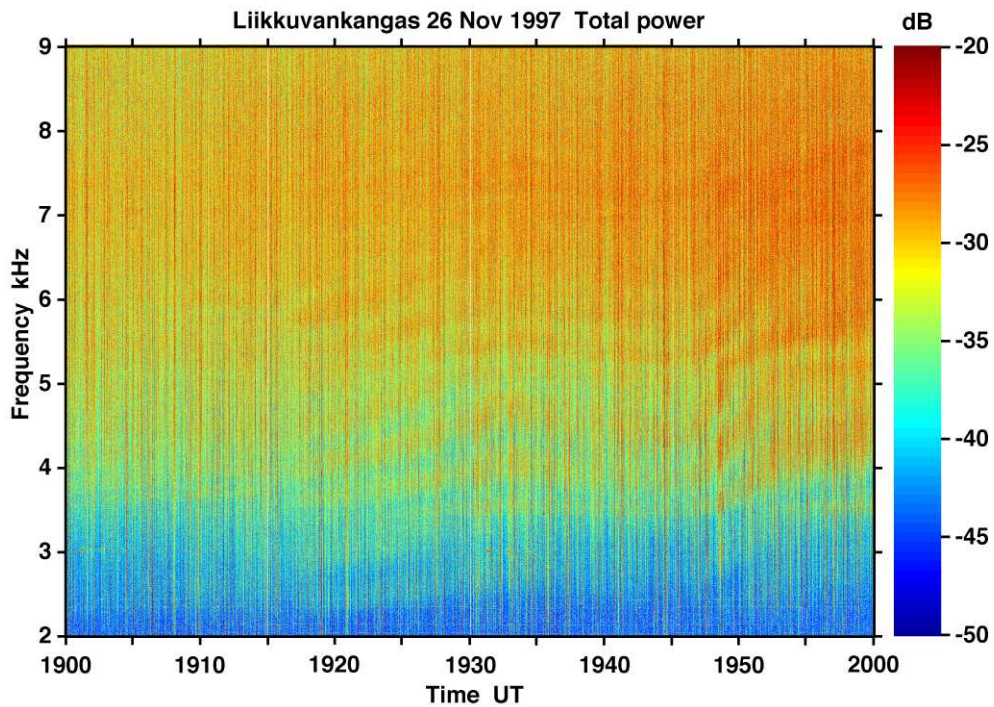


Figure 11.1: Banded VLF hiss event observed on 26 November 1997 at Liikkuvankangas. The banded structure is seen between 3.3 and 9.0 kHz.

in January 1993, November 1993, November 1995, and January 1997, which are collected in Table 11.1. There were altogether 23 banded hiss events, whose average duration was 85 min, i.e. about 1.5 hours. Most events were related to the low-frequency chorus and hiss. Sometimes the maximum frequency was difficult to determine, because of sferics.

Another example of a banded hiss event is presented in Figure 11.2, where there are four panels showing total, right-hand circular and left-hand circular powers, and horizontal angle of arrival, respectively.

A possible explanation could be that the band minima occur at harmonics ( $n$  around 8) of the proton gyrofrequency at an altitude of 1000 km on an  $L = 6$  field line. Slight changes of the band gap could be interpreted as changes of the source altitude from 1000 km. Perhaps Bernstein modes and/or ion conics may be involved. Maybe a proton beam is expected to be generated. [*M. Rycroft, private communication, 2003*].

Some preliminary investigations about the location of the auroral oval and the location of the proton precipitation region have been made using DMSP satellite data. For one case (23 November 1995) the satellite observation showed that Porojärvi is equatorward of the auroral oval and near the maximum of the proton precipitation region. [*E. Titova and A. Demekhov, private communication, 2004*].

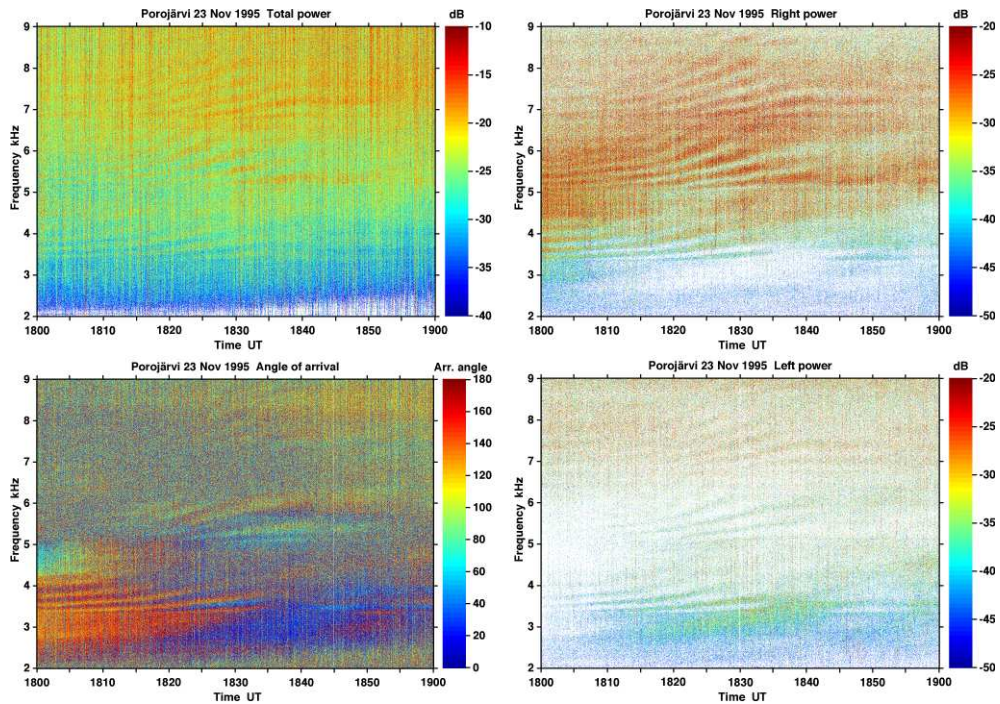


Figure 11.2: Another example of banded VLF hiss event observed at 1800-1900 UT on 23 November 1995 at Porojärvi. There are total power (upper left panel), right-handed circular power (upper right panel), horizontal angle of arrival (lower left panel), and left-handed circular power (lower right panel).

One interesting coincidence is that many banded hiss events occurred during the evenings of ionospheric Alfvén resonators (IAR). *Polyakov* [1976] predicted the existence of IAR, equivalent to the ionospheric waveguide, but operating in vertical direction with shear Alfvén waves. The so-called spectral resonance structures (SRS) discovered by *Belyaev et al.* [1989, 1990] are considered to be an evidence for IAR. They are thought to form within the IAR from electromagnetic emissions of lightning discharges, just like the Schumann resonances. Up to fifteen bands can be observed, from the 1-2 Hz (Pc 1 range) to well above the second Schumann resonance frequency at 14 Hz. After the original finding of SRS at mid-latitudes, they have now been observed also at high-latitudes [*Belyaev et al.*, 1998]. A theoretical approach was presented by *Demekhov et al.* [2000]. The most recent papers devoted to IAR are *Yahnin et al.* [2003] and *Prikner et al.* [2004].

Our recent observations in September-October 2005 may bring some new ideas for banded hiss events. This was the first campaign during which the dynamic range of the receiver was high enough to avoid saturation due to sferics. It allows us to observe several Earth-ionosphere wave guide modes, which can be seen, for example,

Date	Start UT	End UT	Dur. Min	Start kHz	End kHz	ELF obs.
18 Jan 1993	1920	2020	60	2.1	3.6	h, c 0.2-0.6 kHz
20 Jan 1993	2225	2340	75	5.4	6.5	h, c 0.2-0.7 kHz
22 Jan 1993	2200	2300	60	4.0	6.0	h, c 0.2-0.6 kHz
27 Jan 1993	1920	1955	35	4.0	5.5	h, c 0.2-0.6 kHz
28 Jan 1993	2225	2340	75	3.7	4.4	h, c 0.2-0.6 kHz
9 Nov 1993	1720	1800	40	3.6	6.0	h, c 0.2-0.7 kHz
11 Nov 1993	1920	2000	40	5.5	6.0	-
	2230	2300	30	2.1	2.6	-
12-13 Nov 1993	1800	0200	480	4.0	5.5	h, c 0.2-0.6 kHz
16 Nov 1993	1730	1900	90	3.7	4.5	aur. hiss 2-10 kHz
	2000	2100	60	4.0	6.0	h, c 0.2-0.7 kHz
17 Nov 1993	1900	2100	120	?	?	-
17 Nov 1995	1700	1900	120	3.6	5.4	h, c 0.2-2.3 kHz
18 Nov 1995	1920	2020	60	2.6	5.8	h, c 0.2-0.7 kHz
20 Nov 1995	1915	2030	75	3.7	5.0	h, c 0.2-0.7 kHz
21 Nov 1995	1725	1800	35	3.4	5.8	h, c 0.2-0.7 kHz
23 Nov 1995	1730	1925	115	3.4	6.6	h, c 0.2-0.5 kHz
	1815	1840	25	7.0	9.0	-
27 Nov 1995	1715	1850	95	4.2	5.8	h, c 0.2-0.6 kHz
28 Nov 1995	1710	1845	95	3.8	6.0	h, c 0.2-0.5 kHz
11 Jan 1997	0307	0320	13	4.2	5.7	-
	2115	2240	85	3.8	4.5	-
26 Nov 1997	1910	2000	50	2.3	8.2	-
27 Nov 1997	1910	2000	50	2.3	8.2	-

Table 11.1: Banded hiss events observed during campaigns in January 1993, November 1993, November 1995, January 1997, and November 1997. Parameters like start and end times, the minimum frequencies and the maximum frequencies are shown. The last column shows if there were the some ELF events at the same time (h=hiss, c=chorus).

in evening and night-time sferics data. Evening wide-band data either for 6 or 12 hours are shown for four successive days in Figure 11.3.

The varying structures above 1.8 kHz are due to wave-guide modes of 1,2,3,... The strong ELF part below 1.5 kHz is due to wave-guide mode 0. The cutoff between modes 0 and 1 is the well-known Earth-ionosphere wave-guide cutoff at about 1.6 kHz, which can vary a few hundreds of Hz as seen on 30 September 2005. At higher frequencies, similar cutoff frequencies exist, but usually they are swamped by sferics arriving from different directions and distances.

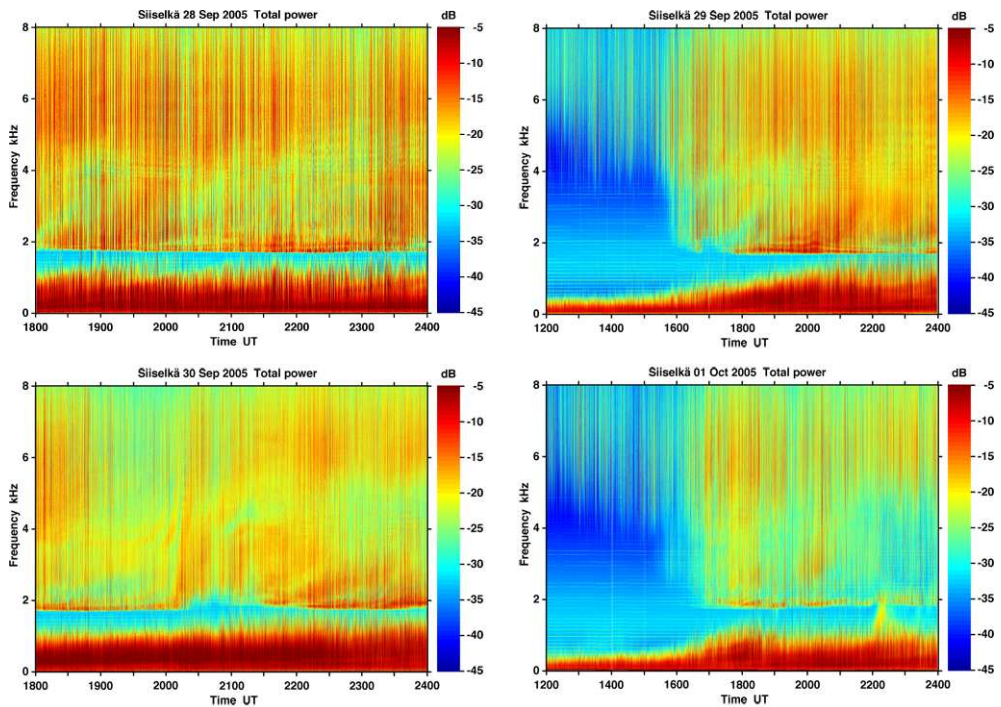


Figure 11.3: Wide-band data either for 6 or 12 hours are shown for four successive days starting from 28 September 2005. There are two plots with 6 hours of data in 1800-2400 UT and two plots with 12 hours of data in 1200-2400 UT. The varying structures above 1.8 kHz are due to wave-guide modes of 1,2,3,... The strong ELF part below 1.5 kHz is due to wave-guide mode 0.

There are also other possible physical reasons to have banded structures in the evening VLF data. It might be that these two banded structures are entirely separate phenomena, but further studies are needed.

## 11.2 Mysterious Man-made ELF-VLF Bursts

Clearly artificial ELF-VLF bursts were observed in spring 1992. They were short lasting bursts, whose start and/or end could be very sharp. In Figure 11.4 it can be seen that the first burst at 1.5 s from the beginning of the plot had a sharp start, but a fuzzy end, while the second burst at 3.5 s had a fuzzy start, but a sharp end. The third burst at 8 s had both edges sharp. The fourth burst at 14 s was very short and its start was sharp, but the end was fuzzy. The long bursts at 18 s and 21 s had again both edges fuzzy, as well as the last short burst at 24 s.

An interesting feature is seen in Figure 11.4, where the upper panel shows the signal observed by the NS antenna, and the lower panel shows the simultaneous signal received by the EW antenna. It is evident that in the NS component the strongest signal sits at exact kHz (at 1, 2, 3, 4, 5, and 6 kHz), and in the EW component the strongest signal is between exact kHz.

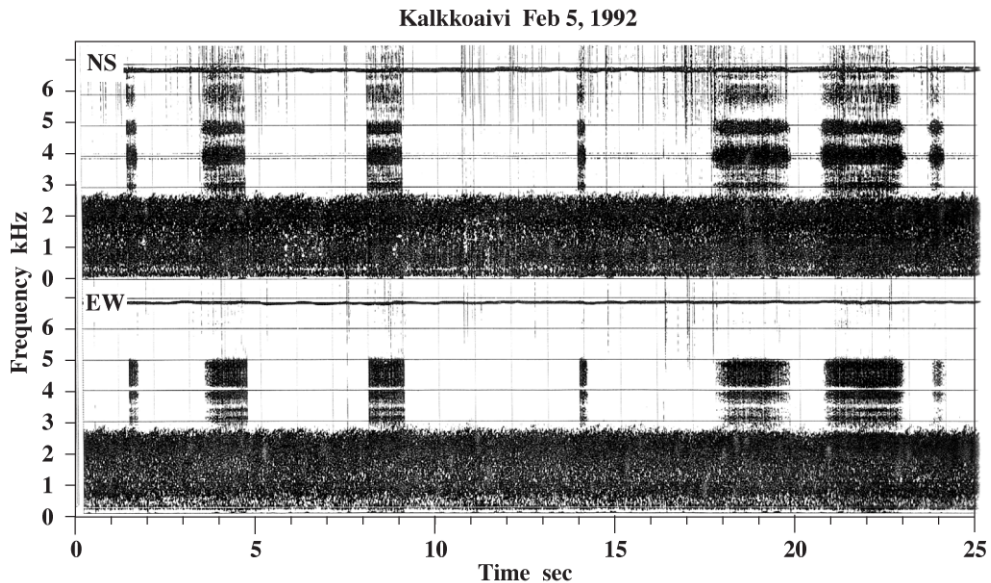


Figure 11.4: ELF-VLF bursts observed during the passes of the Russian APEX satellite. The upper panel shows the NS component and the lower panel shows the EW component of the signal. There were 7 bursts, whose duration varied from 0.2 s to 2 s. Note, that start and/or end could be either very sharp or fuzzy.

Figure 11.5 presents the third burst in detail. The burst clearly consisted of short pulses, whose period was about 20 ms, i.e. it had 50 Hz modulation. Therefore, the source of the signals could be, for example, a radar. However, the observed separation of different frequencies between antennae is extremely difficult to understand.

Surprisingly, these events have been observed only when the Russian APEX satellite transmitter signals have been observed. If the source of the mysterious signals

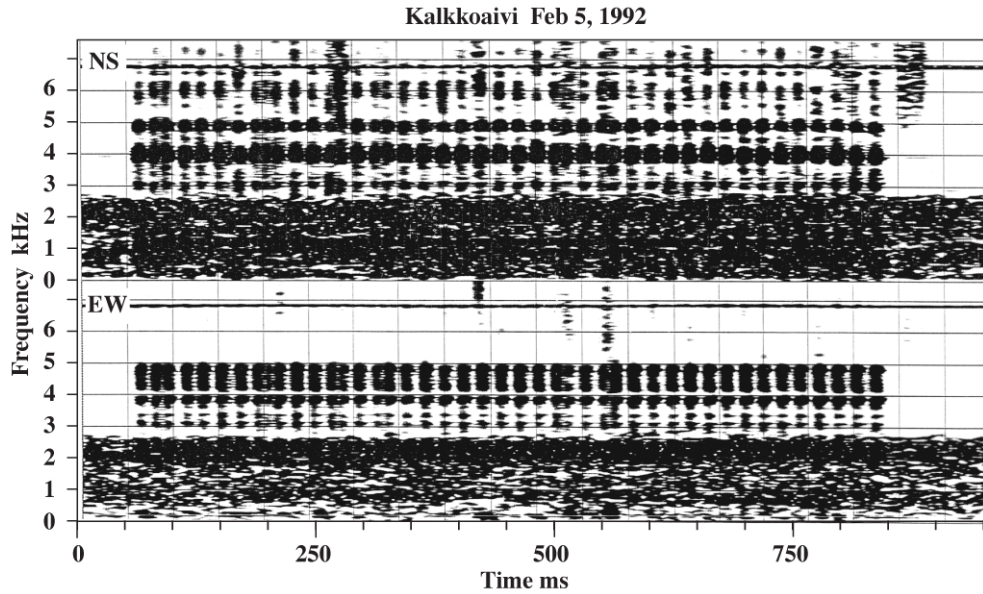


Figure 11.5: Magnification of the third burst in Figure 11.4. The burst consisted of short pulses, whose period was about 20 ms, i.e. it had 50 Hz modulation.

was the satellite transmitter, this kind of frequency separation could be observed only for a very short time, because the satellite was moving. A moving source should be seen as a changing frequency at the receiver due to the Doppler effect. Although, one group of bursts lasted for 25 s, such frequency change was not observed.

These mysterious bursts occurred about 1-2 min before the estimated satellite pass. There is a possibility that these signals came from some very powerful (military) radar operating in connection with the APEX satellite somewhere in Kola peninsula.

It would be interesting to study these bursts with new analysis method in detail. That could be done in future if the original video tape can still be read.



## Chapter 12

# Conclusions

This thesis is the first ELF-VLF related Ph.D. thesis in Finland. I have collected here different kinds of phenomena, which have been observed on the ground during our measurement campaigns between 1992 and 2005 in Northern Finland. The main difference between our recordings and other recordings made mostly in Antarctica is that during our campaigns we have recorded continuous wide-band (0-10 kHz) data. Also the L value of our receiver site is about 6.1, which is much higher than that of many other ELF-VLF receivers in the world. All ELF-VLF receivers used during our campaigns have been made at the Sodankylä Geophysical Observatory (SGO).

Also the digital analysis of ELF-VLF data is based on the software developed by SGO. The analysis is applied to recordings from two orthogonal sets of antennae. The computations are based on complex Fast Fourier Transforms using a window length, which gives the desired frequency and time resolution. The parameters given by the described analysis are mostly presented in frequency-time plots, usually as colour surface plots. Quick-look data plots of our measurement campaigns in 1993-2005 have been produced. The 1-hour, 6-hour, 12-hour, and 24-hour plots were made using two frequency ranges, from 0 to 4 kHz and from 0 to 8 kHz.

The new analysis package produces total, right-handed circular, and left-handed circular power plots, as well as horizontal angle of arrival plots, axis ratio of polarisation ellipse, and sense of rotation. This has been used throughout the thesis.

Power line harmonic radiation (PLHR) is a fascinating geophysical phenomenon in the near-Earth space environment that has excited much interest. We have put lots of our efforts into describing many PLHR-triggered or PLHR-related phenomena. Due to some reason, which is not yet understood, the PLHR-triggered emissions were systematically left-handed polarised. However, many of these emissions obviously bounced between the hemispheres, which means that in the magnetosphere the emissions must have been right-handed polarised.

The left-hand polarisation of the PLHR-triggered emissions is due to the mode conversion from the right-hand to the left-hand polarisation in the Earth-ionosphere wave-guide. This causes that all night-time sferics between  $\approx 1.7$  kHz and  $\approx 5$  kHz are left-hand polarised starting from almost pure circular polarisation just above  $\approx 1.7$  kHz, changing to elliptic polarisation, and ending at linear polarisation above

$\approx 5$  kHz.

Our results extend the explanation of the left-hand polarised ELF-VLF waves in comparison with observational results of *Yearby and Smith* [1994] and theoretical simulations of *Strangeways and Rycroft* [1980]. There might also be some latitudinal effect, because the left-handed waves are observed more frequently at high-latitudes. A theoretical explanation for mode conversion in the Earth-ionosphere wave-guide is required in the future. Furthermore, diurnal and seasonal behaviour should be studied carefully.

Some special features of PLHR-related phenomena were also shown. One of them was the signals from the Russian ELF transmitter Zevs, whose frequencies are in the range of 81-83.3 Hz. Other signals causing a huge amount of additional noise are the power line control signals transmitted along the 20 kV power lines. Their frequencies are mainly 3025 Hz and 4825 Hz. These signals have become one of the most disturbing factors in ELF-VLF range.

The most important part of my thesis is dealing with the magnetospheric line radiation (MLR). The phenomenon is extremely interesting, because it combines PLHR-type structure, natural discrete emissions, and it can have an enormous amount of fine structures. Sometimes there were clear peaks near the sub-harmonics of 50 Hz in the spacing frequency of individual MLR lines. Spacing as small as 5 Hz have been found in some events.

The MLR events are most likely produced during very quiet geomagnetic conditions at low altitudes over wide spatial areas, initially triggered by PLHR, but then moving away from the PLHR frequencies and becoming self-sustaining. Our new observations suggest that MLR contains, simultaneously, fast and slow time processes, which are completely locked to one another. Such MLR is made up of many narrow band rising elements existing in an “envelope” that slowly changes in frequency but guides the small bandwidth fast elements.

At the same time, evidence for wave-energy coupling is also present in other ways, from our other new observation that all MLR events are accompanied by Pc 5 magnetic pulsations.

We narrowed down the source region of MLR, and provided evidence that it is, initially, triggered by PLHR. It is clearly a complex and finely balanced plasma wave process occurring on multiple time scales, but both self-sustaining and self-stabilising. On the basis of our observations low-level PLHR can act as the “seed” for the MLR, after which the multiple wave processes occurring in the MLR decouple from the PLHR. As such, the dominant energy source is unlikely to be PLHR, which probably explains the earlier results of *Rodger et al.* [1995, 1999, 2000a,b].

The fact that many MLR events were left-hand polarised may be explained by the mode conversion in the Earth-ionosphere wave-guide, as proposed in the case of PLHR-triggered emissions.

Very narrow band hiss bursts were observed above 6 kHz only during one morning during our campaigns, but they are worth presenting in this thesis, because this is the first time they have been observed. They might be related to the hydromagnetic (HM) emission bursts below 1 Hz.

High latitudes ( $L > 5$ ) are usually lacking whistlers, because ducted whistlers propagate mostly just inside the plasmopause. However, we were able to analyse 860

whistlers observed near Sodankylä before, during, and after an auroral substorm above Sodankylä. Whistler analysis showed that all whistlers propagated between  $L=3.0$  and  $L=4.0$ , i.e. south of Sodankylä. When comparing the relative movement of the equatorward boundary of the observable auroral forms, the whistler ducts moved accordingly.

The HM emission bursts seemed to be related to ELF-VLF chorus in a very fascinating way. The upper cutoff frequencies of chorus and HM emission bursts had the mass ratio of protons to electrons, i.e. gyrofrequency ratio of electron to proton at the same place in the magnetosphere. There was also a relationship between the intensity of the HM emission bursts and the occurrence of chorus bursts above 4.5 kHz.

Quasi-periodic (QP) emissions have similar periods to magnetic Pc 3-5 pulsations. In this thesis I have presented such an event, where magnetic pulsations had a lag of about 40 s with QP emissions. On the same morning also optical pulsations had the period of simultaneously observed Pc 3 pulsations.

The hiss clouds are most likely observed during quiet or moderate geomagnetic conditions over wide spatial areas. Most of the observed hiss clouds occurred in the morning hours during the recovery phase of the auroral activity, when diffuse aurora still prevailed. The duration (2-11 hours) and wide frequency range (0.5-7.0 kHz) separate the hiss clouds from other hiss-types.

The lower cutoff frequency of 1.85 kHz may be related to PLHR, but more likely it is due to the cutoff in the Earth-ionosphere wave-guide. The latter supports the idea that the hiss clouds propagated over long distances in the wave-guide.

The hiss clouds and MLR events tend to occur on the same days. If they are connected the interaction should occur relatively close to the topside ionosphere. Proving this idea certainly requires some morning-side satellite observations at auroral latitudes. The phenomenon must be studied more carefully in the future.

In the last chapter we have shown a few unusual ELF-VLF events, which are worth mentioning, but they require much more work to be published in the scientific journals.

The continuous wide-band recordings were found to be essential to study many of the ELF-VLF phenomena described in this thesis. The present experience in ELF-VLF research is widely based on either narrow band recordings or so-called synoptic (1 min every 15 min) recordings. Of course, numerous individual short-duration events need still to be studied in detail, but modern powerful computers with large hard disk capacities open up an entirely new era in ELF-VLF research. Hopefully, human activity will not pollute the plasma physical environment of the Earth too much before many new phenomena have got their explanations.



# Bibliography

- Akimoto, K., and D. Winske (1989), Nonlinear generation of whistler waves by an ion beam, *J. Geophys. Res.*, *94*, 17,259–17,265.
- Alford, J., M. Engebretson, R. Arnoldy, and U. Inan (1996), Frequency variations of quasi-periodic ELF-VLF emissions: A possible new ground-based diagnostic of the outer high-latitude magnetosphere, *J. Geophys. Res.*, *101*, 83–97.
- Anderson, B. J. (1994), An overview of spacecraft observations of 10 s to 600 s period magnetic pulsations in the Earth's magnetosphere, in *Solar Wind Sources of Magnetospheric Ultra-Low-Frequency Waves*, *Geophys. Monograph 81*, edited by M. J. Engebretson, K. Takahashi, and M. Scholer, pp. 25–43, American Geophysical Union, Washington, D.C.
- Anderson, R. R., and W. S. Kurth (1989), Discrete electromagnetic emissions in planetary magnetospheres, in *Plasma Waves and Instabilities at Comets and in Magnetospheres*, *Geophys. Monograph 53*, edited by B. T. Tsurutani and H. Oya, pp. 81–117, American Geophysical Union, Washington, D.C.
- Ando, Y., M. Hayakawa, and O. A. Molchanov (2002), Theoretical analysis on the penetration of power line radiation into the ionosphere, *Radio Sci.*, *37*, 1093, doi: 10.1029/2001RS002486.
- Angerami, J. J. (1970), Whistler duct properties deduced from VLF observations made with OGO-3 satellite near the magnetic equator, *J. Geophys. Res.*, *75*, 6115–6135.
- Angerami, J. J., and D. L. Carpenter (1966), Whistler studies of plasmopause in the magnetosphere. II. Equatorial electron density and total tube electron content near the knee in magnetospheric ionization, *J. Geophys. Res.*, *71*, 711–725.
- Barkhausen, H. (1919), Zwei mit Hilfe der neuen Versterker entdeckte Erscheinungen, *Physik A.*, *20*, 401–403.
- Barkhausen, H. (1930), Whistling tones from the Earth, *Proc. Inst. Radio Eng.*, *18*, 1155–1159.
- Barrington, R. E., and J. S. Belrose (1963), Preliminary results from the very-low-frequency receiver aboard Canada's Alouette satellite, *Nature*, *198*, 651.

- Baumback, M. M., and W. Calvert (1987), The minimum bandwidths of auroral kilometric radiation, *Geophys. Res. Lett.*, *14*, 119–122.
- Bell, T. F. (1985), High amplitude VLF transmitter signals and associated sidebands observed near the magnetic equatorial plane on the ISEE 1 satellite, *J. Geophys. Res.*, *90*, 2792–2806.
- Bell, T. F., U. Inan, and R. A. Helliwell (1981), Nonducted coherent VLF waves and associated triggered emissions observed on the ISEE 1 satellite, *J. Geophys. Res.*, *86*, 4649–4670.
- Bell, T. F., J. P. Lurette, and U. S. Inan (1982), ISEE-1 observations of VLF line radiation in the Earth's magnetosphere, *J. Geophys. Res.*, *87*, 3530–3536.
- Belyaev, P. P., S. Polyakov, V. O. Rapoport, and V. Yu. Trakhtengerts (1989), Experimental studies of the spectral resonance structure of the atmospheric electromagnetic noise background within the range of short-period geomagnetic pulsations, *Radiophysika*, *32*, 663–672.
- Belyaev, P. P., S. V. Polyakov, V. O. Rapoport, and V. Yu. Trakhtengerts (1990), The ionospheric Alfvén resonator, *J. Atmos. Terr. Phys.*, *52*, 781–788.
- Belyaev, P. P., T. Bösinger, S. V. Isaev, V. Yu. Trakhtengerts, and J. Kangas (1998), First evidence at high latitudes for ionospheric Alfvén resonator, *J. Geophys. Res.*, *104*, 4305–4317.
- Bernard, L. P. (1973), A new nose extension method for whistlers, *J. Atmos. Terr. Phys.*, *35*, 871–880.
- Bernhardt, P. A., and C. G. Park (1977), Protonospheric-ionospheric modeling of VLF ducts, *J. Geophys. Res.*, *82*, 5222–5230.
- Bespalov, P. A., and V. Y. Trakhtengerts (1986), Cyclotron instability of the Earth's radiation belt, *Rev. Plasma Phys.*, *10*, 155–212.
- Block, L. P., and D. L. Carpenter (1974), Derivation of magnetospheric electric fields from whistler data in a dynamic geomagnetic field, *J. Geophys. Res.*, *79*, 2783–2789.
- Bortnik, J., U. S. Inan, and T. F. Bell (2002), L dependence of energetic electron precipitation driven by magnetospherically reflecting whistler waves, *J. Geophys. Res.*, *107*, 1150, doi:10.1029/2001JA000303.
- Bortnik, J., U. S. Inan, and T. F. Bell (2003), Energy distribution and lifetime of magnetospherically reflecting whistlers in the plasmasphere, *J. Geophys. Res.*, *108*, 1199, doi:10.1029/2002JA009316.
- Bullough, K. (1983), Satellite observations of power line harmonic radiation, *Space Sci. Rev.*, *35*, 175–183.
- Bullough, K. (1995), Power line harmonic radiation: Sources and environmental effects, in *Handbook of atmospheric electrodynamics*, vol. 2, edited by H. Volland, pp. 291–332, CRC Press Inc., N.W., Boca Raton, Florida, U.S.

- Burke, C., and D. L. Jones (1992), An experimental investigation of ELF attenuation rates in the Earth-ionosphere duct, *J. Atmos. Terr. Phys.*, *54*, 243–250.
- Burton, E. T. (1930), Submarine cable interference, *Nature*, *126*, 55.
- Burton, E. T., and E. M. Boardman (1933a), Effects of solar eclipse on audio-frequency atmospheric, *Nature*, *131*, 81.
- Burton, E. T., and E. M. Boardman (1933b), Audio-frequency atmospheric, *Proc. IRE*, *21*, 1476–1494.
- Cannon, P. (1981), A ground based investigation of high latitude ELF radio signals, Ph.D. thesis, Dept. of Physics, University of Southampton, Southampton, UK.
- Carpenter, D. L. (1963), Whistler evidence of a ‘knee in the magnetospheric ionization density profile, *J. Geophys. Res.*, *68*, 1675–1682.
- Carpenter, D. L. (1966), Whistler studies of the plasmopause in the magnetosphere, 1. Temporal variations in the position of the knee and some evidence on plasma motions near the knee, *J. Geophys. Res.*, *71*, 693–709.
- Carpenter, D. L., and C. G. Park (1973), On what ionospheric workers should know about the plasmopause-plasmaphere, *Rev. Geophys. Space Phys.*, *11*, 133–154.
- Carpenter, D. L., R. R. Anderson, T. F. Bell, and T. R. Miller (1981), A comparison of equatorial electron densities measured by whistlers and by a satellite radio technique, *Geophys. Res. Lett.*, *8*, 1107–1110.
- Carson, W. B., J. A. Koch, J. H. Pope, and R. M. Gallet (1965), Long period very low frequency emissions, *J. Geophys. Res.*, *70*, 4293–4303.
- Chang, H. C., and U. S. Inan (1983a), Quasi-relativistic electron precipitation due to interactions with coherent VLF waves in the magnetosphere, *J. Geophys. Res.*, *88*, 318–328.
- Chang, H. C., and U. S. Inan (1983b), A theoretical model study of observed correlations between whistler mode waves and energetic electron precipitation events in the magnetosphere, *J. Geophys. Res.*, *88*, 10,053–10,058.
- Chapman, S. (1931), Audibility and lowermost altitude of aurora, *Nature*, *127*, 341–342.
- Chmyrev, V. M., A. B. Draganov, and Yu. N. Taranenko (1990), On the theory of whistler precursors on a VLF transmitter signal, *J. Atmos. Terr. Phys.*, *52*, 797–800.
- Cornilleau-Wehrin, N., J. Solomon, A. Korth, and G. Kremser (1993), Generation mechanism of plasmaspheric ELF/VLF hiss: A statistical study from GEOS 1 data, *J. Geophys. Res.*, *98*, 471–479.
- Coroniti, F. V., and C. F. Kennel (1970), Electron precipitation pulsations, *J. Geophys. Res.*, *75*, 1279–1289.

- Cummer, S. A. (1997), Lightning and ionospheric remote sensing using VLF/ELF radio atmospherics, Ph.D. thesis, Dept. of Electrical Engineering, Stanford University, Stanford, U.S.A.
- Demekhov, A. G., and V. Yu. Trakhtengerts (1994), A mechanism of formation of pulsating aurorae, *J. Geophys. Res.*, *99*, 5831–5841.
- Demekhov, A. G., P. P. Belyaev, S. V. Isaev, **Manninen, J.**, T. Turunen, and J. Kangas (2000), Modeling the diurnal evolution of the resonance spectral structure of the atmospheric noise background in Pc 1 frequency range, *J. Atmos. Sol.-Terr. Phys.*, *62*, 257–265.
- Doolittle, J. H., and D. L. Carpenter (1983), Photometric evidence of electron precipitation induced by first hop whistlers, *Geophys. Res. Lett.*, *10*, 611–614.
- Dowden, R. L. (1971), VLF discrete emissions deduced from Helliwell's theory, *J. Geophys. Res.*, *76*, 3046–3054.
- Draganov, A. B., U. S. Inan, V. S. Sonwalkar, and T. F. Bell (1992), Magnetospherically reflected whistlers as a source of plasmaspheric hiss, *Geophys. Res. Lett.*, *19*, 233–236.
- Dunckel, N., and R. A. Helliwell (1969), Whistler mode emissions on the OGO 1 satellite, *J. Geophys. Res.*, *74*, 6731–6785.
- Eckersley, T. L. (1931), 1929-1930 developments in the study of radio wave propagation, *Marconi Rev.*, *5*, 1–8.
- Eckersley, T. L. (1935), Musical atmospherics, *Nature*, *135*, 104–105.
- Edgar, B. C. (1976), The upper and lower frequency cutoffs of magnetospherically reflected whistlers, *J. Geophys. Res.*, *81*, 205–211.
- Ellis, G. R. A. (1957), Low frequency radio emission from aurorae, *J. Atmos. Terr. Phys.*, *10*, 302–306.
- Ellis, G. R. A. (1960), Observations of atmospheric noise, *Nature*, *186*, 229.
- Ellis, G. R. A. (1961), Spaced observations of the low frequency radiation from the Earth's upper atmosphere, *J. Geophys. Res.*, *66*, 19–23.
- Engebretson, M. J., C. I. Meng, R. L. Arnoldy, and L. J. Cahill Jr. (1986), Pc3 pulsations observed near the South Polar Cusp, *J. Geophys. Res.*, *91*, 8909–8918.
- Engebretson, M. J., J. R. Beck, D. L. Detrick, T. J. Rosenberg, R. L. Rairden, S. B. Mende, R. L. Arnoldy, and L. J. Cahill Jr. (1994a), Optical evidence that modulated electron precipitation near the magnetospheric boundary drives high latitude Pc 3-4 magnetic pulsations, in *Physical Signatures of Magnetospheric Boundary Layer Processes, NATO ASI Series*, edited by A. Egeland, J. Holtet, and P. E. Sandholt, pp. 361–373, Kluwer Acad. Publ.

- Engebretson, M. J., J. R. Beck, R. L. Rairden, S. B. Mende, R. L. Arnoldy, L. J. Cahill Jr., and T. J. Rosenberg (1994b), Studies of the occurrence and properties of Pc 3-4 magnetic and auroral pulsations at South Pole, Antarctica, in *Solar Wind Sources of Magnetospheric Ultra-Low-Frequency Waves*, edited by M. J. Engebretson, K. Takahashi, and M. Scholer, pp. 345–353, American Geophysical Union.
- Engebretson, M. J., J. L. Posch, A. J. Halford, G. A. Shelburne, A. J. Smith, M. Spasojević, U. S. Inan, and R. L. Arnoldy (2004), Latitudinal and seasonal variations of quasiperiodic and periodic VLF emissions in the outer magnetosphere, *J. Geophys. Res.*, *109*, A05216, doi:10.1029/2003JA010335.
- Francis, C. R., H. J. Strangeways, and K. Bullough (1983), Discrete VLF emissions (7–9 kHz) displaying unusual banded and periodic structure, *Planet. Space Sci.*, *31*, 537–557.
- Fukunishi, H., T. Toya, K. Koike, M. Kuwashima, and M. Kawamura (1981), Classification of hydromagnetic emissions based on frequency-time spectra, *J. Geophys. Res.*, *86*, 9029–9039.
- Gendrin, R. (1965), Gyroresonance radiation produced by proton and electron beams in different regions of the magnetosphere, *J. Geophys. Res.*, *70*, 5369–5383.
- Ginzburg, M. A. (1961), Electromagnetic radiation from solar corpuscular streams, *Phys. Rev. Lett.*, *7*, 399–401.
- Green, J. L., S. Boardsen, L. Garcia, W. W. L. Taylor, S. F. Fung, and B. W. Reinisch (2005), On the origin of whistler mode radiation in the plasmasphere, *J. Geophys. Res.*, *110*, A03201, doi:10.1029/2004JA010495.
- Guglelmi, A. V., T. A. Plyasova-Bakunina, and R. V. Shchepetnov (1973), Relation between the period of geomagnetic pulsations Pc 3,4 and the parameters of the interplanetary medium at the earth's orbit, *Geomagn. Aeron.*, *13*, 331–334.
- Gurnett, D. A., and L. A. Frank (1972), VLF hiss and related plasma observations in the polar magnetosphere, *JGR*, *77*, 172–190.
- Gurnett, D. A., and U. S. Inan (1988), Plasma wave observations with the Dynamics Explorer 1 spacecraft, *Rev. Geophys.*, *26*, 285–316.
- Gurnett, D. A., S. D. Shawhan, and R. R. Shaw (1983), Auroral hiss, Z mode radiation, and auroral kilometric radiation in the polar magnetosphere: DE1 observations, *J. Geophys. Res.*, *88*, 329–340.
- Hayakawa, M., and A. Iwai (1975), Magnetospheric ducting of low-latitude whistlers as deduced from the rocket measurement of their wave normal directions, *J. Atmos. Terr. Phys.*, *37*, 1211–1218.
- Hayakawa, M., and K. Ohta (1992), The propagation of low-latitude whistlers: a review, *Planet. Space Sci.*, *40*, 1339–1351.

- Hayakawa, M., and S. S. Sazhin (1992), Mid-latitude and plasmaspheric hiss: a review, *Planet. Space Sci.*, *40*, 1325–1338.
- Hayakawa, M., Y. Tanaka, T. Okada, and A. Iwai (1981), Goniometric direction finding for low-latitude whistlers and their propagation mechanism, *J. Geophys. Res.*, *86*, 6781–6793.
- Hayakawa, M., M. Parrot, and F. Lefeuvre (1986), The wave normals of ELF hiss emissions observed on board GEOS 1 at the equatorial and off-equatorial regions of the plasmasphere, *J. Geophys. Res.*, *91*, 7989–7999.
- Hayakawa, M., K. Ohta, and S. Shimakura (1990), Spaced direction finding of nighttime whistlers at low and equatorial latitudes and their propagation mechanism, *J. Geophys. Res.*, *95*, 15,091–15,102.
- Helliwell, R. A. (1965), *Whistlers and Related Ionospheric Phenomena*, Stanford University Press, Stanford, California, U.S.
- Helliwell, R. A. (1967), A theory of discrete emissions from the magnetosphere, *J. Geophys. Res.*, *72*, 4773–4790.
- Helliwell, R. A. (1975), Coherent VLF waves in the magnetosphere, *Phil. Trans. Roy. Soc. Lond. A.*, *280*, 137–149.
- Helliwell, R. A. (1983), Controlled stimulation of VLF emissions from Siple Station, Antarctica, *Radio Sci.*, *18*, 801–814.
- Helliwell, R. A. (2000), Triggering of whistler mode emissions by the band-limited impulse (BLI) associated with amplified Vlf signals from Siple Station, Antarctica, *Geophys. Res. Lett.*, *27*, 1455–1458.
- Helliwell, R. A., J. P. Katsufakis, T. F. Bell, and R. Raghuram (1975), VLF line radiation in the Earth's magnetosphere and its association with power system radiation, *J. Geophys. Res.*, *80*, 4249–4258.
- Helliwell, R. A., S. B. Mende, J. H. Doolittle, W. C. Armstrong, and D. L. Carpenter (1980), Correlations between  $\lambda$ 4278 optical emissions and VLF wave events observed at L $\sim$ 4 in the Antarctic, *J. Geophys. Res.*, *85*, 3376–3386.
- Helliwell, T. A. (1962), Very-low-frequency discrete emissions received at conjugate points, *Nature*, *195*, 64–65.
- Heyborne, R. L. (1966), Observations of whistler-mode signals in the OGO satellites from VLF group station transmitters, *Tech. Rep. 3425/3418-1*, Radioscience Laboratory, Stanford Electronics Labs., Stanford University, Stanford, CA.
- Hirasawa, T. (1980), Interaction between whistlers and quasi-periodic VLF emissions, in *Symposium on Highlights of the Japanese IMS Program*, University of Tokyo, conference paper.

- Ho, D. (1973), Interaction between whistlers and quasi-periodic VLF emissions, *J. Geophys. Res.*, *78*, 7347–7356.
- Hobara, Y., V. Yu. Trakhtengerts, A. D. Demekhov, and M. Hayakawa (2000), Formation of electron beams by the interaction of a whistler wave packet with radiation belt electrons, *J. Atmos. Sol.-Terr. Phys.*, *62*, 541–552.
- Hoffman, R. A., and T. Laaspere (1972), Comparison of very-low-frequency auroral hiss with precipitating low-energy electrons by the use of simultaneous data from two OGO-4 experiments, *J. Geophys. Res.*, *77*, 640–650.
- Inan, U. S., and T. F. Bell (1977), The plasmapause as a VLF guide, *J. Geophys. Res.*, *82*, 2819–2827.
- Inan, U. S., M. Platino, T. F. Bell, D. A. Gurnett, and J. S. Pickett (2004), Cluster measurements of rapidly moving sources of ELF/VLF chorus, *J. Geophys. Res.*, *109*, A05214, doi:10.1029/2003JA010289.
- Isted, G. A., and G. Millington (1957), The “dawn chorus” in radio observation, *Nature*, *180*, 716.
- James, H. G. (1976), VLF saucers, *J. Geophys. Res.*, *81*, 501–514.
- Jasna, D., U. S. Inan, and T. F. Bell (1990), Equatorial gyroresonance between electrons and magnetospherically reflected whistlers, *Geophys. Res. Lett.*, *17*, 1865–1868.
- Johnson, M. P., and U. S. Inan (2000), Sferics clusters associated with early/fast VLF events, *Geophys. Res. Lett.*, *27*, 1391–1394.
- Kaiser, J. F. (1974), Nonrecursive digital filter design using the  $i_0 - \sin h$  window function, *Proc. 1974 IEEE Symp. Circuits and Systems*, pp. 20–23.
- Karinen, A., K. Mursula, Th. Ulich, and **Manninen, J.** (2002), Does the magnetosphere behave differently on weekends?, *Ann. Geophys.*, *20*, 1137–1142.
- Karpman, V. I., J. N. Istomin, and D. R. Shklyar (1974), Nonlinear theory of a quasi monochromatic whistler mode wave packet in inhomogeneous plasma, *Plasma Phys.*, *16*, 685–703.
- Kennel, C. F., and H. E. Petschek (1966), Limit on stably trapped particle flux, *J. Geophys. Res.*, *71*, 1–28.
- Kikuchi, H. (1983), Power line transmission and radiation, *Space Sci. Rev.*, *35*, 59–81.
- Kimura, I. (1961), Amplification of the VLF electromagnetic wave by a proton beam through the exosphere – an origin of the VLF emissions, *Rep. Ionosph. Space Res. Japan*, *15*, 171–191.
- Kimura, I. (1985), Whistler mode propagation in the Earth and planetary magnetospheres and ray tracing techniques, *Space Sci. Rev.*, *42*, 449–466.

- Kimura, I. (1989), Ray paths of electromagnetic and electrostatic waves in the Earth and planetary magnetospheres, in *Plasma Waves and Instabilities at Comets and in Magnetospheres*, *Geophys. Monograph 53*, edited by B. T. Tsurutani and H. Oya, pp. 161–171, American Geophysical Union, Washington, D.C.
- Kitamura, T., J. A. Jacobs, T. Watanabe, and R. B. Flint Jr (1969), An investigation of quasi-periodic VLF emissions, *J. Geophys. Res.*, *74*, 5652–5664.
- Kokubun, S., K. Hayashi, and T. Oguti (1969), VLF emission study at Syowa Station, Antarctica: Polar chorus emissions and worldwide geomagnetic variation, *JARE Sci. Rep. Ser. A*, *6*, 1–34.
- Koons, H. C. (1985), Whistlers and whistler-stimulated emissions in the outer magnetosphere, *J. Geophys. Res.*, *90*, 8547–8551.
- Koons, H. C., B. C. Edgar, R. L. Dowden, C. G. Carrington, and L. E. S. Amon (1974), Multipath Doppler shifts in man-made VLF signals, in *ELF-VLF Radio Wave Propagation*, edited by J. A. Holtet, pp. 311–316, D. Reidel Publishing Company, Dordrecht-Holland.
- Koons, H. C., M. H. Dazey, and B. C. Edgar (1978), Satellite observation of discrete VLF line radiation within transmitter-induced amplification bands, *J. Geophys. Res.*, *83*, 3887–3889.
- Kornilov, I., **Manninen, J.**, J. Kultima, and T. Turunen (1998), Sunrise effect on chorus type VLF emissions, *Geomagn. Aeron.*, *38*, 155–160.
- Kozyra, J. U., C. E. Rasmussen, R. H. Miller, and L. R. Lyons (1994), Interaction of ring current and radiation belt protons with ducted plasmaspheric hiss 1. Diffusion coefficients and timescales, *J. Geophys. Res.*, *99*, 4069–4084.
- Kraus, J. D., and R. J. Marhefka (2001), *Antennas For All Applications*, McGraw-Hill Science/Engineering/Math, 3rd edition, U.S.
- Laaspere, T., and W. C. Johnson (1973), Additional results from an OGO-6 experiment concerning ionospheric electric and electromagnetic fields in the range 20 Hz to 540 kHz, *J. Geophys. Res.*, *78*, 2926–2944.
- Lauben, D. S., U. S. Inan, and T. F. Bell (2001), Precipitation of radiation belt electrons induced by obliquely propagating lightning-generated whistlers, *J. Geophys. Res.*, *107*, 29,745–29,770.
- Lauben, D. S., U. S. Inan, T. F. Bell, and D. A. Gurnett (2002), Source characteristics of ELF/VLF chorus, *J. Geophys. Res.*, *107*, 1429, doi:10.1029/2000JA003019.
- Lester, M., and A. J. Smith (1980), Whistler duct structure and formation, *Planet. Space Sci.*, *28*, 645–654.
- Lindemann, F. A., and G. M. B. Dobson (1923), Theory of meteors, *Proc. Roy. Soc. (London)*, *102*, 411–437.

- Lorentzen, K. R., J. B. Blake, U. S. Inan, and J. Bortnik (2001), Observations of relativistic electron microbursts in association with VLF chorus, *J. Geophys. Res.*, *106*, 6017–6027.
- Lurette, J. P. (1983), Power line radiation in the magnetosphere, Phd thesis, Department of Electrical Engineering, Stanford University.
- Lurette, J. P., C. G. Park, and R. A. Helliwell (1979), The control of magnetospheric chorus by power line radiation, *J. Geophys. Res.*, *84*, 2657–2660.
- Lundin, B. (1979), The effects of the interaction of resonant particles with monochromatic whistler waves propagating obliquely to the ambient magnetic field under magnetospheric conditions, Phd thesis, Institute of Terrestrial Magnetism, Ionosphere and Radio Wave Propagation, IZMIRAN, Moscow, Russia.
- Lundin, B. (1983), The new approach to the identification of the waveguide propagation of the VLF waves: the investigation of the polarization features of the wave field pattern, in *The propagation of the radiowaves in the ionosphere*, pp. 107–112, IZMIRAN, Moscow, Russia, in Russian.
- Lundin, B. (1985), On the polarization features of radiowaves reflected from the ionosphere, in *Investigations of structure and waves' properties of the near Earth's plasma*, pp. 95–103, IZMIRAN, Moscow, Russia, in Russian.
- Lundin, B., and C. Krafft (2002), Ion sense of polarization of the electromagnetic wave field in the electron whistler frequency band, *Ann. Geophys.*, *20*, 1153–1165.
- Maggs, J. E. (1976), Coherent generation of VLF hiss, *J. Geophys. Res.*, *81*, 1707–1724.
- Maggs, J. E. (1978), Electrostatic noise generated by auroral electron beam, *J. Geophys. Res.*, *83*, 3173–3188.
- Makita, K. (1979), VLF-LF Hiss emissions associated with aurora, *Mem. Natl. Inst. Polar Res., Ser. A. No. 16*, p. 127.
- Manninen, J., T. Turunen, J. Kultima, and E. Titova (1994), Correlating optical emissions, quasi-periodic VLF emissions and magnetic Pc3 pulsations, *Geomagn. Aeron.*, *34*, 42–47.
- Manninen, J., N. G. Kleimenova, O. V. Kozyreva, and A. Ranta (2002), High latitude morning ionosphere response to the front edge of the interplanetary magnetic cloud on January 10, 1997, *J. Atmos. Sol.-Terr. Phys.*, *64*, 23–32.
- Masson, A., U. Inan, H. Laakso, O. Santolík, and P. Décréau (2004), Cluster observations of mid-latitude hiss near the plasmapause, *Ann. Geophys.*, *22*, 2565–2575.
- Matsumoto, H., and I. Kimura (1971), Linear and nonlinear cyclotron instability and VLF emissions in the magnetosphere, *Planet. Space Sci.*, *19*, 567–608.

- Matthews, J. P., and K. Yearby (1981), Magnetospheric line radiation observed at Halley, Antarctica, *Planet. Space Sci.*, *29*, 97–105.
- Molchanov, O. A., M. Parrot, M. M. Mogilevsky, and F. LeFeuvre (1991), A theory of PLHR emissions to explain the weekly variation of ELF data observed by a low-altitude satellite, *Ann. Geophys.*, *9*, 669–680.
- Morrison, K., M. J. Engebretson, J. R. Beck, J. E. Johnson, R. L. Arnoldy, L. J. Cahill Jr., D. L. Carpenter, and M. Gallani (1994), A study of quasiperiodic ELF-VLF emissions at three Antarctic stations – Evidence for off-equatorial generation?, *Ann. Geophys.*, *12*, 139–146.
- Mosier, S. R. (1976), Observations of magnetospheric ionization enhancements using upper hybrid resonance noise band data from RAE 1 satellite, *J. Geophys. Res.*, *81*, 253–256.
- Neufeld, J., and H. Wright (1964), Multiple instability in a plasma-beam system, *Phys. Fluids*, *7*, 1527–1534.
- Nunn, D. (1986), A nonlinear theory of sideband stability in ducted whistler mode wave, *Planet. Space Sci.*, *34*, 429–451.
- Nunn, D. (1990), The numerical simulation of VLF non-linear wave particle interactions in collision free plasmas using the Vlasov hybrid simulation technique, *Comput. Phys. Comm.*, *60*, 1–25.
- Nunn, D. (1993), A novel technique for the numerical simulation of hot collision free plasma; Vlasov hybrid simulation, *J. Computat. Phys.*, *108*, 180–196.
- Nunn, D., and A. J. Smith (1996), Numerical simulation of whistler-triggered VLF emissions observed in Antarctica, *J. Geophys. Res.*, *101*, 5261–5277.
- Nunn, D., Y. Omura, H. Matsumoto, I. Nagano, and S. Yagitani (1997), The numerical simulation of VLF chorus and discrete emissions observed on the Geotail satellite using a Vlasov code, *J. Geophys. Res.*, *102*, 27,083–27,097.
- Nunn, D., **Manninen, J.**, T. Turunen, V. Yu. Trakhtengerts, and N. Erokhin (1999), On the nonlinear triggering of VLF emissions by power line harmonic radiation, *Ann. Geophys.*, *17*, 79–94.
- Ohta, K., M. Hayakawa, and S. Shimakura (1989), Frequency dependence of arrival direction and polarization of low-latitude whistlers and their ducted propagation, *J. Geophys. Res.*, *94*, 6975–6978.
- Okada, T., A. Iwai, and M. Hayakawa (1977), The measurement of incident and azimuthal angles and the polarization of whistlers at low-latitudes, *Planet. Space Sci.*, *25*, 233–241.
- Omura, Y., and H. Matsumoto (1982), Computer simulations of basic processes of coherent whistler wave particle interactions in the magnetosphere, *J. Geophys. Res.*, *87*, 4435–4444.

- Omura, Y., D. Nunn, H. Matsumoto, and M. J. Rycroft (1991), A review of observational, theoretical and numerical studies of VLF triggered emissions, *J. Atmos. Terr. Phys.*, *53*, 351–368.
- Ondoh, T. (1976), Magnetospheric whistler ducts observed by ISIS satellites, *J. Radio Res. Labs.*, *23*, 139–147.
- Ondoh, T. (1993), Narrow-band plasmopause hiss observed by ISIS satellites, *Radio Sci.*, *28*, 629–642.
- Ondoh, T., Y. Nakamura, S. Watanabe, and T. Murakami (1981), Narrow-band 5 kHz hiss observed in the vicinity of the plasmopause, *Planet. Space Sci.*, *29*, 65–72.
- Park, C. G. (1972), Methods of determining electron concentrations in the magnetosphere from nose whistlers, *Tech. rep.*, Radiosci. Lab., Stanford Electron. Lab., Stanford University, Stanford, California.
- Park, C. G. (1977), VLF wave activity during a magnetic storm: A case study of the role of power line radiation, *J. Geophys. Res.*, *82*, 3251–3260.
- Park, C. G. (1978), Whistler observations of substorm electric fields in the nightside plasmasphere, *J. Geophys. Res.*, *83*, 5773–5777.
- Park, C. G. (1982), Whistlers, in *CRC handbook of Atmospheric, Vol II*, edited by H. Volland, pp. 21–77, CRC Press, Inc., Boca Raton, Florida.
- Park, C. G., and D. C. D. Chang (1978), Transmitter simulation of power line harmonic radiation effects in the magnetosphere, *Geophys. Res. Lett.*, *5*, 861–864.
- Park, C. G., and R. A. Helliwell (1971), The formation by electric fields of field-aligned irregularities in the magnetosphere, *Radio Sci.*, *6*, 299–309.
- Park, C. G., and R. A. Helliwell (1977), Whistler precursors: a possible catalytic role of power line radiation, *J. Geophys. Res.*, *82*, 3634–3642.
- Park, C. G., and R. A. Helliwell (1978), Magnetospheric effects of power line radiation, *Science*, *200*, 727–730.
- Park, C. G., and R. A. Helliwell (1981), Power line radiation in the magnetosphere, *Adv. Space Res.*, *1*, 423–437.
- Park, C. G., and T. R. Miller (1979), Sunday decreases in magnetospheric vlf wave activity, *J. Geophys. Res.*, *84*, 943–950.
- Park, C. G., R. A. Helliwell, and F. LeFeuvre (1983), Ground observations of power line radiation coupled to the ionosphere and magnetosphere, *Space Sci. Rev.*, *35*, 131–137.
- Parrot, M. (1995), Observations of power-line harmonic radiation by the low-altitude AUREOL-3 satellite, *J. Geophys. Res.*, *100*, 5681–5689.

- Parrot, M., and Y. Zaslavski (1996), Physical mechanisms of man-made influences on the magnetosphere, *Surv. Geophys.*, *17*, 67–100.
- Paschal, E. W. (1990), Whistler precursors on a VLF transmitter signal, *J. Geophys. Res.*, *95*, 225–231.
- Pasmanik, D., V. Trakhtengerts, A. Demekhov, A. Lyubchich, E. Titova, T. Yahnina, M. Rycroft, **Manninen, J.**, and T. Turunen (1998), A quantitative model for cyclotron wave-particle interaction at the plasmopause, *Ann. Geophys.*, *16*, 322–330.
- Peter, W. B., and U. S. Inan (2004), On the occurrence and spatial extent of electron precipitation induced by oblique nonducted whistler waves, *J. Geophys. Res.*, *109*, A12215, doi:10.1029/2004JA010412.
- Polyakov, S. V. (1976), On properties of an ionospheric Alfvén resonator, in *Proc. Symposium KAPG on Solar-Terrestrial Physics*, vol. III, pp. 72–73, Nauka, Moscow, conference paper.
- Potter, R. K. (1951), Analysis of audio-frequency atmospherics, *Proc. IRE N. Y.*, *39*, 1067–1069.
- Preece, W. H. (1894), Earth currents, *Nature Lond.*, *49*, 554.
- Prikner, K., K. Mursula, J. Kangas, R. Kerttula, and F. Z. Feygin (2004), An effect on the ionospheric Alfvén resonator on multiband p1 pulsations, *Ann. Geophys.*, *22*, 643–651.
- Rietveld, M. T., H.-P. Mauelshagen, P. Stubbe, H. Kopka, and E. Nielsen (1987), The characteristics of ionospheric heating-produced ELF/VLF waves over 32 hours, *J. Geophys. Res.*, *92*, 8707–8722.
- Riihimaa, J. J. (1972), Observations of radio noise in the VLF region, *Tech. rep.*, Report S 33, Department of Electrical Engineering, University of Oulu.
- Rodger, C. J. (1999), Red sprites, upward lightning, and VLF perturbations, *Rev. Geophys.*, *37*, 317–336.
- Rodger, C. J., N. R. Thomson, and R. L. Dowden (1995), VLF line radiation observed by satellite, *J. Geophys. Res.*, *100*, 5681–5689.
- Rodger, C. J., M. A. Clilverd, K. H. Yearby, and A. J. Smith (1999), Magnetospheric line radiation observations at Halley, Antarctica, *J. Geophys. Res.*, *104*, 17,441–17,447.
- Rodger, C. J., M. A. Clilverd, K. H. Yearby, and A. J. Smith (2000a), Temporal properties of magnetospheric line radiation, *J. Geophys. Res.*, *105*, 329–336.
- Rodger, C. J., M. A. Clilverd, K. H. Yearby, and A. J. Smith (2000b), Is magnetospheric line radiation man-made?, *J. Geophys. Res.*, *105*, 15,981–15,990.

- Rycroft, M. J. (1976), Gyroresonance interactions in the outer plasmasphere, *J. Atmos. Terr. Phys.*, *38*, 1211–1214.
- Rycroft, M. J. (1991), Interaction between whistler-mode waves and energetic electrons in the coupled system formed by the magnetosphere, ionosphere and atmosphere, *J. Atmos. Terr. Phys.*, *53*, 849–858.
- Safargaleev, V., T. Turunen, W. Lyatsky, **Manninen, J.**, and A. Kozlovsky (1996), Imaging and EISCATradar measurements of an auroral prebreakup event, *Ann. Geophys.*, *14*, 1170–1176.
- Sagredo, J. L., and K. Bullough (1973), VLF goniometer observations at Halley Bay, Antarctica–II. Magnetospheric structure deduced from whistler observations, *Planet. Space Sci.*, *21*, 913–914.
- Sagredo, J. L., I. D. Smith, and K. Bullough (1973), The determination of whistler nose-frequency and minimum group delay and its implication for the measurement of the east-west electric field and tube content in the magnetosphere, *J. Atmos. Terr. Phys.*, *35*, 2035–2046.
- Salvati, M. A., U. S. Inan, T. J. Rosenberg, and A. T. Weatherwax (2000), Solar wind control of polar chorus, *Geophys. Res. Lett.*, *27*, 649–652.
- Santolik, O., and D. A. Gurnett (2002), Propagation of auroral hiss at high latitudes, *Geophys. Res. Lett.*, *29*, 1481, doi:10.1029/2001GL013666.
- Sato, N. (1980), Quasi-periodic (QP) ELF-VLF emissions observed in high latitudes, *Mem. Natl. Polar Res., Ser. A17*.
- Sato, N., and H. Fukunishi (1981), Interaction between ELF-VLF emissions and magnetic pulsations: Classification of quasi-periodic ELF-VLF emissions based on frequency time spectra, *J. Geophys. Res.*, *86*, 19–29.
- Sato, N., and S. Kokubun (1980), Interaction between ELF-VLF emissions and magnetic pulsations: Quasi-periodic ELF-VLF emissions associated with pc 3-4 magnetic pulsations and their geomagnetic conjugacy, *J. Geophys. Res.*, *85*, 101–113.
- Sato, N., and S. Kokubun (1981), Interaction between ELF-VLF emissions and magnetic pulsations: Regular period ELF-VLF pulsations and their geomagnetic conjugacy, *J. Geophys. Res.*, *86*, 9–18.
- Sazhin, S. S., and M. Hayakawa (1992), Magnetospheric chorus emissions: a review, *Planet. Space Sci.*, *40*, 681–697.
- Sazhin, S. S., and M. Hayakawa (1994), Periodic and quasiperiodic VLF emissions, *J. Atmos. Terr. Phys.*, *56*, 735–753.
- Sazhin, S. S., A. J. Smith, and E. M. Sazhina (1990), Can magnetospheric electron temperature be inferred from whistler dispersion measurements?, *Ann. Geophys.*, *8*, 273–285.

- Sazhin, S. S., A. E. Sumner, and N. M. Temme (1992), Relativistic and nonrelativistic analysis of whistler-mode waves in a hot anisotropic plasma, *J. Plasma Phys.*, *47*, 163–174.
- Sazhin, S. S., K. Bullough, and M. Hayakawa (1993), Auroral hiss: a review, *Planet. Space Sci.*, *41*, 735–753.
- Shawhan, S. D. (1979), Magnetospheric plasma waves, in *Solar System Plasma Physics*, vol. III, edited by E. N. Parker, C. F. Kennel, and L. J. Lanzerotti, chap. 1.6., pp. 211–270, North-Holland Publishing, Amsterdam, The Netherlands.
- Shimakura, S., T. Okada, M. Hayakawa, and Y. Tanaka (1986), The relationship between the polarisation of whistlers and their dispersion, *J. Geophys.*, *59*, 140–141.
- Shklyar, D. R., D. Nunn, A. J. Smith, and S. S. Sazhin (1992), An investigation into the nonlinear frequency shift in magnetospherically propagated pulses, *J. Geophys. Res.*, *97*, 19,389–19,402.
- Singh, R., R. P. Patel, R. P. Singh, and Lalmani (2000), An experimental study of hiss-triggered chorus emissions at low latitude, *Earth Planets Space*, *52*, 37–40.
- Skellett, A. M. (1931), Effect of meteors on radio transmission through the Kennelly-Heavyside layer, *Phys. Rev.*, *37*, 1668.
- Smith, A. J. (1995), VELOX: a new VLF/ELF receiver in Antarctica for the Global Geospace Science mission, *J. Atmos. Terr. Phys.*, *57*, 507–524.
- Smith, A. J., M. J. Engebretson, E. M. Klatt, U. S. Inan, R. L. Arnoldy, and H. Fuku-nishi (1998), Periodic and quasiperiodic ELF/VLF emissions observed by an array of Antarctic stations, *J. Geophys. Res.*, *103*, 23,611–23,622.
- Smith, R. L. (1960), VLF observations of auroral beams as sources of a class of emissions, *Nature*, *224*, 351.
- Smith, R. L., and J. J. Angerami (1968), Magnetospheric properties deduced from OGO 1 observations of ducted and non-ducted whistlers, *J. Geophys. Res.*, *73*, 1–20.
- Sonwalkar, V. S., and U. S. Inan (1988), Wave normal direction and spectral properties of whistler mode hiss observed on the DE 1 satellite, *J. Geophys. Res.*, *93*, 7493–7514.
- Sonwalkar, V. S., and U. S. Inan (1989), Lightning as an embryonic source of VLF hiss, *J. Geophys. Res.*, *94*, 6986–6994.
- Storey, L. R. O. (1953), An investigation of whistling atmospheric, *Phil. Trans. Roy. Soc. A.*, *246*, 113–141.
- Strangeways, H. J. (1980), Systematic errors in VLF direction-finding of whistler ducts-I, *J. Atmos. Terr. Phys.*, *42*, 995–1008.

- Strangeways, H. J. (1981), Determination by ray-tracing of the regions where mid-latitude whistlers exit from the lower ionosphere, *J. Atmos. Terr. Phys.*, *43*, 231–238.
- Strangeways, H. J., and M. J. Rycroft (1980), Systematic errors in VLF direction-finding of whistler ducts–II, *J. Atmos. Terr. Phys.*, *42*, 1009–1023.
- Swift, D. W., and J. R. Kan (1975), A theory of auroral hiss and implications on the origin of auroral electrons, *J. Geophys. Res.*, *80*, 985–992.
- Tanaka, Y., M. Hayakawa, and M. Nishino (1976), Study of auroral VLF hiss observed at Syowa Station, Antarctica, *Mem. Natl. Inst. Polar Res. Ser. A*, *13*, 1–58.
- Tarcsai, Gy. (1975), Routine whistler analysis by means of accurate curve fitting, *J. Atmos. Terr. Phys.*, *37*, 1447–1457.
- Thomson, R. J. (1977), PL whistlers, *Planet. Space Sci.*, *25*, 1037–1043.
- Thomson, R. J. (1978), The formation and lifetime of whistler ducts, *Planet. Space Sci.*, *26*, 423–430.
- Thomson, R. J., and R. L. Dowden (1977), Simultaneous ground and satellite reception of whistlers: 2. PL whistlers, *J. Atmos. Terr. Phys.*, *39*, 879–883.
- Thomson, R. J., and R. L. Dowden (1978), Ionospheric whistler propagation, *J. Atmos. Terr. Phys.*, *40*, 215–221.
- Thorne, R. M., and B. T. Tsurutani (1979), Power line harmonic radiation: can it significantly affect the Earth's radiation belts?, *Science*, *204*, 839–841.
- Thorne, R. M., and B. T. Tsurutani (1981), Comment on 'Sunday decreases in magnetospheric wave activity by C. G. Park and T. R. Miller, *J. Geophys. Res.*, *86*, 1639–1641.
- Tixier, M., G. Charcosset, Y. Corcuff, and T. Okada (1984), Propagation modes of whistlers received aboard satellites over Europe, *Ann. Geophys.*, *2*, 211–220.
- Trakhtengerts, V. Yu. (1995), Magnetosphere cyclotron maser: BWO generator regime, *J. Geophys. Res.*, *100*, 17,205–17,210.
- Trakhtengerts, V. Yu., and M. J. Rycroft (2000), Whistler–electron interactions in the magnetosphere: new results and novel approaches, *J. Atmos. Sol.-Terr. Phys.*, *62*, 1719–1733.
- Trakhtengerts, V. Yu., V. R. Tagirov, and S. A. Chernous (1986), Flow cyclotron maser and impulsive VLF emissions, *Geomagn. Aeron.*, *26*(1), 99–106.
- Trakhtengerts, V. Yu., M. J. Rycroft, and A. G. Demekhov (1996), Inter-relation of noise-like and discrete ELF/VLF emissions generated by cyclotron interaction, *J. Geophys. Res.*, *101*, 13,293–13,301.

- Troitskaya, V. A., T. A. Plyasova-Bakunina, and A. V. Gugelmi (1971), Relationship between Pc2-4 pulsations and the interplanetary magnetic field, *Dokl. Akad. Nauk. USSR*, *197*, 1312–1315.
- Troitskaya, V. A., A. V. Gugelmi, O. V. Bolshakova, E. T. Matveyeva, and R. V. Schepetnov (1972), Indices of geomagnetic pulsations, *Planet. Space Sci.*, *20*, 849–858.
- Tsurutani, B. T., and R. M. Thorne (1981), A skeptic's view of PLR effects in the magnetosphere, *Adv. Space Res.*, *1*, 439–444.
- Tsurutani, B. T., S. R. Church, and R. M. Thorne (1979), A search for geographic control on the occurrence of magnetospheric ELF emissions, *J. Geophys. Res.*, *84*, 4116–4124.
- Turunen, T., and J. Oksman (1979), On the relative location of the plasmapause and the HF backscatter curtains, *J. Atmos. Terr. Phys.*, *41*, 345–350.
- Turunen, T., P. S. Cannon, and M. J. Rycroft (1980), Generation of ELF radio signals in the auroral ionosphere by non-linear demodulation of LF and/or MF transmissions, *Nature*, *286*, 375–377.
- Volland, H. (1995), Long-wave sferics propagation within the atmospheric waveguide, in *Handbook of atmospheric electrodynamics*, vol. 2, edited by H. Volland, pp. 65–93, CRC Press Inc., N.W., Boca Raton, Florida, U.S.
- Walker, A. D. M. (1978a), Formation of whistler ducts, *Planet. Space Sci.*, *26*, 375–379.
- Walker, A. D. M. (1978b), The theory of whistler propagation, *Rev. Geophys. Space Phys.*, *14*, 629–638.
- Watt, A. D. (1967), *VLF Radio Engineering*, Pergamon Press, Oxford, U.K.
- Weidman, C. D., and E. P. Krider (1986), The amplitude spectra of lightning radiation fields in the interval from 1 to 20 MHz, *Radio Sci.*, *21*, 964–970.
- Williams, J. L. (1932), The sound of the aurora, *Literary Digest*, *112*, 28.
- Yahnin, A. G., N. V. Semenova, A. A. Ostapenko, J. Kangas, **Manninen, J.**, and T. Turunen (2003), Morphology of the spectral resonance structure of the electromagnetic background noise in the range of 0.1–4 Hz at L=5.2, *Ann. Geophys.*, *21*, 779–786.
- Yamagishi, H. (1989), ELF emissions at high latitudes – Ray path calculation and ground-satellite observations, *Mem. Natl. Polar Res., Ser. A*, *19*, 1–120.
- Yamamoto, T. (1979), On the amplification of VLF hiss, *Planet. Space Sci.*, *27*, 273–284.
- Yearby, K. H. (1982), Magnetospheric VLF line radiation, Phd thesis, Department of Physics, The University of Sheffield.

- Yearby, K. H., and A. J. Smith (1994), The polarisation of whistlers received on the ground near  $L = 4$ , *J. Atmos. Terr. Phys.*, *56*, 1499–1512.
- Yearby, K. H., J. P. Matthews, and A. J. Smith (1981), VLF line radiation observed at Halley and Siple, *Adv. Space Res.*, *1*, 445–448.
- Yearby, K. H., A. J. Smith, T. R. Kaiser, and K. Bullough (1983), Power line harmonic radiation in Newfoundland, *J. Atmos. Terr. Phys.*, *45*, 409–419.





**VERÖFFENTLICHUNGEN DES GEOPHYSIKALISCHEN OBSERVATORIUMS  
DER FINNISCHEN AKADEMIE DER WISSENSCHAFTEN  
(PUBLICATIONS FROM SODANKYLÄ GEOPHYSICAL OBSERVATORY)**

- No.
- |        |  |         |  |
|--------|--|---------|--|
| 1 J.   | KERÄNEN: Ergebnisse der magnetischen Beobachtungen des Observatoriums zu Sodankylä im Jahre 1914   | 45 E.   | KATAJA: Ergebnisse 1961  |
| 2 J.   | KERÄNEN: Ergebnisse 1915   | 46 E.   | KATAJA: Ergebnisse 1962  |
| 3 J.   | KERÄNEN: Ergebnisse 1916   | 47 E.   | KATAJA: Ergebnisse 1963  |
| 4 J.   | KERÄNEN: Ergebnisse 1917   | 48 E.   | KATAJA: Ergebnisse 1964  |
| 5 E.R. | LEVANTO: Ergebnisse 1918   | 49 E.   | KATAJA: Ergebnisse 1965  |
| 6 E.R. | LEVANTO: Ergebnisse 1919   | 50 E.   | KATAJA: Ergebnisse 1966  |
| 7 E.R. | LEVANTO: Ergebnisse 1920   | 51 E.   | KATAJA: Ergebnisse 1967  |
| 8 H.   | HYRYLÄINEN: Ergebnisse 1921  | 52 E.   | KATAJA: Ergebnisse 1968  |
| 9 H.   | HYRYLÄINEN: Ergebnisse 1922  | 53 E.   | KATAJA: Ergebnisse 1969  |
| 10 H.  | HYRYLÄINEN: Ergebnisse 1923  | 54 E.   | KATAJA: Ergebnisse 1970  |
| 11 H.  | HYRYLÄINEN: Ergebnisse 1924  | 55 E.   | KATAJA: Ergebnisse 1971  |
| 12 H.  | HYRYLÄINEN: Ergebnisse 1925  | 56 J.   | KERÄNEN and C. SUCKSDORFF (ed.): Collected papers to commemorate the 60 <sup>th</sup> anniversary of the Sodankylä Observatory |
| 13 H.  | HYRYLÄINEN: Ergebnisse 1926  | /1 J.   | KERÄNEN: Ueber die Verteilung des erdmagnetischen Feldes in Sodankylä  |
| 14 E.  | SUCKSDORFF: Ergebnisse 1927  | /2 E.   | KATAJA: The Sodankylä Geophysical Observatory in 1973  |
| 15 E.  | SUCKSDORFF: Ergebnisse 1928  | /3 W.   | DIEMINGER: 20 years of cooperation in ionospheric research with Finland  |
| 16 E.  | SUCKSDORFF: Ergebnisse 1929  | /4 J.C. | GUPTA: The solar and lunar daily geomagnetic variations at Sodankylä, 1914-1966  |
| 17 E.  | SUCKSDORFF: Ergebnisse 1930  | /5 S.   | KOIVUMAA: Solar-cycle variation of ionospheric F2-layer profile parameters at Sodankylä  |
| 18 E.  | SUCKSDORFF: Ergebnisse 1931  | /6 H.   | RANTA and E. KATAJA: Bibliography of the geophysical observatories at Sodankylä  |
| 19 E.  | SUCKSDORFF: Ergebnisse 1932  | 57 E.   | KATAJA: Magnetic results 1972  |
| 20 E.  | SUCKSDORFF: Ergebnisse 1933  | 58 E.   | KATAJA: Magnetic results 1973  |
| 21 E.  | SUCKSDORFF: Berichtungen der in den magnetischen Jahrbüchern des Observatoriums zu Sodankylä veröffentlichten Werte der Deklination 1925-1933 und der Horizontalintensität 1932-1933 | 59 E.   | KATAJA: Magnetic results 1974  |
| 22 E.  | SUCKSDORFF: Ergebnisse 1934  | 60 E.   | KATAJA: Magnetic results 1975  |
| 23 E.  | SUCKSDORFF: Ergebnisse 1935  | 61 E.   | KATAJA: Magnetic results 1976  |
| 24 E.  | SUCKSDORFF: Ergebnisse 1936  | 62 E.   | KATAJA: Magnetic results 1977  |
| 25 E.  | SUCKSDORFF: Die erdmagnetische Aktivität in Sodankylä in den Jahren 1914-1934  | 63 J.C. | GUPTA: The solar and lunar daily geomagnetic variations at Sodankylä 1914-1966. Supplement.                                    |
| 26 E.  | SUCKSDORFF: Ergänzende Daten betreffs der erdmagnetischen Aktivität in Sodankylä in den Jahren 1914-1934   | 64 E.   | KATAJA: Magnetic results 1978  |
| 27 E.  | SUCKSDORFF: Ergebnisse 1937  | 65 E.   | KATAJA: Magnetic results 1979  |
| 28 E.  | SUCKSDORFF: Ergebnisse 1938  | 66 E.   | KATAJA: Magnetic results 1980  |
| 29 E.  | SUCKSDORFF: Ergebnisse 1939  | 67 E.   | KATAJA: Magnetic results 1981  |
| 30 E.  | SUCKSDORFF: Die erdmagnetischen Aktivitätszahlen AZ von Sodankylä in den Jahren 1935-1944  | 68 E.   | KATAJA: Magnetic results 1982  |
| 31 E.  | SUCKSDORFF: Ergebnisse 1940  | 69 E.   | KATAJA and J. KULTIMA: Magnetic results 1983   |
| 32 E.  | SUCKSDORFF: Ergebnisse 1941  | 70 E.   | KATAJA and J. KULTIMA: Magnetic results 1984   |
| 33 E.  | SUCKSDORFF: Ergebnisse 1942  | 71 E.   | KATAJA and J. KULTIMA: Magnetic results 1985   |
| 34 E.  | SUCKSDORFF: Ergebnisse 1943-1944   | 72 E.   | KATAJA and J. KULTIMA: Magnetic results 1986   |
| 35 H.  | LÄHTI: Ueber das Auftreten der magnetischen Pulsationen in Sodankylä und Vuotso in den Jahren 1935 und 1936  | 73 J.   | KULTIMA and E. KATAJA: Magnetic results 1987   |
| 36 M.  | SEPPÄNEN and E. KATAJA: Ergebnisse 1946  | 74 J.   | KULTIMA and E. KATAJA: Magnetic results 1988   |
| 37 M.  | SEPPÄNEN and E. KATAJA: Ergebnisse 1947  | 75 J.   | KULTIMA and E. KATAJA: Magnetic results 1989   |
| 38 T.  | HILPELÄ: Ergebnisse 1948-1949  | 76 K.   | KAURISTIE et al.: Homogeneity of geomagnetic variations at the Sodankylä Observatory   |
| 39 E.  | KATAJA: Ergebnisse 1950-1951   | 77 J.   | KULTIMA and E. KATAJA: Magnetic results 1990   |
| 40 E.  | KATAJA: Ergebnisse 1952-1953   | 78 J.   | KULTIMA and E. KATAJA: Magnetic results 1991   |
| 41 E.  | KATAJA: Ergebnisse 1954-1956   | 79 J.   | KULTIMA: Magnetic results 1992   |
| 42 E.  | KATAJA: Ergebnisse 1957-1958   | 80 J.   | KULTIMA: Magnetic results 1993   |
| 43 E.  | KATAJA: Ergebnisse 1959  | 81 J.   | KULTIMA: Magnetic results 1994   |
| 44 E.  | KATAJA: Ergebnisse 1960  | 82 J.   | KULTIMA: Magnetic results 1995   |
|        |  | 83 J.   | KULTIMA: Magnetic results 1996   |

**SPEZIELLE UNTERSUCHUNGEN  
VON DEM INTERNATIONALEN POLARJAHRE 1932-1933**

- 1 M. TOMMILA: Ergebnisse der magnetischen Beobachtungen des Polarjahr-Observatoriums zu Petsamo im Polarjahre 1932-1933
- 2 J. KERÄNEN and H. LUNELUND: Ueber die Sonnen- und Himmelsstrahlung in Sodankylä während des Polarjahres 1932-1933

**SODANKYLÄ GEOPHYSICAL OBSERVATORY  
PUBLICATIONS**

- 84 H. NEVANLINNA: Magnetic results Sodankylä Polar Year Observatory 1882-1883
- 85 J. KULTIMA: Magnetic results Sodankylä 1997
- 86 J. KULTIMA: Magnetic results Sodankylä 1998
- 87 TH. ULICH: Solar variability and long-term trends in the ionosphere; PhD thesis
- 88 J. KULTIMA: Magnetic results Sodankylä 1999
- 89 I. USOSKIN: Oulu neutron monitor cosmic ray data, January 2000 - December 2000
- 90 J. KULTIMA: Magnetic results Sodankylä 2000
- 91 J. KULTIMA: Magnetic results Sodankylä 2001
- 92 K. KAILA, H. HOLMA and J. JUSSILA: Proceedings of the 28<sup>th</sup> annual European meeting on atmospheric studies by optical methods, 19 – 24.8.2001, Oulu, Finland
- 93 A. KOZLOVSKY: Structure and dynamics of the magnetosphere inferred from radar and optical observations at high latitudes; PhD thesis
- 94 J. KULTIMA: Magnetic results Sodankylä 2002
- 95 J. KULTIMA: Magnetic results Sodankylä 2003
- 96 VLF-WORKSHOP: Abstracts, Sodankylä 2004
- 97 J. KULTIMA and T. RAITA: Magnetic results Sodankylä 2004
- 98 J. MANNINEN: Some aspects of ELF-VLF emissions in geophysical research; PhD thesis

ISBN 951-42-6047-3  
ISBN 951-42-6048-1 (pdf)  
ISSN 1456-3673